THE BELL SYSTEM TECHNICAL JOURNAL
Vol. 56, No. 10, December 1977
Printed in U.S.A.

WT4 Millimeter Waveguide System:

Introduction

By W. D. WARTERS

(Manuscript received April 7, 1977)

In this special WT4 issue of the B.S.T.J., we describe the design of a long-haul millimeter waveguide transmission system capable of carrying up to 475,000 two-way voice circuits, and give the results of measurements on a 14-km test system. The WT4/WT4A system transmits high-speed digital bit streams in the DS-4 format (274 Mbits/sec), which can carry any form of voice, data, or video communications. The bit error rate is designed to be 10^{-7} or better on a coast-to-coast circuit. The waveguide medium is designed to be installed on readily obtainable right-of-way, utilizing standard construction techniques for most operations. The installed medium features low signal loss, allowing extremely wide repeater spacings, and rugged construction, providing significantly higher reliability than any existing medium. Maintenance and restoration procedures and equipment have been developed and demonstrated for both repeaters and medium. For a fully loaded system, the cost per circuit mile will be significantly below that of any existing long-haul system.

This development is the direct result of over four decades of Bell System research and development activities on waveguides, which began with the experimental identification of waveguide modes by G. C. Southworth in 1931 and 1932, and the theoretical discovery of the low-loss property of the TE_{01} mode by J. R. Carson, S. P. Mead, and S. A. Schelkunoff in 1933.

After the early discoveries, interest and effort in waveguides and high frequencies grew steadily at Bell Laboratories, forming the basis for the development of radar during World War II, and of microwave radio relay and satellite communications after the war. In the 1950s and early 1960s, many fundamental contributions to the understanding and realization of waveguide transmission via the TE_{01} mode and to millimeter-wave repeater concepts and components were made at the Holmdel and Crawford Hill laboratories by H. T. Friis, S. E. Miller, and their co-

workers. An exploratory development effort was begun in 1959 on a system utilizing 2-inch waveguide and traveling-wave-tube repeaters, but was abandoned in 1962 because of TWT cost and reliability problems and because the capacity exceeded then-current Bell System needs.

In 1968, after six years of continuous long-haul growth and with high-frequency solid-state devices such as IMPATTs a reality, exploratory development of an all solid-state system was undertaken as a joint project of Bell Laboratories, Western Electric Company, and the Long Lines Department of AT&T. This effort has led to the results described in this issue.

As Southworth himself wrote in 1962, referring to the early years when millimeter waves were only a dream,

> "Almost from the first, however, the possibility of obtaining low attenuations from the use of circular-electric waves, carrying with it, at the same time, the possibility of extremely high frequencies and accordingly vastly wider bands of frequencies appeared as a fabulous El Dorado always beckoning us onward."

The path has, of course, not been an easy one nor have we yet reached its end. Although the technical problems have been solved, the economic ones have proven more formidable. Being a high-technology right-of-way system, waveguide is inherently expensive. But because of its loss characteristic, it is also inherently a high-capacity system, so that its cost per circuit is still attractively low. However, for its low costs to be realized, it must be used on routes of sufficiently large circuit cross-section and growth rate that it fills in a reasonable length of time. In recent years, after several decades of consistently rapid growth and continuing need for ever-larger systems, the growth rate of the Bell System long-haul network has declined. Thus the immediate need for a system of such large capacity as WT4 has decreased and, as of this writing, the date of first commercial deployment of waveguide is uncertain.

Since the responsibility for system design, specification and testing resided with Bell Telephone Laboratories, the authors of the papers in this issue are primarily Bell Labs people. However, that fact in no way reflects the relative contributions of the other partners in the project. The close interaction with Western and Long Lines at every stage of the development has had a profound effect on the tradeoffs in the design, manufacture, installation and operation of the system, and has resulted in many of the most attractive system features.

M. P. Eleftherion and his coworkers at Western Electric's Engineering Research Center were responsible for the development of the waveguide manufacturing processes and the incorporation of these processes into a pilot plant which fabricated the waveguide for the 14-kilometer field

test. The wide repeater spacings realized were in a large part due to the Western Electric work on controlling steel tube geometry and on processes which led to low waveguide ohmic dissipation. The Western Electric manufacturing engineers at Merrimack Valley, in particular D. P. Farley and J. W. Thomas, provided the guidance to bring the electronics from the "brassboard" stage to the state of being a manufacturable product.

D. E. Derringer of Long Lines Headquarters and his co-workers in Engineering and Operations continually stressed the realities of right-of-way construction and the importance of reliability and maintenance of both the medium and the electronics. They encouraged the development of and made many contributions to the two-stage waveguide installation technique described in this issue.

The Northeastern Area of Long Lines had the responsibility for right-of-way procurement, engineering, and installation of the 14-km field test. Much of the success of the field test must be credited to the excellent work performed by these groups.

THE BELL SYSTEM TECHNICAL JOURNAL
Vol. 56, No. 10, December 1977
Printed in U.S.A.

WT4 Millimeter Waveguide System:

The WT4/WT4A Millimeter-Wave Transmission System

By D. A. ALSBERG, J. C. BANKERT, and P. T. HUTCHISON

(Manuscript received April 7, 1977)

The WT4/WT4A millimeter-wave, long-haul transmission system is described. The description includes overall characteristics of the various system components, their interrelationship, and performance. Results of the field evaluation test are summarized.

I. INTRODUCTION

The WT4/WT4A communication system is designed to provide long-distance communication service at a lower per circuit cost when fully loaded and with an order of magnitude higher reliability then has been achieved previously in right-of-way systems. In the WT4 version, capacity is almost two times that of any existing system, and in the WT4A version, capacity is twice that of WT4. Digital signal transmission is used which can accommodate any mix of voice, high-speed data, TV, and *PICTUREPHONE*® service. The system can be installed readily on any terrain and any right-of-way. Methods and procedures have been developed for easy low-cost maintenance.

II. GENERAL DESCRIPTION

The WT4/WT4A system uses 60-mm internal diameter waveguide as the transmission medium. It is designed to provide a total of 124 broadband channels of which 59 are used for signal transmission and three for protection in each direction. The specific designs of the experimental system described in this paper and the companion papers in this issue operate in the 40- to 110-GHz frequency band.

Based on the results of a field evaluation test conducted in northern New Jersey from 1974–76, the frequency band is being shifted to 38–

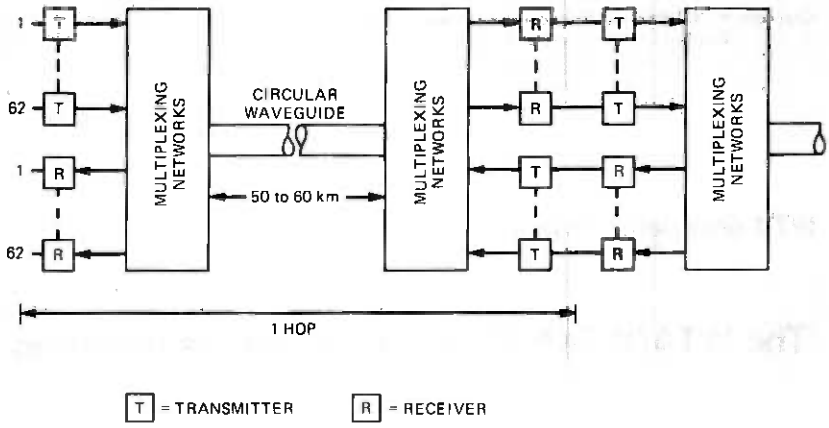

Fig. 1—Block diagram of a repeater hop.

104.5 GHz to maximize the repeater spacing using 60-mm diameter waveguide. The repeater spacing for commercial systems will be a maximum of approximately 60 kilometers (37 miles) in relatively gentle terrain and on superhighway rights-of-way. In very rugged terrain, such as the mountains of Pennsylvania, the maximum repeater spacing will be reduced to about 50 kilometers (31 miles).

The system uses solid-state regenerative repeaters which carry a DS-4 digital signal stream (274 megabits per second). The system error rate is less than 10^{-7} for 6000 kilometers (4000 miles) transmission distances and a service availability of better than 0.9998. On initial installations (WT4) two-level, differentially coded, phase-shift-keyed modulation can be used to furnish up to 238,000 two-way voice circuits. As traffic demand increases, the system may be upgraded to four-level modulation (WT4A) up to a total capacity of 476,000 voice channels. This increased capacity can be achieved without changing repeater spacing by retrofitting only the electronics. To allow system management flexibility, as many as six of the repeater stations within a protection span [up to 500 km (300 miles)] can be arranged to add or drop signal channels.

A block diagram of one fully equipped hop or span of the system is shown in Fig. 1. Sixty-two transmitters which operate at different millimeter-wave carrier frequencies in one-half of the frequency spectrum carry east-west signals to 62 receivers at the next repeater station. Correspondingly, another set of 62 receivers and transmitters carry west-east signals in the opposite direction in the other half of the frequency spectrum. A multiplexer connects the 124 individual channels to the single waveguide broadband transmission medium.

An important system feature is that the multiplexing network configuration and the waveguide parameters are selected so that their total

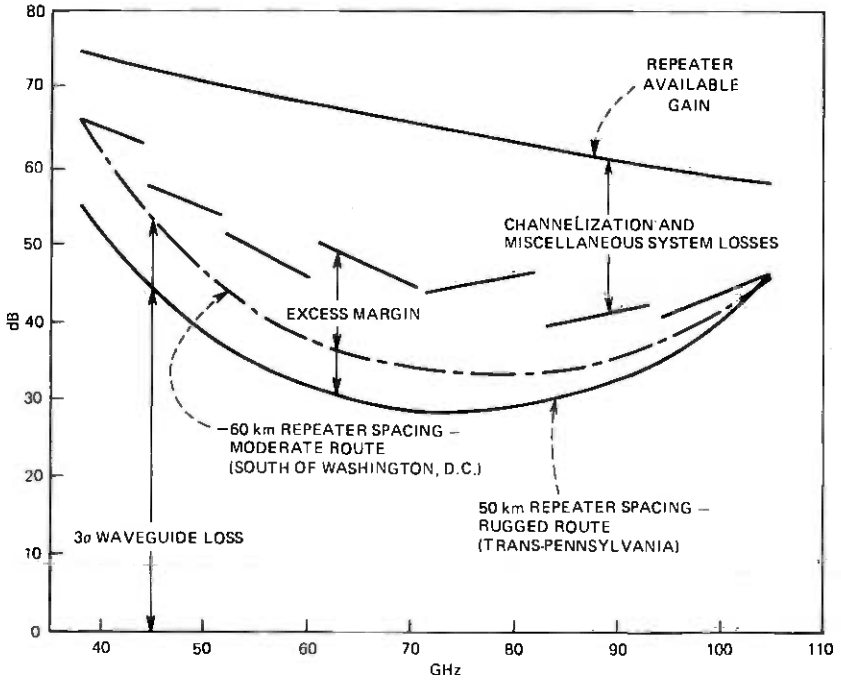

Fig. 2—WT4A system loss composite.

loss-versus-frequency characteristic closely matches the available gain and noise-figure-versus-frequency characteristic of the repeaters.

Figure 2 shows the individual and combined loss design parameters of the commercial WT4A design for repeater station spacings of 50 kilometers for the difficult terrain of the trans-Pennsylvania route and 60 kilometers for the moderate terrain model typical of routes on the United States East Coast south of Washington. 3σ values are used for the installed waveguide losses.

The overall loss budget shown also includes a 3-dB margin to accommodate repairs and future route realignments. The loss ceiling or available repeater gain curve in Fig. 2 is based on having a transmitted power 10 dB lower at 104.5 GHz than at 38 GHz and on having the receiver noise figure 3 dB higher at 104.5 GHz than at 38 GHz.

Because of the large traffic-carrying capacity, the highest possible reliability and service availability are important features. High reliability in the electronics is achieved by operating solid-state circuits in a dry nitrogen environment. The large distance between repeaters minimizes the number of repeaters required and therefore also contributes to service availability. The transmission medium is extraordinarily resistant

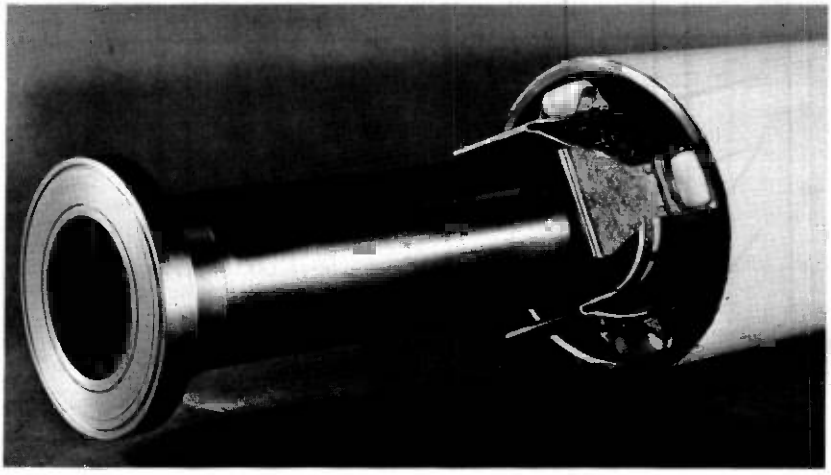

Fig. 3—Waveguide with flange, spring roller supports, and steel sheath.

to damage since its basic structure is made up of fusion-joined steel tube sections encased in a fusion-joined protective steel outer casing. It is impervious to lightning damage and highly resistant to damage from most construction machinery which often causes damage to other buried communication systems. Restoration methods have been developed even for the rare cases where a waveguide failure should occur. To enhance the reliability, no manholes or expansion joints interrupt the transmission medium between repeater stations. The overall built-in reliability is such that minimal routine maintenance is anticipated.

Because the reliability of the waveguide medium is so much higher than that of a buried cable, it is also used to carry the protection-system signaling and order wire. These are interleaved into the digital data streams of designated channels. Should a service channel fail, automatic transfer to a protection channel is provided.

Particular attention was paid in the design of the waveguide medium to provide for easy installation on any commercially feasible right-of-way. Conventional pipeline construction methods are used, and the waveguide has been designed so it can follow the horizontal bends and vertical contours of the right-of-way without undue performance penalties.

Because of the heavy shielding provided by the sheath and the waveguide, even high-voltage power line rights-of-way can be utilized without incurring any interference.

Protection against electromagnetic radiation to and from outside sources is of increasing concern in the design of new systems. In the WT4 repeaters all parts that carry radio-frequency and intermediate-frequency signals are shielded. Since the radio-frequency signals in the

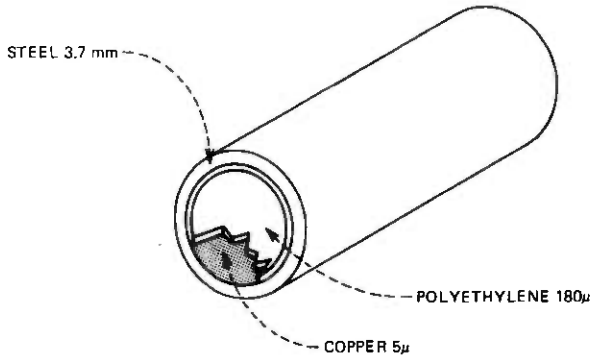

Fig. 4—Dielectric-lined waveguide.

multiplexer networks and circular waveguide are also shielded, the WT4 system causes no radiation pollution.

The repeater stations[1] are above-ground buildings spaced up to 60 kilometers apart, as stated previously. They also contain the various auxiliary services needed to operate the repeaters, protection switching, etc. They are powered from commercial sources, but self-contained emergency standby power is provided. The system is safe for maintenance personnel since no high voltages are required for any of the active circuits.

In the remainder of this paper, we will first discuss some salient features of the waveguide medium, its installation, reliability and maintenance. This will be followed by discussion of the multiplexers, repeaters, protection switching, order wire, and telemetry, and the results of the field evaluation test.

III. THE WAVEGUIDE TRANSMISSION MEDIUM

The transmission medium for the millimeter wave system is a waveguide with a circular cross section of 60 mm (~2 3/8 in.) inside diameter. Supported by spring roller supports, it is installed in a 140-mm (5 1/2 in.) outside diameter steel sheath buried a minimum of 0.6 meter (2 ft) below the surface. Individual sections of waveguide as well as the sheath are joined by fusion welding. The waveguide with its flange, spring roller supports, and steel sheath are shown in Fig. 3. The installed waveguide consists of a mix of 99 percent dielectric-lined guide and 1 percent helix-type mode-filter guide. The dielectric-lined guide has an inner conducting surface of plated high-conductivity copper and a thin polyethylene lining (Fig. 4). The helix guide consists of a layer of millimeter-wave-absorbing material and a copper helical structure inside the steel tube (Fig. 5). This combination of waveguide types provided a total

installed loss below 1 dB/km from 40–110 GHz on the field evaluation test route.

To achieve the lowest installed loss in the design of the waveguide, two loss mechanisms must be considered. One is the heat (resistive and dielectric) loss which is controlled by choice of waveguide diameter and by the quality of the manufacturing process. The second is the so-called mode conversion loss. Since the waveguide is much larger in diameter (60 mm) than the wavelengths of the signals in the system (2.7–7.5 mm)

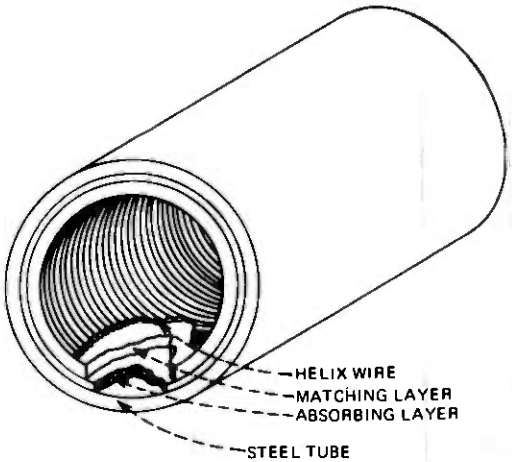

Fig. 5—Helix waveguide.

electromagnetic energy can propagate in many field patterns called modes. Only one of these, the TE_{01} mode, has the low-loss transmission property desired. When signal energy is converted from the TE_{01} mode to any of the other modes some additional signal loss results. This energy transfer and consequent loss is minimized by the dielectric liner applied to the guide,[2,3,4] by proper controls of the manufacturing process, and by the installation design and route engineering. In the following, the various losses are examined in some more detail. The addition of the various loss components is shown in Fig. 6.

3.1 Heat loss

In Fig. 6, curve a is the idealized loss curve for intrinsic pure copper. For various reasons, such as conductor impurities, surface roughness and dielectric-liner-induced losses, this ideal is not attained in practice.[5] The heat loss which was achieved consistently under manufacturing conditions for the field evaluation test is shown in curve b, Fig. 6. This loss is about 0.06 dB/km higher than the ideal at 40 GHz.

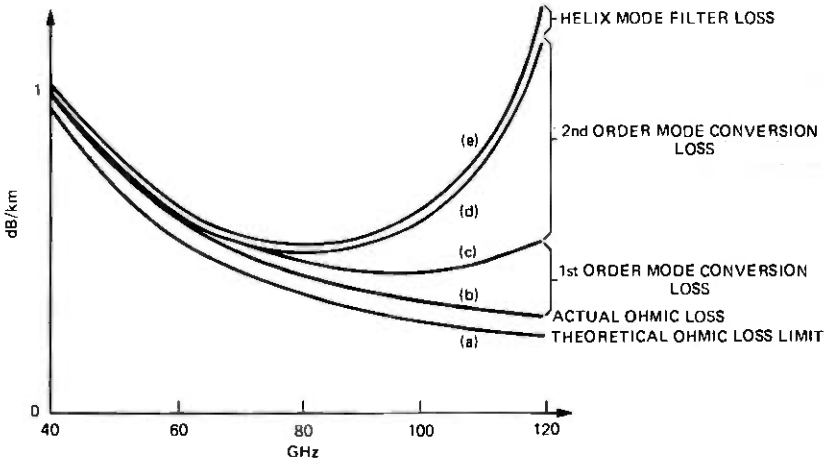

Fig. 6—Addition of the various loss components.

3.2 Mode conversion loss

Mode conversion results whenever the geometry of the waveguide departs from a perfectly true cylinder. The three principal sources of geometric distortion are:

(*i*) Manufacture of the waveguide
(*ii*) Installation
(*iii*) Horizontal and vertical route bends

Since it is easier to control tolerances in a factory environment than in the field, much of the mode conversion control is achieved by attention to waveguide design details and by careful design of factory processes, tooling, and inspection. To avoid excessively stringent tolerances, advantage was taken of the theoretical understanding of the relation between waveguide geometry and mode generation.[6]

The geometry of the waveguide is inspected in the factory by mechanical gauges which rapidly measure the waveguide distortions. As the data are being taken they are fed into a minicomputer for evaluation of their level of distortions and particularly their periodic components. The computer outputs are simple go, no-go displays for the machine operator and inspector.

The application of minicomputer-aided inspection as part of a manufacturing specification has resulted in an excellent yield of high-grade waveguide-quality tubing and finished product at reasonable cost using only slight modifications of standard manufacturing processes, as described by Boyd et al.[5]

The installation process adds distortions on top of the manufacturing distortions and also contributes to unwanted modes. Modes caused by

trench bottom irregularities are reduced by suspending the waveguide on spring roller supports inside the protective steel sheath. The steel sheath and spring supports in conjunction with the stiffness of the waveguide act as mechanical filters between the waveguide and trench bottom irregularities.[7] Other important sources of installation distortion are tilt and offset of the waveguide flanges. These are controlled by the flange design, the manufacturing process, and by the tooling used in the field-weld joining process.

Another important potential source of periodic geometric distortions are diameter discontinuities at waveguide couplings which would generate undesired modes. The waveguide lengths are therefore pseudo-randomized by a small amount with a uniform distribution during the sizing process in the factory to avoid the cumulative effects of periodic coupling spacing.

Because of terrain features, changes in waveguide horizontal and vertical direction through bends are unavoidable. These bends will also generate various spurious modes. Energy coupling to these modes and loss are minimized by the dielectric lining and by the natural tapering of the installed waveguide bends. Bends with radii as tight as 75 m (250 ft) can be negotiated with minimal loss. The total mode conversion loss due to direct or "first-order" mode generation from these various geometrical distortions is shown added to the heat loss as curve c in Fig. 6.

During the field evaluation test an important mode generation mechanism was discovered in the interaction between several modes in the presence of tight horizontal or vertical bends and long mechanical periodicities of wavelengths in the order of 20 m (~65 ft). This is described in detail by Carlin and Moorthy.[8] These long wavelength periodicities are caused by the natural undulations of the terrain and are not filtered out by the sheath stiffness. The resulting mode generation increases as the sixth power of frequency and the fourth power of route curvature and is shown as added loss in curve d, Fig. 6. This rapid increase in mode conversion at the highest frequencies of the WT4/WT4A band when coupled with route curvature was an important finding of the field evaluation test. This provided a major incentive to shift the WT4/WT4A frequency band slightly downward for the commercial system which allows increased repeater spacing and makes route selection and engineering much easier.

3.3 Mode filtration

Even with optimal manufacturing and installation techniques a small residual level of excess unwanted modes must be suppressed. Helix guide[9] is therefore used as a mode filter. Since mode conversion losses

in helix guide are particularly sensitive to bends in the installation, an important design objective is to minimize the amount of helix used and then to insert it where possible into relatively straight parts of the waveguide run. This minimizes the overall installed loss and permits considerable latitude in following natural terrain features. Sections of 9-m (~30 ft) long helix guide inserted at about 800-m (0.5 mile) intervals are adequate to limit the buildup of unwanted mode levels. The choice of a mode filter spacing of approximately 800 m was aided by a Monte Carlo computer program which simulated the effects of first-order mode conversion losses on the received signal. The simulation showed only modest sensitivity to mode filter spacings in the range of 800–1500 meters. Since the helix guide has higher loss than dielectric-lined waveguide, short mode filter spacings lead to higher overall waveguide losses because there is then a greater percentage of helix waveguide in the transmission medium. Excessively long mode filter spacings, though they have low loss, can result in unacceptable delay distortion of the signal. The difference between curves d and e, Fig. 6, shows a typical added loss from helix mode filters for a helix to dielectric-lined guide ratio of approximately 1:100.

IV. ROUTE ENGINEERING

Route selection and engineering for waveguide differs from that for a coaxial cable system in three respects.

(*i*) The mechanical properties of the waveguide and its sheath restrict the permissible bending configuration of this structure. For engineering purposes plan bends can be laid out simply as two straight tangents connected by a circular arc; a method of profiling based on transparent plastic beam-curve overlays has also been developed to assist in the engineering process.

(*ii*) The loss depends on the configuration as well as the length of the medium. Therefore, computer-aided techniques were developed to take into consideration the configuration of the waveguide plan and profile and to determine waveguide loss and, thereby, assist in the siting of repeater stations.

(*iii*) The rights-of-way which are not available for coaxial cable systems but which can be utilized for waveguide include joint routes with high-voltage power lines (because of decoupling from inductive interference) and interstate highways (because of the large repeater spacing and absence of manhole access requirements).

V. INSTALLATION

To achieve minimum costs, the installation method was carefully integrated with the overall system design.[10,11] The sheath [nominal 5½

inch (140 mm) O.D. pipe] is installed first using pipeline technology; there are no special bedding requirements for the trench bottom. Two minor modifications from pipeline practice are: (*i*) changes in plan and profile must be made in such a way that the sheath is not bent beyond the elastic limit; (*ii*) the welds used in joining the pipe are partial penetration welds to prevent protrusions on the inside which might interfere with the insertion process.

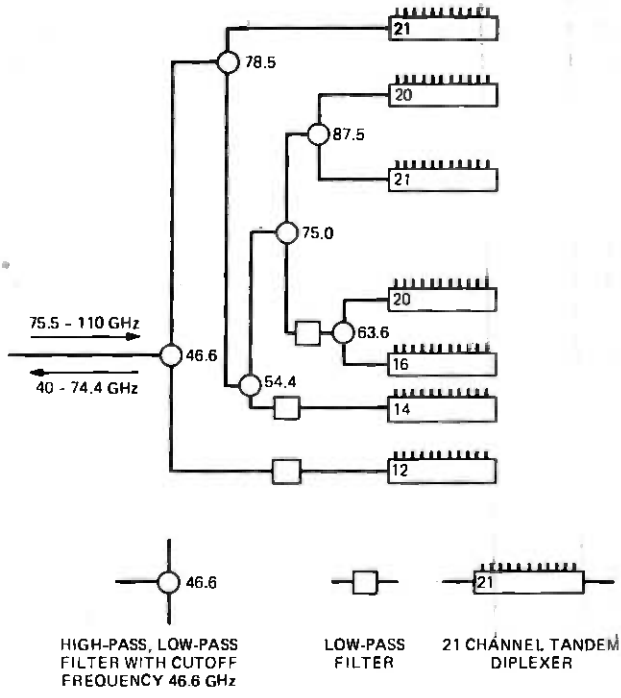

Fig. 7—Multiplexing network plan.

In a second operation the waveguide is installed by field-welding waveguide sections and pushing (inserting) them into the previously installed sheath. The equipment designed to perform the welding and insertion operations requires a five-worker crew and is capable of installing 160 km (100 miles) of waveguide per year with a single-shift operation. Waveguide installation cost (equipment and crew) represents less than 3 percent of the first cost of the system.

VI. MULTIPLEXING NETWORKS

Band diplexers are used to split the overall experimental band from 40 to 110 GHz (38–104.5 GHz commercial) into seven subbands. Tan-

dem-connected channel diplexers consecutively drop or add broadband channels within each subband. Figure 7 shows the actual arrangement of the various filters to give the desired loss shape over the band. The lowest-frequency subband is dropped first and the highest-frequency subband is dropped next. In the lowest-frequency subband, the lowest-frequency broadband channel is dropped first by the string of channel diplexers. In the highest-frequency subband, the highest-frequency broadband channel is dropped first. As shown in Fig. 2, the repeater spacing is maximized by this channelization plan because at frequencies where the waveguide loss is high, the multiplexer loss is low. Further details on the remainder of the Fig. 7 layout are covered by Harkless et al.[12] in a companion paper. The low-pass filters shown are required to control harmonics because the total operating band covers more than one octave.

The band diplexers, high-pass low-pass constant resistance filters, and the low-pass filters are made with circular guide operating in the TE_{01} mode. The input and output ports are 50.8 mm (2 in.) in diameter. The channel diplexers are two-section constant-resistance filters with half-power bandwidths of 475 MHz and center-frequency spacings of 525 MHz (500 MHz commercial). The channel diplexer resonant cavities are in dominant mode rectangular waveguide and are aperture-coupled to semicircular waveguide large enough to support the TE_{01} mode but not large enough to support the TE_{02} mode. These mode restrictions limit the subband bandwidth to about 17 percent. Waveguide tapers and circular-to-semicircular transducers are used as needed between the tandem channel diplexers and the 50.8-mm guide.

The hardware realization of the diplexer components and the four-section modular aluminum frame which supports them and the repeaters is shown in Fig. 8. Modular construction makes the test and installation of the diplexer array very simple. Two frames, each 13 m (43 ft) long, 2.4 m (8 ft) high, and 0.3 m (1 ft) deep, are required at each repeater station. The frame design is controlled mainly by the six individual band diplexers which are about 1.6 m (5 ft, 2 in.) long. The channel diplexers are much smaller; each is about 7.5–10 cm (3–4 in.) long, and 248 are required at each fully equipped repeater station. The frame is very rigid because component alignment is much more important for overmoded waveguide than for dominant-mode waveguide. The band diplexers and low-pass filters are made of aluminum and the channel diplexers are made of high-conductivity copper. Plans to make the critical resonators in the channel diplexers of INVAR to lessen detuning with temperature variations were quickly dropped because tolerances of 2.5 μm (0.1 mil) were required. To meet requirements, temperature control of the multiplexer environment is utilized and the entire multiplexing array is filled with low-pressure dry nitrogen at 180 mm H_2O (¼ psi).

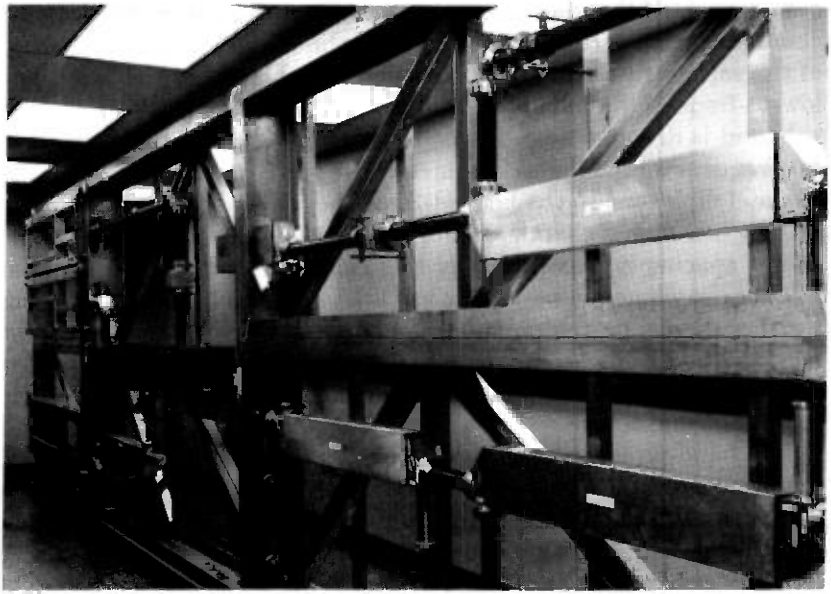

Fig. 8—Diplexer components with four-section aluminum frame.

VII. REGENERATIVE LINE REPEATER

The physical realization of the repeater consists of four units: the transmitter, receiver, power supply and passive line equalizer. A two-level repeater block diagram, without the power supply, is shown in its simplest form in Fig. 9. A CW millimeter-wave signal is generated in the

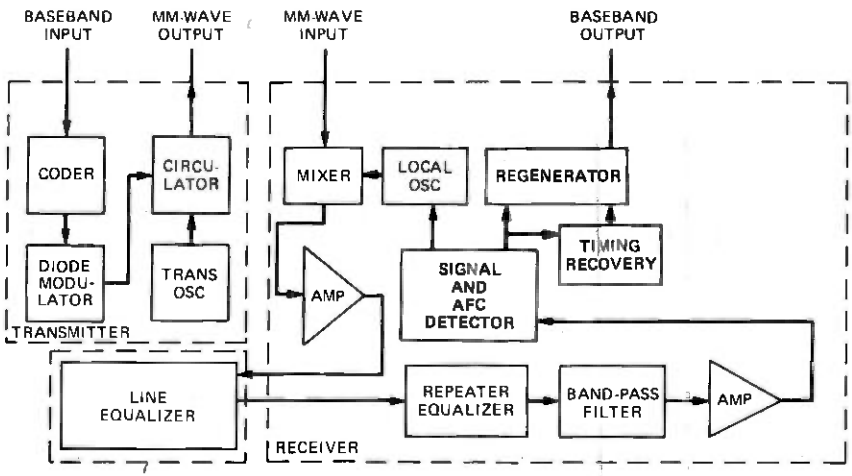

Fig. 9—Repeater block diagram.

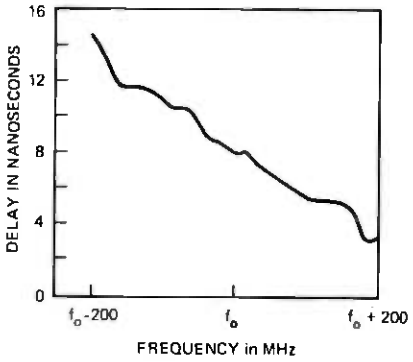

Fig. 10—Typical delay of the line.

transmitter by the silicon IMPATT diode oscillator. The phase modulator, a PIN diode and its associated network, are adjusted so the phase difference between the reflected signals in the conducting and nonconducting states of the diode differ by 180 deg. This phase-modulated millimeter-wave signal is transmitted through the multiplexers and the circular waveguide to the receiver at the next repeater station. At the receiver, the signal is shifted in a mixer, made with a beam-lead GaAs Schottky barrier diode, to an intermediate frequency of 1371 MHz for amplification. The amplified signal goes through the line and repeater equalizers before it undergoes more amplification and is fed into a differential phase detector. The purpose of the line equalizer is to compensate for delay distortion and undesirable loss-frequency shaping caused by the "line." The "line" is defined as the combination of the circular waveguide between repeater stations and the two multiplexing networks between a transmitter and the following associated receiver. The transmission distortion of a particular hop depends on its length and its routing since route curvature affects the characteristics. The dispersion caused by one 60-km hop of 60-mm circular waveguide will introduce as much as 40 ns of almost linear delay across a 400-MHz band. Above about 85 GHz the delay caused by this dispersion is less than 4 ns. The shape of the delay introduced by a typical line will be similar to the curve shown in Fig. 10. The equalizer compensates only for the gross shape shown in Fig. 10; no attempt is made to equalize fine-structure ripple.

The line equalizer is adjusted in the field to compensate for the distortions unique to the specific line and is thereafter associated with the line and is not removed if the transmitter-receiver pair are replaced for any reason. Details of the adjustment of the line equalizer are covered in a companion paper by P. Brostrup-Jensen et al.[13] A line equalizer failure should be a rare event because all its components are passive and

experience no dc voltages. In addition to the line, each circuit through which the signal travels introduces some delay distortion and some gain shaping other than that desired. These distortions can cause intersymbol interference. To compensate for these distortions a repeater equalizer is provided which contains delay and loss networks which are adjusted in the factory.

The system was designed so the signal-to-noise ratio at the repeater would assure an error rate better than 10^{-9} even under adverse conditions such as temperature extremes, supply voltage variations, etc. The repeater intermediate frequency is kept fixed through an automatic frequency control circuit, but no control is applied to the transmitter. The transmitter frequency can drift ±25 MHz without causing excessive unequalized delay in the system.

The baseband 274-Mb/s bit stream is scrambled by the nature of the DS4 signal, which uses pseudorandom bit generators located in the time-division multiplexers that feed the WT4 system. The baseband circuits therefore, can be ac-coupled with minimal concern about baseline wander.

Physically the repeater is made in four parts; each part is enclosed in a cast aluminum housing. All parts except the power supply have radio-frequency interference shielding and are pressurized with dry nitrogen to about 180 mm H_2O (¼ psig), available from the waveguide. This controlled atmosphere improves component reliability. All parts of the repeater are flush-mounted on the aluminum frame that also supports the tandem channel diplexers. This type repeater installation is a "plug-in" operation. Some of the channels that make up the frame carry circulating water at about 13°C (55°F). The transmitter and receiver are mounted on these channels, so they are water-cooled. The physical locations of the IMPATT oscillators inside the housings are placed as close to the water-cooled channels as possible. No routine maintenance of the repeaters will be required. At each repeater station there is an error-rate detector which can be connected by command to the output of any repeater at that station. In the event of a repeater failure, the E2A status reporting and control system quickly locates the bad repeater by making use of the error-rate detectors.

Three distinct technologies are required in making repeaters. First, the millimeter-wave parts all use standard rectangular waveguide; three sizes are required to cover the 38 to 104.5 GHz band. Because we operate at such high frequencies, the dimensional tolerances required are stringent. Tolerances of 2.5 μm (0.1 mil) are common and some requirements are even tighter. The mixer uses a beam-lead diode on a gold conductor pattern on a quartz substrate. Second, the IF and most of the baseband circuits are made using hybrid integrated circuits (HIC). The baseband circuits are standard HIC technology but the IF circuitry is

more demanding. The line widths in some of the IF networks are 75 ± 6 μm (3 ± 0.15 mils) and line separations must be controlled to ±10 μm (±0.25 mils). Some of the IF circuits require that the dielectric constant of the alumina substrate be held to within ±1 percent of a fixed value. The fixed value itself is not critical, but delay circuits and couplers must be designed for a specific dielectric constant. The third technology is printed circuitry, the least demanding of the three. This technology is used in the AFC and AGC circuits associated with the IF amplifiers, and the power supply circuits.

VIII. PROTECTION SWITCHING

The introduction mentioned that for a fully loaded WT4 system, three broadband channels in each direction are required for protection switching and maintenance. Two of these channels are used for conventional protection switching and the other one is used as a manual patch channel associated with maintenance.[14] Because the waveguide is so much more reliable than any cable,[15] the protection switching signals are sent over waveguide channels. For redundancy, these signals are transmitted over both protection channels. The protection switching signals are digitized and inserted in positions in the DS4 bit stream reserved specifically for auxiliary communications use. These specific time slots are called x-bit slots and the bits are referred to as x-bits. Each x-bit slot has a capacity of 58.3 kb/s and there are three such slots in each DS4 bit stream.

Initially, parity bits are inserted in the DS4 bit stream by M34 time-division multiplex equipment. At the end of each protection switching span there is an error-rate detector called a violation monitor and remover (VMR) which has the following functions. First, it measures the bit error rate by measuring parity in a frame and comparing measured parity with transmitted parity. From this, the error rate for each broadband channel is calculated. Second, the VMR resets the parity bits transmitted to the next switching section so that the next VMR will measure only errors made in its protection switching span.

When the error rate in an east-west broadband channel exceeds 10^{-6}, the VMR in that channel calls for a protection switch. The switch is initiated by signaling the head end of the protection switching span to bridge the bad channel and one of the protection channels. This signaling is sent over the west-east protection channels. When the VMR in the east-west protection channel shows the performance is good, the tail-end switch is executed to complete the protection switching operation. When the VMR in the previously bad channel after repair again shows proper operation, the protection line is automatically switched out and is thus available in case of another channel failure. The actual switching is done with relays that transfer in about 1.5 ms, so a hit or loss of frame results

when protection switching occurs. If the switching were associated only with routine testing of broadband channels, loss of frame could be avoided by using fast solid-state switches. However, when there is an unexpected broadband channel failure, the signaling delay caused only by propagation time in a 800-km (500-mile) protection span is enough to cause a loss of frame. Since the WT4 plan does not call for routine testing of broadband channels, switching is done with relays.

In order to extend the repair time available for a failed repeater, one of the three protection channels has been designated a patch channel.[14] It is not part of the automatic protection switching system. It is a fully equipped channel, so by proper baseband patching, any single hop of this channel can be used to replace the hop associated with a failed repeater. Thus, making manual patches at two adjacent repeater stations allows craft personnel ample time to restore the previously bad channel. After this patching, the automatic protection channel is returned to normal operation and is available to protect other failures. Without such a plan, either the time permitted to replace a bad repeater would have to be reduced significantly or at least two more automatic protection channels would be necessary.

IX. ORDER WIRE AND TELEMETRY

Signals associated with the voice order-wire system and the telemetry system are carried in the x-bits transmitted by a specified service channel. The SS3 analog order-wire system and the analog signals associated with the E2A status reporting and control system (telemetry) are put in digital form and multiplexed to form a 58 kb/s signal which in turn is multiplexed with the 274 Mb/s DS4 bit stream. Three adjacent x-bits carry the same information for triple redundancy. Delta modulation is used on the order-wire signals; 29 kb/s is the actual rate needed to carry the signals. The multiplexer which inserts the x-bits into the main bit stream and the associated demultiplexer are hard-wired into the specified service channel so that they are inside the switches in a protection switching span and are not affected by any protection switching operation. How the order wire and telemetry systems function when there is a failure in this specified service channel is covered in a companion paper by Bonomi et al.[14]

The E2A system is modular and can, when properly equipped, provide monitoring of over a thousand points in the WT4 system and can provide momentary grounds for over a thousand points. With proper relays, these grounds provide the command feature for the system. As stated earlier, this system used in conjunction with an error-rate detector at each repeater station can quickly locate a faulty repeater.

X. FIELD EVALUATION TEST

In order to prove in the various manufacturing, installation and service features of the mm-wave transmission system, a field evaluation test was conducted starting in 1974 in northern New Jersey. A 14-km (8.7-mile) waveguide line was installed between the AT&T Metropolitan Junction Station in Netcong and a temporary experimental station in Long Valley. The waveguide was fabricated to manufacturing specifications in an experimental pilot plant at Forsgate, New Jersey, by Western Electric Engineering Research Center and Kearny Works personnel who had developed the manufacturing, test, and inspection techniques in cooperation with Bell Labs.

The terrain used for the 14-km waveguide run offered a variety of construction situations including route bends, road and stream crossings, a steep grade, rocky terrain which required blasting, and swampy areas. The actual sheath installation was done by commercial subcontractors under the direction of AT&T Long Lines Northeastern Area. Long Lines Northeastern Area craft personnel installed the waveguide using tooling and equipment specially developed for waveguide installation by Bell Laboratories and in cooperation with commercial suppliers. Waveguide repair and maintenance procedures were tried out and refined.[15] This demonstrated the viability of the installation and maintenance methods on a commercial basis.

Complete band diplexer modules were installed in both terminal stations but only 12 frequencies in the range from 40–110 GHz were fully equipped with repeaters and channel-dropping networks. The electronics included all elements of the complete operating system such as protection switching, span terminating, fault locating, auxiliary communications, and maintenance.

Twelve repeaters were made by Bell Laboratories to test the system at 12 frequencies in the 40–110 GHz band. The DS4 baseband signal is available at the output of each receiver and tests were made first on the 12 individual hops and then with the 12 connected in tandem. Since the waveguide length used in this test was so much shorter than the proposed spacing of repeaters, it was necessary to use pads to simulate normal repeater operation. By using adjustable pads, the repeaters were tested over a range of input power to the repeaters. These tests showed that the operation in the field was essentially the same as in the laboratory and that the system met all objectives. Periodic tests, however, will be continued to look for changes in line characteristics, receiver sensitivity, frequency stability, etc.

Tests of the protection switching system, electronic fault-locating system, and order-wire circuits showed they met all the design objectives. Experience with measured characteristics of the diplexers and low ad-

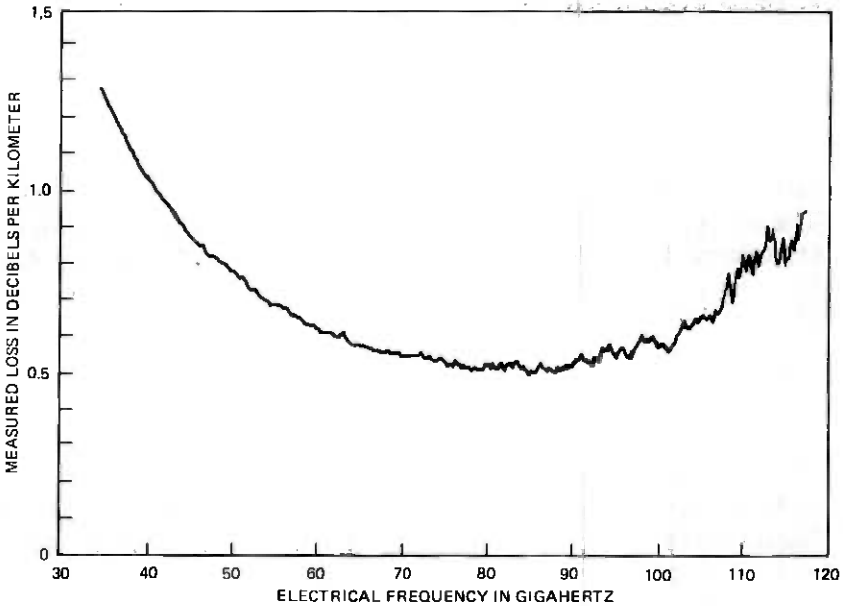

Fig. 11—WT4 field evaluation test measured loss.

jacent-channel interference of repeaters indicated that the guard bands used could be narrowed, permitting a tighter packing of channels.

The results of the measurements on the transmission medium are shown in Fig. 11. The loss of the transmission medium was 1 dB/km or less over the entire frequency band from 40 to 110 GHz. To verify the line behavior outside the operating band, measurements were actually taken from 35 to 117 GHz. The entire line has also been remeasured periodically over the past two years; during this time its loss has remained unchanged within the accuracy of measurement. In addition to overall measurements of the guide, individual sections were measured as they were being installed, both for mechanical distortions of the installed guide and for electrical transmission performance. This permitted refinement and reconciliation of waveguide theory and actual performance.

The calculated 3σ losses for both the moderate-terrain, private ROW route model (south of Washington, D.C.) and the rugged-terrain, private ROW route model (trans-Pennsylvania) are shown on Fig. 12 for comparison. Also shown are the permissible waveguide losses per kilometer for repeaters operating in the 40–110 GHz band over distances of 42 kilometers (26 miles) and 54 kilometers (34 miles) respectively. The difference between these two route models illustrates one of the most important new findings of the test of the transmission medium, namely the sensitivity of loss at the highest frequencies of the WT4/WT4A band

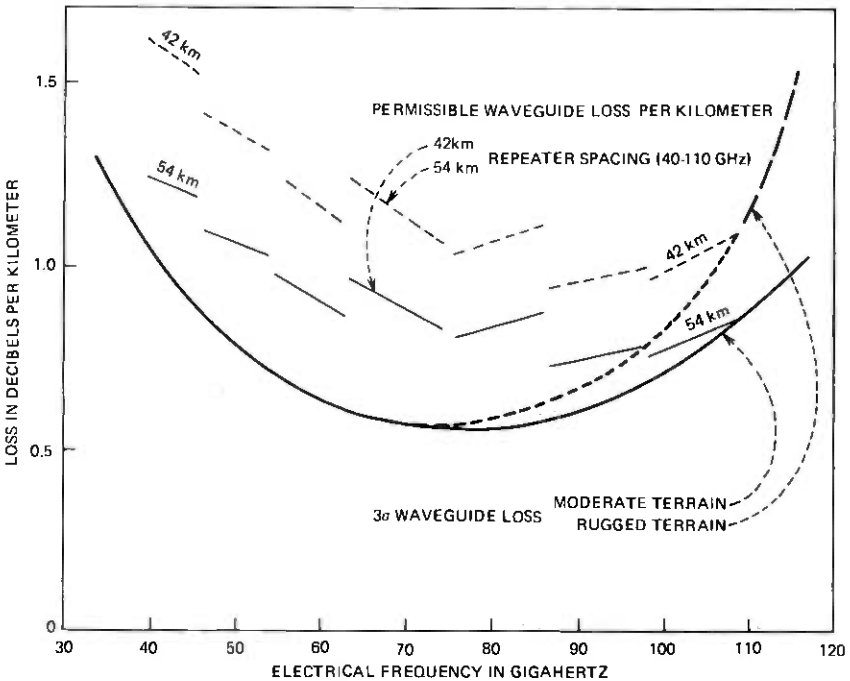

Fig. 12—Waveguide loss and repeater spacing.

to a combination of tight route bends and the natural undulations of the land. This finding was the major stimulus for shifting the frequency band downward to 38 to 104.5 GHz. This downward bandshift also exploits the large margin available at the low-frequency end. A 50 to 60 km repeater spacing can then be attained, rather than a 42 to 54 km repeater spacing corresponding to the 40 to 110 GHz band. This downward shift also includes a slight compression of the guard bands between diplexers and channel-dropping filters as mentioned.

XI. CONCLUSION

The WT4 system provides for economical transmission of a very large communication cross section. Design concepts, manufacturing techniques, and installation methods were proven and demonstrated in a field environment.

XII. ACKNOWLEDGMENTS

Many individuals, too numerous to give credit by name, at Bell Laboratories, Western Electric, Western Electric Engineering Research Center, American Telephone and Telegraph, Long Lines Department,

and several commercial suppliers contributed to this success. Their ideas, help and devotion are gratefully acknowledged.

REFERENCES

1. W. J. Liss et al., "The WT4 Repeater Station", B.S.T.J., this issue.
2. S. E. Miller, "Waveguide as a Communication Medium," B.S.T.J., *33*, No. 9 November 1954), pp. 1209–1266.
3. H. G. Unger, "Circular Electric Wave Transmission in Dielectric Lined Waveguide," B.S.T.J. *36*, No. 6 (September 1957), pp. 1253–1278.
4. J. W. Carlin and P. D'Agostino, "Normal Modes in Overmoded Dielectric Lined Circular Waveguide," B.S.T.J. *52*, No. 4 (April 1973), pp. 453–486.
5. R. J. Boyd et al., "Waveguide Design and Fabrication", B.S.T.J., this issue.
6. H. E. Rowe and W. D. Warters, "Transmission in Multimode Waveguide with Random Imperfections," B.S.T.J. *41*, No. 3 (March 1962), pp. 1031–1170.
7. R. W. Gretter et al., "Mechanical Design of Sheathed Waveguide Medium," B.S.T.J., this issue.
8. J. W. Carlin et al., "Waveguide Transmission Theory," B.S.T.J., this issue.
9. H. G. Unger, "Helix Waveguide Theory and Applications," B.S.T.J., *37*, No. 9, (November 1958), pp. 1599–1662.
10. J. C. Anderson et al., "Route Engineering and Sheath Installation," B.S.T.J., this issue.
11. H. A. Baxter et al., "Waveguide Installation," B.S.T.J., this issue.
12. E. T. Harkless et al., "Channelization Plan and Network," B.S.T.J., this issue.
13. P. Brostrup-Jensen et al., "Line and Repeater Equalization," B.S.T.J., this issue.
14. M. J. Bonomi et al., "Protection Switching, Auxiliary Communications and Maintenance," B.S.T.J., this issue.
15. R. P. Guenther et al., "Reliability and Maintenance of the WT4 Transmission Medium," B.S.T.J., this issue.

THE BELL SYSTEM TECHNICAL JOURNAL
Vol. 56, No. 10, December 1977
Printed in U.S.A.

WT4 Millimeter Waveguide:

TE_{01} Transmission in Waveguide with Axial Curvature

By J. W. CARLIN and S. C. MOORTHY

(Manuscript received April 7, 1977)

In this paper we examine the relationship between the loss of the TE_{01} mode in a multimode circular waveguide and the waveguide geometry. First-order perturbation theory solutions of the coupled line equations were used to predict the loss from measurements of the waveguide geometry. The predicted loss disagreed with the measured loss for the 14 km long waveguide line in the WT4 field evaluation test. An analysis of the coupled line equations which considers the effects of both first- and second-order mode conversion is described. The appropriate coupling coefficients are derived and discussed. Second-order perturbation theory solutions of the coupled line equations are developed and examined. Losses predicted from the measured waveguide curvature and the second-order theory agree well with measured loss data. The results indicate that axial curvature leads to significant mode conversion-reconversion effects between the TE_{01}–TM_{11}, TE_{01}–TE_{12}, TM_{11}–TM_{21}, TE_{12}–TM_{21} modes in the installed waveguide of the WT4 field evaluation test. The TM_{21} conversion is due to curvature fluctuations with a characteristic wavelength of 10 to 30 m.

I. INTRODUCTION

The transmission characteristics of the TE_{01} mode in circular waveguide are quite different from the characteristics of cable or wire transmission media currently used in the Bell System. The waveguide medium has the unique property that its heat loss decreases with increasing frequency. Heat losses[1] as low as 0.3 dB/km are obtained at 110 GHz in 60 mm diameter waveguide. However, since the diameter of the

waveguide is much larger than the operating wavelength of 2.75 mm at 110 GHz, several hundred spurious modes can also propagate, in addition to the TE_{01} mode. The spurious modes have slightly different phase and group velocities than the TE_{01} mode. Spurious modes are excited in practice because the waveguide is not a geometrically perfect right circular cylinder, and there is a continuous exchange of energy between the TE_{01} and spurious modes. This mode conversion-reconversion results in added loss and delay distortion. A detailed understanding of the relationship between spurious mode generation and waveguide geometry is required since even small distortions in the guide cross section (of the order of 1 μm) can cause substantial loss.[2]

The mode conversion problem can be modeled by an infinite system of coupled transmission line equations[3] for which approximate solutions have been obtained by first-order perturbation theory.[4] At the beginning of the WT4 field evaluation test the first-order theory was considered to be a valid and accurate method for predicting the TE_{01} mode conversion loss. Detailed measurements of the waveguide cross-section geometry were carried out in the laboratory on 9 m long individual sections of waveguide. The curvature of the waveguide axis, in two orthogonal planes, was also measured over the 14 km field evaluation test route. The curvature and cross-section geometry data and the first-order perturbation theory solutions were used to predict the TE_{01} mode conversion loss. Waveguide curvature was found to be a significant source of TM_{11} and TE_{12} mode generation with a predicted TE_{01} mode conversion loss of approximately 0.2 dB/km at 110 GHz. All other predicted first-order mode conversion effects resulted in an additional TE_{01} loss of less than 0.03 dB/km at 110 GHz.

The measured loss disagreed substantially with those first-order predictions. The measured loss indicated a total TE_{01} mode conversion loss of approximately 0.5 dB/km at 110 GHz.

In this paper, we show that the generation of the TM_{21} mode is a significant source of TE_{01} mode conversion loss in curved waveguide. The TM_{21} mode is not coupled directly to the TE_{01} mode and therefore is ignored in the first-order perturbation theory. It is excited via the TM_{11} and TE_{12} modes and hence can be thought of as a "second-order" phenomenon. However, as we shall see, the energy coupled into the TM_{21} mode exceeds the energies coupled into the "first-order modes" TM_{11} and TE_{12} under certain conditions. Therefore the term "second order" is used to describe any theory which includes the TM_{21} mode, only in the sense that it is a mode which is indirectly excited from the TE_{01} mode.

An approximate model and a second-order perturbation theory is developed for the TM_{21} conversion in curved waveguide, which, in conjunction with the first-order theory for TM_{11} and TE_{12} conversion,

yields results which agree well with measured results. The source of the TM_{21} generation is identified as waveguide curvature with low spatial frequency components with a characteristic wavelength of 10 to 30 meters.

II. PROBLEM FORMULATION

Maxwell's equation in the deformed waveguide may be transformed to an infinite set[3,5] of coupled transmission line equations expressed in terms of the normal modes of the undeformed guide:

$$\frac{d}{dz} A_m(z) = \sum_{n \neq m} K_{m,n}(z) A_n(z) - j h_m A_m \tag{1}$$

The unknowns in eq. (1) are the normal mode amplitudes A_m while h_m are the normal mode propagation constants in the undeformed guide. The sum over n extends over an infinite number of modes, and the coefficients $K_{m,n}$ in the infinite system of equations consist of the product of a geometry deformation factor and a normalized coupling[4,5,6,7] coefficient $C_{m,n}$. The derivation of the coupled line equations and the normalized coupling coefficients, as well as some notation for normal modes, is outlined in the appendix.

We shall use single subscripts m and n when referring to a general normal mode. A double subscript pn is used in referring to a specific normal mode such as TE_{pn} or TM_{pn}. Here the p refers to the order of the azimuthal variation ($\cos p\phi$ and $\sin p\phi$) while the n is the order of the radial variation $J_p(x_n r)$. The modes in dielectric-lined waveguide, the principal transmission medium in the field evaluation test, are not strictly[6,7,8] "transverse electric" TE or "transverse magnetic" TM but we will retain the notation. The axis of the installed waveguide is a curve in three-dimensional space. The polarizations of the locally excited spurious modes are related to the orientation of the osculating plane, and since this is continuously changing, the polarizations of the modes are also changing continuously along the waveguide axis. The net spurious mode amplitude is the sum of the locally generated modes, and to determine this sum it is necessary to resolve the local polarization into two orthogonal polarizations. Furthermore, it has been shown[4] that the same results are obtained by using the curvature of the projections of the waveguide axis on two orthogonal planes. We shall use superscripts $\uparrow$ and $\rightarrow$ to denote the two distinct polarizations, e.g., $TE^{\uparrow}_{pn}$ or $TE^{\rightarrow}_{pn}$. We shall use TE_{pn} with no superscripts in discussions which apply for both polarizations. The two polarizations for the $TM^{\uparrow}_{11}$ and $TM^{\rightarrow}_{11}$ modes are given in Fig. 1. Note that the plane of curvature determines which polarization is generated. The waveguide installed for the field evaluation test has independent curvature characteristics for the two planes, hor-

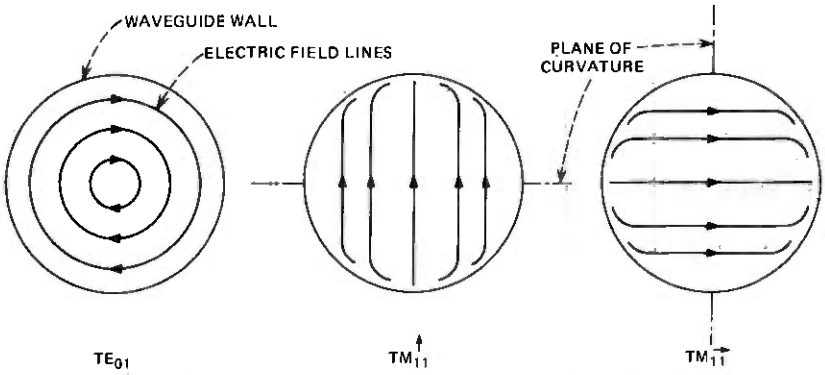

Fig. 1—Normal mode electric fields in dielectric-lined waveguide.

izontal and vertical, shown in Fig. 1, and the polarization of the spurious mode must be carefully accounted for when estimating the TE_{01} loss.

Previous analyses[4] assume $K_{m,n}(z)$ to be sufficiently small so that the total loss can be obtained by a superposition of a number of two mode problems in each of which the TE_{01} mode and one spurious mode is considered. As a specific example, the TE_{01}–TM_{11} mode conversion loss due to axial curvature $c(z)$ in a single plane may be determined from

$$\frac{d}{dz}\begin{bmatrix} A_{01} \\ A_{11} \end{bmatrix} = -j\begin{bmatrix} h_{01} & 0 \\ 0 & h_{11} \end{bmatrix}\begin{bmatrix} A_{01} \\ A_{11} \end{bmatrix} + j\begin{bmatrix} 0 & C_{01,11} \\ C_{01,11} & 0 \end{bmatrix}\begin{bmatrix} A_{01} \\ A_{11} \end{bmatrix} c(z) \quad (2)$$

An approximate[4] expression for the expected TE_{01}–TM_{11} mode conversion loss (α_{01}^{11}) in eq. (2) is

$$\alpha_{01}^{11} = \frac{1}{2} C_{01,11}^2 S_c(\Delta\beta_{01,11}/2\pi) \quad (3)$$

Here S_c is the spectral density function for c and the differential propagation constant $\Delta\beta_{01,11}$ is defined as

$$\Delta\beta_{01,11} = h_{01} - h_{11} \quad (4)$$

Expression (3) is valid in loss-free waveguide, real h_m, and for long lengths of line with a slowly varying power spectrum, S_c.[4] It is an exact solution for (2) in the case of a white power spectrum.[9] Computed power spectral density functions of the installed WT4 field evaluation test waveguide[2,10] diameter, curvature, ellipticity, and higher-order geometric distortions were substituted into the equivalent of (3). The resulting values of loss indicated that approximately 90 percent of the total TE_{01} mode conversion loss, α_{01}^{MC}, was accounted for by $TM_{11}^{\uparrow}$, $TM_{11}^{\rightarrow}$, $TE_{12}^{\uparrow}$, $TE_{12}^{\rightarrow}$ conversions due to the curvatures c_H and c_V of the waveguide axis in the

horizontal and vertical planes, respectively. Thus the predicted mode conversion loss was expected to be

$$\alpha_{01}^{MC} = \frac{1}{2} C_{01,11}^2 \left[S_{cV}(\Delta\beta_{01,11}/2\pi) + S_{cH}(\Delta\beta_{01,11}/2\pi)\right] + \frac{1}{2} C_{01,12}^2 \left[S_{cV}(\Delta\beta_{01,12}/2\pi) + S_{cH}(\Delta\beta_{01,12}/2\pi)\right] \quad (5)$$

The mode conversion loss predicted by (5) differed significantly from the measured loss[10] as discussed in greater detail in Section IV. Moving piston measurements[11] in regions of the field evaluation test line with high curvature indicated the presence of significant levels for the TM_{21} mode as well as TM_{11} and TE_{12} modes.

The measured results implied that second-order conversion processes of the form $TE_{01} \leftrightarrow TM_{11} \leftrightarrow TM_{21}$ are also significant and must be considered along with the first-order processes, $TE_{01} \leftrightarrow TM_{11}$, in estimating the total TE_{01} loss. Instead of considering the two-mode model in (2), we must examine a three-mode model of the form

$$\frac{d}{dz}\begin{bmatrix} A_{01} \\ A_{11} \\ A_{21} \end{bmatrix} = -j \begin{bmatrix} h_{01} & 0 & 0 \\ 0 & h_{11} & 0 \\ 0 & 0 & h_{21} \end{bmatrix} \begin{bmatrix} A_{01} \\ A_{11} \\ A_{21} \end{bmatrix} + j\,c(z) \begin{bmatrix} 0 & C_{01,11} & 0 \\ C_{01,11} & 0 & C_{11,21} \\ 0 & C_{11,21} & 0 \end{bmatrix} \begin{bmatrix} A_{01} \\ A_{11} \\ A_{21} \end{bmatrix} \quad (6)$$

In (6) we are considering only one of the possible TM_{21} conversion paths, as the curvature $c(z)$ is assumed to be in a single plane. The other paths are given in Fig. 2. The coupling model in Fig. 2 leads to the following set of coupled transmission line equations for the determination of TE_{01} mode conversion loss due to curvature of the waveguide axis:

$$\frac{d}{dz}[A] = -j[h][A] + jc_H(z)[C_H][A] + jc_V(z)[C_V][A] \quad (7)$$

where

$$A = [A_{01}, A_{11}^{\uparrow}, A_{12}^{\uparrow}, A_{21}^{\updownarrow}, A_{11}^{\rightarrow}, A_{12}^{\rightarrow}, A_{21}^{\rightarrow}]^T \quad (8)$$

Here the A_m's are the transmission line voltages corresponding to the TE_{01}, $TM_{11}^{\uparrow}, \ldots, TM_{21}^{\rightarrow}$ modes. The propagation constants $h_{01}, h_{11}^{\uparrow}, \ldots, h_{21}^{\rightarrow}$ of the modes in straight waveguide are the elements of the diagonal matrix $[h]$. Note that $h_m^{\uparrow} = h_m^{\rightarrow}$ and that no superscript is required for the TE_{01} mode. Corresponding differential propagation constants, $\Delta\beta_{m,n}$ are given in Fig. 3.

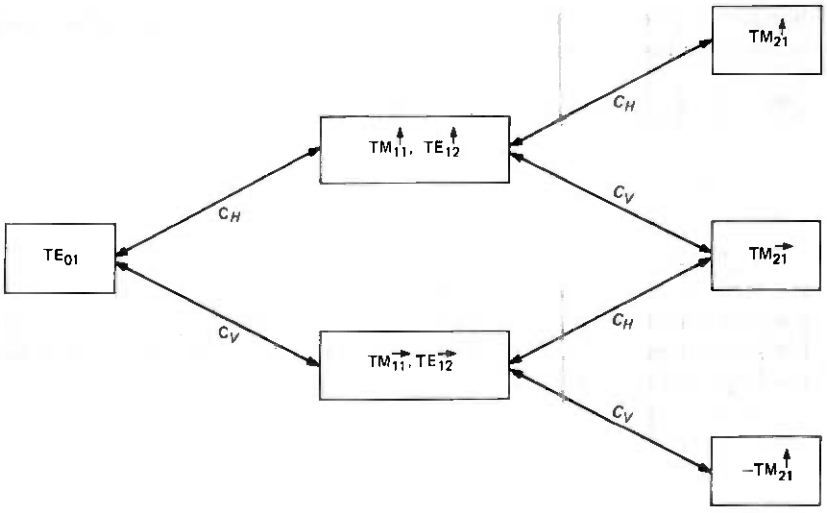

Fig. 2—Curvature coupling mechanisms.

The coupling coefficient matrices $[C_H]$ and $[C_V]$ consist of the normalized curvature coupling coefficients $C_{m,n}$ from mode m to mode n. They may be determined from eq. (57) in the appendix. The normalized curvature coupling coefficients in 60 mm diameter guide, with a 180-μm polyethylene liner are shown in Fig. 4. $[C_H]$ and $[C_V]$ must be multiplied by the local horizontal or vertical curvature, $c_H(z)$ or $c_V(z)$, respectively, to obtain the local coupling coefficients. From Fig. 2 we have

$$j[C_H] = \begin{bmatrix} 0 & jC_{01,11} & jC_{01,12} & 0 & 0 & 0 & 0 \\ jC_{01,11} & 0 & 0 & jC_{11,21} & 0 & 0 & 0 \\ jC_{01,12} & 0 & 0 & jC_{12,21} & 0 & 0 & 0 \\ 0 & jC_{11,21} & jC_{12,21} & 0 & 0 & 0 & 0 \\ 0 & 0 & 0 & 0 & 0 & 0 & jC_{11,21} \\ 0 & 0 & 0 & 0 & 0 & 0 & jC_{12,21} \\ 0 & 0 & 0 & 0 & jC_{11,21} & jC_{12,21} & 0 \end{bmatrix} \quad (9)$$

$$j[C_V] = \begin{bmatrix} 0 & 0 & 0 & 0 & jC_{01,11} & jC_{01,12} & 0 \\ 0 & 0 & 0 & 0 & 0 & 0 & jC_{11,21} \\ 0 & 0 & 0 & 0 & 0 & 0 & jC_{12,21} \\ 0 & 0 & 0 & 0 & -jC_{11,21} & -jC_{12,21} & 0 \\ jC_{01,11} & 0 & 0 & -jC_{11,21} & 0 & 0 & 0 \\ jC_{01,12} & 0 & 0 & -jC_{12,21} & 0 & 0 & 0 \\ 0 & jC_{11,21} & jC_{12,21} & 0 & 0 & 0 & 0 \end{bmatrix} \quad (10)$$

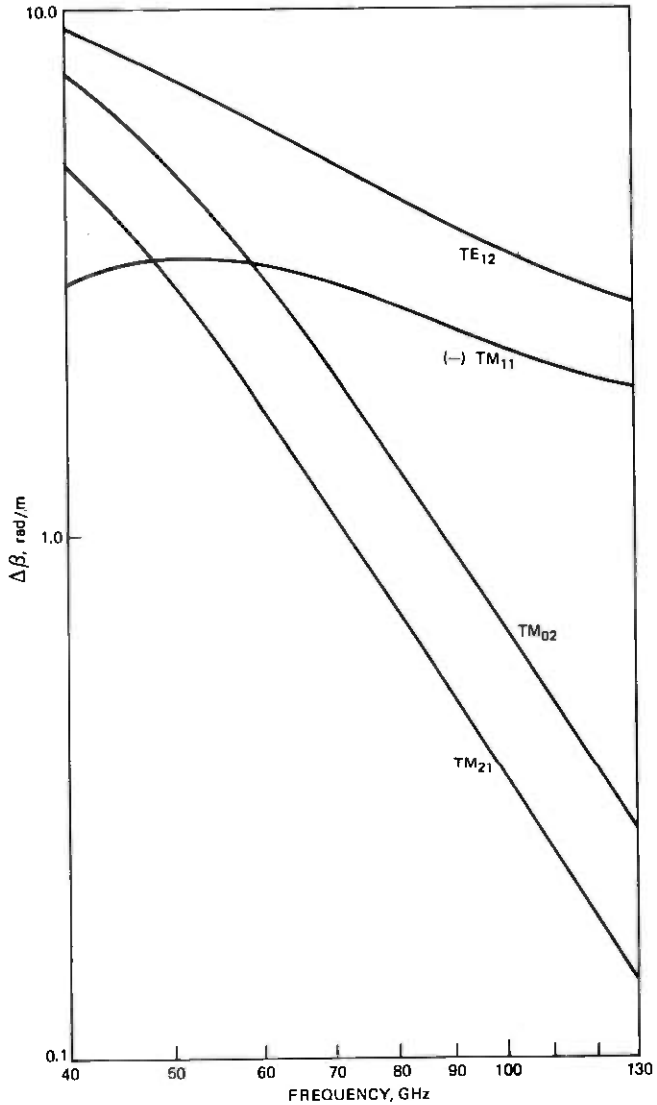

Fig. 3—Differential propagation constants in 60-mm lined waveguide.

Prediction of TE_{01} loss based on the set of coupled line equations in (7) agrees well with measured results as discussed in Section IV.

III. SOLUTIONS—COUPLED LINE EQUATIONS

The set of seven coupled line equations in (7) has been integrated numerically for sets of measured curvature data up to 800 m in length.

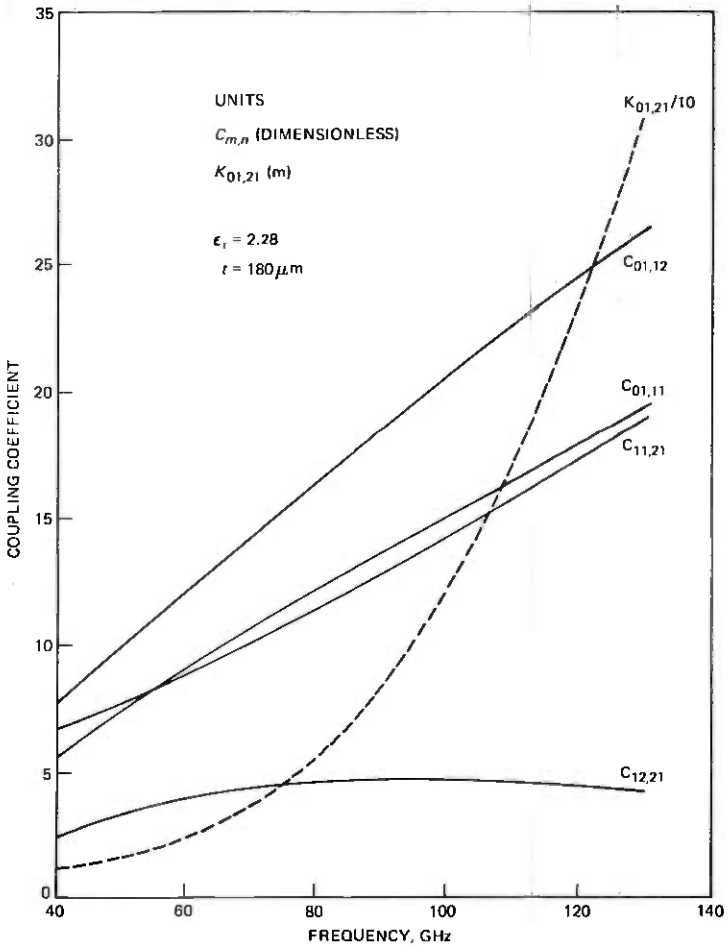

Fig. 4—Coupling coefficients for 60-mm-diameter lined waveguide.

The numerical method yields solutions with an accuracy of better than 1 percent. The method consists of a direct numerical evaluation of the transmission matrix for incremental sections 5 cm long. Direct multiplication of the individual matrices yields the transmission matrix for the desired sections of line. The results agree well with measured data as discussed in Section IV and are a confirmation of the validity of the mode conversion model in Fig. 2. The numerical integration must be carried out at a number of discrete frequencies to determine the loss characteristics over a given frequency band and is an expensive process, since 10 minutes or more of computer time may be required for a 500 m length. Thus approximate solutions are required.

For the case of weak coupling, the seven-mode system of equations in (7) can be reduced to a superposition of three-mode equations similar to (6). It is convenient to define a normalized mode amplitude G_m in terms of A_m

$$A_m = e^{-jh_m z} G_m \tag{11}$$

On applying Picard's method[4] of successive approximations to (6), we find that G_{11} and G_{21} are given to first- and second-order respectively by

$$G_{11} = j \int_0^z C_{01,11} c(s) e^{-j\Delta\beta_{01,11} s} ds \tag{12}$$

$$G_{21} = - \int_0^z C_{11,21} c(s) e^{-j\Delta\beta_{11,21} s} \int_0^s C_{01,11} c(t) e^{-j\Delta\beta_{01,11} t} dt\, ds \tag{13}$$

For slowly varying curvature, $c(z)$, it can be shown that

$$G_{21} \approx j \int_0^z \left\{ C_{11,21} c(s) \left(\frac{C_{01,11}}{\Delta\beta_{01,11}} c(s) \right) \right\} e^{-j\Delta\beta_{01,21} s} ds \tag{14}$$

There is a simple physical interpretation for the terms in (14) which we will examine instead of presenting the details of the analysis. As the TE_{01} mode travels through a region of waveguide with slowly varying curvature in a single plane, the local field structure for the TE_{01} mode is slightly distorted from the structure in the straight waveguide. The degree of distortion can be quantified by expanding the fields in the curved guide in terms of the normal modes for the straight waveguide.[12] In doing so, it is found that the TM_{11} component has a magnitude given by

$$\left(\frac{C_{01,11}}{\Delta\beta_{01,11}} c(z) \right)$$

which is one of the terms in (14). The TM_{11} component travels with the *same* phase velocity as the TE_{01} mode and couples to the TM_{21} mode with a coupling of strength $C_{11,21}\, c(z)$. This is the second coupling term in (14).

Thus the net coupling between the TE_{01} and TM_{21} modes in waveguide with slowly varying curvature, c, is

$$\frac{C_{01,11} C_{11,21}}{\Delta\beta_{01,11}} c^2(z)$$

Equation (14) is similar in form to (12) and thus the three-mode mechanism, $TE_{01} \leftrightarrow TM_{11} \leftrightarrow TM_{21}$, has been converted to an equivalent simple two-mode mechanism $TE_{01} \leftrightarrow TM_{21}$ with an effective normalized

coupling coefficient, $C_{01,21}$, given by

$$C_{01,21} = \frac{C_{01,11}C_{11,21}}{\Delta\beta_{01,11}} \tag{15}$$

The waveguide geometry enters (14) via the factor $c^2(z)$. The reader is cautioned against confusing (15) with the normalized coupling coefficient between the TE_{01} and TM_{21} modes due to ellipticity of the waveguide.

The formula for the expected value of the $TE_{01} \leftrightarrow TM_{21}$ mode conversion loss, α_{01}^{21}, is similar to (3) and is given by

$$\alpha_{01}^{21} = \frac{1}{2} C_{01,21}^2 S_{c^2}(\Delta\beta_{01,21}/2\pi) \tag{16}$$

The loss in (16) is proportional to the spectral density function for the square of the waveguide curvature at a spatial frequency of $\Delta\beta_{01,21}/2\pi$ c/m. From Fig. 3 it may be observed that $\Delta\beta_{01,21}/2\pi$ is less than 0.1 c/m for frequencies greater than 80 GHz, and thus curvatures with long wavelengths, 10m or more are the source of TE_{01}–TM_{21} mode conversion loss in (16).

In Ref. (10) it is shown that the curvature power spectral density for the field evaluation test waveguide in the 0 to 0.1 c/m region of the spectrum is three orders of magnitude larger than the spectrum in the 0.3–1 c/m region which causes TM_{11}, TE_{12} conversion. Thus the assumptions in previous analyses[4] of a slowly varying spectrum are clearly not true and the existence of additional mode conversion loss components is not surprising.

In general, for curvature in two planes, we must consider all of the mechanisms in Fig. 2 to determine the total TE_{01} loss. It is convenient to define an equivalent normalized coupling coefficient, $K_{01,21}$

$$K_{01,21} \equiv 2\left[\frac{C_{01,11}C_{11,21}}{\Delta\bar{\beta}_{11}} + \frac{C_{01,12}C_{12,21}}{\Delta\bar{\beta}_{12}}\right] \tag{17}$$

where

$$\Delta\bar{\beta}_{11} = \frac{\Delta\beta_{11,21} + \Delta\beta_{11,01}}{2}, \quad \Delta\bar{\beta}_{12} = \frac{\Delta\beta_{12,21} + \Delta\beta_{12,01}}{2} \tag{18}$$

A plot of $K_{01,21}$ vs. frequency is given in Fig. 4.

We then find that the mode conversion due to curvature may be approximately treated as a superposition of the two-mode process shown in Table I.

Table I — Mode conversion due to curvature

Conversion process	Geometrical factor	Normalized coupling coefficient	$\Delta\beta$	Loss
TE_{01}–$TM_{11}^{\uparrow}$	c_H	$C_{01,11}$	$\Delta\beta_{01,11}$	$\frac{1}{2}C_{01,11}^2 S_{c_H}(\Delta\beta_{01,11}/2\pi)$
TE_{01}–$TM_{11}^{\rightarrow}$	c_V	$C_{01,11}$	$\Delta\beta_{01,11}$	$\frac{1}{2}C_{01,11}^2 S_{c_V}(\Delta\beta_{01,11}/2\pi)$
TE_{01}–$TE_{12}^{\uparrow}$	c_H	$C_{01,12}$	$\Delta\beta_{01,12}$	$\frac{1}{2}C_{01,12}^2 S_{c_H}(\Delta\beta_{01,12}/2\pi)$
TE_{01}–$TE_{12}^{\rightarrow}$	c_V	$C_{01,12}$	$\Delta\beta_{01,12}$	$\frac{1}{2}C_{01,12}^2 S_{c_V}(\Delta\beta_{01,12}/2\pi)$
TE_{01}–$TM_{21}^{\uparrow}$	$c_H^2 - c_V^2$	$K_{01,21}/2$	$\Delta\beta_{01,21}$	$\frac{1}{2}[K_{01,21}/2]^2 S_{c_H^2-c_V^2}(\Delta\beta_{01,21}/2\pi)$
TE_{01}–$TM_{21}^{\rightarrow}$	$c_H c_V$	$K_{01,21}$	$\Delta\beta_{01,21}$	$\frac{1}{2}K_{01,21}^2 S_{c_H c_V}(\Delta\beta_{01,21}/2\pi)$

IV. COMPARISON OF APPROXIMATE AND EXACT SOLUTIONS WITH MEASURED RESULTS

In this section the approximate results obtained in the last section for TE_{01}—TM_{21} mode conversion, the measured results, and the results from a numerical integration of the coupled line equations in (7) are compared for different curvatures of the waveguide axis. Let us first consider an idealized bend, as shown in Fig. 5a, having constant curvature in the horizontal plane and a sinusoidally varying curvature in the vertical plane

$$c_H(z) = 1/R_H$$

$$c_V(z) = A_V \sin \frac{2\pi}{\lambda_m} z \tag{19}$$

From Table I, we can approximately model the $TM_{21}^{\rightarrow}$ conversion process with the following set of two coupled equations. Since $S_{c_H c_V}$ is much greater than $S_{c_V}^2$ and $S_{c_H}^2$ at $\Delta\beta_{01,21}/2\pi$ c/m the $TM_{21}^{\rightarrow}$ level is much greater than the $TM_{21}^{\uparrow}$ level, which is neglected.

$$\frac{d}{dz}A_{01} = -jh_{01}A_{01} + jK_{01,21}\frac{1}{R_H}A_V \sin\left(\frac{2\pi}{\lambda_m}z\right)A_{21}^{\rightarrow}$$

$$\frac{d}{dz}A_{21}^{\rightarrow} = jK_{01,21}\frac{1}{R_H}A_V \sin\left(\frac{2\pi}{\lambda_m}z\right)A_{01} - jh_{21}A_{21}^{\rightarrow} \tag{20}$$

The coupling term in (20), $\sin(2\pi/\lambda_m)z$, is sinuosoidal, and an analytic solution for this case has been obtained by Miller.[13] Miller's solution for (20) will be compared with both the numerical solution and the sec-

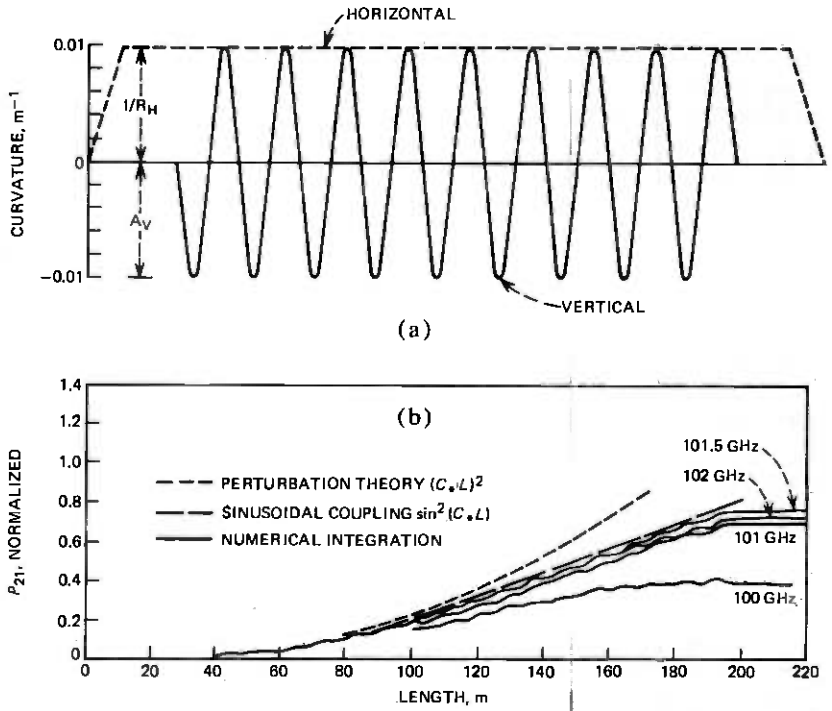

Fig. 5—Comparison of predicted losses for constant curvature bend with sinusoidal curvature in orthogonal plane.

ond-order perturbation theory solution in the following. After the solutions for A_{01} and $A_{21}^{\rightarrow}$ in (20) are determined as in Miller,[13] the normalized $TM_{21}^{\rightarrow}$ level, $G_{21}^{\rightarrow}$, follows from (11):

$$G_{21}^{\rightarrow}(L) = \frac{C_* L \sin\left\{C_*\left|1+\left(\frac{\Delta\beta_*}{2C_*}\right)^2\right|^{1/2} L\right\}}{\left\{C_*\left|1+\left(\frac{\Delta\beta_*}{2C_*}\right)^2\right|^{1/2} L\right\}} \tag{21}$$

where

$$C_* = \frac{1}{2} K_{01,21} \frac{1}{R_H} A_V, \qquad \Delta\beta_* = \Delta\beta_{01,21} - \frac{2\pi}{\lambda_m} \tag{22}$$

The corresponding value of G_{01} is

$$|G_{01}(L)|^2 = 1 - |G_{21}^{\rightarrow}(L)|^2 \tag{23}$$

from which the loss is readily obtained. From (14) we obtain the second-order perturbation theory solution for $G_{21}^{\rightarrow}$ for the two curvature

functions in (19) as

$$G_{21}^{\rightarrow}(L) = C_{\bullet}L \tag{24}$$

In Figure 5b, we compare the results from (21) and (24) with a direct numerical integration of the corresponding seven-mode system in (7) for the curvature data in Fig. 5a. We see that there is a substantial disagreement at 100 GHz, the frequency at which $\Delta\beta_{01,21}$ is equal to $2\pi/\lambda_m$, because the propagation constant of TE_{01} in a bend is slightly different from that in the straight waveguide. This causes the frequency at which we obtain coherent coupling to differ slightly from 100 GHz. On performing the numerical integration at a number of frequencies in the vicinity of 100 GHz, it was found that a frequency of 101.5 GHz resulted in a maximum $TM_{21}^{\rightarrow}$ conversion as also shown in Fig. 5b. The 101.5 GHz curve differs by less than 2 percent from the result predicted by (21). The second-order perturbation theory solution in (24) is also in good agreement for small $TM_{21}^{\rightarrow}$ levels, as for $C_{\bullet}L < 0.1$, $C_{\bullet}L \approx \sin C_{\bullet}L$. From the results in Fig. 5 we draw two important conclusions. The equivalent two-mode model in (20) can be summed to give an accurate representation of the seven-mode system in (7) and the second-order perturbation theory solution (14) is valid for small couplings, $C_{\bullet}L < 0.1$.

A controlled experiment was conducted in order to compare the analytic results discussed above with measured data. An experimental bend was constructed having constant curvature in the horizontal plane and either "zero or very small" curvature or a sinusoidally varying curvature in the vertical plane. The measured curvature for this line is given in Fig. 6. Shuttle pulse loss[14] measurements were carried out on this bend for the two different vertical curvature cases. From the difference of the two measurements the loss due to $TM_{21}^{\rightarrow}$ conversion was determined and is shown in Fig. 7 (curve A). Two predicted loss curves are also given in Fig. 7; curve B from a numerical integration of the coupled line equations (7) for the data in Fig. 6, and curve C from the sinusoidal coupling theory (21). There is excellent agreement between all three sets of curves with the exception of some slight frequency shifts. The frequency shift between B and C has been discussed. The shift between A and B is probably due to small errors (<1 percent) in our estimated values for the differential propagation constant $\Delta\beta_{01,21}$.

A similar comparison has been carried out on a 720 m long section in the WT4 field evaluation test. The measured curvature for this section is given in Fig. 8. There are substantial changes in profile in this section and vertical curvatures greater than 0.020 m^{-1} were measured in several regions. The measured loss characteristic for this section is given in Fig. 9. A numerical integration of the coupled line equations, for the measured curvature data in Fig. 8, was carried out at discrete frequencies, as indicated by a circle or cross in Fig. 9 for two cases. The first case allowed

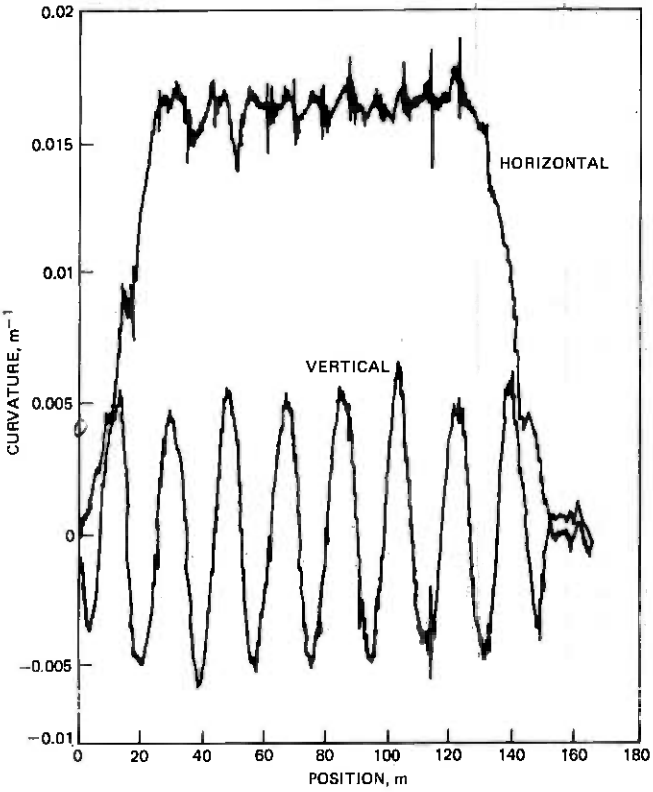

Fig. 6—Measured curvature data for experimental route bend.

only for first order $TM_{11}^{\uparrow}$, $TM_{11}^{\rightarrow}$, $TE_{12}^{\uparrow}$, and $TE_{12}^{\rightarrow}$ conversion, and it can be seen that the predicted losses are much lower than the measured losses. The second case allowed for $TM_{11}^{\uparrow}$, $TM_{11}^{\rightarrow}$, $TE_{12}^{\uparrow}$, $TE_{12}^{\rightarrow}$, $TM_{21}^{\downarrow}$, and $TM_{21}^{\rightarrow}$ conversion. It can be seen in Figure 9 that there is excellent agreement between the measured loss and the numerical integration results. The absolute loss for the peak at 114 GHz is $\approx$ 1.5 dB. This is a fairly large loss, and because of this the perturbation theory will yield losses that are too large. The perturbation theory losses are approximately 30 percent greater than the numerical integration estimate, as also shown in Fig. 9.

The large measured loss peak at 112 GHz is principally due to $TM_{21}^{\downarrow}$ conversion occurring at the large vertical curvature peaks at 125 and 250 m in Fig. 8. This is readily seen in the measured "moving piston" trace of Fig. 10. Here we are measuring[11] the reflected TE_{01} level at the end of the line as a perfectly reflecting piston is moved through this mode filter section in a left-to-right direction in Fig. 8. The large increase in

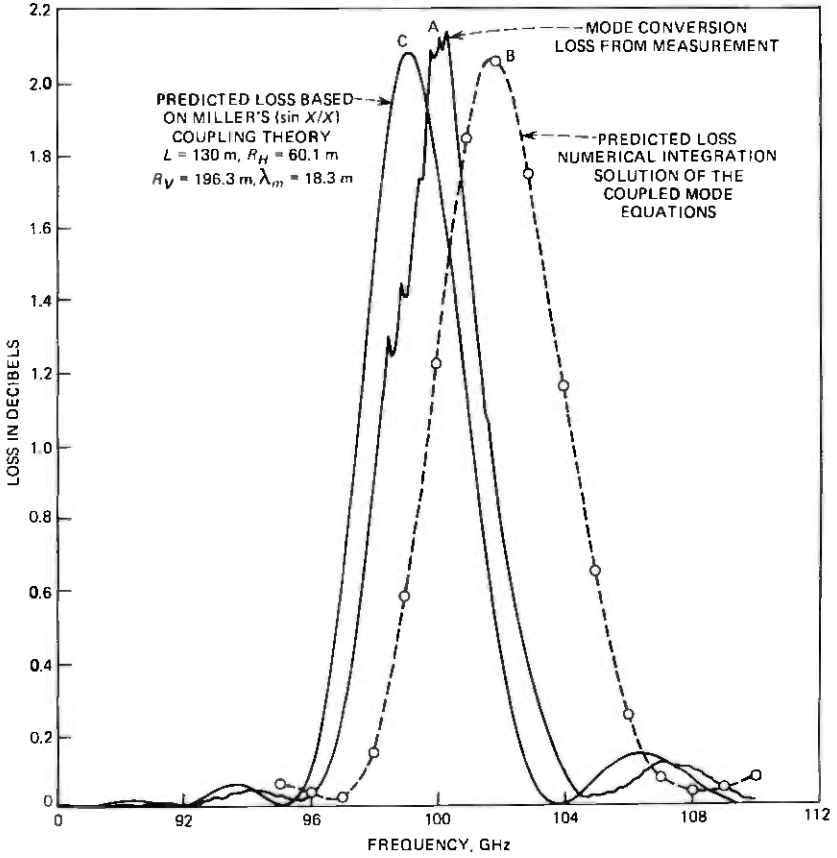

Fig. 7—TE_{01} loss due to mode conversion in modulated bend at Chester.

the TE_{01} ripple at points A and B corresponds to regions of high vertical curvature in Fig. 8.

The numerical integration used in solving (7) consists of an evaluation of the transmission matrix for 5 cm long incremental sections of the waveguide line. A predicted moving piston trace is readily obtained on multiplying the transmission matrix with its transpose. The final result, given in Fig. 11, agrees well with the measured trace in Fig. 10.

V. LOSS VARIATION IN BENDS

In the preceding discussion we have seen that TE_{01}–TM_{21} mode conversion effects result in sizable losses for the TE_{01} mode in bends. This will have a significant impact on repeater siting and spacing for a commercial system and it is desirable to determine the sensitivity of this loss component to system parameters such as guide size (a), frequency

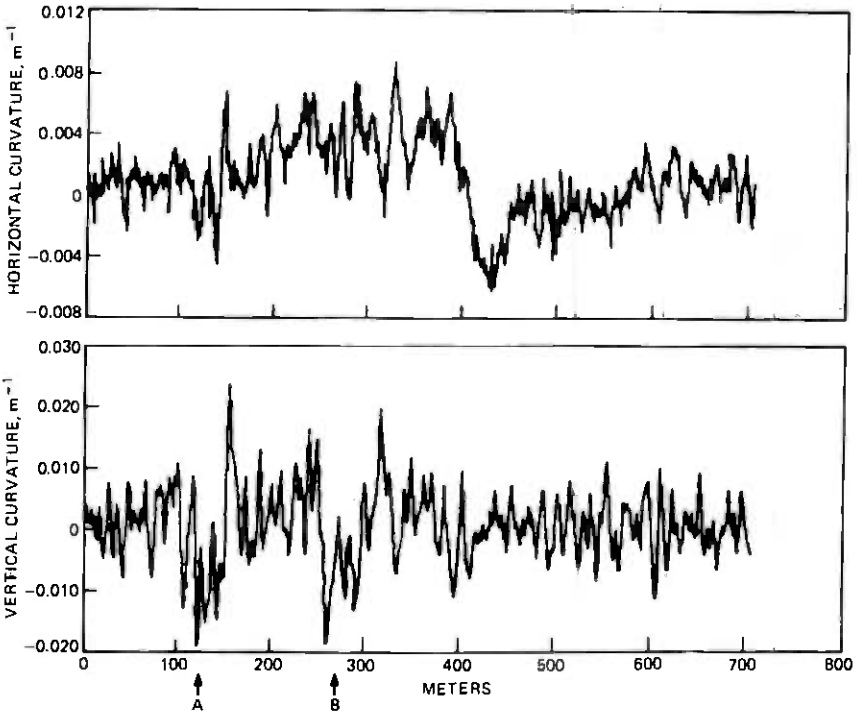

Fig. 8—Measured curvature for 720-m-long section in WT4 field evaluation test.

(f), bend radius (R_B), rms curvature ($c_{V_{rms}}$), etc. On examination of the loss components in Table I, we see that the TM_{21} loss depends on the product of a coupling coefficient $K_{01,21}$ and a geometrical factor $S_{c_{HcV}}$ or $S_{c_H^2 - c_V^2}$. The coupling coefficient $K_{01,21}$ is the product of two curvature coupling coefficients, e.g., $C_{01,11}$ and $C_{11,21}$ which vary as af, and the inverse of a differential propagation constant, e.g., $\Delta\beta_{01,11}^{-1}$, which varies as $a^2 f$. Thus $K_{01,21}$ varies approximately as $a^4 f^3$. The TM_{21} conversion loss is proportional to $K_{01,21}^2$, and varies as $a^8 f^6$.

In a plan bend with an arc length >100 m and a constant radius R_B < 100 m, the geometrical factor $S_{c_{HcV}}(\Delta\beta_{01,21}/2\pi)$ is approximately equal to $1/{R_B}^2\, S_{cV}(\Delta\beta_{01,21}/2\pi)$. The magnitude of $S_{c_{HcV}}$ is much greater than in nominally straight waveguide. Thus the TE_{01} loss due to $TM_{21}^{\rightarrow}$ conversion is much greater in a plan bend than in straight waveguide. Conversely, the value of $S_{c_H^2 - c_V^2}(\Delta\beta_{01,21}/2\pi)$ is increased to a lesser degree from the value in straight waveguide for spatial frequencies greater than 0.04 c/m and thus the increase in TE_{01} loss due to $TM_{21}^{\downarrow}$ conversion is of less significance.

With the above assumptions the additional TE_{01} loss per unit length in a plan bend may be approximately written as

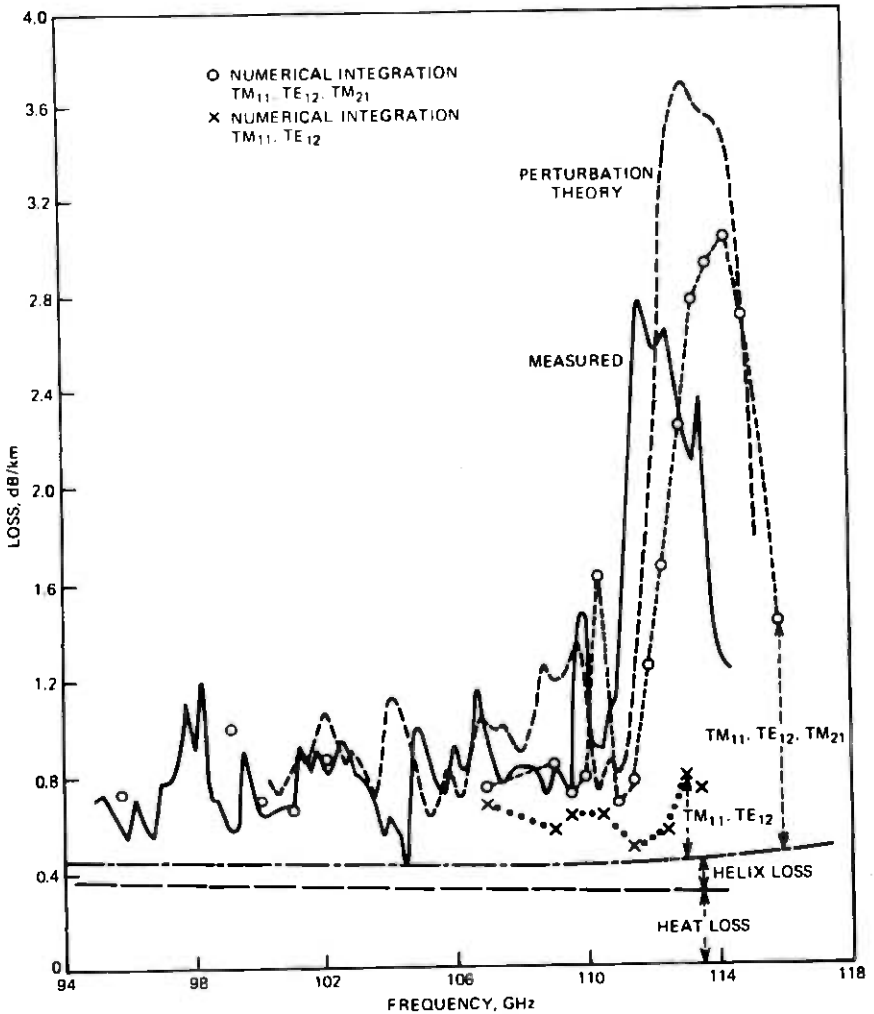

Fig. 9—Loss comparison for 720-m section.

$$\Delta\alpha_{\text{Bend}} = 4.5 \times 10^{-4} \left(\frac{a}{30}\right)^8 \left(\frac{f}{100}\right)^6 \left(\frac{100}{R_B}\right)^2 \left(\frac{S_{cv}}{7 \times 10^{-5}}\right) \quad \text{dB/m} \quad (25)$$

Here a is the guide radius in mm, f is the frequency in GHz, R_B the bend radius in m, and S_{cv} the vertical curvature power spectral density in $1/m^2/c/m$. As an example, from (25) a 95 m radius bend with a net angle of 75 degrees or an arc length of 131 m has an average added loss of 0.12 dB at 110 GHz assuming a value of 7×10^{-5} $1/m^2/c/m$ for S_{cv}. This value of S_{cv} is typical of the WT4 field evaluation test.[10]

Figure 12 is the measured curvature for a bend in the WT4 field evaluation test with nominal parameters similar to those in the preceding

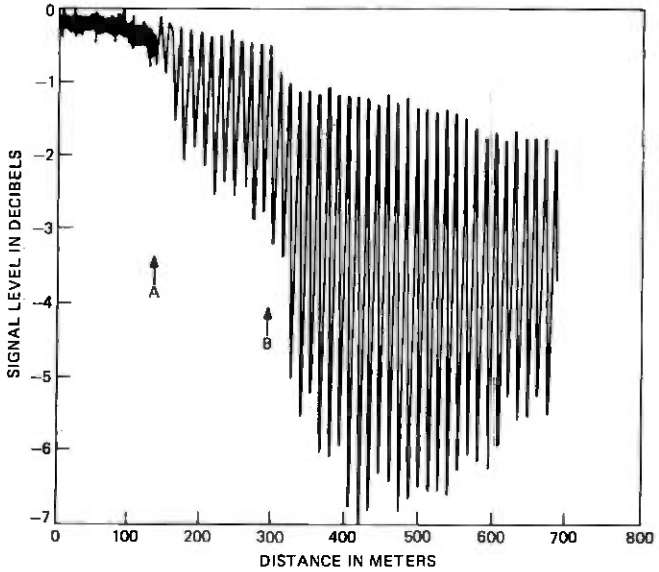

Fig. 10—Moving piston measurement of relative TE_{01} level for 720-m-long section at 113 GHz.

paragraph. The TM_{21} mode conversion loss for this bend was calculated directly using the result of perturbation theory from Table I in Section IV. This agrees fairly well with the numerical integration of the coupled line equation as shown in Fig. 13. Several bends from the field evaluation test were analyzed and exhibited similar agreement. The perturbation theory losses were generally 10 to 20 percent higher than the losses predicted from the numerical integration. The fine structure of the loss, with the exception of small shifts in the loss peaks, was similar for both cases. Figure 13 also gives a comparison of the average added loss predicted from (25) and the actual loss for the bend. In general (25) is useful only for estimating the average loss for a given bend. The actual loss for a given bend exhibits significant fluctuation about this average value as shown in Fig. 13. Any practical installation will contain several route bends in a given repeater span. These bends are independent and thus an expression similar to (25) is useful as it gives an accurate estimate of the average added bend loss.

VI. CONCLUSION

A coupled line system of equations has been presented which predicts the effect of second-order TM_{21} mode conversion on TE_{01} loss. A numerical integration of the coupled line equations developed from this

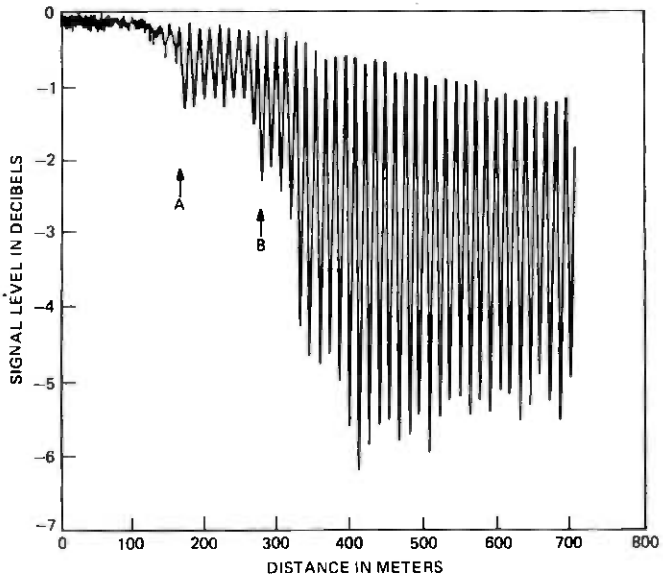

Fig. 11—Calculated TE_{01} level for 720-m-long section at 113 GHz.

model agreed very well with measured results for a bend experiment designed to have high TM_{21} conversion and also agreed with measurements on sections of the WT4 field evaluation test. A second-order perturbation theory solution for the TE_{01} loss due to TM_{21} conversion was derived and discussed. The perturbation theory results agreed well with the results obtained by numerical integration of the coupled line equations for typical sets of curvature data from the WT4 field evaluation test. The perturbation loss estimates were approximately 20 percent higher but the two loss predictions had the same fine structure except for slight shifts in the frequencies of the loss peaks.

An approximate formula for the additional loss due to route bends was given. The added loss is proportional to the inverse square of the bend radius. The added loss increases as the eighth power of guide radius and the sixth power of frequency. The added loss is approximately proportional to the mean squared vertical curvature. This approximate formula works well on the average but does not predict the fine structure of the loss for a given route bend.

There are several areas worthy of further investigation. Additional work is required on the statistics of the TM_{21} mode conversion loss, particularly the loss statistics for a single bend or pair of bends. We have also assumed, without proof, that the TM_{11} and TE_{12} loss is given by the first-order perturbation theory[4] and is little affected by TM_{21} conversion.

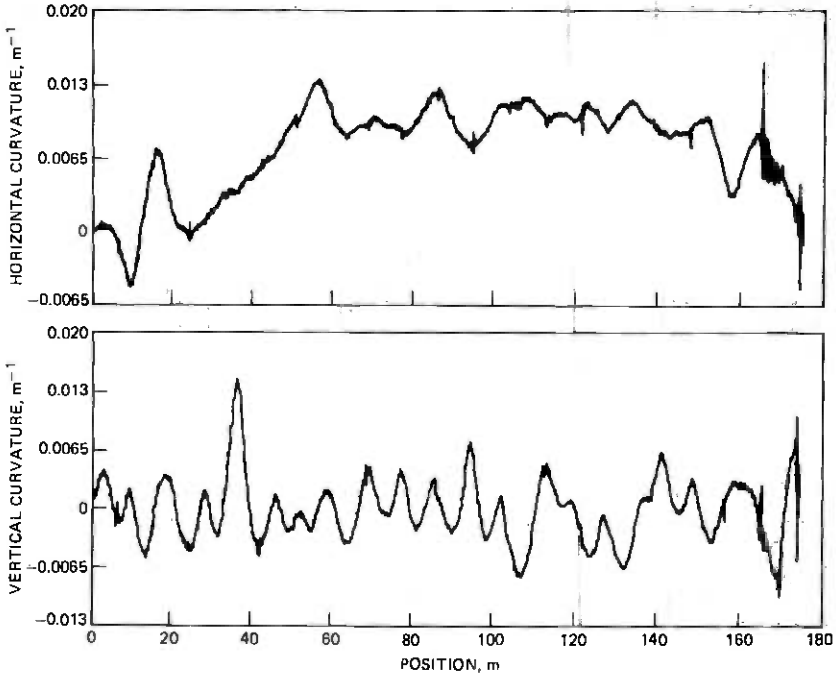

Fig. 12—Measured curvature for plan bend in WT4 field evaluation test.

Note that significant energy passes through these modes to the TM_{21} mode and an examination of higher-order terms is desirable. Finally, the three-mode set of equations (10) has great significance for a practical dielectric-lined waveguide system and is of as much interest as the two-mode systems investigated to date. Improved approximate solutions for systems of this type would be desirable.

ACKNOWLEDGMENT

The authors wish to thank Eli Bochner and Pat Synefakis for their

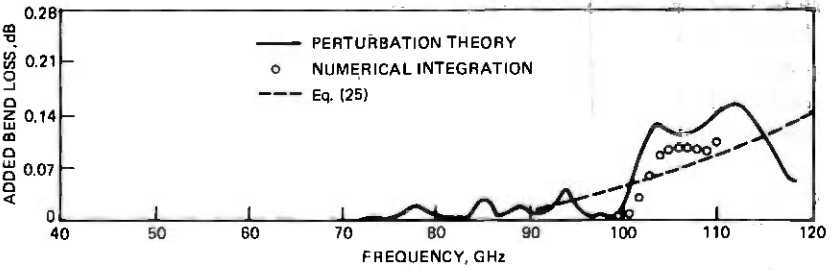

Fig. 13—Added TE_{01} loss for plan bend in WT4 field evaluation test.

assistance with the measurements and computations and Don Rutledge for directing the construction of the experimental route bend.

APPENDIX

Derivation of coupling coefficients

In many cases of interest[1,2,3] circular waveguide with a complex jacket structure may be replaced with a simpler "wall impedance" model with a resultant simplification in the analysis. This is true for the WT4 waveguide and thus we have the following set of equivalent boundary conditions at the inner waveguide surface $r = a$:

$$\begin{aligned} Z_\phi &= E_\phi/H_z|_{r=a} \\ Z_z &= -E_z/H_\phi|_{r=a} \end{aligned} \tag{40}$$

The total fields within the guide can be expressed as a superposition of two scalar functions.

$$\begin{aligned} T_\nu &= N_\nu J_p(x_\nu r) \sin p\phi \\ T'_\nu &= N_\nu J_p(x_\nu r) \cos p\phi \end{aligned} \tag{41}$$

Here ν and p are integers and the eigenvalue $x_\nu a$ is defined by

$$\begin{aligned} k_\nu &= x_\nu a \\ \omega^2\mu_0\epsilon_0 &= k^2 = x_\nu^2 + h_\nu^2 \end{aligned} \tag{42}$$

The fields vary as $e^{-jh_\nu z}$ in the axial direction and k_ν is the solution of the characteristic equation

$$j\omega\epsilon_0 a Z_z$$

$$- \frac{k_\nu J_p(k_\nu)\left[J'_p(k_\nu) + j\omega\epsilon_0 Z_\phi \dfrac{x_\nu}{k^2} J_p(k_\nu)\right]}{-\dfrac{p}{k_\nu^2}\dfrac{h_\nu^2}{k^2} J_p^2(k_\nu) + J'_p(k_\nu)\left[J'_p(k_\nu) + j\omega\epsilon_0 Z_\phi \dfrac{x_\nu}{k^2} J_p(k_\nu)\right]} = 0 \tag{43}$$

The total fields are expressible as a superposition of normal mode fields

$$\overline{E} = \sum_\nu A_\nu^+(z)\bar{e}_\nu^+ e^{-jh_\nu z} + \sum_\nu A_\nu^-(z)\bar{e}_\nu^- e^{+jh_\nu z} \tag{44}$$

$$\overline{H} = \sum_\nu A_\nu^+(z)\bar{h}_\nu^+ e^{-jh_\nu z} + \sum_\nu A_\nu^-(z)\bar{h}_\nu^- e^{+jh_\nu z}$$

where

$$\bar{e}_\nu^\pm = \hat{r}\sqrt{\frac{h_\nu}{\omega\epsilon_0}}\left(\frac{\partial T_\nu}{\partial r} + d_\nu \frac{\partial T'_\nu}{r\partial\phi}\right) + \hat{\phi}\sqrt{\frac{h_\nu}{\omega\epsilon_0}}\left(\frac{\partial T_\nu}{r\partial\phi} - d_\nu \frac{\partial T'_\nu}{\partial r}\right) + \hat{z}(\pm)j\omega\mu_0\sqrt{\frac{\omega\epsilon_0}{h_\nu}}\frac{x_\nu^2}{k^2}T_\nu \tag{45}$$

$$\bar{h}_\nu^{\pm} = \hat{r}(\mp)\sqrt{\frac{\omega\epsilon_0}{h_\nu}}\left(\frac{\partial T_\nu}{r\partial\phi} - d_\nu\frac{h_\nu^2}{k^2}\frac{\partial T_\nu'}{\partial_r}\right)$$
$$+ \hat{\phi}(\pm)\sqrt{\frac{\omega\epsilon_0}{h_\nu}}\left(\frac{\partial T_\nu}{\partial r} + d_\nu\frac{h_\nu^2}{k^2 r\partial\phi}\frac{\partial T_\nu'}{}\right) + \hat{z}j\omega\epsilon_0\sqrt{\frac{h_\nu}{\mu\epsilon_0}}\,d_\nu\frac{x_\nu^2}{k^2}T_\nu'$$

The separation constant d_ν is given by

$$d_\nu = \frac{p}{k_\nu^2}\left\{y_\nu + \frac{j\omega\epsilon_0 a Z_\phi}{k^2a^2}\right\}^{-1}$$
$$= \frac{k_\nu^2}{p}\frac{k^2}{h_\nu^2}(y_\nu + j/\omega\epsilon_0 a Z_z) \tag{46}$$
$$y_\nu = J_p'(k_\nu)/k_\nu J_p(k_\nu)$$

The modes are orthonormal as the vector cross product

$$\int\int_s \bar{e}_\mu^{+} x \bar{h}_\nu^{\pm}\cdot d\bar{s} = \pm\,\delta_{\nu\mu} \tag{47}$$

The normalization constant N_ν is given by

$$\frac{\pi}{2}N_\nu^2 k_\nu^2 J_p^2(k_\nu)\left[\left(1+\frac{d_\nu^2 h_\nu^2}{k^2}\right)\left(1-\frac{p^2}{k_\nu^2}+2y_\nu+k_\nu^2y_\nu^2\right)\right.$$
$$\left. - 2\left(1+\frac{h_\nu^2}{k^2}\right)d_\nu\frac{p}{k_\nu^2}\right] = 1 \tag{48}$$

for $p \neq 0$, and by

$$\pi N_\nu^2 k_\nu^2 J_0^2(k_\nu)\frac{d_\nu^2 h_\nu^2}{k^2}\{(1+k_\nu^2y_\nu^2+2y_\nu)\} = 1 \tag{49}$$

for $TE_{0\nu}$ modes, and by

$$\pi N_\nu^2 k_\nu^2 J_0^2(k_\nu)\{(1+k_\nu^2y_\nu^2+2y_\nu)\} = 1 \tag{50}$$

for $TM_{0\nu}$ modes.

For a nonideal waveguide where the inner surface is of the form $r = a + \epsilon\rho_1(\phi,z)$ where $\epsilon \ll 1$, we may express the total field in the distorted guide $(\bar{E},\bar{H})$ as a superposition of the normal modes[5] in an ideal guide of radius a. On taking Maxwell's equations, multiplying by $\bar{h}_\mu^{\pm}$ or $\bar{e}_\mu^{\pm}$, integrating by parts over the guide cross section and adding we find

$$\int\int_s (\nabla\times\bar{E} = -j\omega\mu_0\bar{H})\cdot\bar{h}_\mu^{\pm}\,ds + \int\int_s (\nabla\times\bar{H} = j\omega\epsilon_0\bar{E})\cdot\bar{e}_\mu^{\pm}\,ds$$

reduces to

$$\frac{\partial}{\partial z}A_\mu^{\pm}(z) = \pm\frac{1}{2}\left\{\oint_{r=a}\bar{E}\times\bar{h}_\mu^{\pm}\cdot\hat{r}\,dl + \oint_{r=a}\bar{H}\times\bar{e}_\mu^{\pm}\cdot\hat{r}\,dl\right\} \tag{51}$$

We now apply the boundary condition in (1) at $r = a + \epsilon\rho_1(\phi,z)$. For any initial field $\bar{E}_0$, $\bar{H}_0$ in undistorted guide the distortion $\epsilon\rho_1$ yields a distorted field $\bar{E}$, $\bar{H}$ to first order of

$$\begin{aligned} \bar{E} &= \bar{E}_0 + \epsilon\bar{E}_1 \\ \bar{H} &= \bar{H}_0 + \epsilon\bar{H}_1 \end{aligned} \tag{52}$$

At $r = a + \epsilon\rho_1$ we have to first order from (40)

$$\frac{1}{a}\frac{\partial\rho_1}{\partial\phi}E_{0r} + \rho_1\frac{\partial E_{0\phi}}{\partial r} + E_{1\phi} = Z_\phi\left\{\frac{\partial\rho_1}{\partial z}H_{0r} + \rho_1\frac{\partial H_{0z}}{\partial r} + H_{1z}\right\} \tag{53}$$

$$\frac{\partial\rho_1}{\partial z}E_{0r} + \rho_1\frac{\partial E_{0z}}{\partial r} + E_{1z} = -Z_z\left\{\frac{1}{a}\frac{\partial\rho_1}{\partial\phi}H_{0r} + \rho_1\frac{\partial H_{0\phi}}{\partial r} + H_{1\phi}\right\}$$

From (51) we need to determine

$$[\bar{E}\times\bar{h}_\mu^{\mp} + \bar{H}\times\bar{e}_\mu^{\mp}]|_{r=a}\cdot\hat{r}$$

On substituting [from (52)] for $\bar{E}$ and $\bar{H}$ and using boundary conditions (40) at $r = a$ for $\bar{E}_0$ and $\bar{H}_0$ we find

$$[\bar{E}\times\bar{h}_\mu^{\mp} + \bar{H}\times\bar{e}_\mu^{\mp}]\cdot\hat{r}|_a = \epsilon[\bar{E}_1\times\bar{h}_\mu^{\mp} + \bar{H}_1\times\bar{e}_\mu^{\mp}]\cdot\hat{r}|_a \tag{54}$$

The right-hand side of (54) may be reduced to terms containing only $\bar{E}_0$, $\bar{H}_0$, and $\bar{h}_\mu^{\mp}$ by expanding and substituting for $(E_{1\phi} - Z_\phi H_{1z})$ and $(E_{1z} + Z_z H_{1\phi})$ from (53).

On letting

$$\bar{E}_0 = \sum_\nu A_\nu\bar{e}_\nu \quad\text{and}\quad \bar{H}_0 = \sum_\nu A_\nu\bar{h}_\nu^{-}$$

we finally obtain a system of coupled equations of the form

$$\frac{\partial}{\partial z}A_\mu^+(z) = \sum_\nu K_{\mu\nu}^{(+,+)}A_\nu^+(z)e^{j(h_\mu - h_\nu)z} + K_{\mu\nu}^{(+,-)}A_\nu^-(z)e^{j(h_\mu+h_\nu)z} \tag{55}$$

Only forward coupling is significant as $h_\nu \approx h_\mu$ and we need concern ourselves only with the forward coupling coefficient, $K_{\mu,\nu}^{(+,+)}$ which is of the form

$$K_{\mu,\nu}^{(+,+)} = \frac{1}{2}\int_0^{2\pi}\epsilon\left\{-h_{\mu\phi}\left[\frac{\partial\rho_1}{\partial_z}e_{\nu r} + \rho_1\frac{\partial e_{\nu z}}{\partial r} + Z_z\left(\frac{1}{a}\frac{\partial\rho_1}{\partial\phi}h_{\nu r} + \rho_1\frac{\partial h_{\nu\phi}}{\partial r}\right)\right]\right.$$

$$\left. + h_{\mu z}\left[-\frac{1}{a}\frac{\partial\rho_1}{\partial\phi}e_{\nu r} - \rho_1\frac{\partial e_{\nu\phi}}{\partial r} + Z_\phi\left(\frac{\partial\rho_1}{\partial z}h_{\nu r} + \rho_1\frac{\partial h_{\nu z}}{\partial r}\right)\right]\right\}a\,d\phi \tag{56}$$

This is similar to Unger's[15] result for helix waveguide ($Z_\phi = 0$) coupling coefficients but contains several additional terms.

$K_{\mu,\nu}^{+,+}$ is the coupling coefficient for displacement of the waveguide walls from a right circular cylinder. If $\rho_1(\phi,z)$ is of the form

$$\epsilon\rho_1(\phi,z) = \epsilon \cos \phi f(z)$$

we can determine the curvature coupling coefficient ($C^{+,+}_{\mu,\nu}$) from $K^{+,+}_{\mu,\nu}$ as in Rowe and Warters. Since the curvature $1/R(z)$ is approximately equal to $-\epsilon f''(z)$ we have

$$C^{(+,+)}_{\mu,\nu} = K^{(+,+)}_{\mu,\nu}/[j(h_\mu - h_\nu)]^2 \tag{57}$$

This is the normalized curvature coupling coefficient referred to in the main text of this paper.

REFERENCES

1. D. A. Alsberg et al., "WT4 Millimeter-Wave Transmission System Overview," B.S.T.J., this issue.
2. R. D. Tuminaro et al., "Waveguide Design and Fabrication," B.S.T.J., this issue.
3. S. A. Schelkunoff, "Conversion of Maxwell's Equations into Generalized Telegraphists Equations," B.S.T.J., *34,* No. 7 (September 1955), pp. 995–1043.
4. H. E. Rowe and W. D. Warters, "Transmission in Multimode Waveguide with Random Imperfections," B.S.T.J., *41,* No. 5 (May 1962), pp. 1031–1170.
5. S. P. Morgan, "Mode Conversion Losses in Transmission of Circular Electric Waves through Slightly Noncylindrical Guides," J. Appl. Phys., *21,* April 1950, pp. 329–338.
6. H. G. Unger, "Lined Waveguide," B.S.T.J., *41,* No. 3 (March 1962), pp. 745–768.
7. H. L. Kreipe and H. G. Unger, "Imperfections in Lined Waveguide," B.S.T.J., *41,* No. 7 (September 1962), pp. 1589–1619.
8. J. W. Carlin and P. D'Agostino, "Normal Modes in Overmoded Dielectric Lined Circular Waveguide," B.S.T.J., *52,* No. 4 (April 1973), pp. 453–486.
9. H. E. Rowe and D. T. Young, "Transmission Distortion in Multimode Random Waveguides," IEEE Trans. Microwave Theory Tech., *MTT-20,* June 1972, pp. 349–365.
10. J. C. Anderson et al., "Field Evaluation Trial—Medium Objectives and Results," B.S.T.J., this issue.
11. M. A. Gerdine et al., "Electrical Transmission Measurement System," B.S.T.J., this issue.
12. H. G. Unger, "Circular Electric Wave Transmission in Dielectric-Coated Waveguide," B.S.T.J., *36,* No. 7 (September 1957), pp. 1253–1278.
13. S. E. Miller, "Some Theory and Application of Periodically Coupled Waves," B.S.T.J., *48,* No. 7 (September 1969), pp. 2189–2219.
14. A. P. King and G. D. Mandeville, "The Observed 33–90 kMc Attenuation of 2-Inch Improved Waveguide," B.S.T.J., *40,* No. 7 (September 1961), pp. 1323–1330.
15. H. G. Unger, "Noncylindrical Helix Waveguide," B.S.T.J., *40,* No. 1 (January 1961), pp. 233–254.

THE BELL SYSTEM TECHNICAL JOURNAL
Vol. 56, No. 10, December 1977
Printed in U.S.A.

WT4 Millimeter Waveguide System:

Waveguide Design and Fabrication

By R. J. BOYD, JR., W. E. COHEN, W. P. DORAN, and R. D. TUMINARO

(Manuscript received April 7, 1977)

The WT4 transmission line is a 60 mm diameter string of circular waveguide sections composed of 9 m long dielectric-lined and 4.4 m long helix waveguide sections, with dielectric-lined waveguide comprising approximately 99 percent of the transmission line. The dielectric-lined waveguide is manufactured from steel tubing whose geometric distortions are controlled on a power spectral density basis. The steel tubing is processed into waveguide by the application of copper and dielectric layers along its inner bore and by the attachment of flanges at its ends. The materials system and processes were chosen for extremely low ohmic losses, minimum geometric distortions, and high long-term reliability. The helix waveguide is formed from a closely spaced array of helically wound wires cast into an epoxy system, which is in turn enclosed in a steel jacket. The key design features of this helix waveguide are (i) the specially prepared iron-loaded epoxy which provides ohmic dissipation to spurious mode energy and (ii) the precision temperature control applied to the curing of the epoxy to assure minimum geometry distortion.

I. INTRODUCTION

The waveguide medium is composed of a string of 60 mm internal diameter, 9 m long, flanged dielectric-lined and 4.4 m long helix waveguide sections. Dielectric-lined waveguide consists of a copper-plated steel tube, the inner surface of which is lined with a thin dielectric layer. Helix waveguide consists of a steel tube encompassing an insulated copper wire which is helically wound and is cast within the steel tubing with an epoxy. Dielectric-lined waveguide was selected to be the principal transmission medium, comprising approximately 99 percent of the total

waveguide length. The remainder of the transmission medium consists of helix waveguide sections deployed at 800 m intervals.

In this paper the factors leading to the choice of dielectric-lined waveguide as the principal waveguide medium will be reviewed. In addition, the designs and fabrication techniques associated with each type of waveguide will be discussed.

II. CHOICE OF DIELECTRIC-LINED WAVEGUIDE AS THE PRINCIPAL TRANSMISSION MEDIUM

Multiwavelength diameter TE_{01} circular waveguide has two classes of loss.[1,2] The first is that which would exist for a pure TE_{01} wave guided by a perfect right circular cylinder having a wall surface with finite dissipation. The second is due to the scattering of TE_{01} energy into other modes as a result of geometric imperfections in the waveguide surface. This second component can be calculated from the normal mode propagation constants, coupling coefficients, and the geometry of the waveguide.[3] Practically speaking, the type of geometric distortion that contributes the largest amount of loss is curvature of the waveguide axis.[4]

Waveguide curvature affects propagation differently in dielectric waveguide than in helix waveguide. For example, a waveguide route bend is typically constructed to have linearly varying curvature profiles at the input and output sections of the bend and a constant radius of curvature in the central section. For such a bend, it can be shown[5] that the increase in loss relative to a straight waveguide is given by a summation of terms; each of these terms is proportional to the absolute magnitude of the difference in attenuation coefficients between the TE_{01} mode and one of the spurious modes to which the TE_{01} mode is coupled when the waveguide axis is curved. Dielectric-lined waveguide is characterized by low differential attenuation constants; helix waveguide, by high differential constants. Hence, dielectric-lined waveguide has lower route bend losses than helix waveguide.

Another example which demonstrates the more tolerant behavior of dielectric-lined waveguide to curvature is that associated with unintentional curvature introduced in waveguide manufacture and installation. Although first-order average curvature losses are related to the power spectral density (PSD) of the curvature for both types of waveguide, the relationship is different for each type. In the case of dielectric-lined waveguide there is only a limited band of mechanical frequencies which gives rise to first-order mode conversion losses.[6,7] This band is from $\frac{1}{3}$ to $1\frac{1}{2}$ cycle/meter (c/m) for 60-mm waveguide as illustrated in Fig. 1. Helix waveguide, however, responds to a much larger mechanical frequency band,[8] including the high magnitude of the low-frequency curvature associated with installation.[9,10] The processes de-

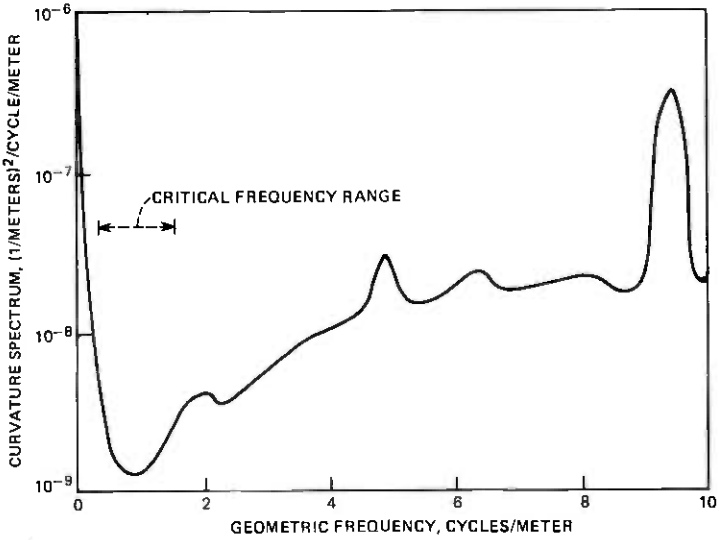

Fig. 1—Curvature spectrum of installed 60-mm waveguide.

veloped for the manufacture and installation of waveguide resulted in curvature PSDs which were lower in the ⅓ to 1 ½ c/m range than in the balance of the band. Thus, to minimize curvature losses, dielectric-lined waveguide was selected for the majority of the medium.

At the outset of the project, these advantages were recognized. However, it was also recognized that some helix waveguide would have to be deployed in order to limit the amount of reconverted spurious-mode energy and its attendant transmission distortion. Initially a 90%/10% mixture of dielectric-lined/helix waveguide was believed to be reasonable. However, improvements in the curvature of installed waveguide reduced spurious mode levels, permitting the use of less helix. The ratio was changed to 99%/1%.

The choice of waveguide system described above led to a decision to concentrate heavy effort on achieving a dielectric waveguide design which had an extremely low curvature spectrum over the limited mechanical frequency band. The helix design concentrated on the efficient absorption of the spurious modes rather than on achieving ultra-low TE_{01} helix loss.

III. DIELECTRIC-LINED WAVEGUIDE

3.1 General Considerations

The configuration of dielectric-lined waveguide is shown in Fig. 2. The principal structural element consists of a 60-mm internal diameter steel

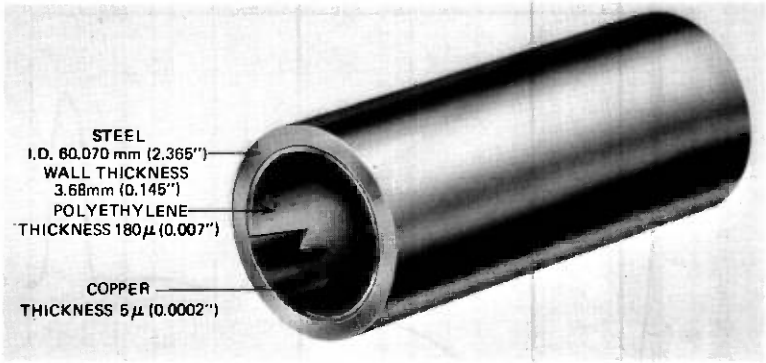

Fig. 2—Dielectric-lined waveguide configurations.

tube. The inner surface of the steel tube is plated with copper to which a thin layer of polyethylene is subsequently bonded.

This particular design was intended to provide an approximate balance of the heat and mode conversion components of loss over the 40 to 110 GHz frequency band, as shown in Fig. 3. (The loss at high and low ends of the bands are not made exactly equal since system balance requires lower transmission line loss at the high end of the band in view of the poorer solid state device performance at high frequencies.) In addition, the design had to be compatible with manufacturing technology, reliability objectives, and the installation techniques which were being developed in parallel with the waveguide. Finally, the overall program had to be carried out economically so waveguide costs would compare favorably to other technologies in new high-capacity routes.

The steel tube shown in Fig. 2 was chosen for waveguide manufacture. Other materials such as copper and aluminum were ruled out on the basis of technical performance and economics. It was found that steel tubing could be made to have extremely low power spectral densities over the critical mechanical frequency regions, not only for curvature, but also for diameter, ellipticity, and other forms of geometric distortion. It also provided rigidity and strength, making the waveguide medium difficult to damage. It lent itself to plating techniques and is dimensionally stable. Finally the use of steel was completely compatible with welding techniques, thereby permitting the use of welded flanges to facilitate the joining of contiguous waveguide sections.

The use of copper as a conducting surface over the steel substrate was based primarily on achieving low ohmic loss, while at the same time achieving a high degree of reliability. The two metallic elements with the highest conductivity are silver and copper, with copper having a conductivity of 0.97 that of silver. Offsetting this slight advantage of silver is the fact that silver is more vulnerable to sulfide attack from the

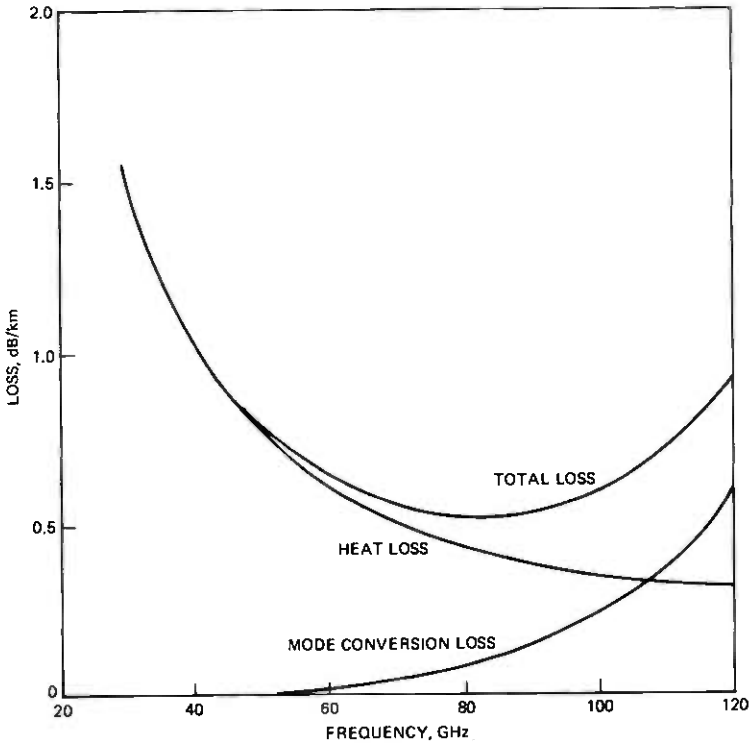

Fig. 3—Waveguide loss components.

atmosphere than copper. Thus the possibility of attack during manufacture and storage prior to installation weighed heavily against choosing silver. Finally, copper could be directly deposited in a dense, high-purity layer on the steel surface by electrolytic means.

The purpose of the dielectric liner is to break the degeneracy between the TE_{01} and curvature coupled TM_{11} modes. In idealized waveguide having infinitely conducting metallic walls, both the TE_{01} and TM_{11} modes have identical propagation constants. In waveguides with metallic walls having finite conductivity, the attenuation portions of the propagation constant for the two modes are different, but the phase portions of the propagation constants are almost equal. This situation makes simple copper-walled waveguide intolerant to bends. Low-loss propagation in bends can be achieved if the phase constants of the TE_{01} and TM_{11} modes are significantly different. One method of achieving the desired separation of the phase constants of these two modes is by application of a dielectric liner to the conducting wall. This liner has a pronounced effect on the propagation constant of the TM_{11} mode and a much lesser effect on the propagation constant of the TE_{01} mode.[11,12,13]

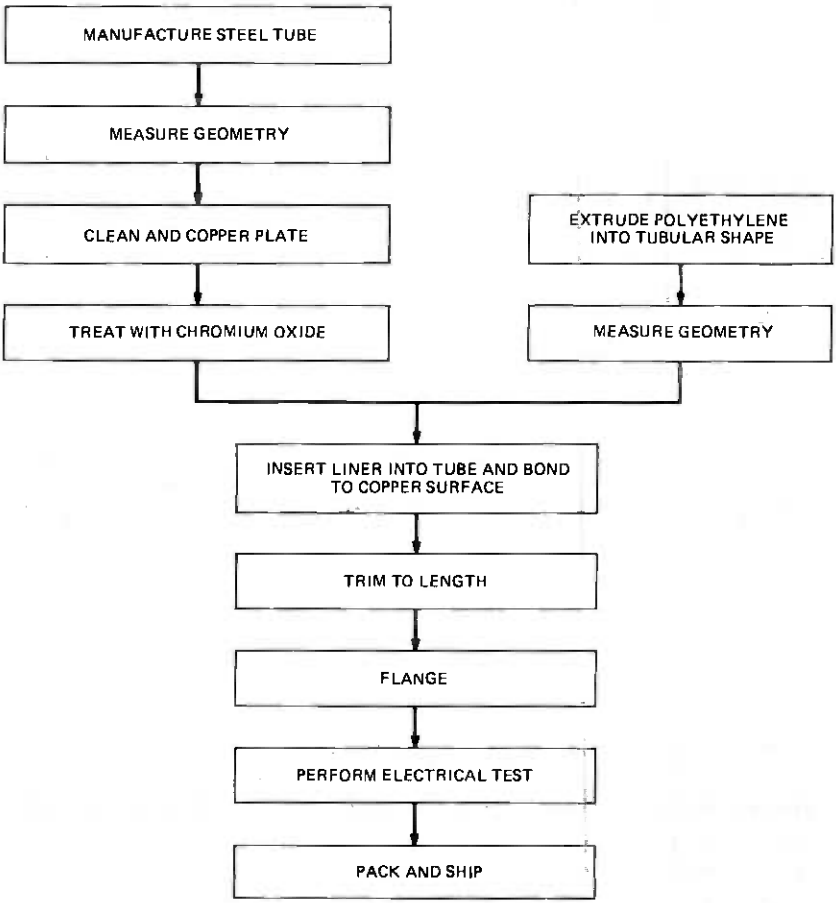

Fig. 4—Manufacturing process for dielectric-lined waveguide.

The choice of polyethylene for the dielectric liner was made for a variety of reasons. First, when free of all additives except antioxidants, polyethylene has an extremely low loss tangent over the 40 to 110 GHz band. Second, the particular polyethylene composition used in waveguide is one that had been used for many years in Bell System submarine cable applications; the submarine cable experience had shown that this particular composition was extremely stable chemically, even when bonded to copper for long periods of time. Third, polyethylene liner material could be made into prefabricated thin-walled tubing using modified commercially available extrusion techniques.

The foregoing discussion has reviewed, in general terms, the choice of waveguide configuration for dielectric-lined waveguide. In the paragraphs that follow, attention will be focused on specific elements of the

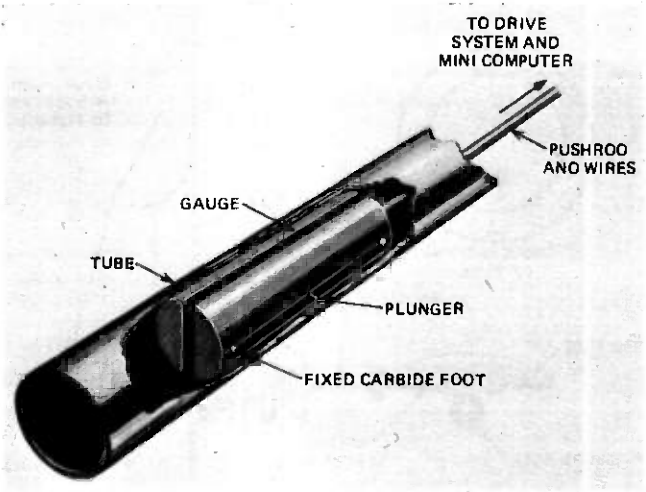

Fig. 5—Mouse.

dielectric waveguide design. To facilitate this discussion, reference is made to Fig. 4, which depicts the manufacturing process. Each of the key elements of the process will be reviewed along with performance data achieved for each of the processes.

3.2 Steel tubing

A number of commercially available steel tubing processes were analyzed to determine their suitability for waveguide. This evaluation consisted of having 2 inch or 51 mm diameter steel tubes fabricated at commercial facilities under scrutiny of Bell System engineering personnel, and measuring the resultant internal curvature and diameter with a gauge called a mouse (Fig. 5).[14] The output of the mouse was converted into curvature and diameter PSDs.

In this exploratory phase, it was soon recognized that each particular process had its own characteristic signature. It was also noticed that various periodicities revealed by the PSD plots could be related to periodic anomalies introduced by different components of the machinery that manufactured the steel tubes.

Of several commercial steel tube manufacturing methods investigated, one had significantly lower curvature PSD in the critical $\frac{1}{3}$ to $1\frac{1}{2}$ c/m range. This method, illustrated in Fig. 6, is the drawn-over-mandrel process (DOM). Flat steel strip is formed into a cylinder and welded longitudinally to form a tube. After a full anneal, the tubes are cold-drawn over a mandrel. They are then roller-straightened twice. Except for the double straightening, this is a standard commercial process.[15]

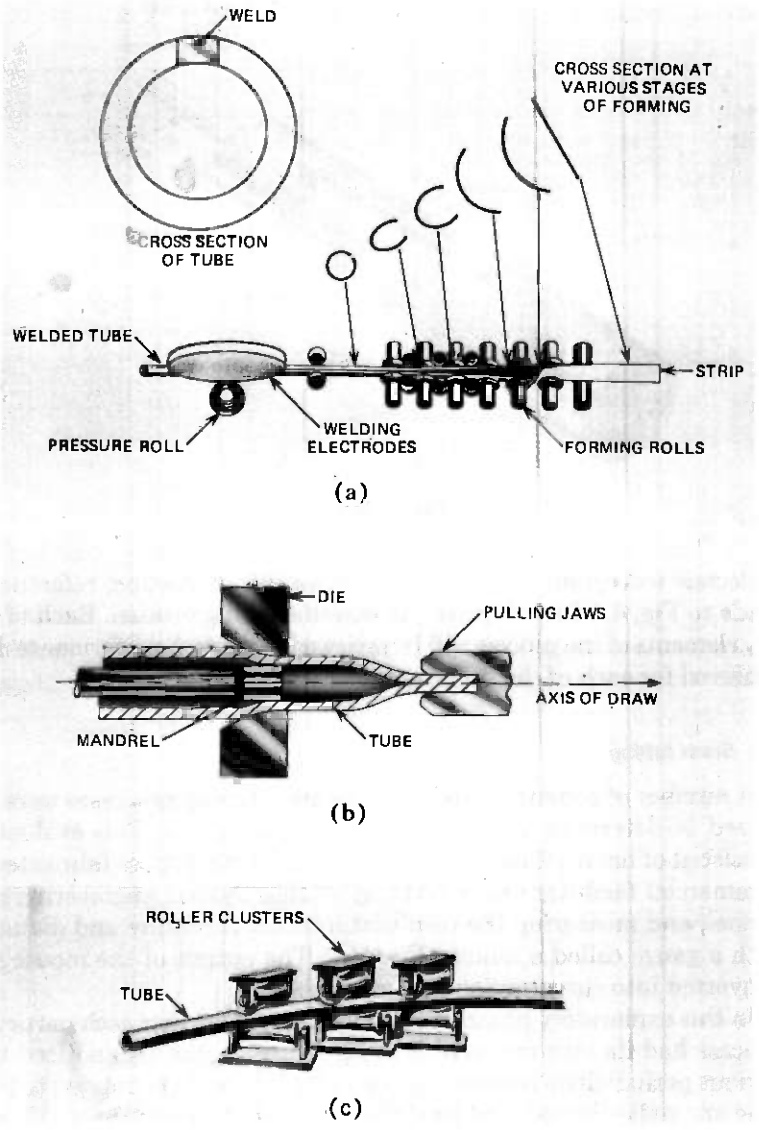

Fig. 6—Manufacturing process for steel tube. (a) Tube forming and welding. (b) Cold drawing. (c) Roller straightening.

To make waveguide-quality tubing, equipment tolerances were tightened and operating parameters were carefully controlled.

The types of tubing material that were considered were rimmed and aluminum-killed low carbon steel. Aluminum-killed was selected instead of rimmed to avoid impurity blow-out problems that could have occurred

in the high-vacuum electron beam welding of the flanges to the tubes. (Flanging will be discussed later.) Steel having a 0.1 percent carbon content (1010 steel) was selected because it could be easily formed and cold drawn, would maintain long-term dimensional stability, was readily plateable, and is relatively free of martensite formation during the flange welding operation. Experiments on the drawing operation focused on the sensitivity of tube geometry to changes in operating conditions. A 3-milliradian misalignment of the draw and die axes produced tubes with long curvature bows of 200-meter radius. The tubes also had slightly higher curvature PSD in the 0 to 10 c/m range than tubes with aligned axes. No effect on curvature was seen when the axes were offset up to 3 mm. Tubes that were drawn on chain benches loaded to greater than 80 percent of drawing capacity had curvature spikes corresponding to the length of the chain links. These geometric distortions were controlled by carefully aligning a bench with sufficient drawing capacity. In addition, the maintenance of tight tolerances in the draw bench tooling is essential to achieving a round tube with the proper final diameter.

The final processing step for steel tubing is the straightening operation. Simply stated, the machine operates by imparting both longitudinal and rotary motion to the tube, with the center roll cluster offset from the imaginary straight line path extending between the end roll clusters. In this manner a beam bending action is provided. The degree of center roll cluster displacement relative to the end rolls is such that a straight section of tubing passing through the machine is deformed elastically and hence remains straight, while a curved section is bent beyond its elastic limit and springs back to a straight configuration after passing through the machine.

Roller straightener configurations other than the six roll cluster, which is shown in Fig. 6, were studied. The six roll cluster was found to be most desirable because the tube was supported on opposing sides at each cluster. The squeezing action of the opposing rolls substantially reduced the ellipticity of the drawn tubes.

The double roller straightening was primarily responsible for the low curvature PSD in the mechanical frequency range of $\frac{1}{3}$ to 1 $\frac{1}{2}$ c/m. However, due to high stresses at the contact area, a helical deformation at 9 c/m was introduced. Engineers at Western Electric Engineering Research Center designed contoured rolls that increased the roll-tube contact area, thus reducing the contact stresses and the resultant PSD spike at 9 c/m. Further reductions in the level of the spike were achieved by altering the temper of the tube by eliminating the prestraightening anneal and by improving drawn straightness and roundness. The curvature PSD of the tubes, both before and after straightening, is shown in Fig. 7.

Steel tubing development started with the objective of producing

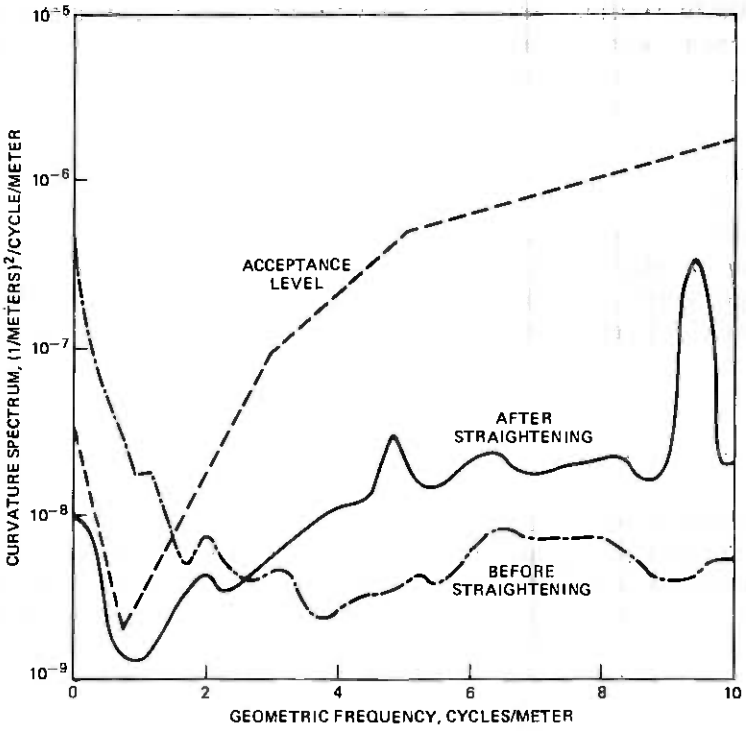

Fig. 7—Steel tubing curvature.

51-mm internal diameter tubes that were 5 meters long. For 51-mm tubing, the critical mechanical frequency band associated with curvature was from ½ to 2 c/m. It was found that curvature could readily be controlled not only in this band, but even at lower mechanical frequencies corresponding to ⅓ c/m. Indeed with the low curvatures that were being obtained, it was found that most of the losses were ohmic, not mode conversion, and that the repeater spacing was limited by waveguide ohmic losses at the lower frequencies. By increasing the inner diameter to 60 mm, these ohmic losses were reduced. Since the 60 mm tubes still had low curvature PSD levels in the now critical ⅓ to 1 ½ c/m range, the losses were brought into balance resulting ultimately in a repeater spacing of 50–60 km for the commercial 38–104.5 GHz system instead of the initial objective of 33 km.[16] Experiments showed that the tubing length could be increased to 9 meters—the maximum length that could then be processed—without sacrificing quality. This resulted in fewer joints and reduced construction costs. Thus 60-mm, 9-meter-long dielectric tubes were used in the field evaluation test. Subsequent experiments have demonstrated that 10 ½-meter-long tubes can be produced without loss of quality.

The tube-forming operation leave residual stresses in the tubes in both the circumferential and longitudinal directions. Experiments indicated that the stress relief expected over the lifetime of the tube would result in negligible distortions.

The steel tubes used in the field evaluation test were manufactured by Babcock & Wilcox Co., Alliance, Ohio, in cooperation with Bell System personnel. All tubes produced were inspected at the mill by Western Electric engineers. The inspection consisted of "mouse" measurements of curvature and diameter. An on-line computer was used to compute the curvature PSD. The acceptance rate was 70 percent.

After copper plating, samples of the tubes were measured with the rotary-head mouse for more detailed analyses of geometry.[17,18] A summary of the geometry spectra of the principal components of distortion achieved for the final 60-mm waveguide used in the field evaluation test is shown in Fig. 8. In this figure the different circular harmonic components of geometric distortion are presented in terms of power spectral density functions. It can be seen, that the zero foil (Fig. 8a) objective is easily met with a large margin. On the other hand, the other distortion components (Fig. 8b, c, d) exceed the objective at certain mechanical frequencies. Allowances for these higher spectral responses have been made in the administration of the overall loss budget and geometry specifications for the steel tube.

3.3 Copper plating

Copper plating was required to deposit a highly conductive layer on the inner surface of the steel tube. The objectives in the plating development were to: (*i*) achieve the highest possible conductivity, (*ii*) provide a uniform layer of copper, and (*iii*) present a reliable bond to the steel substrate and be receptive to the polyethylene layer.

At the outset of the program, various methods for plating were considered. These included electroless plating, the use of a nickel layer followed by an electrolytically deposited acid copper layer, etc. The results of scanning electron microscope studies, coupled with the desirability of achieving the plating with a single electrolyte, favored the use of the alkaline copper cyanide electrolytic chemistry applied with the setup shown in Fig. 9. This particular system yielded a copper plating performance that exceeded our original objectives. It has been found that the ratio of measured loss to theoretical loss for this plating is given by the following empirical equation:[19]

$$\frac{\alpha_{\text{meas}}}{\alpha_{\text{theory}}} = 1 + 0.2\left(\frac{f}{100}\right)^{1.5}$$

where f is the electrical frequency in GHz. It is emphasized that the above

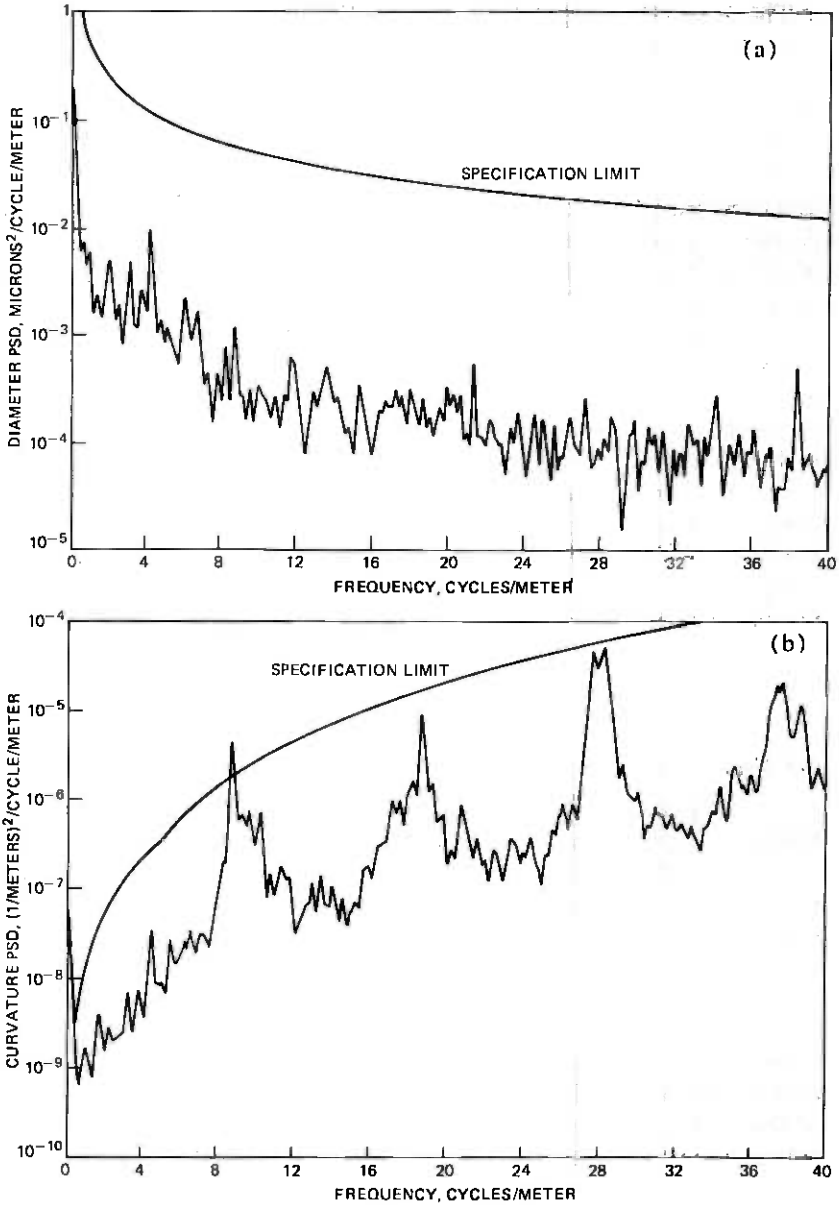

Fig. 8—Measured geometry spectra of dielectric-lined waveguide: (a) diameter, (b) curvature, and on opposite page (c) ellipticity, (d) trifoil.

equation translates to a loss that is only 6 percent higher than theoretical at 40 GHz. Further, this loss was achieved on a production basis, and has been found to be completely stable over a three-year testing period.

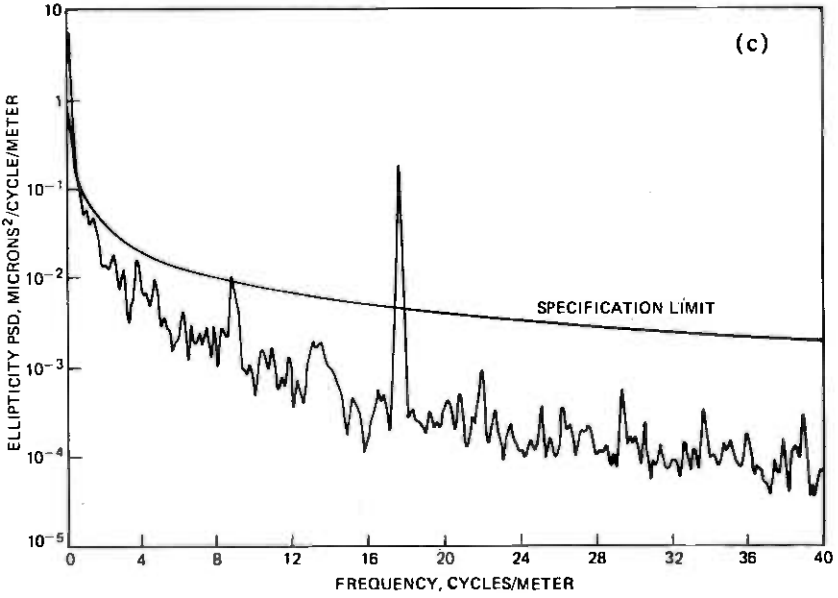

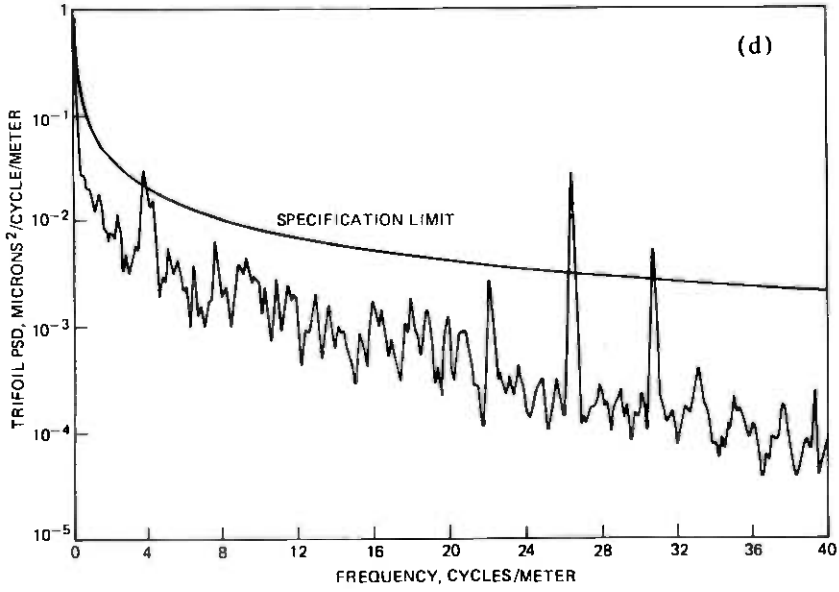

In addition to achieving high conductivity, the peculiar needs of the waveguide system led to the selection of additional plating requirements. Copper, even at the lowest frequency used in the system (40 GHz), has a skin depth of approximately ⅓ micron. Since only about 5 skin depths are needed to support propagation inside the waveguide, 2 microns of

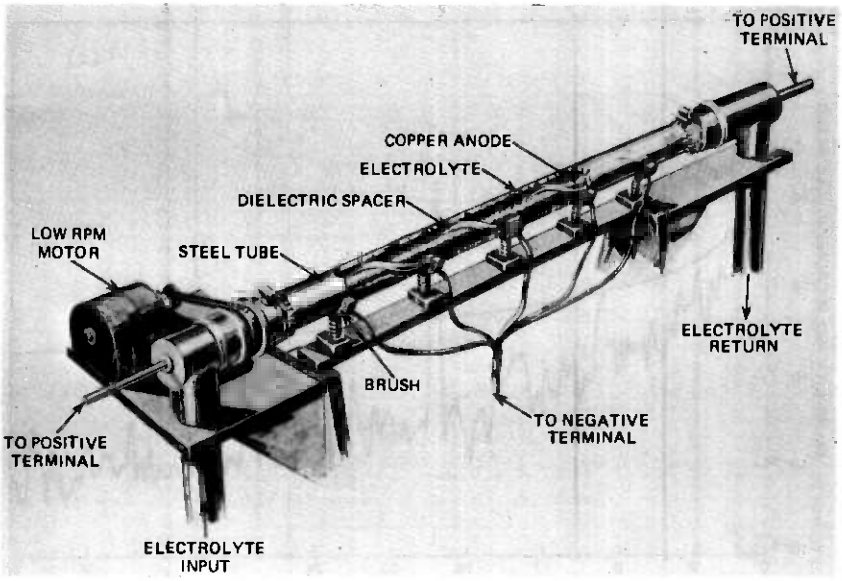

Fig. 9—Copper plating system.

plating would meet this requirements. Nevertheless, a plating thickness of approximately 5 microns was deemed to be optimal. With this thickness, the plating was for the most part free of porosity and was found to be adequate to cover most of the microscopic imperfections in the steel substrate. Thicker platings, such as the 15-micron coating used at the outset of the program, actually degraded the quality of the waveguide product. This degradation arose because the rotation applied to the tube to ensure a circumferentially uniform coating of copper, when combined with the gravitational sag of the anode and its helical dielectric support, resulted in an unacceptably high level of periodic diameter distortion. This periodicity was minimized by the use of a thinner plating and a slower tube rotation.

3.4 Chromium oxide layer

The previously described copper plating, when exposed to the atmosphere prior to being lined with polyethylene, will develop a very thin surface layer of cuprous oxide. Polyethylene, when bonded to this surface layer, can readily be delaminated at the ends of the waveguide tube in the presence of moisture. The electrolytic application of a thin chromium oxide layer to the copper surface prevents atmospheric attack and the formation of a copper oxide surface layer; when used in conjunction with the other elements of the bonding system, it contributes to a highly reliable bond. The chromium oxide layer, being very thin (~20 Å), does

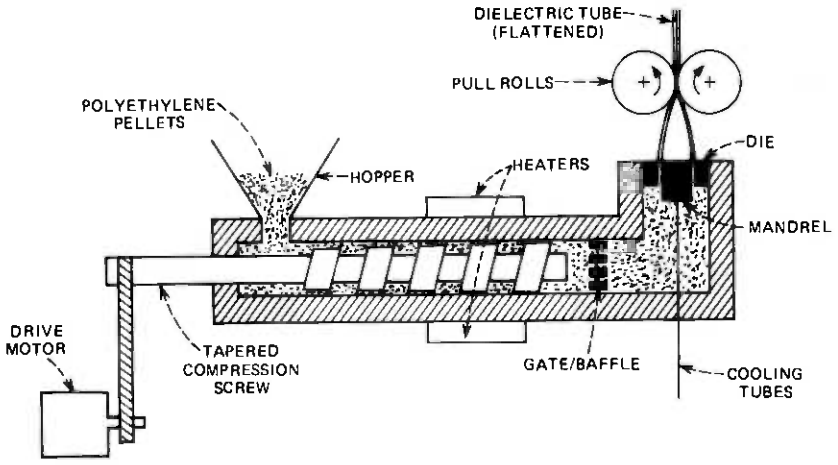

Fig. 10—Dielectric extruder.

not have to be included in the ohmic loss calculations applicable to a cylindrically stratified medium.

3.5 Dielectric lining

The dielectric material used for the manufacture of dielectric tubing is manufactured in pellet form; it contains 0.06 percent ethyl 330 antioxidant. The particular composition used has a density of 0.92 g/cm^3 and a melt index of 0.2. The transformation of pelletized polyethylene into homogeneous precision thin-walled tubing was accomplished by a commercial vendor using a heavy-duty extruder with a specially designed adjustable cross head. The very low melt index of the material required that the liquification of the pelletized material be carried out at higher-than-normal temperatures, with extensive mechanical shearing of pelletized material. The extruder system is shown schematically in Fig. 10.

During its passage through the extruder, a portion of the ethyl 330 oxidant is expended due to the combination of dissolved oxygen and high melt temperature; however, maintaining the maximum extruder temperature at or below 200°C allowed a sufficient amount of antioxidant to be present for the high-temperature copper-to-polyethylene bonding operation.

One of the major elements of the dielectric tubing program was associated with producing thin-walled tubing that satisfied the geometric PSD requirements. The most troublesome geometric component proved to be small periodic changes in thickness that occurred over entire circumferential zones as a function of length along the dielectric tube. This type of distortion, if present, generates TE_{on} modes which are not at-

tenuated by the helix mode filters. Following the experience gained in the steel tubing program, periodic pulsations associated with the dielectric processing machinery were identified and suppressed. With the machinery optimized, these thickness periodicities have a PSD which is shown in Fig. 11.

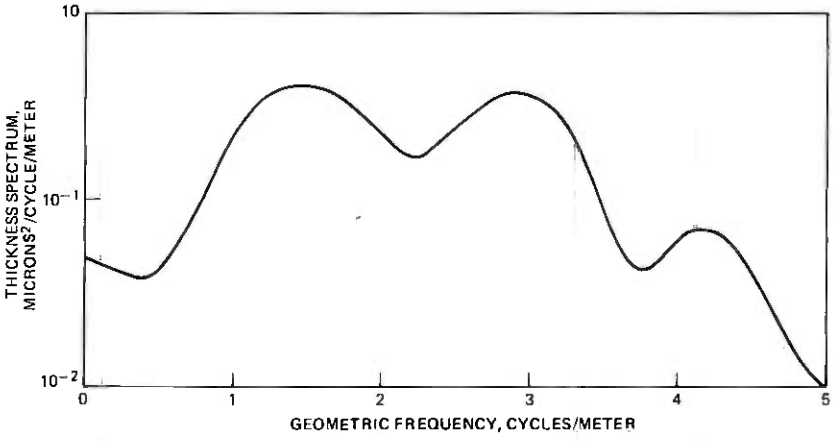

Fig. 11—PSD of dielectric tubing thickness.

The final version of the gauging used to measure dielectric tubing geometry is shown in Fig. 12. The measurement is carried out by longitudinally slitting samples of dielectric tubing and passing these samples through an array of eight pairs of differential air gauges. Changes in dielectric thickness give rise to changes in sensor pressure. These pressure changes are converted to voltage changes, which, after computer processing, yield the PSD of the thickness of dielectric tubing.

The dielectric liner thickness of 180 microns was chosen after the following parameters were analyzed: (*i*) differential phase and attenuation constants of the TM_{11} mode relative to the TE_{01} mode and their effects on route bend and installation losses; (*ii*) TE_{01} ohmic loss due to the current enhancement effect caused by the presence of the dielectric; (*iii*) TE_{01} loss due to dielectric loss tangent effects; (*iv*) sensitivity to mode conversion effects due to dielectric thickness distortions; and (*v*) liner tubing manufacturability. The above analysis had shown that there is a fairly broad choice of nominal liner thickness (from approximately 150 to 200 microns) which would be compatible with system objectives; the thickness of 180 microns was chosen because it appeared to be not only close to the midpoint of the broad optimum range, but also because it presented fewer difficulties in the liner manufacturing and subsequent bonding operations.

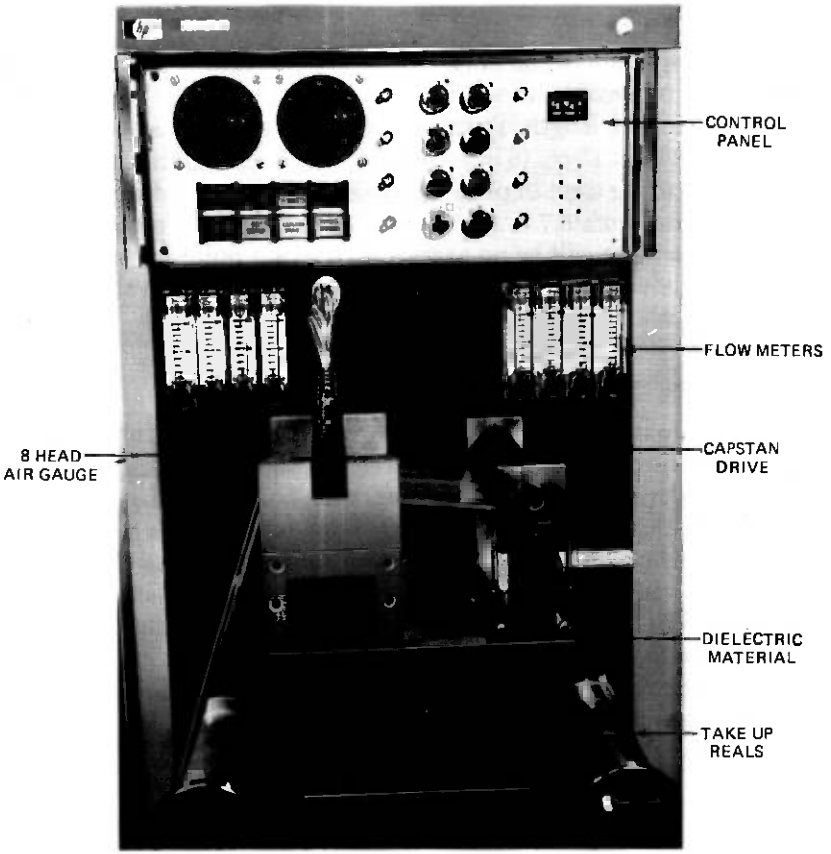

Fig. 12—Dielectric thickness gauge.

3.6 Dielectric bonding

The details of the dielectric bonding philosophy have been reported elsewhere.[20] Accordingly, only the following brief summary is included in this paper. The previously described liner tubing is subjected to a corona discharge prebond treatment at the regions corresponding to the ends of the tubing; this treatment enhances the bondability of the liner. The liner tubing is introduced into the copper-plated and chromated steel tube. The annular region between the outer surface of the dielectric liner and the inner surface of the plated steel tube is evacuated, and high-purity nitrogen is introduced inside the dielectric liner tubing. The assembly is raised to a temperature of 300°C, effecting a high-strength bond between the dielectric and metallic tubes. This system meets all requirements—low ohmic loss, bond integrity even in the presence of moisture and temperature cycling, and manufacturability.

3.7 Trim to length

After completion of the lining operation, the tube is moved into the mechanical processing area where the first operation is trimming the waveguide ends to length. There are two purposes for this operation: (*i*) to remove at least 15 cm (6 in.) from the ends to eliminate the effects of internal fixturing used in prior operations, (*ii*) to introduce a random length varying from 8.7 to 9 m from tube to tube. The random length ensures that there will be no excessive coherent build-up of energy in the TE_{on} modes due to diameter distortions arising from the flanging system discussed below.

3.8 Flanging

Flanges are incorporated at the ends of the waveguide tubes to facilitate field joining by welding. The large precision reference surfaces of the flanges permit accurate alignment of the bores of contiguous tubes. In addition, they provide high thermal impedances to the heat flowing from the field weld toward the liner. The details of the coupling design as they evolved over the course of the waveguide project are treated elsewhere.[21] In this paper, attention will be focused only on those items which relate to waveguide manufacture.

During the course of the program three methods for joining flanges to the waveguide tubing were considered: (*i*) threading both the tube ends and the flange with an adhesive intermediate layer, (*ii*) adhesive bonding without threading, and (*iii*) electron beam welding. The first two approaches offered no long-term cost or performance advantages relative to electron beam welding; moreover, they both involved the introduction of an additional material—adhesive—whose long-term behavior under prolonged shear stress would have to be evaluated. Accordingly, electron beam welding was selected for waveguide application.

Two different approaches for fabrication of flanges and assembly to the tube prior to electron beam welding were considered. In the first method, a precision-finished machined flange was to be applied to a machined surface at each end of each section of waveguide tubing. The tolerances associated with the flange and waveguide machining would assure that proper flange alignment would be obtained after electron beam welding. The second method utilized rough flange forgings which were premachined on a numerically controlled lathe to almost final dimensions, then electron beam welded to the tube, and finish-machined to final dimensions after welding by referencing the machining operation to the waveguide bore. Both methods utilize full circumferential welds at the front face and rear portion of the flange as shown in Fig. 13. Both methods required that an expandable mandrel be inserted into the bore

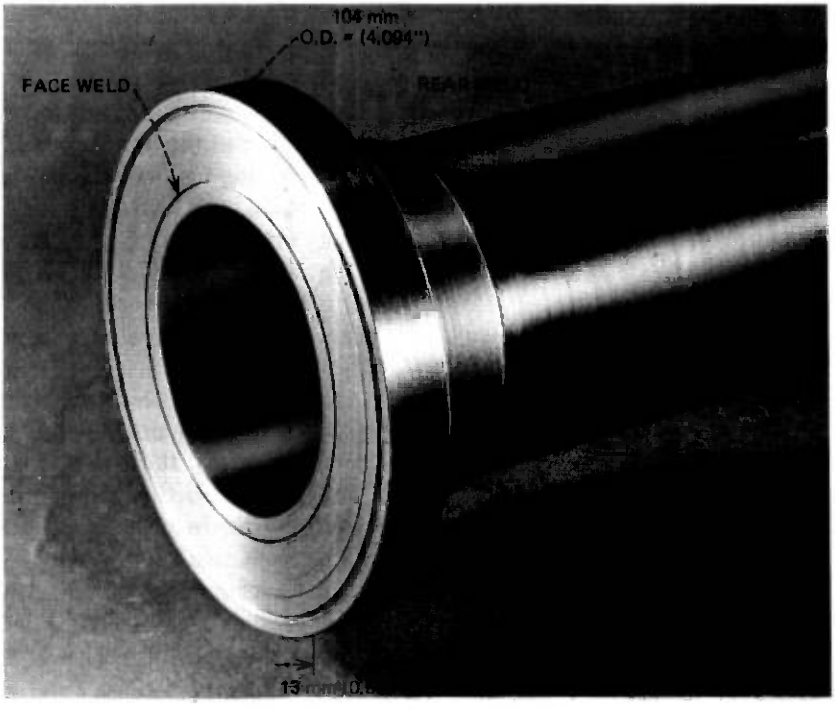

Fig. 13—Flanged end of waveguide.

of the waveguide to maintain precision alignment of the tube axis. The second method was selected since it provided better alignment tolerances.

After locating the flanges at the ends of the tube in accordance with the scheme described above, the tube ends with appropriate fixturing are inserted in a specially designed high-vacuum electron beam chamber where partial-penetration circumferential welds are applied at the face and rear of the flange. After inspection of the welds, the flanged waveguide end is fitted over a precision expandable mandrel on the lathe. Measurements indicated that for all practical purposes the mandrel axis, which was referenced to the dielectric liner, coincided with the electrical axis of the waveguide. The face of the flange is cut to the required squareness, the end of the tube which protrudes beyond the flange face is removed, and the outer diameter of the flange is cut to final dimension concentric with inner bore. The final inspection of the finished flanges showed concentricity of 50 microns, perpendicularity of 0.064 μrad and parallelism of back and front faces of 25 microns.

These tolerances yielded a tube-to-tube tilt alignment in straight waveguide sections of about 0.2 mrad rms. With 9-m waveguide lengths, this corresponds to a random component of tilt loss of 0.02 dB/km at 110 GHz. For offsets, the losses are significantly lower.

IV. HELIX WAVEGUIDE

4.1 General considerations

The dielectric waveguide described above has been designed for low mode conversion loss due to both manufacture and installation. Nevertheless, there is a certain level of mode conversion loss which must be expected, and it is the purpose of helix waveguide to absorb some of the resultant spurious mode energy, and thereby limit its reconversion back to the TE_{01} mode and the transmission degradation which results from this reconversion.

It has been previously shown that over the mechanical frequency band of approximately $\frac{1}{3}$ to $1\frac{1}{2}$ c/m, the highest level of curvature spectral density for installed waveguide occurs at the lower edge of the band. This particular mechanical spectral zone corresponds to TM_{11} and TE_{12} mode conversion at the higher electrical frequencies. At these electrical frequencies, the TM_{11} dielectric-lined waveguide mode has a field distribution which most closely resembles the TE_{11} mode in the lossy-wall helix waveguide described below. The TE_{12} dielectric lined waveguide mode resembles its TE_{12} counterpart in helix waveguide. To significantly attenuate the TM_{11} and TE_{12} modes generated by dielectric lined waveguide, it is essential to have a helix waveguide design that has high TE_{11} and TE_{12} mode losses.

In order to design a helix waveguide that meets the above requirement, the so-called wall impedance representation of waveguide has been used in theoretical modeling studies. Briefly, waveguide propagation is represented in terms of obliquely incident plane waves impinging on a reflecting and/or absorbing surface.[22,23] Thus it is customary to define two surface impedances, $Z_z = -E_z/H_\phi$ and $Z_\phi = E_\phi/H_z$; the former represents wave components having electrical fields parallel to the plane of incidence, and the latter perpendicular to the plane of incidence.

Theoretically at 110 GHz a waveguide with a longitudinal wall impedance $Z_z \approx 50\ \Omega$ will maximize the loss per unit length of the TE_{11} and TE_{12} helix modes (and by extension the TM_{11} and TE_{12} dielectric modes). A practical manufacturable configuration which provides a longitudinal impedance approximating this ideal impedance is a helix waveguide formed from closely spaced insulated wires, directly backed by a lossy material having an impedance $\sqrt{\mu/\epsilon}$ between 50 and 100 Ω.

During the course of the WT4 program, a number of lossy materials were developed and evaluated. One family of materials, carbon-coated glass, had an impedance of approximately $75 + j30\ \Omega$; another family of materials, ferrous metal particles suspended in an epoxy, had an impedance of approximately 85 Ω. Helix waveguide using these materials has the attenuation coefficients shown in Fig. 14.

Both materials described above met the electrical objectives for helix

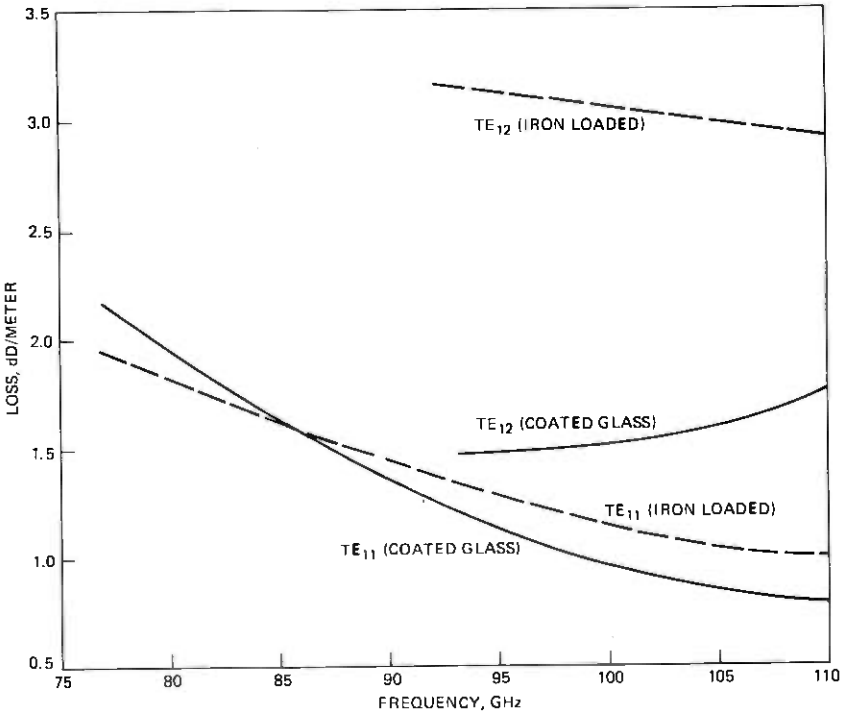

Fig. 14—Measured loss of TE_{11} and TE_{12} modes in helix waveguide.

waveguide. The coated glass material, because of its early development, was used in the field evaluation test. However, during the course of the program, the coated glass material exhibited the following shortcomings: (*i*) the rf resistivity of the coated glass strands exhibited a high degree of variability, leading to the rejection of many batches of glass; (*ii*) the individual glass filaments forming the strands exhibited breaks, which on many occasions caused the helix processing machinery to jam. For these reasons, the use of carbon-loaded glass material in helix waveguide fabrication was abandoned after the field evaluation test. The iron-loaded epoxy system described below has been selected for future waveguide applications.

4.2 Helix process

Iron-loaded epoxy helix waveguide has the finished nominal dimensions shown in Fig. 15. This waveguide can be seen to consist of a helical layer of insulated copper wire impregnated with a conformal low-loss epoxy dielectric. This is followed by a high-loss iron-loaded epoxy layer. The entire spectrum of electrical materials is contained in a flanged steel

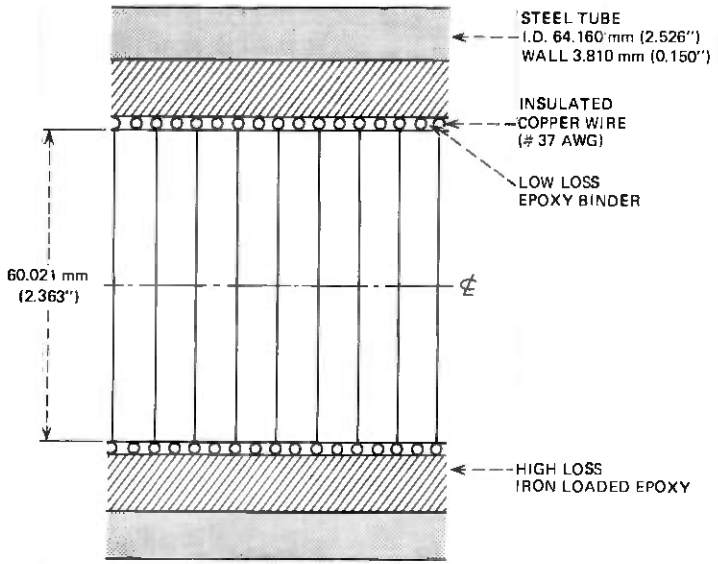

Fig. 15—Helix cross-sectional geometry.

jacket. In this structure, the insulated wire provides circumferential conductivity required for the propagation of the TE_{01} mode. The low-loss epoxy surrounding the helical wires serves as a barrier blocking the flow of high-loss iron-loaded epoxy to the interstices of the wires during the fabrication process; this layer is necessary for low TE_{01} loss. The high-loss iron-loaded epoxy has a wave impedance of approximately 85 Ω and serves to absorb spurious mode energy in accordance with the objectives depicted in Fig. 14. The steel tubing serves as the mechanical strength member of the waveguide. Finally, the flanges permit the welded joining of contiguous sections of either helix or dielectric-lined waveguide.

The basic helix process flow shown in Fig. 16 will now be briefly reviewed. Steel tubes are manufactured to straightness requirements of best commercial tolerance. This steel tube is degreased and flanged via the electron beam welding process described for dielectric waveguide.

In parallel with the steel tubing preparation, a mandrel is cleaned, coated with a mold release agent, and then coated with a thin layer of low-loss epoxy. While still wet with low-loss epoxy, the mandrel is covered with a helical wrap of insulating wire and the low-loss epoxy oozes through the interstices between the wires. The excess low-loss epoxy is wiped conformal to the wire layer and the epoxy is allowed to gel (complete curing is undesirable, because a poor bond would result between the low-loss and iron-loaded high-loss epoxy layers). This mandrel is loaded into the prepared flanged steel tubing, and special pressure fittings are applied at both ends of the assembly.

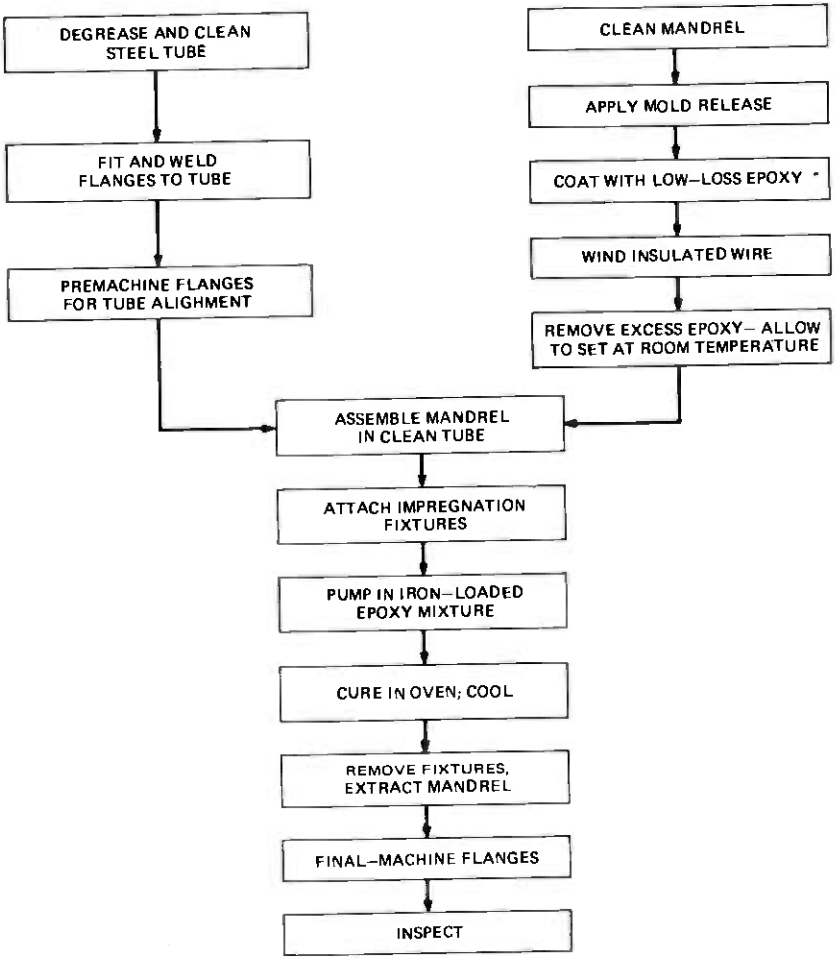

Fig. 16—Helix processing sequence.

A vacuum is applied to one end of the assembly and a heated mixture of iron-loaded epoxy is injected under pressure to the opposite end. When the entire annular region between the wire-loaded mandrel and the steel jacket is filled with iron-loaded epoxy, the pressure fittings at both ends of the tube are sealed off and the entire assembly is placed in an oven to cure under pressure and temperature conditions shown in Fig. 17. In this process both the pressure and temperature parameters have been found to be extremely important in terms of assuring an acceptable final geometry. In the case of pressure, only the initial pressure is set by the epoxy injection machinery. The remaining portion of the pressure curve is determined by the heating and curing stages of the epoxy. In the case of temperature, it has been found to be absolutely imperative to

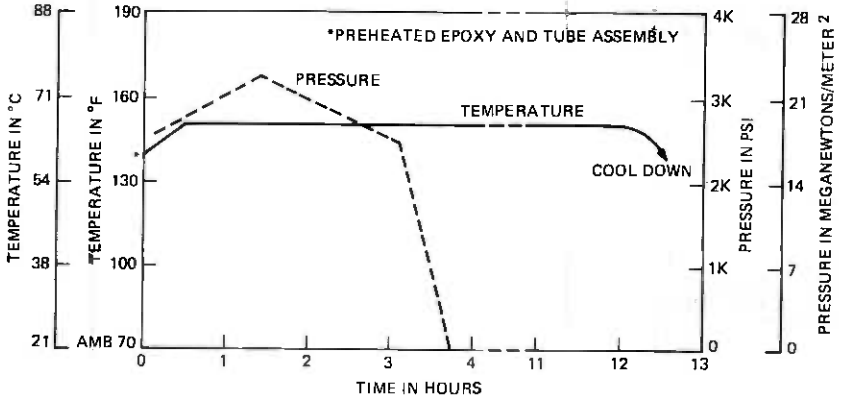

Fig. 17—Iron-loaded epoxy cure cycle.

maintain every portion of the tube within $3\frac{1}{3}$°C; if two portions of the waveguide have different time-temperature profiles, significant geometrical distortions result.

Following the epoxy cure, the mandrel is extracted from the assembly. The flanges are finish-machined in a manner similar to that used for dielectric-lined waveguide.

V. SUMMARY

This paper has reviewed the design philosophies and fabrication implementation of both the dielectric-lined and helix waveguide. Both types of waveguide have received extensive electrical testing and accelerated age stressing. Both have been shown to be readily manufacturable and durable, and can be expected to retain their properties over the typical 40-year life of underground transmission media.

VI. ACKNOWLEDGMENTS

The developments cited in this paper are the results of a large number of contributions at both Bell Laboratories and Western Electric Co. In particular, the authors would like to make note of the contributions by the Western Electric Engineering Research Center for the dielectric-lined waveguide manufacturing process, and to members of the Bell Laboratories materials research laboratories for their consultations during the course of the program.

REFERENCES

1. M. Tanenbaum, "Materials—The Media and the Message," Met. Trans., March 1976.
2. W. P. Doran and R. D. Tuminaro, "Waveguide Medium Design," 1976 International Conference on Communications Conference Record, *1*, June 1976.

3. H. E. Rowe and W. D. Warters, "Transmission in Multimode Waveguide with Random Imperfections," B.S.T.J. *41*, No. 5 (May 1962), pp 1031–1170.
4. H. E. Rowe and W. D. Warters, Op cit.
5. H. G. Unger, "Normal Mode Bends for Circular Electric Waves," B.S.T.J., *36*, No. 7 (September 1957), pp. 1292–1307.
6. W. P. Doran and R. D. Tuminaro, Op cit.
7. J. W. Carlin, and S. C. Moorthy, "Waveguide Transmission Theory," B.S.T.J., this issue.
8. D. T. Young, "Effects of Differential Loss on Approximate Solution to the Coupled Line Equations," B.S.T.J., November 1963.
9. J. C. Anderson, R. W. Gretter, T. J. West, "Route Engineering and Sheath Installation," B.S.T.J., this issue.
10. H. A. Baxter, W. M. Hauser, D. R. Rutledge, "Waveguide Installation," B.S.T.J., this issue.
11. W. P. Doran and R. D. Tuminaro, op cit.
12. J. W. Carlin and P. D'Agostino, "Normal Modes in Over Moded Dielectric Lined Circular Waveguide," B.S.T.J., *52*, No. 4 (April 1973), 487–496.
13. H. G. Unger, "Circular Electric Wave Transmission in Dielectric-Coated Waveguide," B.S.T.J., *36*, No. 7 (September 1957), pp. 1253–1278.
14. S. Harris, P. E. Fox, and D. J. Thomson, "Mechanical Gauging Techniques," B.S.T.J., this issue.
15. Welded Steel Tubing Institute, *Handbook of Welded Steel Tubing*, 1967.
16. D. A. Alsberg, J. C. Bankert, and P. T. Hutchison, "The WT4/WT4A Millimeter-Wave Transmission System," B.S.T.J., this issue.
17. D. J. Thomson, "Spectrum Estimation Techniques for Characterization and Development of WT4 Waveguide," B.S.T.J., this issue.
18. S. Harris, P. E. Fox, D. J. Thomson, op cit.
19. J. C. Anderson, J. W. Carlin, D. J. Thomson, T. J. West, "Field Evaluation Test—Trans mission Medium Achievements." B.S.T.J., this issue.
20. R. D. Tuminaro, G. J. Martyniak, E. Schultz, E. J. Wicks, "Design and Reliability of the Copper-Dielectric Bonding System for Dielectric Lined Waveguide," London—IEE Conference on Millimetric Waves, November 1976.
21. R. W. Gretter, R. P. Guenther, M. Lutchansky, D. Olasin, A. B. Watrous, "Mechanical Design of Sheathed Waveguide Medium," B.S.T.J., this issue.
22. J. W. Carlin, P. D'Agostino, op cit.
23. H. G. Unger, "Lined Waveguide," B.S.T.J., *41*, No. 3 (March 1962), pp. 745–768.

THE BELL SYSTEM TECHNICAL JOURNAL
Vol. 56, No. 10, December 1977
Printed in U.S.A.

WT4 Millimeter Waveguide System:

Mechanical Design of Sheathed Waveguide Medium

By R. W. GRETTER, R. P. GUENTHER, M. LUTCHANSKY, D. OLASIN, and A. B. WATROUS

(Manuscript received April 7, 1977)

The mechanical design of the sheathed waveguide medium for the WT4 System provides means for the fusion joining of waveguide modules into a continuous transmission line and for limiting the distortions added by the joining and installation processes. In addition the fusion-joined steel sheath guarantees a much higher degree of protection for the medium than is present in any of the existing long-haul transmission lines. A summary of the development program of the sheathed waveguide medium used in the recent field evaluation test is presented herein. Results are given of the study conducted to establish the welding procedures used and steps in the evolution of the welded coupling design are reviewed. A discussion is given of the behavior of the two-stage mechanical filter that attenuates the effects of the irregular soil forces acting on the sheath. Estimates of the field test losses attributable to the joining and installation processes are also given.

I. INTRODUCTION

1.1 Sheathed medium components

The installed WT4 transmission medium is composed of four basic mechanical elements; the outer sheath, supports for the waveguide within the sheath, the waveguide couplings, and the cylindrical waveguide tubing (Fig. 1).

The outer sheath is a steel pipe manufactured by conventional methods and coated with a layer of polyethylene extruded over a black mastic undercoating. In addition to filtering the effects of irregular earth forces on the installed medium, the sheath affords protection for the

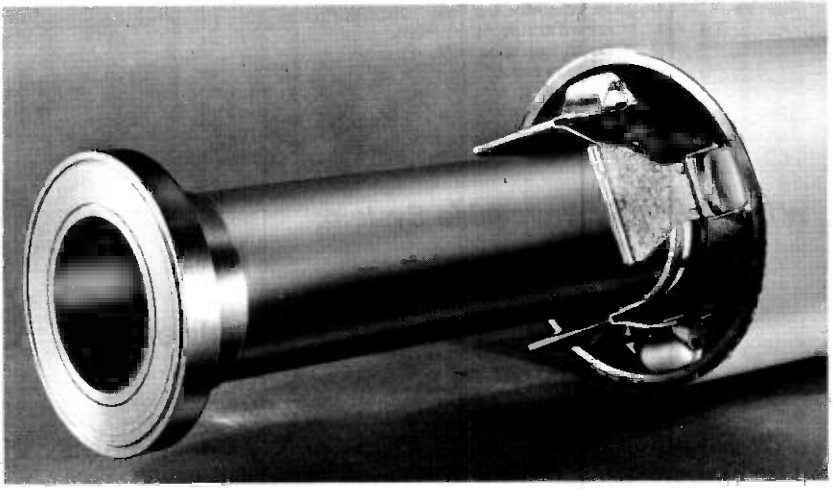

Fig. 1—Components of WT4 sheathed waveguide medium.

waveguide against lightning, corrosion, damage by "foreign" workers, and other hazards.

The roller-spring supports shown in Fig. 1 permit axial motion of the waveguide in the sheath with very low friction. The compliance of the supports in conjunction with the stiffness of the waveguide tubing provides a mechanical filter with respect to the influences, on the waveguide curvature, of the sheath surface distortions as well as the irregularities in the supports themselves.

The couplings, which are all fusion-joined, provide for accurate alignment and reliable connection of the waveguide sections.

The design, fabrication, and characterization of the waveguide tubing are discussed in companion papers by Boyd, et al.[1] and Thomson[2]. This paper covers mechanical design considerations for the other elements of the installed medium and the effects of these elements on transmission losses.

1.2 Transmission constraints on the mechanical design

Electrical transmission considerations establish a number of mechanical design constraints. Both the magnitude and distribution, along the length, of geometric imperfections (deviations from the geometry of a right circular cylinder) in the WT4 waveguide medium are of importance. It has been shown by Rowe and Warters[3] that, for small continuous imperfections in dielectric-lined waveguide, the expected values of average mode conversion losses, from the primary TE_{01} mode, are proportional to the power spectral density levels of the imperfections.

Aside from diametral distortions in the vicinity of the waveguide coupling, imperfections associated with joining and installation are in the form of variations of axis curvature. The most important curvature-coupled spurious modes are the TM_{11} and TE_{12} which, in the 40 to 110 GHz operating frequency range of the field-test system, are produced by high levels of Curvature Power Spectral Density (CPSD) in the 0.3 to 1.5 c/m (cycles per meter) mechanical-frequency range. It is shown in a companion paper by Carlin and Moorthy[4] that significant amounts of loss to the TM_{21} mode can occur for relatively large CPSD amplitudes in the low mechanical-frequency range ($f < 0.15$ c/m). The sheathed medium is an effective mechanical filter with respect to inputs above 0.15 c/m whereas control of the low mechanical-frequency range is a matter of trench design and trench bottom quality, as is discussed in the companion paper by Anderson et al.[5] The present paper deals with inputs associated with waveguide assembly and installation and the action of the sheathed medium in limiting waveguide CPSD levels, particularly in the range of coupling of TE_{01} to the TM_{11} and TE_{12} modes.

II. MECHANICAL FILTERING

2.1 Flow diagram

The WT4 sheathed medium provides two stages of mechanical filtering, one being the sheath stiffness which aids in smoothing the effects of loading irregularities imposed by the surrounding soil, and the second the waveguide stiffness in combination with the waveguide support compliance. The two stages can be considered as independent because the sheath and waveguide are installed in separate operations. Both stages are low-pass filters. A number of inputs influence the net waveguide curvature as indicated in the flow diagram of Fig. 2. The input and output lines of the diagram have been given profiles which roughly illustrate their spatial variations. The trench bottom roughness and soil forces are acted upon by the sheath filter producing the smoothed response referred to in the figure as the "sheath burial curvature." As Fig. 3 illustrates, the sheath makes only partial contact with the trench bottom and therefore its filtering characteristics are nonlinear, depending on the soil loading as well as its own parameters. Other contributions to the net sheath curvature are the imperfections in the sheath splices, in the form of tilts and offsets, and imperfections in the sheath as manufactured.

The deformations in the installed sheath surface act as inputs to the bases of the spring supports. Since nonuniformities in the heights of the springs have the effects of displacements of the spring bases, they are summed with the sheath displacements to give the total input to the next stage of filtering. The output of the second stage, referred to as the

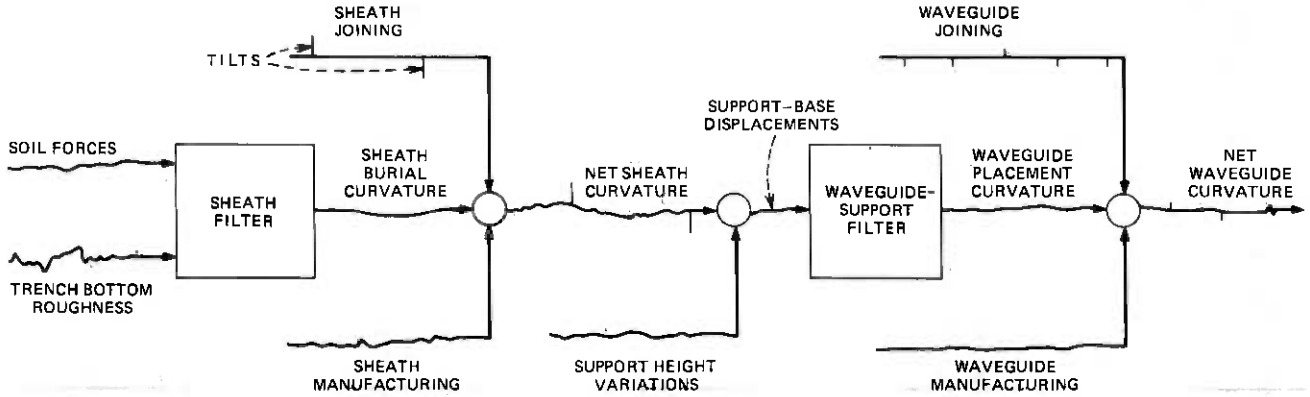

Fig. 2—Waveguide curvature inputs and filtering.

"waveguide placement curvature," reflects all of the deleterious effects of installing a joined string of waveguide sections. To this are added the waveguide manufacturing and joining imperfections to produce the "net waveguide curvature." A conservative simplification is made in this model by assuming that the joining and manufacturing inputs by-pass the filters. Both stages actually behave as high-pass filters with respect to these imperfections, whose low mechanical-frequency content is generally negligible relative to that of the other inputs. Because of the influence of the second-stage filter, tolerances on the sheath and supports are much less stringent than the tolerances associated with the waveguide manufacture and joining. Conversely the waveguide joining imperfections are potentially significant contributors to the higher mechanical frequency portions of the net waveguide CPSD. Achieving the necessary precision in the couplings was recognized at an early stage as a particularly challenging objective.

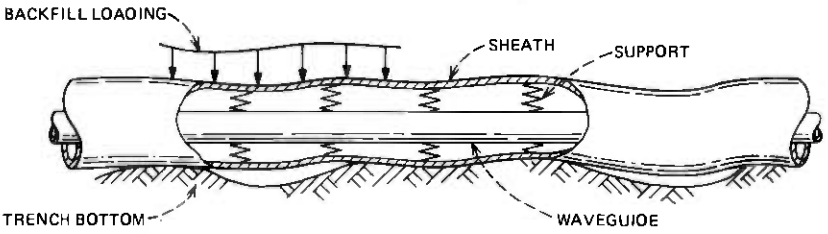

Fig. 3—Two-stage mechanical filter.

2.2 Waveguide CPSD components at 0.325 c/m

The most critical mechanical wavelength is the beat wavelength of the TE_{01} and TM_{11} modes at the highest frequency in the operating band. The mechanical frequency associated with 110 GHz is 0.325 c/m for the dielectric-lined waveguide used in the WT4 field test. Estimates of the various components of the net waveguide CPSD will be given below. Using field test data it was found that the sheath burial, support irregularities, and sheath joining each accounted for contributions to the waveguide CPSD at 0.325 c/m in the order of 10^{-8} l/m^2/c/m while the contributions of sheath manufacturing and waveguide joining were at least an order of magnitude lower. The sum of all of these contributions corresponds to an expected value of average TM_{11} mode conversion loss, at 110 GHz, of less than 0.05 dB/km which is well within acceptable limits for a practical system.

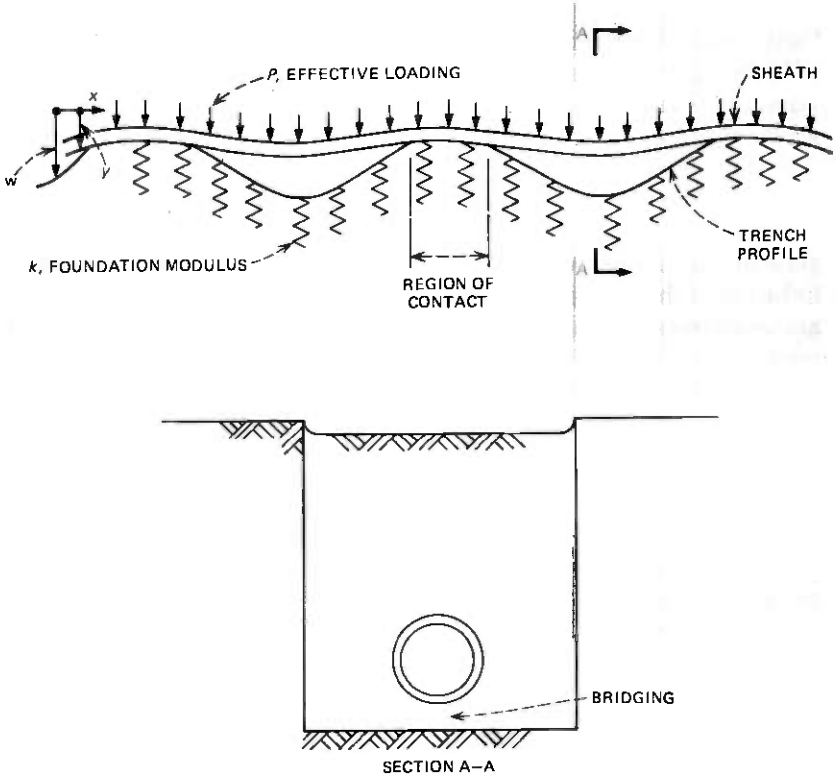

Fig. 4—Sheath-soil interaction model.

2.3 Sheath filtering

2.3.1 Mathematical model

For purposes of understanding the filtering action of the sheath on the soil environment, a mathematical modeling investigation was carried out. The modeling is useful in investigating the effects of trench bottom irregularities as well as sheath parameter and loading variations. The essential features of the sheath deformation process are described by a beam-on-elastic-foundation model where the free surface of the foundation is taken to have the irregular shape of the as-cut trench bottom. The trench bottom is taken to be a continuous elastic foundation of the Winkler type—i.e., composed of an infinite number of independent linear springs of differential width. The beam is assumed to respond to a known loading which reflects not only the weight of the sheath but the effective weight of the backfill.

Referring to Fig. 4, the governing equations for the beam resting on an irregular surface with only partial contact existing are as follows

$$EIy^{IV} = p \qquad y < w \tag{1}$$

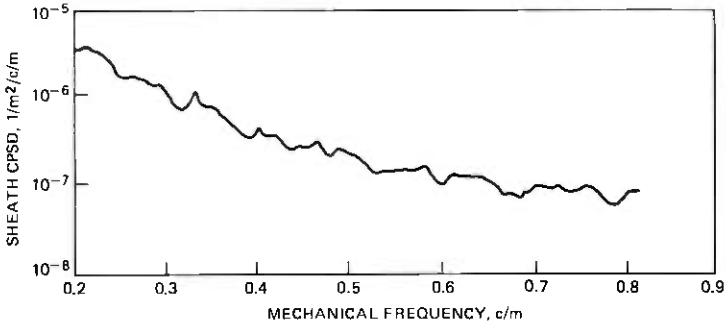

Fig. 5—Average of sheath curvature spectra for field evaluation test.

and

$$EIy^{IV} + ky = p + kw \qquad y \geq w \tag{2}$$

where y is the beam deflection, w is the vertical distance from a horizontal reference line to the soil surface, E is Young's modulus of the sheath material, I is the sheath cross-sectional moment of inertia, k is the foundation modulus, and p is the loading per unit length. Because the regions of contact in which eq. (2) applies are not known in advance, an iterative procedure is required to obtain a solution starting from an initial guess as to where contact exists. A finite difference method was employed to obtain solutions of these equations for trench profiles of arbitrary shape. The computer program written for the sheath analysis was used in obtaining curvature estimates with trench profile data from the field test installation.

2.3.2 Field test results

Figure 5 shows a CPSD estimate obtained using field-test trench profile data. The steel sheath dimensions are $5^9/_{16}$ inch outside diameter and $^3/_{16}$ inch wall thickness. A loading of 8 lb/in. was assumed, which reflects some conservatism as discussed below. The CPSD estimate was obtained by averaging, at each mechanical frequency, sample spectrum values from 12 data sets, each representing 300 feet of trench.

Results of the sheath analysis showed the sheath filtering to be virtually unaffected by the actual value of foundation modulus for typical values ($k > 5000$ lb/in.^{2}).

2.3.3 Sheath loading

Estimates of the loading which was effective in producing bending of the sheath axis were obtained from a limited experimental program. Figure 6 shows some results of these experiments in which deflections were measured for simply supported 20-foot lengths of sheath buried

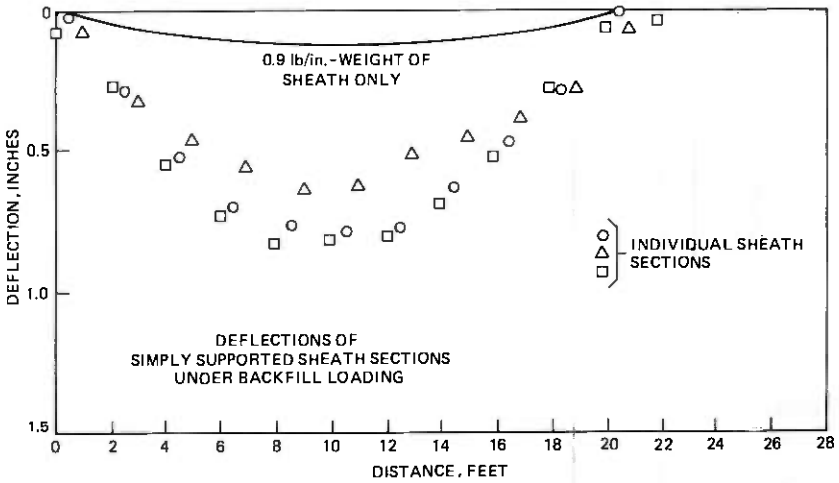

Fig. 6—Experimental determination of effective sheath loading.

in a manner typical of pipeline construction. An effective loading of between 4 and 6 lb/in. was estimated from these tests (about a third of the weight of the backfill directly above the sheath plus the weight of the sheath). As noted above, a somewhat higher loading (8 lb/in.) was used for estimating losses to allow for field conditions not encountered in the experimental installations. It should be noted that the effective sheath loading, referred to here, is a downward beam loading. It is not the same as the crushing loads used in the two-dimensional analysis of uniformly supported buried conduit (cf. Spangler[6]).

2.4 Waveguide-support filtering

2.4.1 Transfer function

The waveguide support within the sheath consists of a set of relatively closely spaced spring elements. The filtering mechanism is very nearly like that of the continuum model of a beam on an elastic foundation as described in the previous section. Here the springs are attached to the beam and the inputs are deflections of the bases of the springs. Because an interference fit between the supports and sheath would increase the effective coefficient of friction for insertion, a slight clearance is allowed. This is ignored in assessing the filtering behavior as the effect is small considering the relatively large amplitude, long wavelength content of the trench profiles observed. Thus, the waveguide-support system is regarded as a linear filter described by eq. (2), if axial loads are ignored. Here w represents the deflections of the bases of the springs.

It is assumed in eq. (2) that the slope of the elastic curve is small everywhere and, accordingly, the waveguide curvature

$$C_g \approx y_g^{II} \tag{3}$$

so that for a uniformly loaded beam having a uniform foundation modulus

$$EI_g C_g^{IV} + kC_g = kC_s \tag{4}$$

where C_s is the curvature of the envelope of the spring bases. The transfer function with respect to sinusoidal input components is

$$H(\omega) = \frac{1}{1 + \dfrac{EI\omega^4}{k}} \tag{5}$$

where $\omega \equiv 2\pi f$.

The CPSD function of the waveguide, S_o, caused by sheath curvature is determined using the input-output relation for linear systems

$$S_o(\omega) = |H(\omega)|^2 S_i(\omega). \tag{6}$$

The parameters used in the WT4 system are: $E = 30 \times 10^6$ lb/in.^{2}, $I = 0.94$ in.^{4}, and $k = 20$ lb/in.^{2} The squared gain function $|H(\omega)|^2$, is shown in Fig. 7 along with the range of mechanical frequencies associated with TE_{01}–TM_{11} and TE_{01}–TE_{12} mode conversion. The magnitude of $|H(\omega)|^2$ is less than 0.01 in the critical range and falls off as the eighth power of mechanical wavelength (24 dB per octave). Because of this high cutoff rate, the design criteria for the inputs acted on by this filter (Fig. 2) are simplified. For all these inputs, peak mode-conversion effects occur at the high end of the operating frequency range with TM_{11} more significant than TE_{12}, although TE_{12} has larger coupling coefficients.[4] Thus a useful figure of merit for assessing the various loss contributions is the CPSD level at a mechanical frequency of 0.325 c/m which, as mentioned earlier, corresponds to TE_{01}–TM_{11} coupling at an operating frequency of 110 GHz for the field test waveguide (180 micron dielectric liner thickness).

Deviations from the continuum filtering behavior occur in two ways as a result of the discrete nature of the supports. Because the supports "sample" the sheath internal surface, aliasing phenomena are present. Also, because the loading impressed on the waveguide is actually a set of discrete forces, the waveguide response to a sinusoidal distortion in the sheath contains response components at shorter wavelengths as well as at the same wavelength as the sheath input. For the 22-inch support spacing used and the field test input data, these deviations have been found negligible.

If an axial force, T, is present in the waveguide, a second-order term

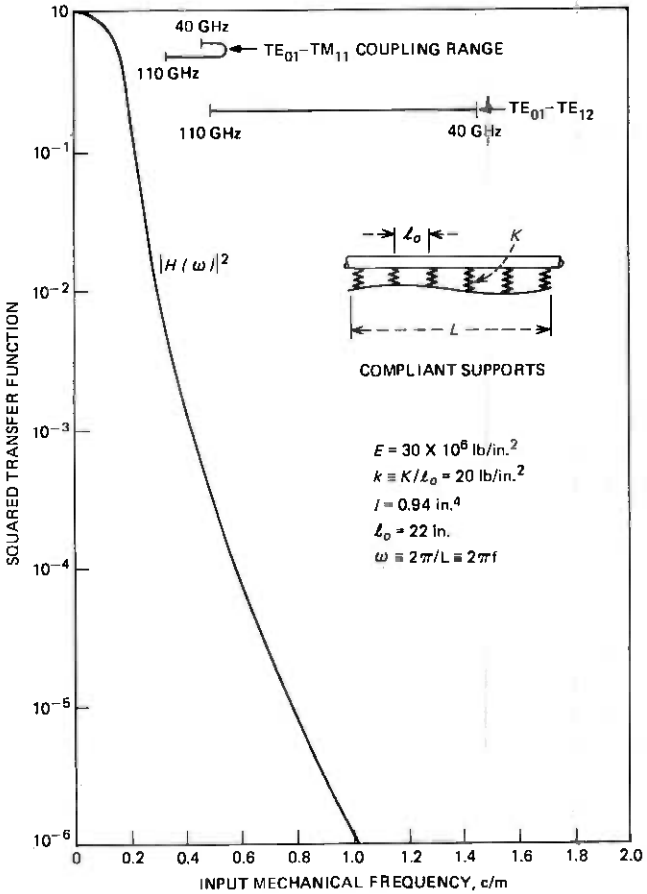

Fig. 7—Response of waveguide-support system.

is added to the left side of eq. (4) and the transfer function is modified to

$$H_T(\omega) = \frac{1}{1 + \frac{T\omega^2}{k} + \frac{EI\omega^4}{k}} \tag{7}$$

The axial force due to temperature fluctuations, with no expansion joints, can be either positive (tensile) or negative (compressive). Adding the axial load, which may reach levels in the order of 10,000 lb, changes the magnitude of the transfer function by less than 15 percent for a 10-foot wavelength input, and by smaller amounts for shorter mechanical wavelengths.

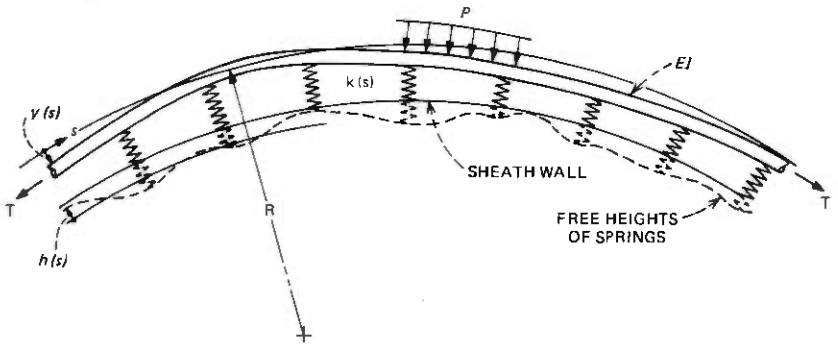

Fig. 8—Effects of support irregularities.

By selecting the support spacing sufficiently small, the mechanical wavelengths of distortions caused by waveguide weight and thermal loading were placed outside the critical range. The shortest wavelength in the range is 27 inches. Buckling of the waveguide under compressive loading is not a problem because the critical buckling load for the WT4 support parameters is in excess of 47,000 lb, which is much greater than any loading anticipated.

2.4.2 Roller-spring support irregularities

Irregularities in the supports are of two types: spring constant variations and variations in the free heights of the supports. The effects of the spring constant variations are only of significance under conditions in which the supports are highly compressed. This occurs when a high axial force exists in the waveguide in a curved region of the trench, as shown in Fig. 8. The waveguide is assumed to be loaded by an axial force, T, which is the result of a temperature variation from that corresponding to a stress free state, and a transverse loading, p, which represents the weight if the curvature is in the vertical plane. (It is assumed that slopes in the vertical plane are sufficiently small that no distinction is needed between the weight and its radial component. Also, changes in T due to the tangential components of weight or frictional effects are ignored.) The radius, R, is taken as constant here because the support variations are much more rapid than the local average curvature. Dropping the subscript g, the waveguide deflection, $y(s)$, is a displacement from the curved reference line. The governing equation is then

$$EI\left[y(s)^{IV} + \frac{1}{R^2}y^{II}\right] - Ty^{II}(s) + k(s)y(s) = \left[p + \frac{T}{R}\right] + k(s)h(s) \quad (8)$$

where $h(s)$ is the variation in the free height of the spring taken positive when the height is less than nominal, and $k(s)$ is the variation in spring constant due to material thickness variations in the roller spring supports and the effects of sliding friction as the support is compressed. Equation (8) reduces to eq. (2) for a uniform support in a nominally straight section of trench and with zero axial force.

An approximate solution of eq. (8) may be obtained by a perturbation technique, putting the spring constant and height variations in the form

$$k(s) = k_o + \epsilon f(s)$$

and

$$h(s) = \epsilon q(s)$$

where ϵ is a small parameter and $f(s)$ and $q(s)$ are assumed to be stationary stochastic processes with zero averages. By expanding the solution in a power series in ϵ and retaining the first two terms the approximate solution is obtained. The waveguide CPSD approximation due to the support irregularities can be expressed

$$S_{ir}(\omega) \approx \omega^4 |H_T(\omega)|^2 \left[S_h(\omega) + \frac{\hat{p}^2}{{k_o}^4} S_k(\omega) \right]$$

where $S_h(\omega)$ is the spectrum of the height variations, $S_k(\omega)$ is the spectrum of the spring constant variations, and the two types of variations are taken as independent. The loading parameter

$$\hat{p} \equiv p + T/R$$

It was found that the field test support data could reasonably be represented as band-limited white noise and the corresponding waveguide CPSD approximation in the critical range is

$$S_{ir}(\omega) = \omega^4 |H(\omega)|^2 \times 10^{-7} \qquad 1/\text{m}^2/\text{c/m} \qquad (9)$$

where ω is in radians/meter and the effect of the axial tension in the transfer function is ignored.

2.4.3 Design considerations for the roller-spring supports

The roller-spring support has two basic functions; to facilitate insertion of the waveguide and to act, in conjunction with the bending stiffness of the waveguide, as a mechanical filter. Since a relatively large number of supports is required, feasibility of the support system is dependent on low unit costs, ease of attachment to the waveguide and high reliability. Fulfilling the insertion objective was primarily a matter of selecting appropriate materials. The roller material chosen is a 30 percent glass-filled nylon and the axle pins are 303 stainless steel coated with

a thin fluorocarbon film. The glass reinforcement provides adequate strength to guarantee dimensional stability of the rollers under the anticipated long-term loading. The effective average coefficient of friction is sufficiently low to permit insertion of the waveguide up to 3 miles from a single push site as discussed in the companion paper by Baxter et al.[7] Very little wear has been observed in testing these rollers for simulated insertion distances far exceeding 3 miles.

The low-cost objective is met by the WT4 roller-spring support (Fig. 9). The carriage for the rollers is a one-piece sheet-steel part incorporating its own attachment clip. The blank is formed into four bow-tie shaped springs by punch-press operations and is made from steel of relatively high ductility as well as high yield stress. Heat-treatment is not required to achieve the necessary spring temper, and design is such that the support may be mass-produced in a completely automated punch-press process. It is estimated that in mass production the cost of a complete assembly will be less than 60 cents. The sheet material is corrosion protected with a zinc coating.

The requirements for the filter are to provide sufficient compliance to achieve adequate attenuation of inputs in the critical mechanical frequency range. The initial objective was to achieve a squared transfer function magnitude of 0.01 or less at a mechanical frequency of 0.325 c/m. For the 20 lb/in.^{2} average support modulus obtained, the value of the squared transfer function is about 0.008 at that frequency. As can be seen from eqs. (5) and (6), the attenuation of spectral inputs is proportional to the square of the spring stiffness. The lower limit on spring stiffness is determined by the reactions to the thermal loading that must be developed within the elastic range of spring deflection and by the geometric constraints within the sheath.

The maximum allowable elastic range of deflection of the supports is less than the radial clearance between the coupling flanges and the sheath inside surface. In the field test waveguide this distance is nominally a little over half an inch. Under the peak lateral loads due to thermal forces, the supports must have some elastic travel remaining for filtering. In the field test supports the transverse loading corresponding to a 10,000-lb axial force in a 250-foot radius route bend displaces the axis of the guide about 75 percent of the elastic range of the supports, which is a little under $\frac{1}{4}$ inch. Supports made since the field test using a newly available steel of higher yield strength has increased this range, for the same support design, by about 25 percent.

To obtain high efficiency in the spring design the supports utilize the increased elastic range of travel available when the support is allowed to deflect well beyond its elastic range during its first loading. For elastic, perfectly plastic materials, the maximum load is up to 1.5 times that for a flat spring loaded only up to yielding of the outer fibers. Although the

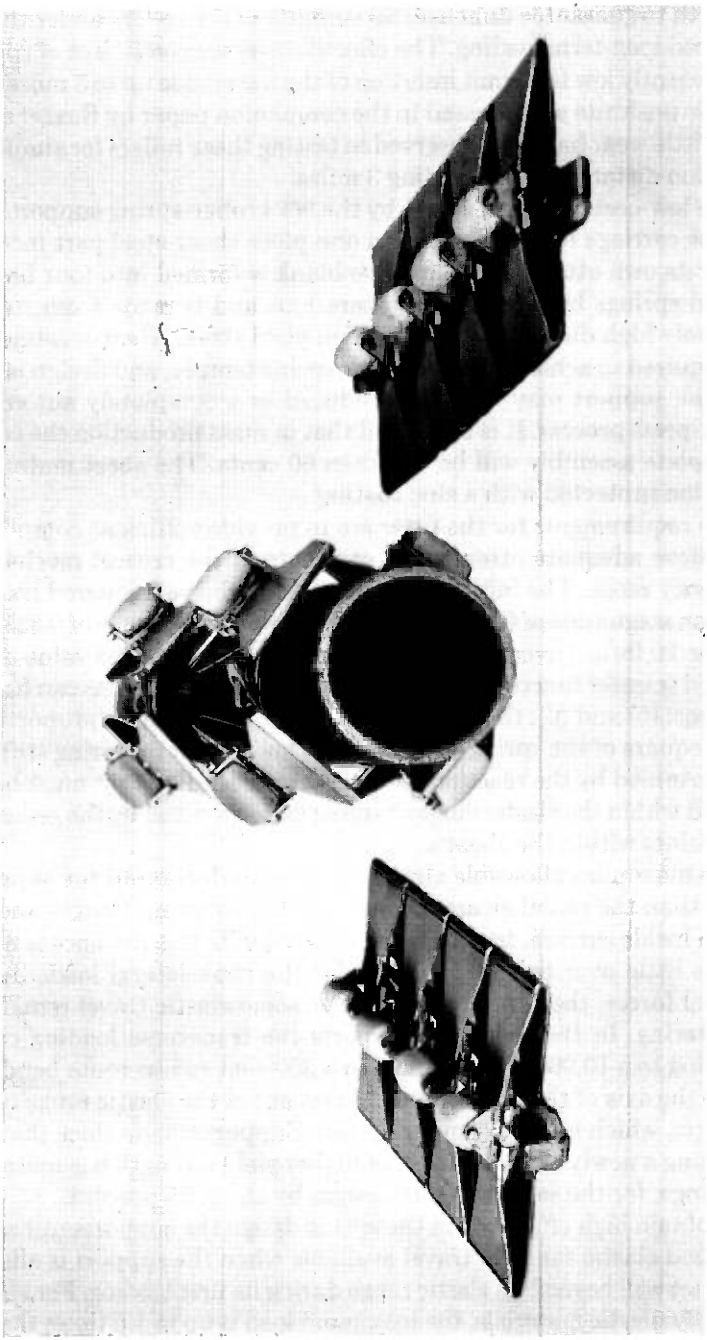

Fig. 9—Roller spring supports.

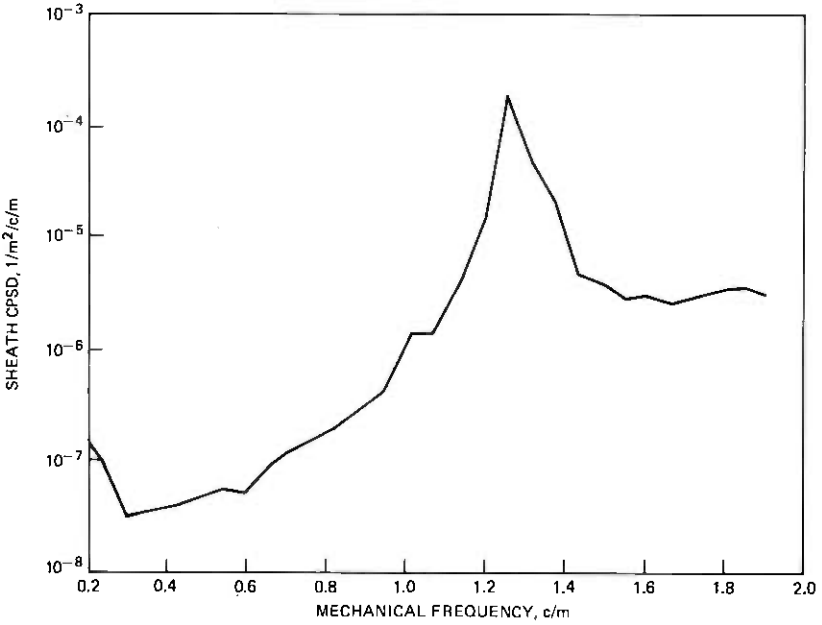

Fig. 10—Average of CPSD plots.

load-deflection curve is somewhat nonlinear during first loading, it is nearly linear on subsequent loadings. In future applications the supports will be subjected to one full deflection in the factory during module preparation. This was not done for the field test modules; therefore more care was required in handling them to prevent changes in the free heights of the springs.

III. SHEATH CONSIDERATIONS

3.1 Manufacturing irregularities

The size and material requirements of the sheath are met by commercially available standard line pipe. To control the effects of sheath manufacturing curvatures on the net waveguide curvature, the specification of sheath straightness tolerance is in terms of an allowable power spectral density limit. The sheath for the field test was inspected using an external curvature gauge, the principles of which are described in the companion paper by Fox et al.[8] Figure 10 shows an average of CPSD plots obtained from 30 of the 60-foot-long field test sheath sections. The relatively high spectrum spike at 1.25 c/m was the result of an eccentricity in a set of sizing rollers through which the sheath passed during manufacture. It is above the "cutoff" frequency of the discrete waveguide supports and is thus aliased by the supports to appear as an input at 0.55

c/m. The amplitude of the effective input spike at 0.55 c/m is reduced in magnitude by the fourth power of the ratio 0.55/1.25 and thus its effect is quite small.

3.2 Sheath joining irregularities

Because, when sheath sections are joined, mating ends are butted together, the magnitude of sheath splice tilts is primarily determined by the out-of-squareness of the sheath ends. A tilt may be considered a delta function in curvature and the curvature power spectral density for a set of equally spaced random tilts in one plane has the simple form[3]

$$S_{t_1}(\omega) = \sigma_t{}^2/L \tag{10}$$

where L is the sheath section length and $\sigma_t{}^2$ is the variance of the tilt magnitudes. Assuming random angular orientations of joining members

$$S_{t_1}(\omega) = \frac{E(A^2)}{L} \tag{11}$$

where $E(A^2)$ is the mean square out-of-squareness of the sheath ends with respect to a plane perpendicular to the sheath axis.

An additional contribution to the tilt may occur if the sheath end faces are not perfectly butted together. The amount of gap allowed by the sheath welding specification was 0.01 inches, which limited this contribution to a negligible level. Using the field test sheath end-squareness data an estimate of the effective tilt spectrum for two orthogonal planes is

$$S_t(\omega) = 9 \times 10^{-7} \quad 1/\text{m}^2 \tag{12}$$

The offsets at sheath joints are characterized as a set of delta functions in slope. Thus the offset curvature power spectral density for one plane is

$$S_{o_1}(\omega) = \frac{\omega^2 \sigma_o{}^2}{L}$$

where σ_o is the standard deviation of offset. From the specified tolerances on wall thickness it can be concluded that the sheath offset contribution is negligible.

3.3 Sheath welding

The sheath welds provide gas-tight joints and sufficient strength for sheath handling. Because the inside surface of the sheath serves as a

runway for the rollers during insertion, it was felt necessary to utilize a weld that created no projections on the inner surface.

The field test sheath sections were joined by SMA (Shielded Metal Arc) welding, a manual process. Other processes are available which can be used satisfactorily for this application. The type of joint selected for the field test differs from standard pipeline practice in that the mating sheath ends are butted together, completely closing the gap, with the weld beads penetrating sufficiently deep to achieve the required joint strength for pipe handling while not completely penetrating to the inner surface. Use of a partial rather than a full penetration weld and zero (nominal) gap between mating ends are the only differences from standard pipeline practice. The sheath wall thickness ($^3/_{16}$ inch) was selected to be the smallest practical value. Thinner-walled pipe could not be reliably joined by butt welding without requiring the use of undesirable reinforcing rings. In addition the thinner-walled pipe is much more prone to denting due to mishandling.

A two-pass weld procedure was used for each splice. The first relatively-thin "root" or "stringer" pass is followed by a final pass using a lateral weaving technique, building up a heavy weld bead on the outer surface. Strength is achieved in this joint nearly equal to the strength of the pipe body. Approximately 750 welded sheath joints were made for the field test with only one failure, which was detected and repaired after completion of the installation.

IV. WAVEGUIDE COUPLING

4.1 Requirements

The waveguide coupling consists of flanges (Fig. 1) that are EB (Electron-Beam) welded to the waveguide tube in the factory and fusion-joined in the field by TIG (Tungsten Inert-Gas) welding, a machine process. The specifications developed to assure reliable joining and satisfactory transmission performance for the coupling are given in Table I.

An all-fusion joined coupling was selected as the joining approach for waveguide modules, primarily because of reliability considerations. An extensive analytical and experimental program, which can be discussed only briefly here, was carried out to develop the coupling.

4.2 Coupling design

The waveguide flanging process (Fig. 11) starts with the machining of flange blanks from forgings or heavy-wall tubing. The material chosen for the flange blanks is aluminum-killed low-carbon (C1010) steel, a choice based on TIG welding requirements.

Table I — Coupling specifications

Item	Requirements	Rationale
Strength (tensile)	1. 40,000 lb min. failure load 2. 100 cycles from 0 to 35,000 lb 3. No yield below 30,000 lb	40°F temp change in 250 ft bend, 2 to 1 safety factor
Leakage (maximum)	1. Average 5×10^{-5} cm^3/sec 2. Max. 1×10^{-3} cm^3/sec	Leak location required in N_2 system
Permeability	(Requirement not necessary with fusion joining)	
Tilt	0.2 millirad rms maximum	Loss objective
Offset	2.0 mils rms maximum	Loss objective
Excess stiffness	No requirement	Optimized after all other requirements met
Diametral distortion	2.0 mil max. at coupling	Loss objective

The shape of the flange was determined at an early stage of the coupling development using finite element analyses. A flange diameter of slightly over 4 inches was found adequate to keep the temperature of the dielectric liner below 250° F (a material requirement) during the TIG welding in the field.

Although the basic flange shape changed little during the latter part of the development, several flange face variations were investigated in an effort to facilitate welding. The large grooves in flange face designs 1, 2, and 3 of Fig. 12 led to pressure-vessel effects (weld blow-out) during the TIG welding process. Flange 4 did not meet strength requirements because of the stress concentration at the TIG weld. Flange 5, which incorporates a small stress relief groove, satisfies both the welding and strength requirements and is the design used for the field test.

The face design of flange 6 has an undercut which is made during the blank machining process. This design is proposed for the next generation of waveguide flanges because it minimizes the final machining effort and eliminates machining the hard martensitic steel region near the electron-beam face weld.

The TIG fusion-joining process uses a specially designed fixture that aligns the flanges, clamps them together with a 10,000-lb preload, rotates the welder head around the coupling, and cools the coupling by means of water-cooled copper heat sinks pressed against the flanges. The preload minimizes the separation of the flange faces when the waveguide is in tension or bending. The welding parameters are critical and are given in Table II.

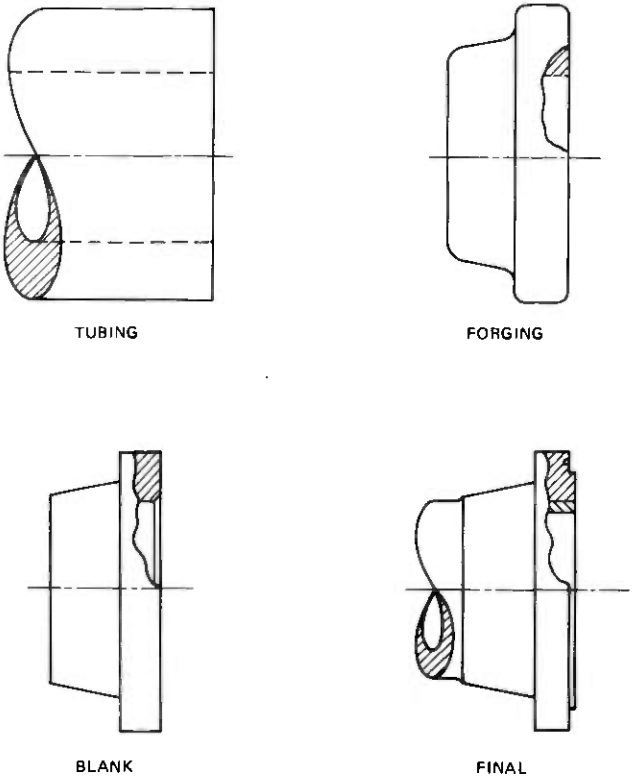

Fig. 11—Flanging process.

4.3 Coupling—field test reliability results

The coupling used in the field test waveguide met or exceeded all of the reliability objectives. Tests demonstrated that:

(*i*) The coupling exceeded strength requirements and is satisfactory for use in bends with radii of curvature as low as 180 ft.

(*ii*) The coupling is very insensitive to stress corrosion cracking.

(*iii*) The 8.7 mile waveguide string, containing over 1500 couplings, has no measurable nitrogen leakage.

The welding process proved to be extremely reliable with only one defective weld, which was easily replaced, out of the over 1500 produced during the field test. Inspection of the welds was visual only.

4.4 Coupling—field-test transmission performance

The waveguide joining imperfections comprise tilts, which result from both flange end-squareness deviations and coupling excess stiffness,

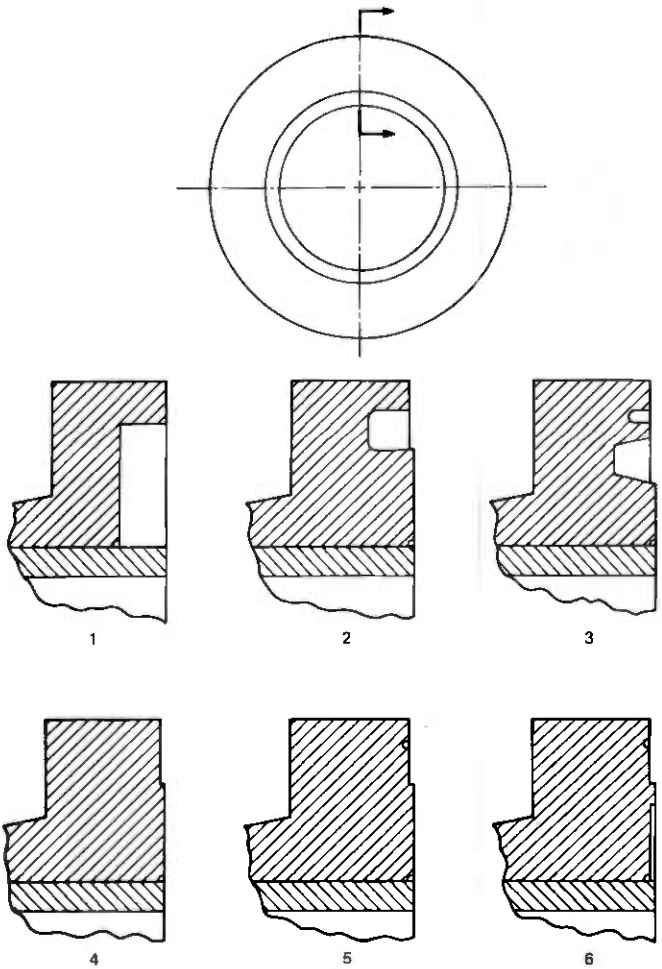

Fig. 12—Flange design stages.

offsets, which result from flange eccentricity and welder misalignments, and diameter distortions in the vicinity of the EB flange attachment welds. These imperfections resulted in a very small contribution to transmission losses in the field test waveguide.

Measurements of end squareness made on over 2600 flanges during Western Electric manufacturing indicated an RMS value of out-of-squareness of 0.064 milliradians. Assuming random joining of the flanges, the couplings would have an effective RMS tilt of 0.09 milliradians.

Thus for the waveguide medium, using eq. (10) with no interface gap assumed, the contribution to the net waveguide CPSD is

$$S_t(\omega) = 9 \times 10^{-10} \quad 1/\mathrm{m}^2/\mathrm{c}/\mathrm{m} \tag{13}$$

Table II — TIG nominal welding parameters

Current	170 amps
Voltage (dc)	16 volts
Welding time	95 sec
Overlap	10 deg
Argon-helium flow rate	15 CFH
Electrode	Thoriated tungsten, 0.093 in. diameter, 60 deg cone tip
Standoff	0.05 in.

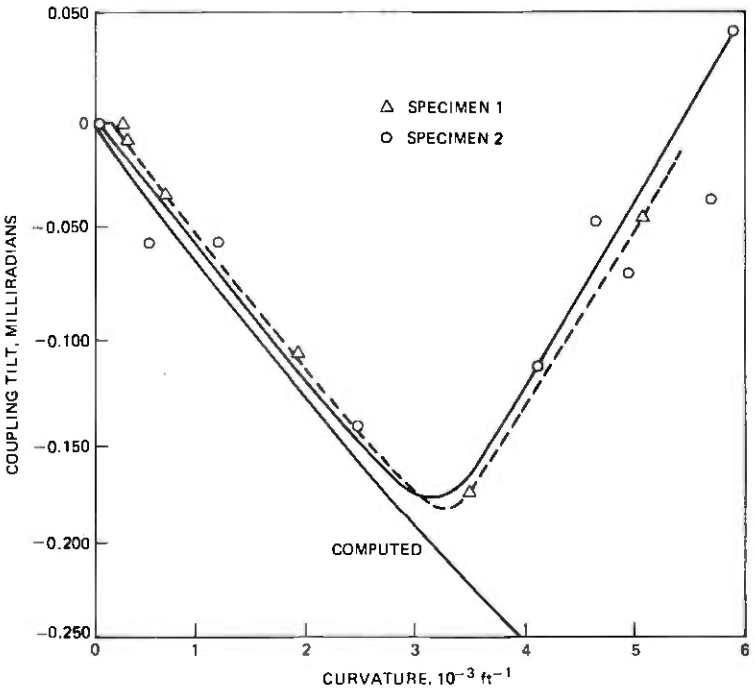

Fig. 13—Apparent tilt due to excess stiffness.

where the waveguide length is taken to be the nominal length of 29 feet. Since the loss is proportional to the square of the tilt, the reduction in tilt to 0.09 mrad from the initial objective of 0.2 mrad reduced the loss contributions of coupling tilt to one-fifth of that allocated.

The effect of excess stiffness of the coupling creates an "apparent tilt" when the waveguide is in a bend. The data in Fig. 13 indicate that the apparent tilt is a function of waveguide curvature. In the field test the RMS curvature of the waveguide in the vertical plane was about 1.33×10^{-3} ft^{-1}. This corresponds to an apparent tilt of 0.07 milliradians, a component almost as high as that resulting from the flange manufacturing irregularities.

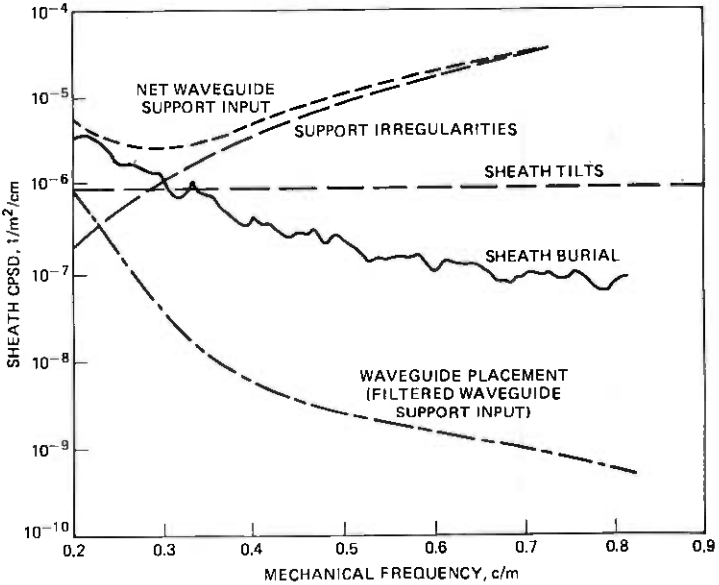

Fig. 14—Components of waveguide placement spectrum.

The offset caused by the eccentricity of the flanges as manufactured was negligible compared with the offset produced by the welder. The welder alignment fixture had a bias that contributed an offset of approximately 1 mil to each pair of flanges. This coherent bias of the welder, which could produce significant loss peaks, was mitigated by the rotation of the waveguide string during insertion. The waveguide string rotated slowly during insertion because of a slight canting of the roller axles in the supports. The potentially significant effects of radial distortions at couplings were removed by a randomization of module lengths.

V. SUMMARY

5.1 Loss contributions

The contributions to the net waveguide curvature of the various inputs associated with installation of the medium, in nominally straight regions, have been discussed in the preceding sections. As indicated earlier, waveguide axis curvature, including coupling tilts and offsets, is the only significant loss-producing effect of the assembly and installation of waveguide, the effects of diameter distortions at couplings having been made negligible by randomization of the waveguide lengths. (Ellipticity that results from bending the waveguide to the relatively large radii allowed is also negligible.)

In Fig. 14 the most important contributions to the net waveguide CPSD above 0.2 c/m are summed graphically. The sheath burial curvature is taken from the plot in Fig. 5. The other significant input contributions are the idealized estimates of support irregularities [eq. (9)] and sheath tilts [eq. (12)]. The squared transfer function for the waveguide support is that shown in Fig. 7. Adding the contributions of the sheath burial, sheath tilts, and support irregularities, one obtains the net WG-support input. Then, multiplying this result by the squared transfer function of Fig. 7, one obtains the waveguide placement spectrum. The expected value of the average combined TM_{11}, TE_{12} mode conversion loss corresponding to the waveguide placement spectrum is less than 0.06 dB/km at 110 GHz.

5.2 Conclusions

The field evaluation test results indicated that the basic objectives of the mechanical design of the sheathed waveguide transmission medium for the WT4 system were met. The field joining of waveguide for the field test was virtually trouble-free and, in addition, the remarkably high degree of machining accuracy achieved in the waveguide flange finishing was sufficient to limit this component of the loss budget to a nearly negligible level. The effectiveness of the mechanical filtering provided by the stiffness of the steel sheath and the action of the waveguide compliant support system permits installation of the sheath using the lowest-cost (conventional) methods of pipeline construction and eliminates the need for potentially troublesome expansion joints in the buried medium. The mechanical filtering is also sufficient to permit the use of pipe manufactured by commercial line-pipe suppliers and is tolerant of a reasonable degree of manufacturing imperfection in the supports themselves. Through use of relatively closely spaced compliant supports, the effects of waveguide weight and thermal loading distortions have been made negligible. The support developed for the field test is a low-cost reliable unit which, in addition to performing the filtering function, permits insertion of the waveguide in lengths of miles from a single point. Because of the substantial protection provided the waveguide by the rugged steel sheath, and the use of fusion joining of both the sheath and waveguide, the WT4 transmission medium is expected to be an order of magnitude higher in reliability than coaxial cable. As brought out by Alsberg et al.,[9] the installation method was carefully integrated with the overall system design[5,7] to achieve minimum costs.

VI. ACKNOWLEDGMENTS

Many people at both Western Electric and Bell Laboratories contributed to the development of the sheathed waveguide medium. Par-

ticularly notable contributions were made to the work reported on here by the following: P. L. Key, who was associated with the resolution of metallurgical problems on all of the elements of the sheathed medium; V. P. Chaudhary, who developed the finite difference solution and iterative procedure for the sheath-soil model; and P. M. Synefakis, who wrote the computer program for the sheath analysis and obtained the numerical results.

REFERENCES

1. R. J. Boyd, W. E. Cohen, W. P. Doran, and R. D. Tuminaro, "Waveguide Design and Fabrication," B.S.T.J., this issue.
2. D. J. Thomson, "Spectrum Estimation Techniques for Characterization and Development of WT4 Waveguide," B.S.T.J., this issue.
3. H. E. Rowe and W. D. Warters, "Transmission in Multimode Waveguide with Random Imperfections," B.S.T.J., *41*, No. 3 (May 1962), pp. 1031–1170.
4. J. W. Carlin and S. C. Moorthy, "Waveguide Transmission Theory," B.S.T.J., this issue.
5. J. C. Anderson, R. W. Gretter, and T. J. West, "Route Engineering and Sheath Installation," B.S.T.J., this issue.
6. M. G. Spangler, *Soil Engineering*, Scranton: International Textbook Co., 1951.
7. H. A. Baxter, W. M. Hauser, and D. R. Rutledge, "Waveguide Installation," B.S.T.J., this issue.
8. P. E. Fox, S. Harris, and D. J. Thomson, "Mechanical Gauging Techniques," B.S.T.J., this issue.
9. D. A. Alsberg, J. C. Bankert, and P. T. Hutchison, "The WT4/WT4A Millimeter Wave Transmission System," B.S.T.J., this issue.

THE BELL SYSTEM TECHNICAL JOURNAL
Vol. 56, No. 10, December 1977
Printed in U.S.A.

WT4 Millimeter Waveguide System:

Waveguide Installation

By D. R. RUTLEDGE, H. A. BAXTER, and W. M. HAUSER

(Manuscript received April 7, 1977)

This paper describes the insertion method for installing WT4 waveguide. The rationale for the selection of the insertion method over competing installation techniques is provided, and the field installation tools and techniques developed to splice and push waveguide are described. Insertion sites are selected by the criteria given in this paper. The analysis of expected push forces is presented, and an example push force problem is solved.

I. INTRODUCTION

The buried portion of the WT4 waveguide system is a coaxial twin pipeline composed of three main elements: waveguide, compliant supports attached to the waveguide, and sheath.[1] When waveguide is installed by the insertion method, described more fully in the sections which follow, the sheath is constructed to completion (including restoration of the right-of-way and acceptance testing of the sheath line) in entire repeater or multirepeater spans before waveguide is installed from access points located at convenient places on the route.

The installation of the sheath is an operation resembling so closely the construction of a conventional pipeline that the familiar equipment and techniques of the pipeline industry have been adopted.[2] In contrast, the flange splicing and push inserting of waveguide required new developments of tools and methods. The particular tools and methods evaluated during the field evaluation test are described in detail in the following sections. Design of a new waveguide insertion system based on the results of the field evaluation test experience is also discussed.

II. BACKGROUND

2.1 Modular Installation

Although direct burial of unsheathed waveguide was the first installation method developed, the very costly trenching and padding specifications which were required to protect the waveguide from backfill pressures quickly led to the introduction of a protective sheath. The resulting coaxial pipeline was initially installed by the so-called modular method in which both waveguide and sheath were weld-spliced over the open trench and buried simultaneously.

For modular installations the units delivered to the field were coaxial modules* in which the waveguide and sheath were carefully matched in length. Because of this precaution, an installation sequence which was begun with the waveguide and sheath weld positions slightly staggered (with the waveguide protruding from the sheath in the direction of construction) set the pattern for staggered weld positions thereafter. With the waveguide flange thus exposed, each coaxial module was simply attached by welding first the waveguide flanges (the waveguide in each new module was accessed by sliding the waveguide a few inches out of its sheath) and subsequently sliding the sheath in the reverse direction to set up a butt weld in the sheath.

Yet, even while this modular method was under active development, the potential economies which could be achieved in manufacturing and construction if the installations of sheath and waveguide could be separated were evident. Modular installation required the manufacture of waveguide-sheath modules, which implied handling sheath in the assembly plant. Furthermore, a sheath trimming operation was needed to match the length of the sheath to its enclosed waveguide. Probably most important, the installation of waveguide-sheath modules required field equipment and construction methods which departed considerably from established pipelining technology. Since a large part of the installed cost of any buried transmission medium is associated with grading, excavation, and restoral work, it is desirable to avoid complicated techniques or unusual equipment which may cause delays during these stages of construction. The insertion installation method so satisfactorily solved these problems that the modular method was abandoned.

2.2 Insertion Feasibility

The insertion method of waveguide installation became feasible with the development of a low-friction roller support[1] and the demonstration

* Herein, a module means a factory-produced length of waveguide flanged at both ends. In the pipeline industry an equivalent meaning is communicated by a "joint" of pipe. Waveguide lines made up by connecting modules together can be installed by the "modular" method discussed here or by the insertion method described in other sections.

by analytical and experimental work that long push distances could be achieved with push forces well under the roller support loading limit (axial load 10,000 lbs). In fact, since the roller support has a coefficient of friction of only 0.058, insertion distances of 7½ miles could be achieved with a push force of 10,000 lbs if the waveguide sheath were perfectly level and straight.

Of course, the sheath is not perfectly straight, and in forcing the waveguide to follow its shape the sheath places increased loads on some roller supports. Furthermore, when waveguide is pushed through a route bend the axial compression (or tension) in the waveguide in the bend causes the waveguide to displace laterally in proportion to the severity of the bend and the axial force so that the roller supports are placed under additional loads. Loads from both of these sources increase the frictional resistance in the bearings and a greater push force is required to move the waveguide through the sheath.

Practically, the forces required to insert waveguide can be predicted from a route-independent "effective" coefficient of friction, which combines the inherent roller support coefficient with the additional clamping resistance caused by imperfect sheath profiles, and the route-dependent additional restraints caused by route bends and elevation changes. Appendixes A and B are devoted to an analytical investigation of these coefficients and restraints—Appendix A to the argument that the "effective" coefficient will not be greater than 0.075 and Appendix B to a method for calculating route bend restraints. To demonstrate their use, an example push force problem is worked out in Appendix C.

Because push forces predicted by the analytical work matched the insertion forces measured during the field evaluation test, it can be quite confidently predicted that 3-mile insertion distances will be routinely achieved with push forces much less than 10,000 lbs.

III. GENERAL PLAN FOR WAVEGUIDE INSTALLATION

The first step in the waveguide installation process is to develop an insertion plan which identifies push sites. In unusual terrain or for routes with many bends it may be necessary to verify that the distance between push sites is not excessive by calculating the insertion forces. A schedule is then prepared for each push site which specifies the sequence of installation of dielectric and helix modules.

At the push site an excavation is made which exposes approximately 100 feet of sheath. The sheath is cut at one end of the excavation, lifted, and supported so that the free end is horizontal and above ground level. An extension is welded to the sheath so it will project beyond the end of the excavation. The components of the insertion equipment are then aligned with and attached to the extension on the sheath.

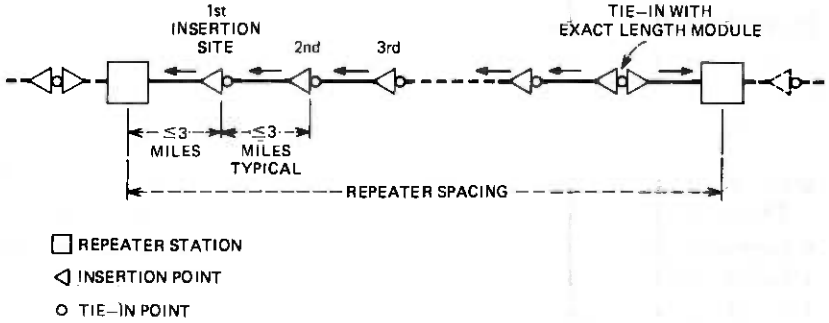

Fig. 1—Insertion segments within a waveguide repeater span.

As shown in Fig. 1 the initial insertion is made toward a repeater station from the first push site beyond the repeater station. Waveguide splices and pushes are made until the leading waveguide flange reaches the repeater station and is secured. At the push site the waveguide and sheath ends are temporarily sealed and lowered to the trench bottom. The insertion equipment is moved to the next adjacent site and is set up to repeat the process except that this time the push is made to the first push site instead of the repeater station. When the leading waveguide flange reaches the waveguide at the first site, the waveguide lines are spliced in the trench with special equipment, the gap in the sheath is closed, and the excavation is filled. This move-ahead-and-push-back procedure is repeated at each successive insertion site. The only variation required is to insert in both directions from the last site. At the last site a special-length waveguide module is fitted and spliced into the final gap in the waveguide line, and the sheath is closed, completing a repeater-to-repeater span.

If desired, insertions can be made in both directions from any site large enough to allow reversal of the insertion equipment. For example, an alternative installation technique might consist of inserting waveguide in both directions from every second site, thereby limiting activities at the remaining sites to the welding together of the abutting waveguide lines.

IV. THE SELECTION OF INSERTION SITES

The following requirements must be considered when push sites are selected:

(*i*) The temporary use of an easement 50 feet in width and 200 feet in length is required at each one-way insertion site. A much shorter span is acceptable for a site (a tie-in site) which will be used only for joining waveguide lines pushed together from adjacent push sites. At two-way

insertion sites, the required easement length is twice that needed for a one-way site.

(*ii*) Access to each push site for heavily laden supply trailers will be necessary.

(*iii*) The distance and the route configuration between push sites must not combine to require a pushing force in excess of 10,000 lb. The force can be calculated as shown in Appendix C.

(*iv*) Well-drained locations are desired, and bends in the sheath should be avoided so that alignments of the waveguide and sheath for the final tie-in splices are simplified.

Since each set-up for waveguide insertion is the second disturbance of right-of-way which was completely restored after the installation of sheath, it is important that insertion sites be carefully selected to avoid areas with substantial improvements and be located as closely as possible to public access. Ideally, affected property owners will be informed from the outset of negotiations for an easement of the two-stage nature of sheath and waveguide installation. However, the large distance allowed between sites should make their selection and acquisition simple.

V. INSTALLATION OF FIELD EVALUATION TEST WAVEGUIDE

5.1 General

During the field evaluation test, 8.75 miles of waveguide were installed using the insertion technique. The waveguide was installed in a series of eight pushes performed according to the general plan for waveguide installation discussed in Section III. The longest segment was 1.5 miles long and required a push force of about 2000 lb.

Each of the three possible kinds of field site was needed. To recount, they are sites used for a push in one direction only and a subsequent tie-in, sites used for pushes in both directions and a tie-in, and sites used only for a tie-in. The decision about the use to be made of a site was usually easily made from an assessment of the available space.

5.2 Insertion operations

Figure 2 shows the arrangement of the equipment used to install the field evaluation test waveguide. The flow of waveguide is from the shipping containers on the right to the sheath on the left. Each waveguide module leaves the sheath-like tube in the shipping container by way of a feeding tray, is delivered to the aligning and splicing fixture in the waveguide splicing vehicle (WSV) through an entry tube where it is joined to the waveguide line, travels from the splicer to the pusher in a second support tube, rolls the length of the pusher (where it picks up the pushing force), and enters the permanent, buried sheath by way of a temporary

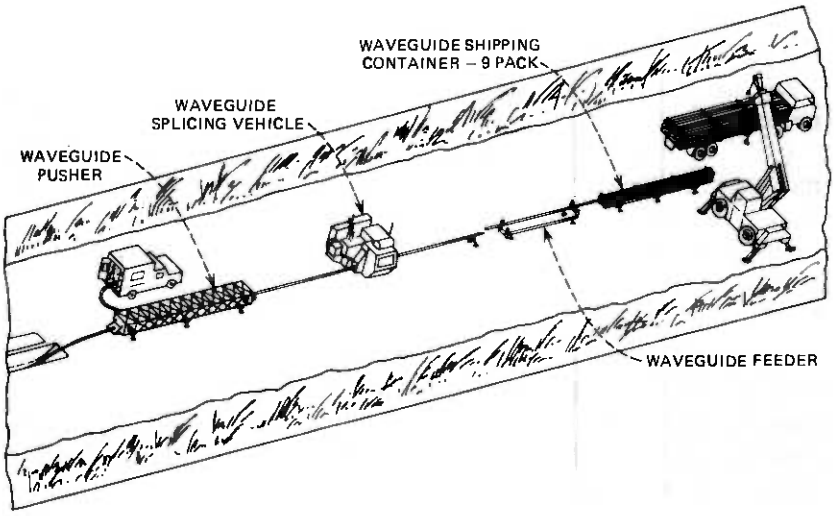

Fig. 2—Arrangement of field evaluation test equipment.

extension from the sheath to the frame of the pusher. The guiding principle in the design of all components which transported waveguide was that the waveguide would be supported at all times by the roller supports on the modules.

The distances separating the equipment shown in Fig. 2 were governed by the nominal length of 9 m (29 feet) for a waveguide module. The following relationships between waveguide and equipment resulted;

(*i*) When a flange pair was in proper position for welding in the WSV, the next flange pair to the left was very near the point of entry to the pusher, but entry had not yet occurred.

(*ii*) The next flange pair in the same direction was gripped in the pusher machine somewhere near the exit end of the pusher.

(*iii*) The right end of the waveguide module which was being welded to the waveguide line in the WSV projected to the right to a point just beyond the end of the support tube providing entry into the WSV.

(*iv*) The waveguide feeder machine was approximately the same length as a waveguide module, and a small separation distance was needed between the feeder and the WSV support tube to avoid interferences with the mobile feeder tray.

(*v*) Another small separation distance was provided between the waveguide feeder and the shipping container frame, also to avoid interferences. Beyond that the shipping container projected another 30 feet.

The entire set-up was approximately 180 feet in length.

Waveguide modules were transported to the site on flat-bed trailers which could carry 12 shipping containers. Each container had nine tubes in which waveguide modules were secured with expanded duct plugs. To use, the containers were first moved from the trailer to the shipping container frame, which was aligned with the feeder. In that position all tube ends and duct plugs were accessible to the feeder operator and were within the ranging zone of the waveguide feeder machine. The feeder operator aligned the feeder tray with the desired tube, removed the duct plug, and pulled the waveguide module into the tray where its length was measured. The tray was then shifted into alignment with the support tube entering the WSV, and the waveguide module was coupled to the protruding end of the module in the WSV with a spring-loaded flange clipping device. At this time the feeder operator's contribution to the feed-splice-push cycle was complete so the operator set a switch in the "ready-to-push" mode and thereby completed a part of the control circuit to the pushing machine.

In the waveguide splicing vehicle the splicer operator removed the clip connecting the waveguide module to the waveguide line. An aligning and preloading fixture was attached to the flanges which were pushed together face-to-face, with a large force, and the flanges were welded. On completion of the weld, the fixture was rolled to the side to permit an unobstructed visual inspection of the splice. When the inspection was completed the operator depressed a "ready-to-push" switch which notified the pusher operator of his readiness and completed another stage in the pusher control circuit.

When both the feeder and splicer operators had completed their tasks and were prepared for waveguide motion under pusher power (signified by their activations of "ready-to-push" switches), the pusher operator could push waveguide. He did so by activating the third in a series of three switches which provided power to the pusher controls (and released the pusher brake) and increasing the swash plate angle in the hydraulic pump to accelerate the pusher. If necessary, either the splicer operator or the feeder operator could stop the push instantly with emergency stop switches located in their areas. The splicer operator had an additional way to stop the waveguide; he was in the best position to determine when the waveguide line had been pushed far enough (one module length), and he stopped the pusher by simply releasing the "ready-to-push" switch when the next pair of flanges was in the proper position for welding.

A cycle of operation consisting of the described feeding, splicing, and pushing tasks hypothetically could be performed in about 5 minutes. The time averaged over all the cycles of the field evaluation test was 9.5 minutes, but this average included time used exchanging empty shipping containers and making test welds for quality checks.

5.3 Ending operations at an insertion site

Since the feeder operator measured each module of waveguide as it crossed the feeder, a record of the total assembled length was available at all times for comparison with the estimated distance to the tie-in point at the opposite end of the insertion section. When this measured length was within five modules of the estimated length, the operation was interrupted. A tie-in crew, dispatched to the opposite end, measured the actual remaining push distance by inserting quick-coupling duct rods into the sheath until the rod string contacted the front end of the waveguide. This remaining push distance minus the measured distance between the centerline of the splicing fixture in the WSV and the point at which the waveguide sheath had been cut at the insertion site determined the number of modules which remained to be spliced and pushed. When a fractional part of a module resulted, the actual number of modules added was equal to the rounded-down whole number.

To make the final positioning pushes, after the waveguide had cleared the pusher, special module-like extensions with mechanically coupled flanges were used to supply a pushing force to the waveguide line. These extensions were fed through the pusher one by one as needed until the gap between waveguide lines at the tie-in site at the opposite end was closed. An observer at the tie-in site directed the operation.

The tie-in crew utilized a special fixture and welder which could be lowered into the trench to make the splice which joined the waveguide lines in the tie-in pit (see Section 5.6). The gap in the sheath was closed by fillet-welding both ends of a special piece of sheath (an oversized tube which was slipped over the waveguide sheath prior to splicing the waveguide) which bridged the gap and slightly overlapped the waveguide sheath ends.

The tie-in anchored the waveguide line and freed the insertion crew to detach the mechanically coupled push links from the line at the opposite end. The sheath extension was removed, and the waveguide sheath was trimmed back to expose the waveguide end. Waveguide and sheath were sealed with temporary caps (and, for the field evaluation test, nitrogen gas was supplied to the waveguide to produce a protective internal pressure of a few psi). The insertion crew then disassembled and moved all equipment to the next push site.

5.4 Waveguide splicing vehicle

The WSV used to splice waveguide during the field evaluation test (Fig. 3) was originally built for waveguide installation by the modular technique. The modular technique, of course, required complete mobility of the aligning fixture and welding machine, and that accounts for the tractor-mounted sidecab which houses the splicing equipment. The

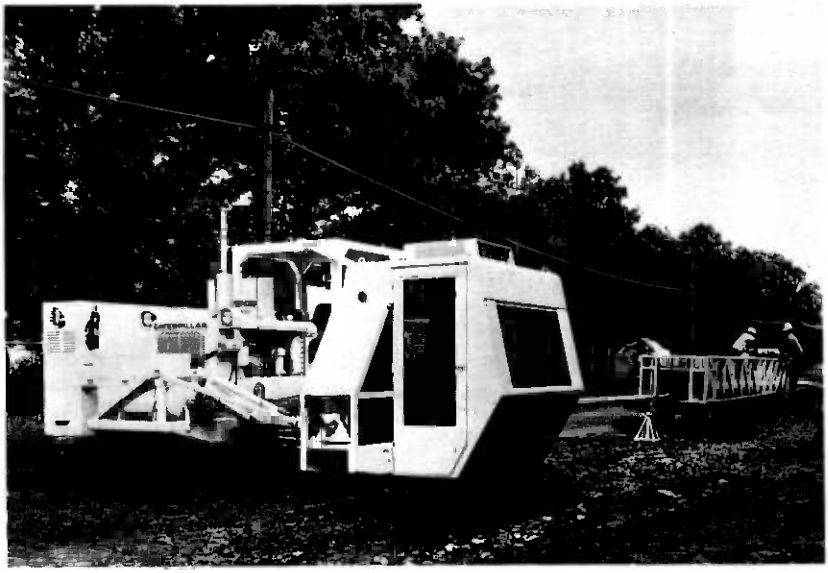

Fig. 3—The waveguide splicing vehicle.

tractor additionally served as a mounting platform for the compressed air, chilled water, hydraulic power, and electric power generators and housed the compressed gas cylinders which supplied the mixture of helium and argon which shielded the weld arc.

5.4.1 Splicing fixture

The flange aligning mechanisms and the welding torch were mounted in the splicing fixture, shown in Fig. 4, which was located in the WSV sidecab. The primary functions of the fixture were locating, aligning, preloading, and welding waveguide flange pairs, and it accomplished them with two waveguide flange clamps located in a C-shaped frame, a preloading mechanism for applying compressive face loads on the pair of flanges to be welded, a welding torch mounted on a ring gear, a torch cable retraction mechanism, and various associated controls, sensors, and indicators. All fixture equipment was mounted within a cabinet on a carriage which permitted movement of the fixture parallel to the axis of the waveguide line. This mobility of the fixture within the WSV permitted the flange clamps and welding torch to "seek out" the flange pair to be welded, which could be in various positions within the sidecab, and, subsequently, to "leave" the freshly welded flange pair to permit a visual inspection.

5.4.2. Torch, torch drive, and cable retraction mechanism

The torch is the welding electrode vise and the terminal for the electrical cable. It was secured in a bracket which permitted precise electrode

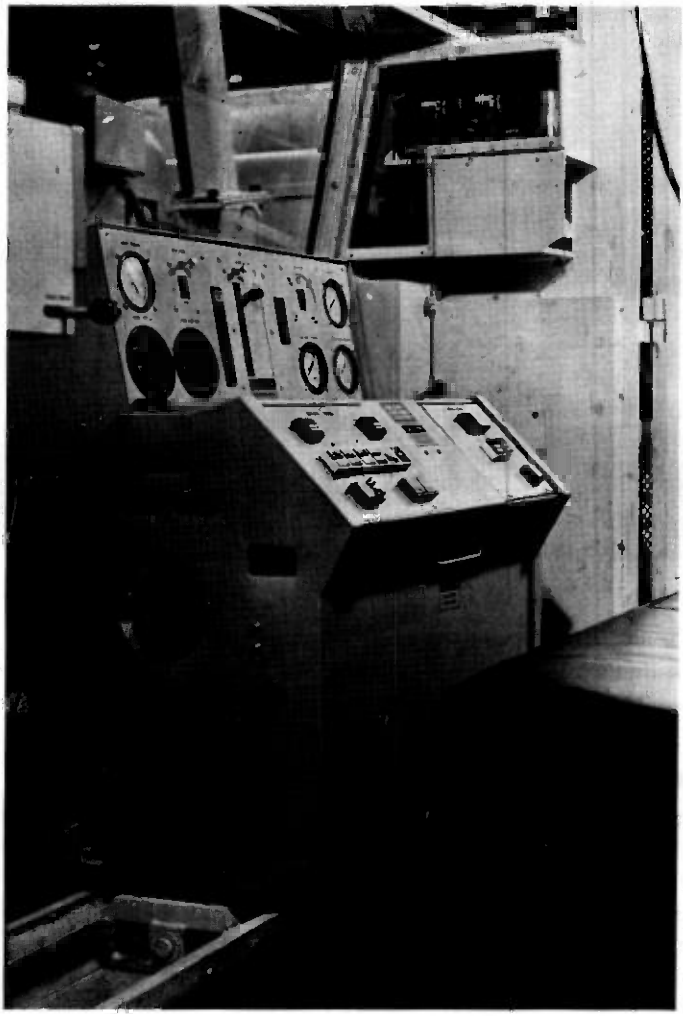

Fig. 4—The WSV aligning and splicing fixture.

adjustments in relation to the flange joint, and this bracket was in turn attached to a ring gear driven by an electric motor which produced one complete revolution of the torch (and therefore a completed weld) in approximately 95 seconds.

The torch was alternately driven in forward and reverse directions so that a torch-driver cycle was completed after two flange pairs had been welded. Sufficient electrical cable was provided to allow a complete revolution of the torch, and this cable was paid out and retracted during a cycle with a pair of sheaves, one of which was mounted on a traveling block in vertically oriented ways under the other. The weight of the

traveling block produced a constant tension on the cable and thereby retained it in guides on the ring gear which held the cable away from the flange and moving fixture parts.

5.4.3 Flange clamps

Actual contact with waveguide flanges was made with flange clamps. Each flange clamp was composed of two halves which traveled in vertical ways to produce a clamp/unclamp action. As shown in Fig. 5, which illustrates the aligning mechanisms, the entire left clamp was in turn mounted on horizontal ways which permitted gripped flanges to be brought together. Figure 5 gives particular emphasis to the method by which the fixture was initially calibrated with shims to produce coincident left and right clamp centerpoints to control offset misalignments of waveguide flanges. To produce automatic centering of gripped waveguide flanges when outside diameters of the flanges varied, in conformance with specifications, as much as 0.0005 inch, each flange clamp had four equally spaced pins with precisely identical contact surfaces arranged on a diameter slightly smaller than the minimum flange diameter permitted. Centering of a flange within a clamp was therefore achieved by the uniform embedment (assuming homogeneous flange materials) of the four contact pins into the outer rim of the flange. Theoretically, optimum fixture calibrations made with the furnished shims should have limited maximum offset misalignments of flange pairs to 0.0007 inch. In practice, the average of misalignments in flange pairs made during the field evaluation test was 0.0011 inch.[1]

Each clamp half was faced with a copper lining which acted as a heat sink to limit the temperature rise of the flanges (and thereby limited the danger to the dielectric lining) during welding. The copper linings, in turn, had cavities through which chilled water was continuously circulated.

5.4.4 Preload mechanism

Tilt misalignment of waveguide at the flanged coupling was controlled with large-surfaced faces on the flanges accurately machined normal to the waveguide axis during manufacture. In the field these faces were pressed together with 10,000-lb forces applied at the outer edges of the flanges prior to welding. This preload force and the flange face relief design[1] results in a residual compressive force between the flange faces after welding, which is particularly effective in controlling gaps or tilts in the couplings when the waveguide is placed under tension or is curved or is subjected to both curves and a tensile force. In the fixture, the movement which brought flange faces together and the force which preloaded the faces were produced with the mobile left flange clamp

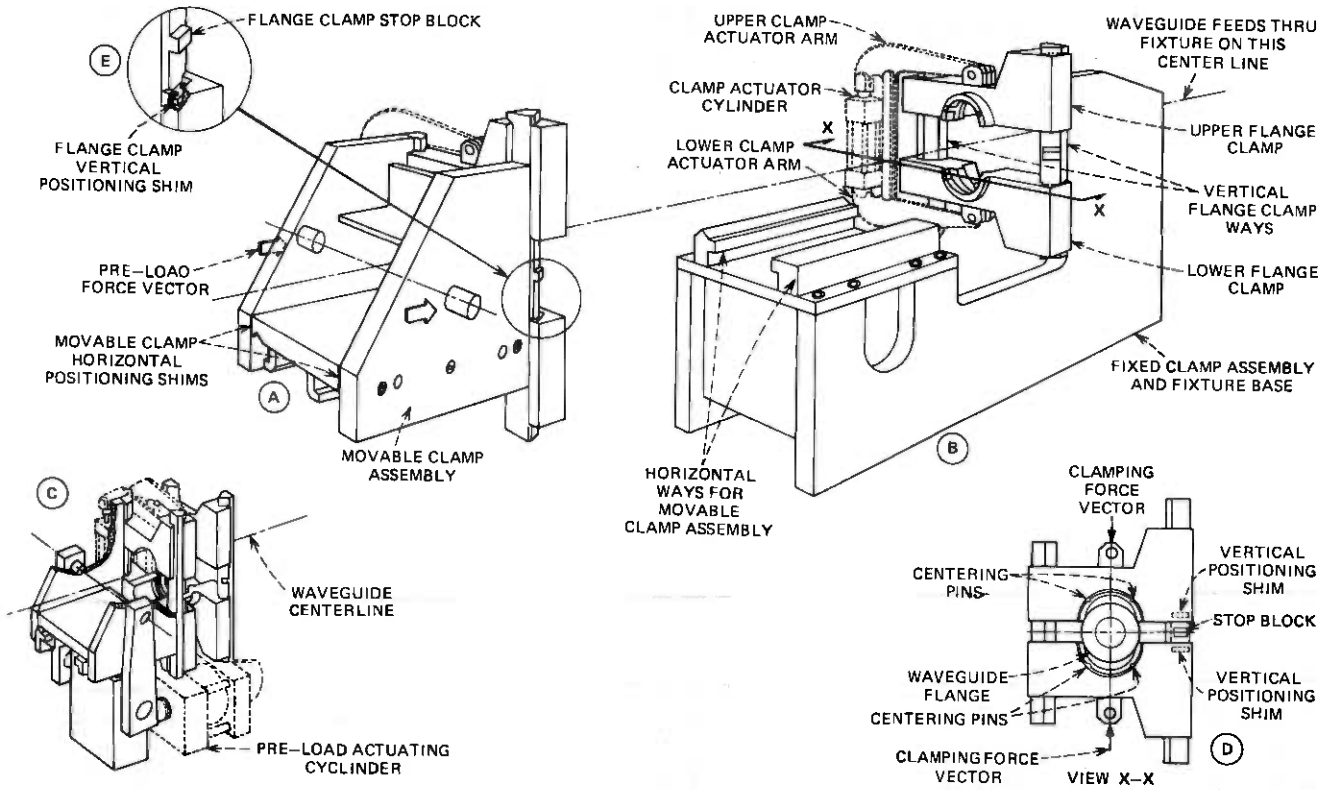

Fig. 5—The WSV aligning and preloading mechanisms.

which was mounted on horizontal ways and linked to a hydraulic cylinder located beneath the clamps in the fixture.

5.4.5 Welder and ozone evacuation

The welding process utilized was the tungsten electrode, inert-gas-shielded-arc process. Because dimensional tolerances of the waveguide flanges were exceptionally small, the material of the flanges could be reliably fused without using filler metal. The Hobart model CT300-DC CYBER-TIG welder was used with a 600 series programmer maintaining control of arc formation, weld current, shield gas application, and cooling water flow.

The fusion of flange pairs by electric arc welding is accompanied by the production of some smoke and ozone. These products were drawn out of the weld chamber through a duct to a blower which exhausted to the exterior of the splicer cab.

The welding machine made over 1600 welds during the field evaluation test and suffered only one malfunction. Although that malfunction damaged a flange pair beyond further use, a suitable flange weld cut-out tool was successfully pressed into service so that the only lasting effects of the malfunction were two lost waveguide modules and an hour of production time. Weld inspection was strictly visual and was adequate to assure that only tight welds free of leaks were installed during the Field Evaluation Test.

5.5 Waveguide pusher

The waveguide pusher, shown in the background in Fig. 3 and in close-up in Fig. 6, applied the insertion force to the waveguide line. It essentially consisted of a pair of endless roller chains which were synchronously turned, when commanded from the pusher operator's control panel, by two reversible hydraulic motors. The hydraulic motors were in turn powered by an electrically driven pump located in the truck shown parked next to the pusher in Figure 2. The source of electrical power was the motor-generator located on the WSV tractor.

The pusher transmitted the pushing force through the roller chains to the waveguide by means of a yoke which was manually placed over each waveguide flange pair just before those flanges entered the pusher. Each yoke had teeth which meshed with the roller chain as it entered the pusher. Meshing was aided by the pair of small synchronizer chains shown clearly in Fig. 6. The forces required to insert, brake, or hold waveguide on inclined routes were in turn transmitted back to the waveguide sheath through a connection between the sheath extension and the pusher frame.

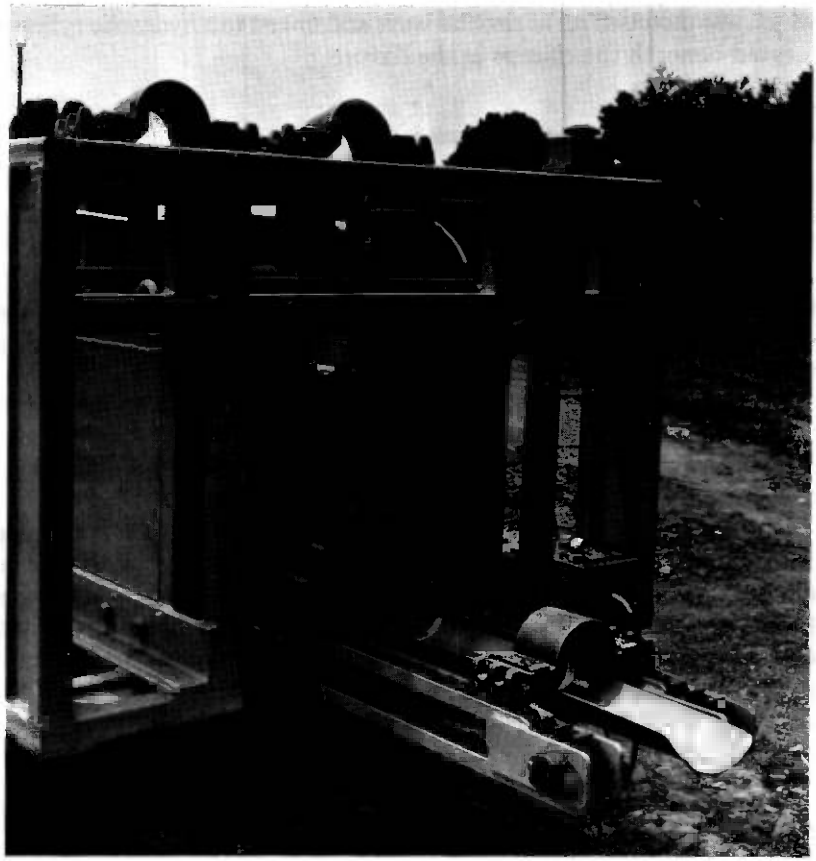

Fig. 6—The pusher.

Since the pusher was 32 feet long and the longest waveguide module was only 29.5 feet long, at least one yoke was fully engaged in the chains at all times, and, during a small part of every push cycle, two yokes on adjacent flange pairs were in the machine at the same time. Two yokes, when both were engaged in the chains, were separated by a unit multiple of the pitch of the chain. Since waveguide modules were manufactured in random lengths unrelated to the roller chain pitch, the yokes had to be designed with clearance around the flange pair equal to the chain pitch, which in this case was in excess of one inch. The load was always carried by the leading yoke and when this yoke was released from the pusher its load was transferred quite suddenly to the trailing yoke. The clearance around the second yoke resulted in an impact which limited the amount of force that could be safely applied to the waveguide, and thereby restricted the maximum insertion distance during the field evaluation test to about 8300 feet.

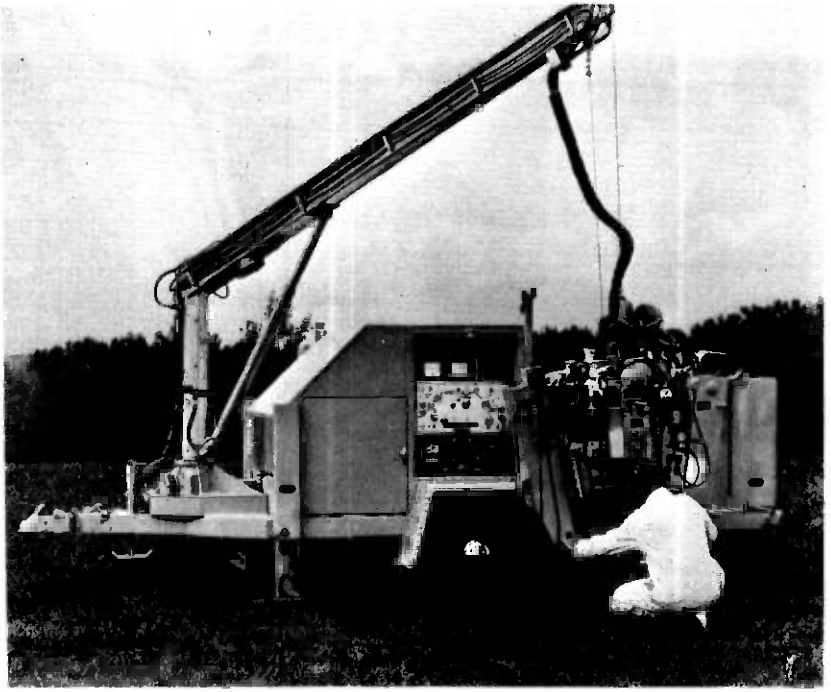

Fig. 7—The in-trench splicer.

5.6 In-trench splicer

The In-Trench Splicer (Fig. 7) does exactly the same waveguide flange splicing job that the WSV does, except that it was designed with an aligning, preloading, and splicing fixture which can be lowered by hoist to the trench bottom to make tie-ins. The welds made with this machine during the field evaluation test were indistinguishable from those made with the WSV.

Figure 8 is a close-up view of the flange clamps of the In-Trench Splicer shown just before they were lowered over the flange pair to be spliced. The small gap seen between the flange faces will be closed by the hydraulic cylinder which supplies the preloading force to squeeze the flange faces.

VI. EVOLUTION OF INSERTION EQUIPMENT SINCE THE FIELD EVALUATION TEST

The field evaluation test waveguide was installed during the fall and winter months using Long Lines craftsmen and operating engineers assigned at random from the local union hall. The insertion technique was demonstrated to be a forgiving and, therefore, practical method to install waveguide. The demonstration equipment was reliable under

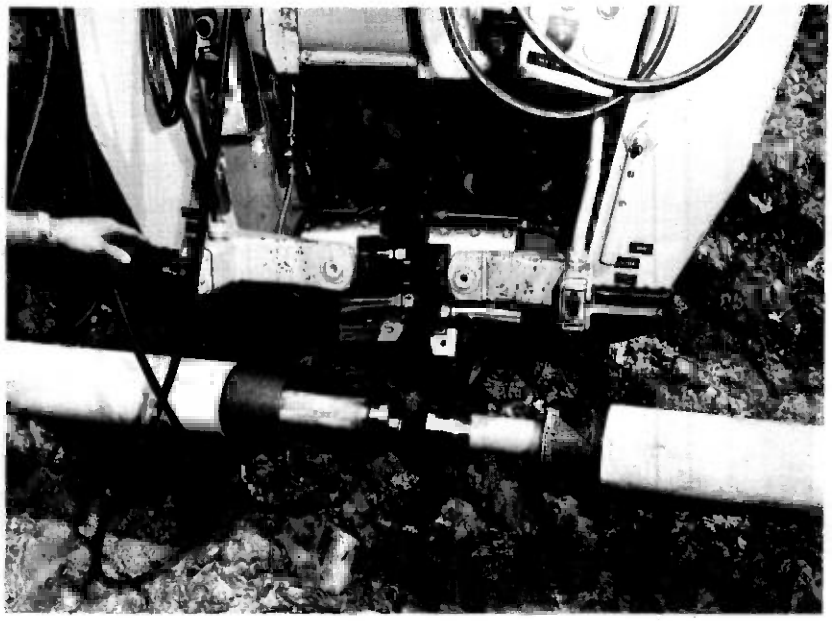

Fig. 8—Close-up of the flange clamps on the in-trench splicer.

sometimes unfavorable weather conditions, but as usual, one of the most useful outcomes of the field test was a list of suggestions, many of them offered by the operators, for improving the waveguide insertion system. Those suggestions which promised major improvements were:

(*i*) Eliminate the need to remove the shipping containers from the trailers, and thereby eliminate the crane.

(*ii*) Make the operation an all-weather operation.

(*iii*) Provide inherent protection against vandalism.

(*iv*) Provide a greater pushing distance capability by eliminating the load transfer problem associated with the waveguide pusher.

(*v*) Reduce the time required to set up the insertion equipment by having fewer components which require independent alignment.

(*vi*) Reduce the time required to make tie-ins and eliminate the need for the in-trench splicer.

Each of these suggestions was incorporated in the design of a new Waveguide Insertion System (WIS). All WIS equipment is contained within two 45-foot-long highway vans designed to be linked in precise alignment in the field. Enclosing the equipment satisfactorily eliminated the weather- and vandal-related problems. To eliminate the crane the feeder concept was expanded to permit bringing the tray into alignment with all shipping tubes when those tubes are in packages still on a flat-

bed trailer. A corollary improvement is reflected in the design of 54-module waveguide shipping packages which increase a trailer-load capacity to 1 mile from the 0.6 mile limit in a load of nine-packs.

New concepts were required to remove the limits on push distance and productivity. Some of these new concepts can be seen in Fig. 9, which illustrates the principal activities in a cycle of operations. As with the demonstration equipment, waveguide modules (which may be either 29 or 34 feet long) are shipped in sheath-like tubes bound into packages, except that the packages are not removed from the delivering trailer. All of the tubes can be reached from within the van containing the feeder equipment without special equipment when the supply trailer is properly docked. One operator rolls waveguide modules into troughs on a mobile tray, as in sequence number 2 in the illustration, and measures the module length. Trays are handled with a carriage and vertical lift mechanism so that a supply of full trays is maintained in a floor-level indexing device. Properly managed, this reserve capacity allows production to continue without external waveguide supplies for 30 minutes. Empty trays are cycled for refilling.

The WSV splicing fixture (Fig. 4) is retained in the WIS and is operated in the familiar way, as depicted in sequences 5 and 6 in Fig. 9. The pushing machine, however, is very different. Waveguide is inserted a distance equal to the length of one module after every weld; however, the push force is transferred to the waveguide by gripping the last welded flange pair in a traveling clamp which is permanently attached to an endless chain. A hydraulic motor supplies power as commanded to the chain; since the motor is reversible, extraction forces can be supplied to the waveguide if necessary. Push loads are continuously monitored and displayed to the operator.

At the end of the push stroke, the traveling clamp delivers the flange pair to a stationary clamp where a transfer of any residual force is made. When released, the traveling clamp can be returned to the splicing fixture for the next push cycle. This decoupling of the two clamps which are required to positively control waveguide overcomes the distance limiting problem of the field evaluation test pusher.

For the safety of the operators, all controls were carefully designed to prevent the unintentional simultaneous release of both clamps. This prevents a possible runaway line for certain right-of-way configurations.

The WIS is designed to be operated in 4-minute cycles with no interruption in splicing provided that exhausted supply trailers are exchanged within 30 minutes. The overall objective is 100 miles of production per year, which can be accomplished with single-shift operations, a five-minute allowance for each splice-and-push cycle, and 200 working days per year.

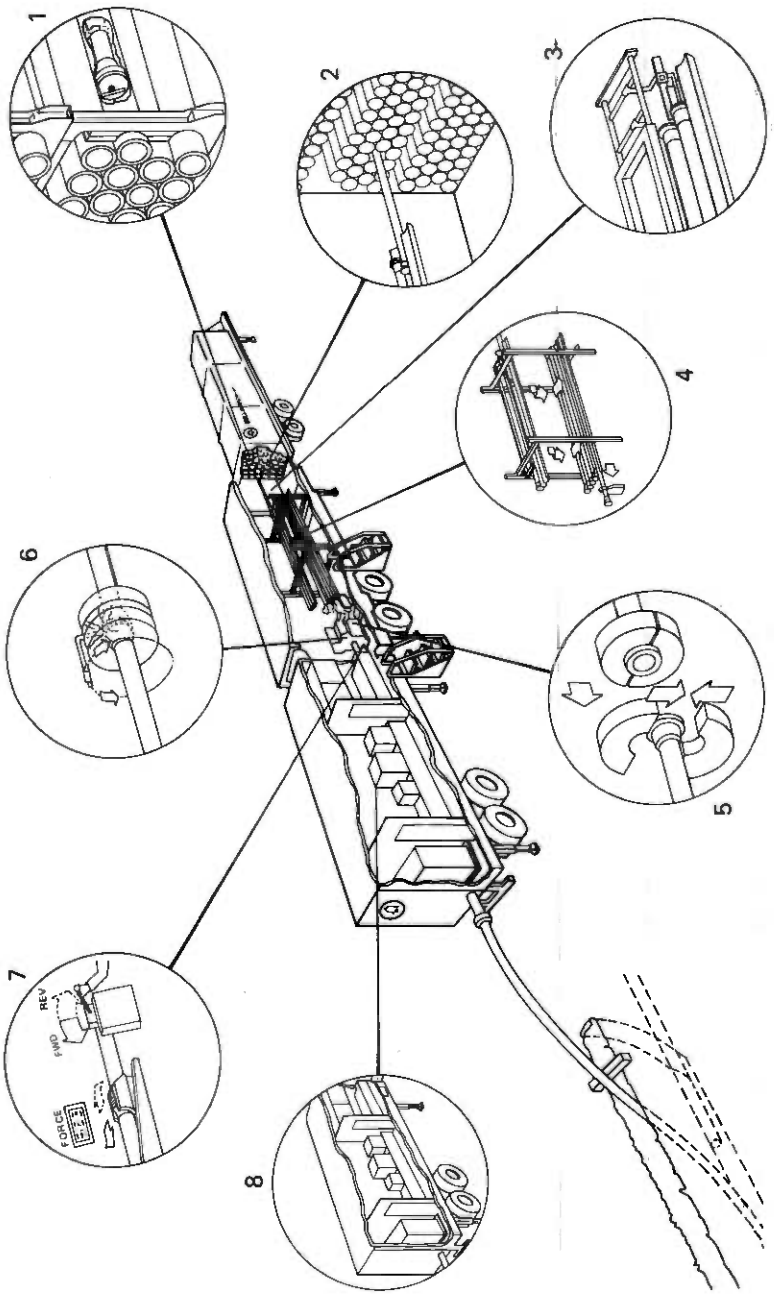

Fig. 9—The operating cycle of the waveguide insertion system.

The in-trench splicer is capable of making fusion splices in waveguide with a quality equal to those produced in the insertion fixture but at a much higher cost per splice. A mechanical coupler which can be used to make tie-in splices in the waveguide has been developed since the field evaluation test. This coupler is self-aligning and provides a gas-tight seal after installation with simple hand tools.

VII. SUMMARY

The insertion method for the installation of WT4 waveguide is the successor to various other methods which included direct burial of waveguide and simultaneous installation of sheath and waveguide. The insertion method is possible because of sheath encasement, discrete waveguide supports with rollers, and the absence of expansion joints in the waveguide. The technique has been tested to a distance of 8300 feet, and theory and test indicate that 3-mile insertion distances will be routinely achieved with push forces less than 10,000 lbs.

Equipment has been developed and used to demonstrate reliable installation of waveguide by the insertion method.

APPENDIX A

The effective coefficient of friction

Installed sheath will not be perfectly straight, and waveguide pushed into imperfect sheath will be forced to deform to follow its shape. Increased loads on some roller supports, and therefore increased resistance to insertion, will result. This increased loading can be accounted for analytically be defining the effective coefficient of friction as that coefficient which produces a reliable prediction of the pushing force needed to insert waveguide in sheath constructed to WT4 system specifications when only the unit weight of waveguide and the length of sheath are known. The effects of route bends and elevation changes are not included in this definition.

The effective coefficient was calculated for those shapes which result when sheath is supported at various regular intervals. Since the inside diameter of the sheath is slightly larger than that of a circle circumscribed about the roller supports, the problem of finding the deflected shape of the waveguide from the sheath's known profile is a nonlinear one. It was solved by a method using an iterative Green's Function solution. Figure 10 shows the results of the calculations. The ordinate of the graph is expressed in terms of the midspan sheath deflection. The contour $M = 1.0$ identifies the deflections below which there is no resistance in excess of that encountered in a truly straight sheath. The curves $M = 1.25$ and $M = 1.5$ identify the deflections for which the insertion force is the stated multiple of the straight sheath value. The lower

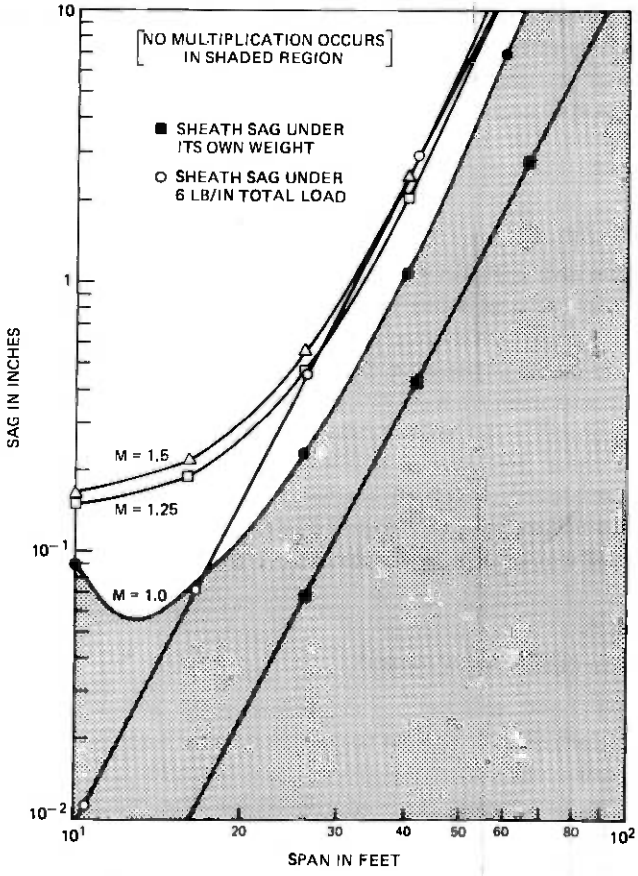

Fig. 10—Friction multiplication factor for the diametral clearance model.

of the two straight lines of the graph represent the maximum midspan sag which a periodically supported sheath could assume under its own weight. The upper straight line gives the maximum midspan sag which the sheath could assume under a 6 pound per inch sheath-weight-plus-backfill load. Six pounds per inch is a backfill load representative of field evaluation test experience. Notice that, for the periodically supported sheath considered, the required insertion force is not greater than 50 percent more than the straight sheath value for unsupported spans of any length.

With the current sheath installation specifications[2] limiting the maximum unsupported sheath span to 30 feet, a periodically supported sheath with 30-foot spans represents a worst-case condition. Under this assumption the friction multiplication contours of Fig. 10 predict a maximum multiplication of about 1.3. Since the straight conduit coef-

ficient of friction is 0.058, a curvature multiplication factor of 1.3 implies an effective coefficient of friction which will, at all times, remain below 0.075. Insertion force measurements during the field evaluation test correspond to an effective coefficient of friction of 0.064 (average), a number which is closer to the truly straight sheath coefficient than to the theoretical upper limit.

An insertion distance of up to 6 miles could be realized in sheath with no route bends assuming a 10,000 pounds pushing force and a 0.075 effective coefficient of friction.

APPENDIX B

Route bends—effect on insertion forces

When waveguide is pushed through a route bend, the loading on the roller supports is increased due to deflection of the waveguide relative to the sheath. The deflections occur at transition zones between the straight and curved sections and along the entire length of the curve due to the axial loading on the waveguide. The increased loading on the roller supports, of course, increases the frictional resistance in the bearings and a greater axial load is required to move the waveguide through bends.

The waveguide deflection at transition zones between straight and curved sections is highly dependent upon the transition curvature and the radius of curvature of the bend. For sheath installations with a minimum radius of curvature of 250 feet it can be shown that the added roller support friction caused by deflections in the transition zones of the waveguide is negligible. The lateral displacement along the entire length of the curve due to the axial loading is the only significant contributor to increased roller support loading. Because of this the waveguide may be treated as a pushable-flexible cable in curves.

The waveguide is modeled as a beam whose neutral axis in the undeformed state forms a circular arc of radius r. The beam is subjected to bending forces acting in the plane of curvature. The roller support reaction is everywhere normal to the axis of the beam and proportional to the radial deflection y of the beam. Vertical plane curvature is not considered, but the effects of elevation changes are included in the analysis.

An infinitesimal element of the beam (Fig. 11) is acted upon by shearing force Q, normal force N, bending moment M, spring reaction $ky\ ds$, and friction force $\mu k|y|$, where μ is the coefficient of friction. These forces all arise from the beam's deformation in the plane of curvature. In addition the beam is acted upon by friction force $\mu w\ ds$ and the projection of gravity onto the beam's axis, $w\alpha\ ds$, where α is the inclination of the axis with respect to the horizontal and w is the beam's weight per unit length.

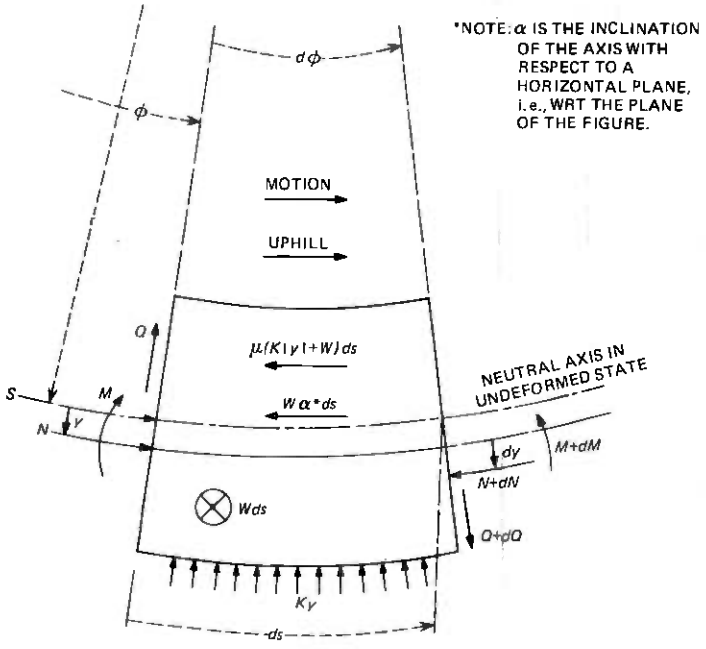

Fig. 11—Equilibrium of an element of waveguide.

The beam is inserted into the sheath from left to right in Fig. 11, and the route slopes uphill in the direction of insertion.

The radial, tangential, and moment equilibrium equations are:

$$\text{(radial) } dQ + N\,d\phi - kyr\,d\phi = 0 \tag{1}$$

$$\text{(tangential) } Q\,d\phi - dN - \mu(k|y| + w)r\,d\phi = w\alpha r\,d\phi \tag{2}$$

$$\text{(moment) } Qr\,d\phi + N\,dy = dM \tag{3}$$

The moment M may be expressed in derivatives of deflection by the relation

$$M = -\frac{EI}{r^2}\left(\frac{d^2y}{d\phi^2} + y\right) \tag{4}$$

to give a set of equilibrium equations expressed in terms of shears, axial forces, and displacements:

$$\frac{dQ}{d\phi} + N - kyr = 0 \tag{5}$$

$$Q - \frac{dN}{d\phi} - \mu(k|y| + w)r = w\alpha r \tag{6}$$

$$Q + \frac{N}{r}\frac{dy}{d\phi} + \frac{EI}{r^3}\left[\frac{d^3y}{d\phi^3} + \frac{dy}{d\phi}\right] = 0 \tag{7}$$

When the intermediate variables are eliminated from these equations the following fundamental differential equation governing waveguide insertion into a curved sheath is obtained:

$$\frac{d^5y}{d\phi^5} + \left[2 + \frac{Nr^2}{EI}\right]\frac{d^3y}{d\phi^3} + \left[1 + \frac{kr^4}{EI} - \frac{Nr^2}{EI}\right]\frac{dy}{d\phi} + \mu\frac{kr^4}{EI}|y| = -\frac{wr^4}{EI}(\mu + \alpha) \tag{8}$$

With the axial loads and bend radii permissible in waveguide, some terms in eq. (8) may be neglected. The following conditions apply:

$$w = 4.34 \text{ lb/ft}$$

$$N < 10^4 \text{ pounds}$$

$$EI = 27.21 \times 10^6 \text{ lb-in}^2$$

$$r \geq 3000 \text{ in}$$

$$k = 20 \text{ lb/in}^2$$

$$\mu \leq 0.1$$

For any axial compression N greater than about 60 pounds, the term Nr^2/EI dominates in the coefficient of $d^3y/d\phi^3$. For all permissible waveguide radii the terms *1* and Nr^2/EI are negligible in the coefficient of $dy/d\phi$. Therefore eq. (8) may be approximated by

$$\frac{d^5y}{d\phi^5} + \frac{Nr^2}{EI}\frac{d^3y}{d\phi^3} + \frac{kr^4}{EI}\frac{dy}{d\phi} + \mu\frac{kr^4}{EI}|y| = -\frac{wr^4}{EI}(\mu + \alpha) \tag{9}$$

If the waveguide deformation y is of one sign only, or if the waveguide in a curve is subdivided for analysis into parts each having a single direction of deflection, then eq. (9) reduces to the linear equation

$$\frac{d^5y}{d\phi^5} + \frac{Nr^2}{EI}\frac{d^3y}{d\phi^3} + \frac{kr^4}{EI}\frac{dy}{d\phi} \pm \mu\frac{kr^4}{EI}y = -\frac{wr^4}{EI}(\mu + \alpha) \tag{10}$$

where the plus sign is chosen for waveguide deflection toward the outside of a curve and the negative sign is chosen for deflection toward the inside of the curve.

The waveguide insertion force may be found by returning to eqs. (5), (6), and (7) and deriving an analytic expression for the axial compression N in terms of derivatives of the displacement. Since the solution of the governing differential equation is known as a sum of exponentials there is conceptually no difficulty in this approach. However, a more direct

approach is possible if we recognize from the beginning that shear and moment effects are negligible in the central section of long route bends. A long route bend is one whose arc length exceeds 80 feet. For the minimum 250-foot radius a long bend is any bend exceeding 18 deg.

Neglecting the shear and bending moment in waveguide is tantamount to equating it to a flexible cable. This equivalence is tempered by the requirement that the waveguide be able to support compressive stress. Careful manipulation of eqs. (5) and (6) preserves this distinction between waveguide and cable while still illustrating their essential similarities.

If the shear Q and its derivative $dQ/d\phi$ are negligible, and if waveguide deflection is assumed positive (outward), then eqs. (5) and (6) may be solved simultaneously to give the first-order differential equation

$$\frac{dN}{d\phi} + \mu N = -wr(\mu + \alpha) \tag{11}$$

with solution

$$N = N_o e^{-\mu\phi} + wr\left(1 + \frac{\alpha}{\mu}\right)(e^{-\mu\phi} - 1) \tag{12}$$

where N_o is the compressive stress at position $\phi = 0$, as illustrated in Fig. 12.

If the shear Q and its derivative $dQ/d\phi$ are negligible, and if waveguide deflection is assumed negative (inward), then $|y| = -y$, and eqs. (5) and (6) may be solved simultaneously to give the first-order differential equation

$$\frac{dN}{d\phi} - \mu N = -wr(\mu + \alpha) \tag{13}$$

with solution

$$N = N_o e^{\mu\phi} + wr\left(1 + \frac{\alpha}{\mu}\right)(1 - e^{\mu\phi}) \tag{14}$$

where again N_0 is the axial compression at position $\phi = 0$. In the case where the deflection y is negative, eq. (5) says that the axial compression N is also negative, i.e., in fact tensile. If then N is replaced by $-T$ in eq. (14), the conventional relation governing tension in a flexible cable is obtained:

$$T = T_o e^{\mu\phi} + wr\left(1 + \frac{\alpha}{\mu}\right)(e^{\mu\phi} - 1), \tag{15}$$

where T_o is the axial tension at position $\phi = 0$.

Equations (12) and (15) apply under the assumption that deflection in a route bend is either everywhere outward or everywhere inward. Since

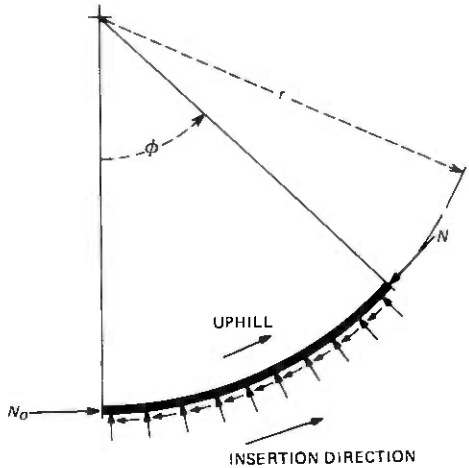

Fig. 12—Plan view of forces on a segment of waveguide in a curve.

waveguide is installed by pushing from the trailing end, it is usually safe to assume a compressive state; however, the axial load is not always compressive. Sometimes the front end of waveguide is pushed into sheath which slopes so steeply downhill that the gravitational pull exceeds the frictional resistance, and therefore at least a part of the waveguide line is in tension. If all of the waveguide line is in tension, then a restraining force is required at the trailing end and eq. (15) is applied without difficulties.

It may be possible to have both compressive and tensile forces in a bend, for example when the leading end of the waveguide is going down a steep hill and the trailing end is in less steeply sloping sheath so that the frictional resistance is greater than gravitational pull. When this happens it is necessary to locate the point where the force is zero and to apply the correct equation [either (12) or (15)] to the segments of the curve either side of the null point.

The null point is equivalent to a free end and can be found by setting N_o equal to zero in eq. (12). If the position in a curve where a null point exists is defined by θ, then

$$\theta = -\frac{1}{\mu} \ln_e \left[\frac{N}{wr\left(1 + \frac{\alpha}{\mu}\right)} + 1 \right] \tag{16}$$

APPENDIX C

Calculating Insertion forces for a hypothetical route

To determine the force required to insert waveguide in any route, the route is partitioned into straight and curved sections, as illustrated on

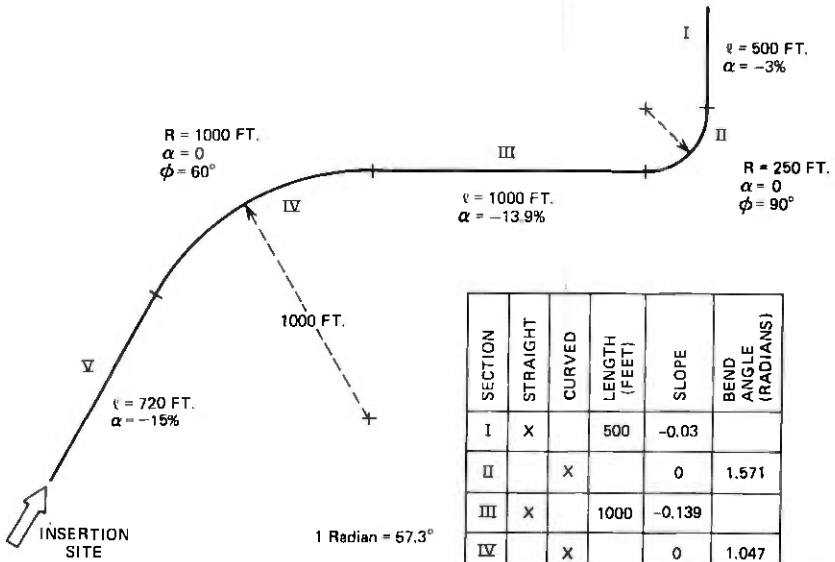

SECTION	STRAIGHT	CURVED	LENGTH (FEET)	SLOPE	BEND ANGLE (RADIANS)
I	X		500	−0.03	
II		X		0	1.571
III	X		1000	−0.139	
IV		X		0	1.047
V	X		720	−0.15	

Fig. 13—Hypothetical route for push force calculation.

the example route shown in Fig. 13. It two adjacent curved sections of different radii had existed, they would have been treated as two distinct sections. Then, for each straight section the length and grade are tabulated, and for each route bend the radius of curvature, r, the included angle, ϕ (measured in radians), and the grade are tabulated. All grades, α, are calculated by

$$\alpha = \frac{\text{Far end elevation} - \text{Near end elevation}}{\text{Section length}}$$

The contribution of each of the partitioned sections to the total resistance to insertion is calculated. In route bends, eq. (12) of Appendix B [or eq. (15) of Appendix B if the tensile condition is discovered] is applied, and the simple relationship

$$N = wl(\mu + \alpha)$$

is used to find the contribution to axial force of each straight section. From eqs. (12) and (15) of Appendix B it can be seen that the thrust N_o and tensile T_o are determined at the *trailing end* of the waveguide. For this reason it is convenient to start at the leading end of the waveguide and work back to the insertion point, calculating the insertion forces segment by segment. The process is described in the flow chart of Fig. 14, and the axial force which results is the push force at the moment the

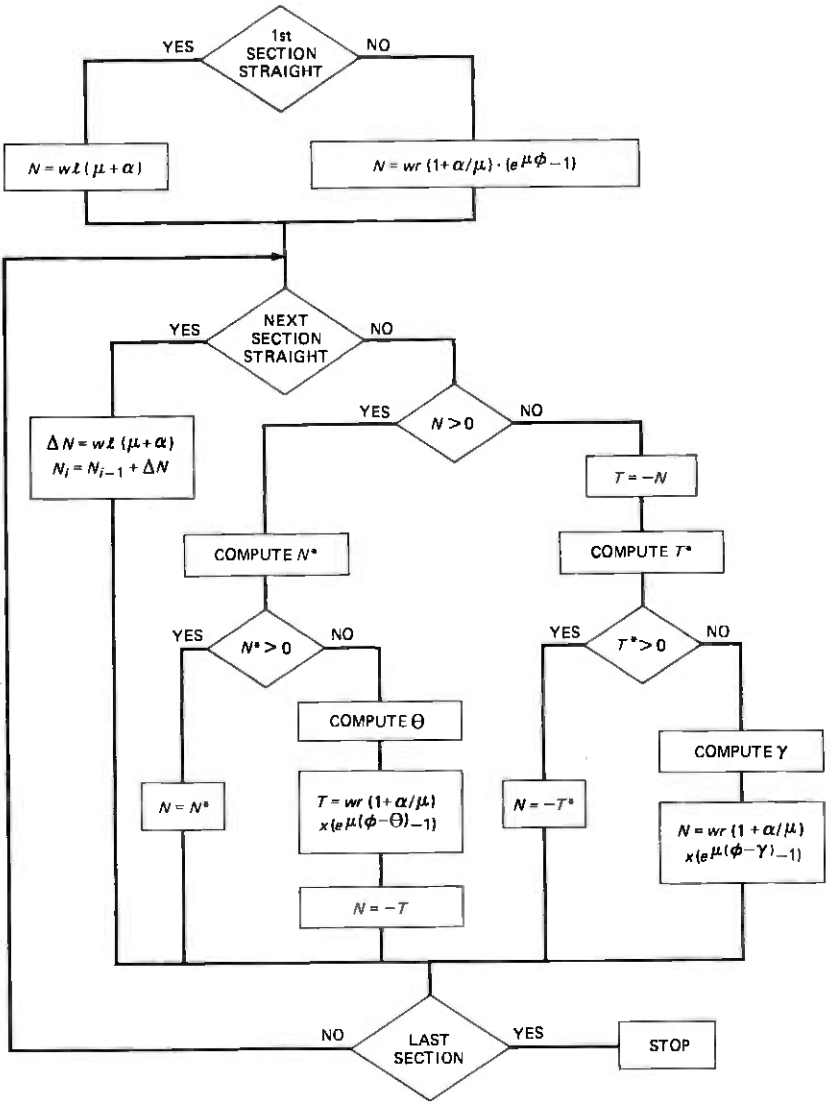

Fig. 14—Insertion force flow diagram.

final piece of waveguide leaves the insertion machine. Depending on the topography of the particular route, the force during insertion may be either higher or lower than the final push force. Computation of the force

history during insertion is more complicated although the procedure is essentially the same.

The hypothetical route of Fig. 13 is now used to illustrate insertion force calculations. The route is divided into five sections.

Section I. This section is straight and unloaded at the front end. The total force at the transition point to Section II is simply the change of force ΔN. The grade in this section is −3 percent.

$$N = wl(\mu + \alpha)$$

$$= 4.34 \text{ lb/ft} \times 500 \text{ ft} \times (0.07 - 0.03)$$

$$= 86.8 \text{ lb}$$

Section II. The next section is curved. The axial compression N at the junction with Section I is greater than zero, and since the slope in this section is zero there is no possibility of sign reversal. The axial force at the junction with Section III is given by

$$N = N_o e^{\mu\phi} + wr\left(1 + \frac{\alpha}{\mu}\right)(e^{\mu\phi} - 1)$$

$$= 86.8 \times \exp(0.07 \times 1.1708) + 4.34 \times 250 \times [\exp(0.07 \times 1.5708) - 1]$$

$$= 223 \text{ lb}$$

Section III. This section slopes steeply downhill. The slope is sufficient to overcome the restraining action of friction. A compression-tension transition is possible, but since the section is straight this possibility is of no particular concern.

$$\Delta N = wl(\mu + \alpha)$$

$$= 4.34 \times 1000 \times (0.07 - 0.139)$$

$$= -229.5$$

$$\text{N} = 223 - 299.5 = -76.5 \text{ lb}$$

The axial force at the junction with curved Section IV is tensile.

Section IV. The axial force at the forward end of this section is tensile, and since the slope in this section is zero, a sign reversal within the section is possible. To test, compute an assumed tension T* at the trailing end.

$$T^* = Te^{-\mu\phi} + wr\left(1 + \frac{\alpha}{\mu}\right)(1 - e^{-\mu\phi})$$

$$= 76.5 \exp(-0.07 \times 1.05) + 4.34 \times 1000 \times (1) \times [1 - \exp(-0.07 \times 1.05)] = -237$$

Since the computed trailing end force is a negative tension, that is, a compression, there is actually a sign reversal somewhere in the bend. The angle at which zero force occurs is found by applying the formula

$$\mu\theta = \ln_e \left\{ 1 + \frac{T}{wr\left(1 + \frac{\alpha}{\mu}\right)} \right\}$$

$$\mu\theta = \ln_e \left\{ 1 + \frac{76.5}{4.34 \times 1000} \right\}$$

$$\theta = 0.2495$$

The point at which the axial force goes to zero is equivalent to an unloaded front end. Since the complete route bend encompasses 1.05 radians, (1.05 − 0.2495) radians remain in which an axial compression can build up from zero.

$$N = wr\left(1 + \frac{\alpha}{\mu}\right) \times \{\exp[\mu(\phi - \theta)] - 1\}$$

$$= 4.34 \times 1000 \times \{\exp[0.07 \times (1.05 - 0.2495)] - 1\}$$

$$= 250 \text{ lb}$$

Section V. The force increment in this long straight section is computed by the same formula used previously.

$$\Delta N = wl(\mu + \alpha)$$

$$= 4.34 \times 720 \times (0.07 - 0.15)$$

$$= -250 \text{ lb}$$

The total force at the insertion site is given by adding this increment to the force at the junction of Sections IV and V:

$$N = 250 - 250$$

$$= 0$$

This route was designed to illustrate one way in which the final insertion force can be zero (or even negative). During insertion in a route which slopes generally downward the insertion force may be expected to assume both positive and negative values during the course of installation.

REFERENCES

1. R. W. Gretter, R. P. Guenther, M. Lutchansky, D. Olasin, and A. B. Watrous, "Mechanical Design of Sheathed Waveguide Medium," B.S.T.J., this issue.
2. J. C. Anderson, R. W. Gretter, and T. J. West, "Route Engineering and Sheath Installation," B.S.T.J., this issue.
3. J. W. Carlin, and S. C. Moorthy, "TE_{01} Transmission in Waveguide with Axial Curvature," B.S.T.J., this issue.

THE BELL SYSTEM TECHNICAL JOURNAL
Vol. 56, No. 10, December 1977
Printed in U.S.A.

WT4 Millimeter Waveguide System:

Spectrum Estimation Techniques for Characterization and Development of WT4 Waveguide—II

By D. J. THOMSON

(Manuscript received April 7, 1977)

In Part I techniques for reliably estimating the power spectral density function for both small and large samples of a stationary stochastic process were described. These techniques have been particularly successful in cases where the range of the spectrum is large. They are resistant to a moderate amount of contaminated or erroneous data. Here these procedures were demonstrated using examples from the development and analysis of the WT4 waveguide medium and compared to conventional techniques.

I. INTRODUCTION

The use of the spectral density function for the characterization of mode conversion effects in millimeter waveguide problems has been in general use since the pioneering paper of Rowe and Warters[2] and has subsequently appeared in several other forms (Morrison and McKenna,[3] Pusey[4]). In this paper the emphasis will not be on mode conversion problems per se but rather on the more fundamental problem of obtaining an accurate estimate of the spectrum for the geometric distortion causing the mode conversion.

In Part I a technique for the estimation of the power spectral density function was described[1] which differs from conventional estimation procedures in several respects. In particular the technique is both *robust*—that is, it is resistant to a moderate amount of erroneous or outlying data—and has the ability to estimate spectra which have very large dynamic ranges. While Part I was primarily theoretical, Part II is devoted primarily to examples of this technique as applied to the analysis

of WT4 waveguide data and comparisons of this method to standard techniques. Because of the complexity of the WT4 system these examples cover a wide range; from the analysis of individual tubes where the sample is very short relative to the resolution required, to the analysis of complete mode filter sections where the amount of data which must be contained in the analysis is almost prohibitive. Some spectra are almost white while some cover ranges of 10 to 16 decades.

Briefly, the method described in Part I begins by forming a *pilot estimate* of the spectrum using a modification of Welch's technique.[5] The pilot estimate is used to form an *autoregressive model* of the process which is used as part of a *robust prewhitening filter*. The final estimate of the spectrum is the *ratio* of the spectrum of the prewhitening residuals to the power transfer function of the autoregressive filter.

While this procedure is clearly motivated by the use of prewhitening techniques it differs from traditional methods in many important aspects:

(*i*) First, extensive use is made of *prolate spheroidal wave functions* as data windows or tapers. These functions, which are described in a series of papers beginning with Slepian and Pollak,[6] are the eigenfunctions of the finite Fourier transform and give greatly improved resolution and dynamic range from that obtained with conventional ad hoc data windows.

(*ii*) Second, adaptive prewhitening forms a central part of this procedure. This is accomplished by using an autoregressive model of the process, obtained from a pilot estimate of the spectrum, as a *prediction error filter*.

(*iii*) Third, by starting with the pilot spectrum estimate an effective autocorrelation function is realized which is both positive definite and also has low bias. A new technique for generating autoregressive models is described.

(*iv*) Fourth, by replacing the subset averaging used in the Welch technique with a robust combination an improved pilot estimate is frequently obtained.

(*v*) Finally, the *robust filter algorithm* permits accurate estimates of the spectrum to be made when the data contains numerous erroneous data points.

Overall the effect is to give estimates of spectra which are much more reliable than those obtained by conventional methods. The loss calculations reported in Anderson et al.[7] are indicative of its accuracy.

II. THEORETICAL CONSIDERATIONS

In the problems considered here measurements are made of a particular geometric distortion in the waveguide over the length, T, of line.

From these measurements it is desired to estimate the spectrum of the particular distortion. The estimated spectrum is commonly used for two purposes; first to estimate the mode conversion loss, and second, to make inferences on the process used to produce the sample. In both cases frequency resolutions of $1/T$ or better are desirable. But, because the range of the spectra typically encountered in waveguide applications is very large, such resolutions cannot be obtained from simple techniques without obtaining unacceptably biased estimates.

In the literature on spectrum estimation there are numerous papers which are concerned with the trade-off between *resolution* and *variance.* Unfortunately this emphasis on a secondary problem has served to obscure the fundamental conflict between *resolution* and *bias.* The source of this conflict between resolution and bias is a result of fundamental properties of the Fourier transform (see Landau and Pollak).[8] Consider a *direct estimate of spectrum*

$$\hat{S}_D(\omega) = \left| \int_0^T e^{i\omega t} D(t)\, x(t)\, dt \right|^2 \tag{1}$$

in which $D(t)$ is a *data window* or *taper.* If the series, $x(t)$, is a sample of a stationary random process having spectral density function $S(\omega)$ the expected value of such an estimate is given by

$$\mathbf{E}\{\hat{S}_D(\omega)\} = S(\omega) * |\tilde{D}(\omega)|^2 \tag{2}$$

where * indicates convolution and $\tilde{D}$ is the Fourier transform of D. From this formula it can be seen that the expected value of an estimate is the true spectrum convolved with the spectral window, $|\tilde{D}(\omega)|^2$, so that estimates of all nonwhite spectra will be biased.

It is convenient to express this convolution as the sum of a "local" term and a "broad band" component. If the "broad band" component of the bias is defined to be the contribution from frequencies differing from ω by an amount Ω or more by using results from Slepian & Pollak[6] it can be shown that the broad band bias is minimized when D is a *prolate spheroidal wave function.* Further it follows from Slepian[9] that when prolate spheroidal wave functions are used as data windows, the broad band bias can be *bounded* by a quantity which decays asymptotically as $4\sigma^2 T\sqrt{\pi c}\, e^{-2c}$ where $c = \Omega T/2$ so that an immense improvement in performance over conventional windows can be guaranteed for moderate values of c.

Two such windows have been extensively used in the analysis of WT4 data. One of these, used for pilot spectrum estimates and exploratory work, has $c = 4\pi$ and so has a dynamic range of over 100 dB while the second, used in situations where the range of the spectrum is lower and high frequency resolution is required uses $c = \pi$. These data windows

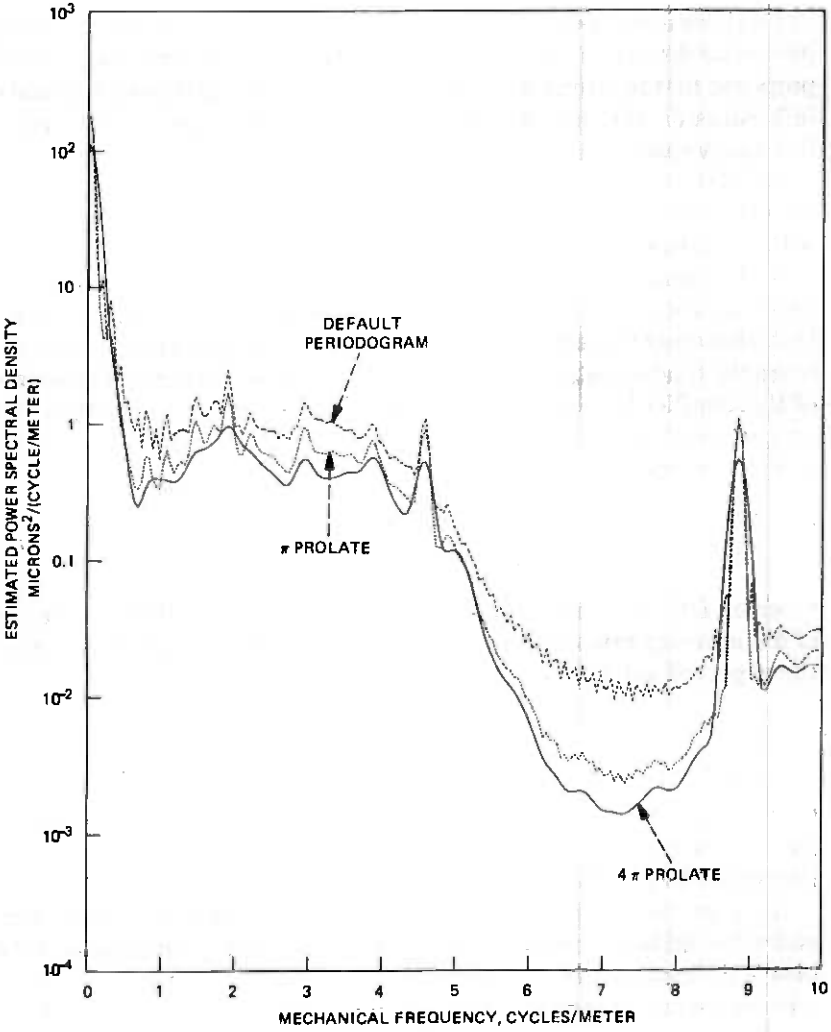

Fig. 1—Comparison of direct spectrum estimates using different data windows. The plotted curves are the average over 2556 data sets.

together with the corresponding spectral windows are shown in Figs. 1 and 2 of Part I.

An example of the different results obtained with different data windows is provided by an analysis of the measured curvature of individual waveguide tubes. The data used here represents the output of a curvature gauge similar to that described in Fox et al.[10] where the curvature is taken from the horizontal sidewall so that the effects of gravitational sag are eliminated and the data are representative of the man-

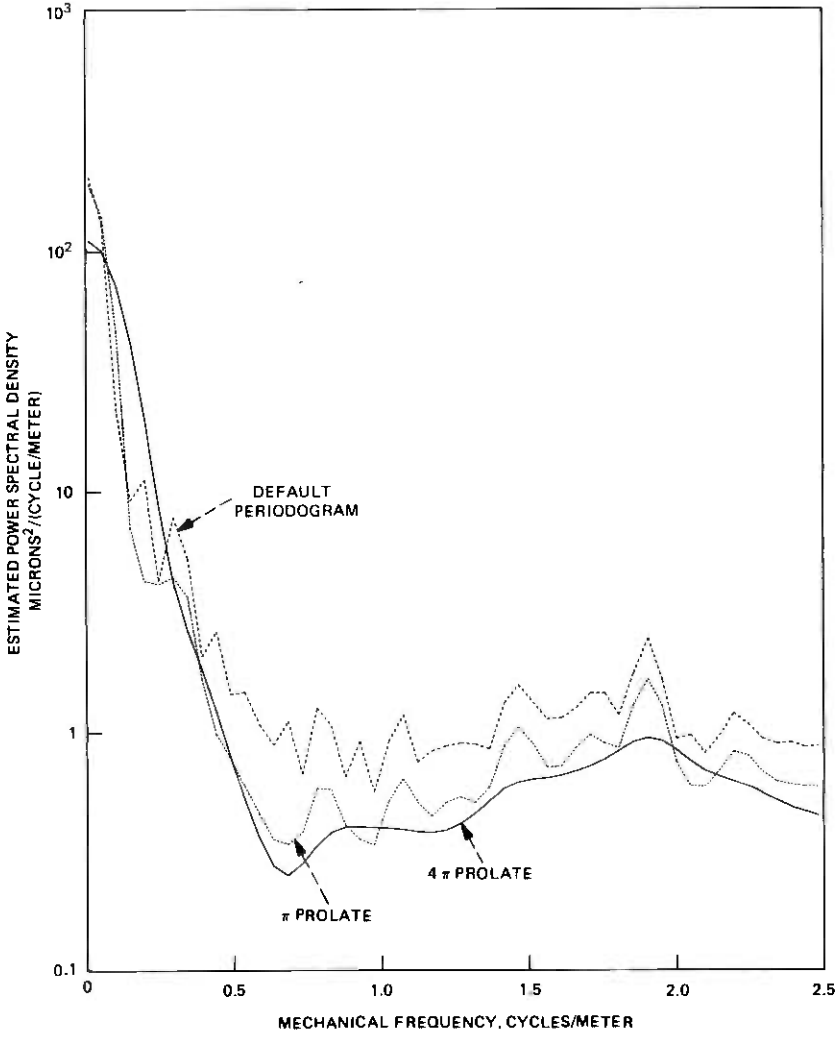

Fig. 2—Low-frequency portion of the data shown in Fig. 1.

ufacturing process. Figure 1 shows the average of 2556 direct estimates of spectra using the two prolate windows described above, and, for comparison, the default periodogram. The differences are most pronounced in the "hole" near 7 cycles per meter but even at low frequencies there are important differences. The region between 0.3 and 1 cycle/meter is particularly important from a mode conversion viewpoint as this region is responsible for the TM_{11} and TE_{12} losses. In this region, shown expanded in Fig. 2, the periodogram is almost a decade higher than the prolate estimates. Also the "structure" evident on the perio-

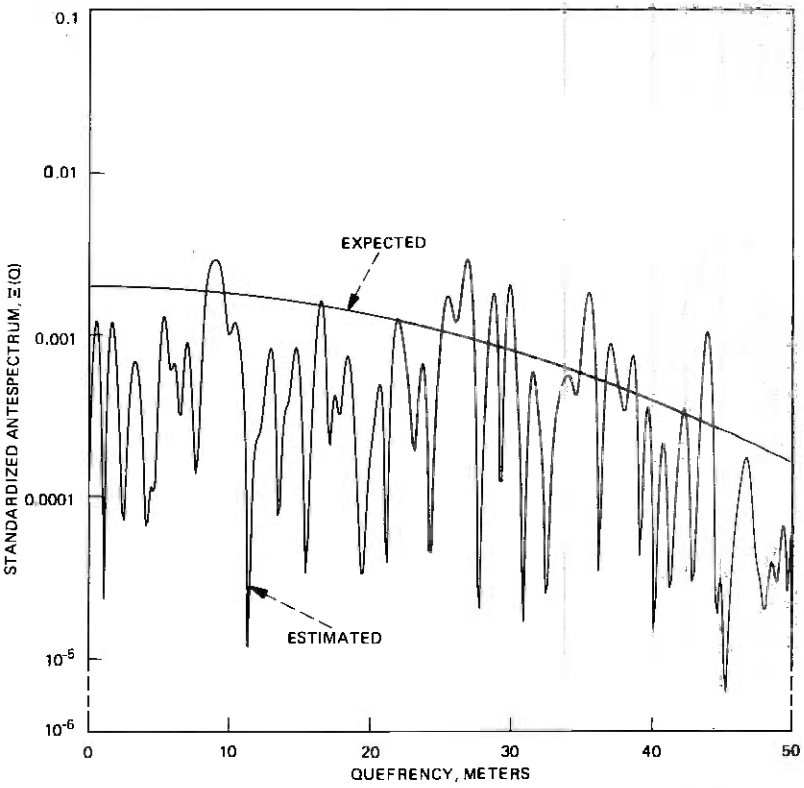

Fig. 3—Expected and standardized sample antespectra for the 19.0 to 20.5 cycle/meter region of the pilot spectrum estimate from mode filter section 17 horizontal curvature.

dogram, for example the peaks at 0.2 and 0.3 cycles per meter, is largely characteristic of it's spectral window (the data sets each contained 808 points spaced 1 cm) rather than the process. It can also be seen that while the π and 4π windows agree in general the narrower window resolves peaks, for example at 0.7 and 1.9 c/m, much better than the broader 4π window but is biased at lower values of the spectrum. In these comparisons it should be noted that since the averages have over 5000 degrees of freedom at each point their standard deviations will be only about 2 percent of their value so that almost all differences between the estimates are significant. Moreover, since the losses are proportional to the spectrum the prolate windows predict losses from the tubes which agrees well with that measured in the field evaluation test whereas those corresponding to the periodogram are considerably larger than the total measured mode conversion loss.

As outlined in Part I a convenient description of the sampling properties of direct estimates is given by the *antespectrum* of the estimate. The antespectrum is the *spectrum of the spectrum estimate* and is ap-

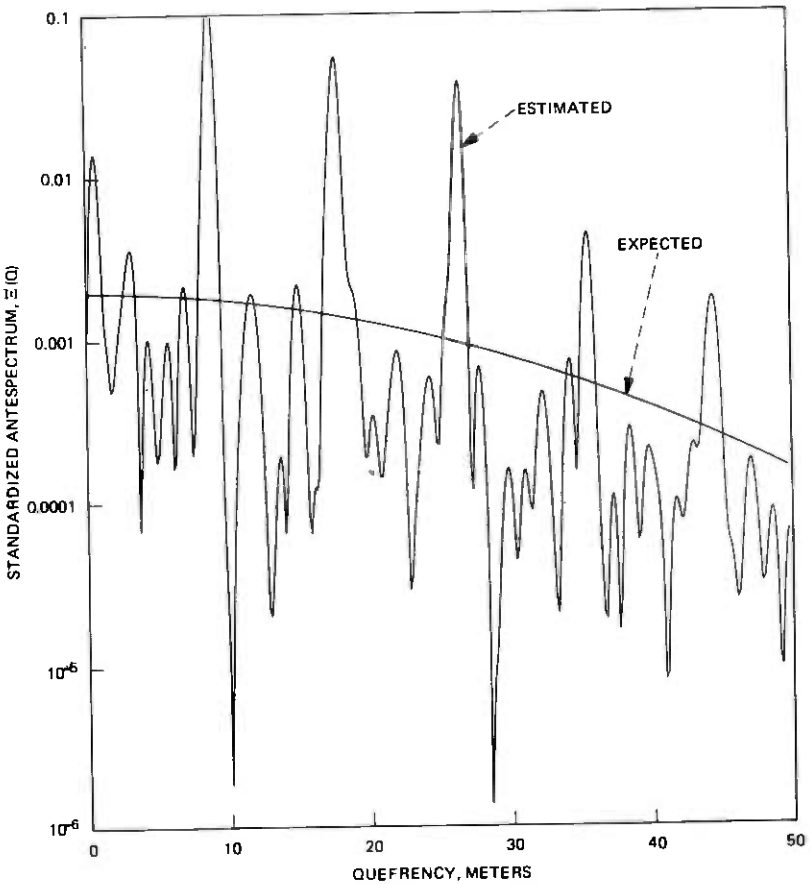

Fig. 4—Antespectra for the 0.5 to 2.0 cycle/meter region.

plicable in regions where the spectrum is constant. In such regions the magnitude of the antespectrum depends on the level of the spectrum and on any smoothing or averaging while its shape depends only on the windows used to generate the spectrum estimate. Since its expected level and shape are known the *sample antespectrum* is a powerful tool for deciding whether a portion of a spectrum is in fact "locally white" or if in fact it contains significant structure. As an example Fig. 3 shows the sample antespectrum corresponding to the 19.0 to 20.5 cycle/meter region† of the pilot spectrum estimate for the horizontal curvature in mode filter section 17 of the field evaluation test (see Anderson et al.[7] for the definition and location of individual mode filter sections such as 17). It

† This region and the one below were chosen as they are both free from obvious peaks and on a plot of the pilot spectrum appear to be flat and very similar.

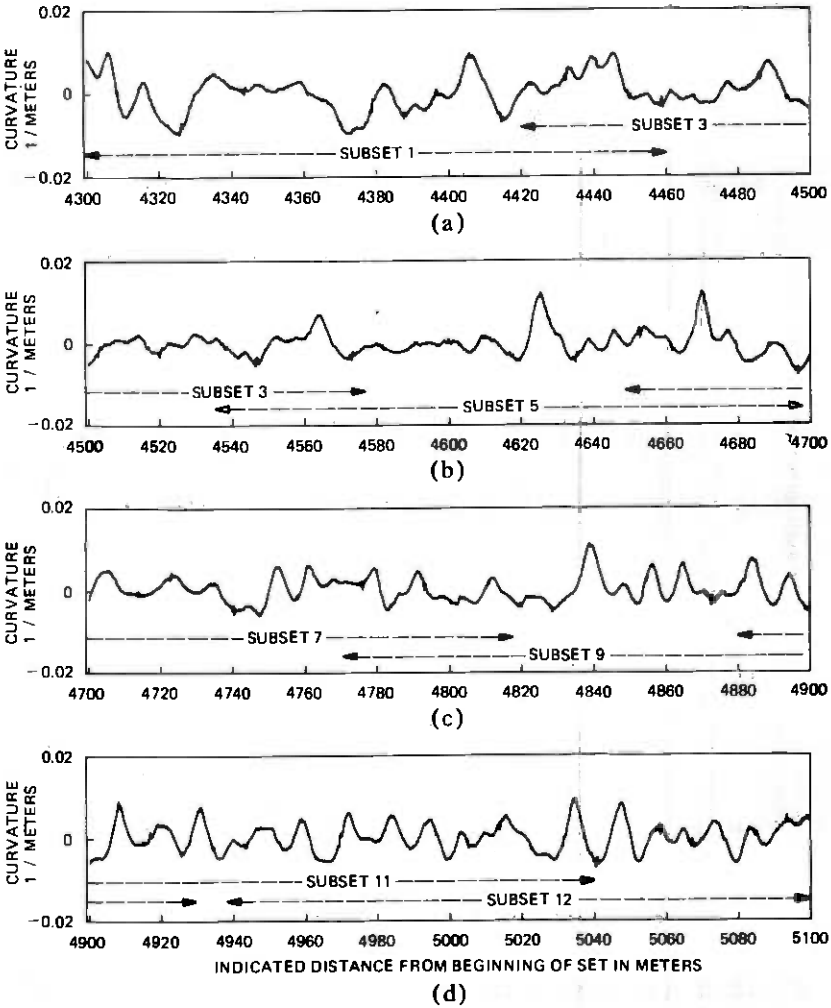

Fig. 5—The vertical curvature for mode filter section 6 as measured by the long-range mouse. Subsets 1, 3, 5, 7, 9, and 11 are used in the test for stationarity; all are used for the pilot estimate.

can be seen that the agreement with the expected behavior is quite good.

In contrast the sample antespectrum shown in Fig. 4, corresponding to the 0.5 to 2.0 cycle/meter region does not conform to the expected shape but rather shows a series of decaying peaks. This shows that a considerable part of the apparent variability of the spectrum in this range is due to the actual fine structure of the spectrum rather than sampling variability. Consequently smoothing must be done very carefully as a smoother with an effective span of only ±8 points will completely obscure

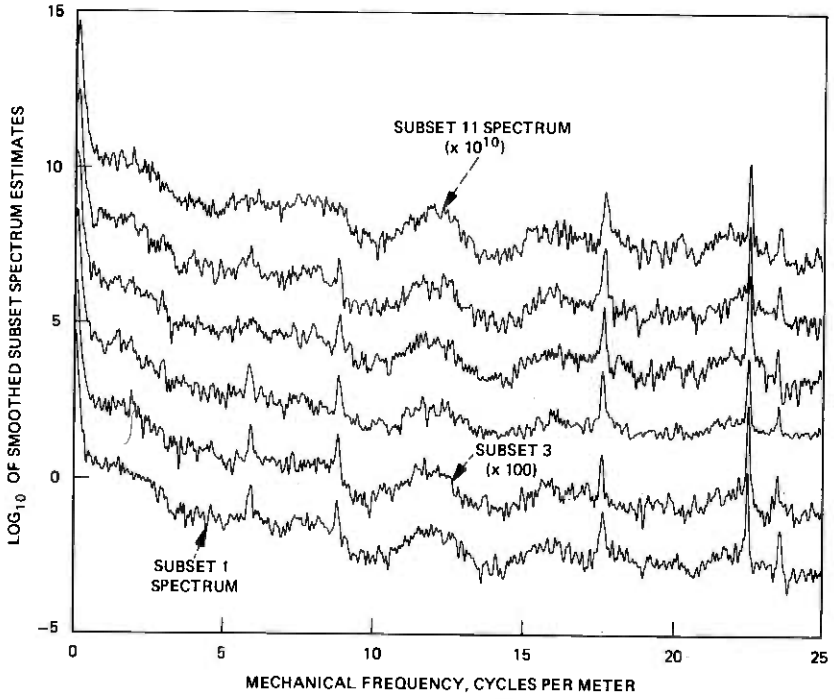

Fig. 6—Smoothed spectrum estimates from alternate subsets of mode filter section 6 vertical curvature. For plotting purposes the estimates have been offset by factors of 100.

this effect. This fine structure in the spectrum is a result of interactions between the tilts and offsets at couplings and, as expected, the random lengths of the individual waveguide tubes is very effective at suppressing the effect at higher frequencies.

III. PILOT SPECTRUM ESTIMATE

The method used to compute the pilot spectrum estimate is a variation of Welch's technique.[5] In this method the data is first divided into several overlapping subsets and a direct estimate of spectrum computed on each subset. For this purpose the prolate data window with $c = 4\pi$ is ideally suited because of its very large dynamic range. For reasons described in Part I the 800-meter mode filter sections were divided into 12 subsets each 160 meters long. These subsets are offset from each other by about 28 to 30 percent of their length so that the information recovery is near optimum. The pilot estimate is a combination of these subset estimates. Originally the combination consisted of a simple arithmetic average over the subsets but in situations where occasional outliers are expected a greatly improved pilot estimate can be obtained by using a simple robust estimate.

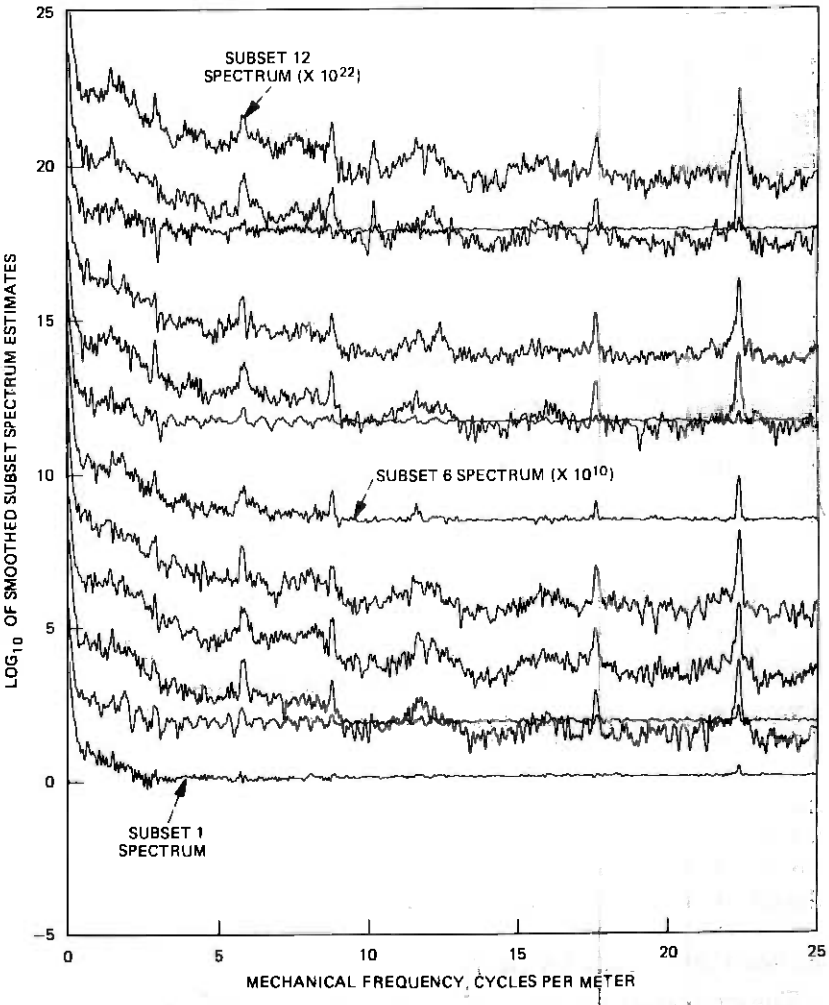

Fig. 7—Smoothed spectrum estimates from all 12 subsets of mode filter section 3 horizontal curvature.

Figure 5 shows a plot of the vertical curvature for mode filter section 6 with the positions of the various subsets indicated. Figure 6 shows alternate subset spectrum estimates and it can be seen that they agree well. So that the plot is readable these estimates have been smoothed and are offset from each other by factors of 100.

By way of contrast, Fig. 7 shows all 12 subset estimates for the horizontal curvature in mode filter section 3 and it can be seen that several of them are "different." The cause of this difference appears to be some small outliers, possibly dust particles. Figure 8 shows the difference between an arithmetic and robust combination of these subsets using

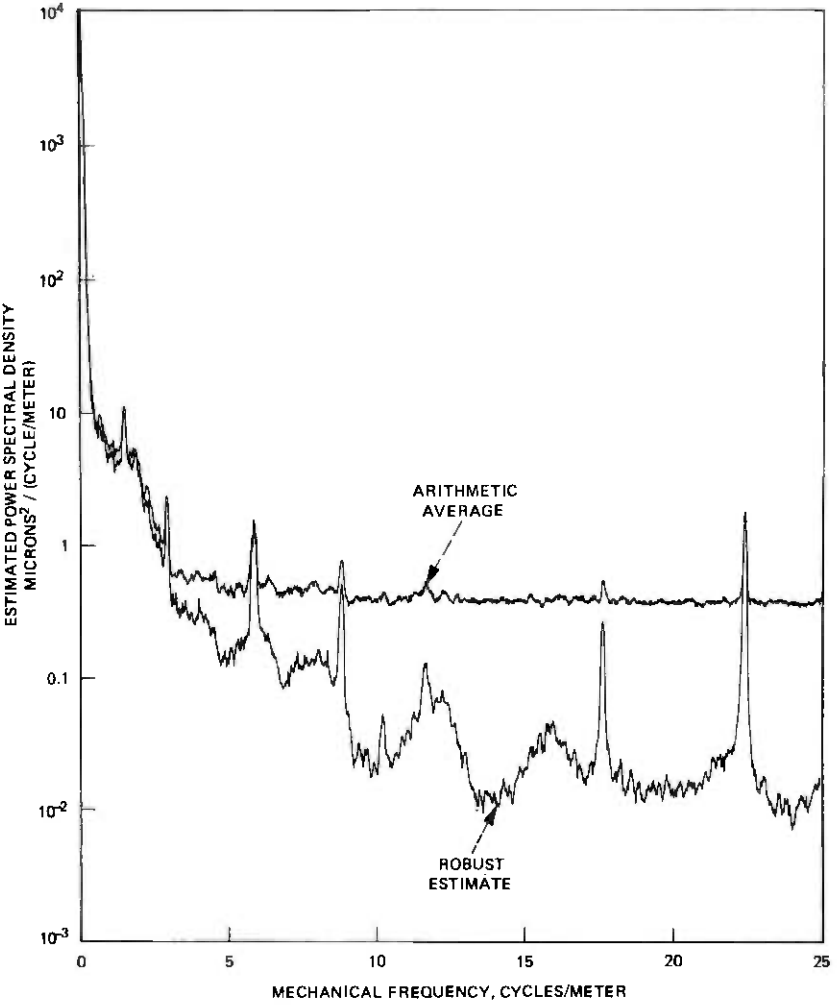

Fig. 8—Comparison of pilot spectrum estimates formed by robust and arithmetic average combinations of the subset spectrum estimates (shown in Fig. 7) for mode filter section 3 horizontal curvature. For plotting purposes both estimates have been smoothed with an adaptive filter having a span of ±10 points.

formula I–5.1 with $k' = 6$. It can be observed that the two differ by more than a decade across much of the frequency band. Integrating the two estimates one finds that the total power decreases by about 10 percent, from 1516 microns^2 for the standard estimate to 1380 microns^2 for the robust estimate. Prediction error, however, is proportional to the integrated logarithm of the spectrum, which decreases dramatically, from 15 microns^2 for the average to 0.101 microns^2 for the robust estimate. Comparisons of these pilot estimates with the spectrum of the individual

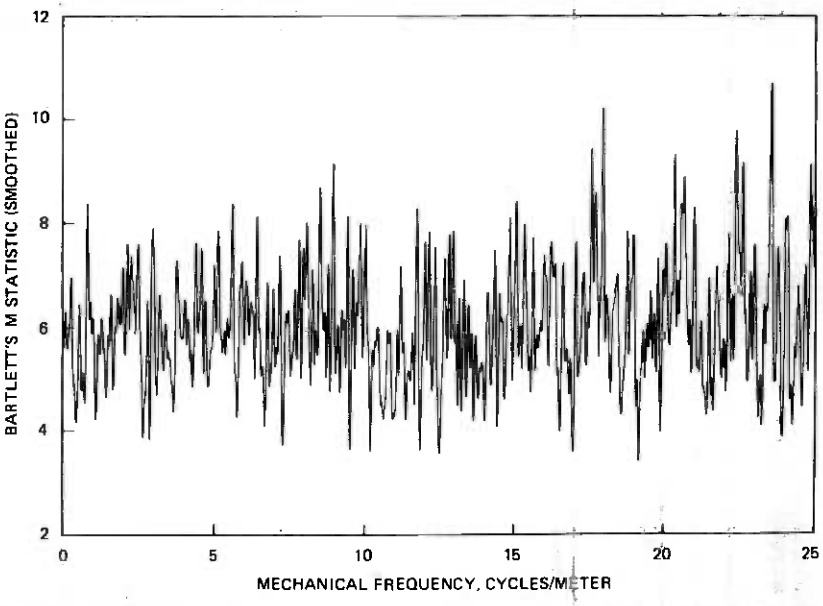

Fig. 9—Comparison of the subset spectrum estimates shown in Fig. 6 for homogeneity using Bartlett's M statistic as a function of frequency. For plotting and interpretative purposes the values shown here have been lightly smoothed.

tubes shown in Fig. 1 indicate that, since the higher frequency portions of the spectrum depend primarily on tubing geometry, the robust estimate is much more believable than the one obtained by simply averaging the subsets.

IV. TESTS FOR STATIONARITY

An important side use of the subset spectrum estimates is in testing the data for stationarity. Tests of this assumption are important in waveguide applications as most models assume that the coupling mechanism between the different modes is driven by a stationary random process and loss estimates made on the basis of such theories will be unreliable of this assumption is violated.

The only test for stationarity which has been found satisfactory is a compound procedure of which the first step is to compute Bartlett's M statistic[11] for heteroscedasticity of variance between subsets as a function of frequency

$$M(\omega) = k\nu \ ln \ \overline{S}(\omega) - \nu \sum_{j=1}^{k} ln \ \overline{S}_j(\omega) \qquad (3)$$

Here $\overline{S}_j(\omega)$ is a slightly smoothed estimate of the spectra of subset j with ν degrees of freedom, and $\overline{S}(\omega)$ is the average, over the k subsets of $\overline{S}_j(\omega)$. If the test is not to be biased constant weight smoothers must be used

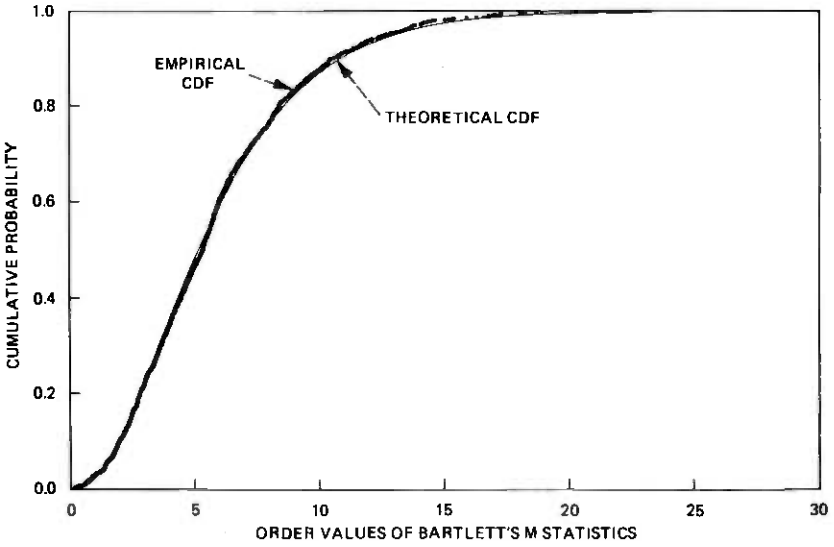

Fig. 10—Comparison of the empirical cumulative distribution function for the *unsmoothed* values of Bartlett's M statistic shown in Fig. 9 with the theoretical distribution. The points used in this test were spaced $4/T$ in frequency. For this comparison the kolmogorov D^- statistic has a value of 0.0264 which is at the 35 percent point.

and smoothing to more than 6 degrees of freedom is inadvisable. Also, so that the test is not biased by correlations between subsets, the subsets used in this test are offset about 57 percent of their length so that, as indicated in Fig. 6, alternate members of the set used to generate the pilot estimate are used in this test.

The second stage of the procedure is to sample $M(\omega)$ at steps greater than $4c/l$, pool the samples, and test for conformance to the known distribution of M. Three primary tests of goodness of fit have been used; the one sided Kolmogorov test D^-, the Anderson-Darling[12] A test, and the Cramer-von Mises W test. (The D and W statistics are described in Durbin.[13]) High values of the Kolmogorov D^+ statistic usually indicate too little variation between the subset spectrum estimates. This condition is normally a result of the subsets being too short.

Figure 9 shows values of M as a function of frequency corresponding to the subset spectrum estimates shown in Fig. 6. The empirical and theoretical distribution functions are plotted in Fig. 10. From this figure it can be seen that the values of M obtained from the different subsets correspond closely to their expected distribution so that the process can be assumed stationary. It should also be noted, see Box,[14] that the M test is very sensitive to departures from the assumed distribution so that, if the spectrum estimates are not closely χ^2 the series will appear nonstationary. Therefore we can conclude that over the frequency band of primary interest, 0 to 25 cycles/meter, the process is stationary and also

that the distribution of losses to a given mode will be χ^2. Other examples are given in Thomson.[15]

V. SMOOTHING

Almost all work on spectrum estimation recommends that various linear smoothers be applied to the raw spectrum estimate and while these procedures are of some value in the present application they can frequently lead to very misleading results. In WT4 applications losses are proportional primarily to the actual value of the spectrum and only to a limited extent to the total power available, and as linear smoothers preserve power rather than spectral amplitudes they cannot be used for loss estimates.

In numerically less critical applications, for example when the spectrum is being "looked at" to study the manufacturing process, conventional smoothing can be seriously misleading and in most applications of this type various adaptive smoothers have been used. While it is impossible to describe the complete details of such smoothers here one of the simpler methods will serve as an example. For this example the bottom curve in Fig. 11 shows a portion of the raw vertical curvature spectrum from mode filter section 14.

(*i*) From a symmetric interval about the frequency of interest values of the raw spectrum estimate are pooled and sorted. From these values a robust estimate of location is made by methods similar to those described in Section 5, Part I, that is, the initial estimate is a systematic function of the order statistics. In this case both ends of the distribution are censored, typically at the 25 percent points, instead of just the upper tail. This initial robust location is shown, offset by a factor of 10, as the second curve of Fig. 11.

(*ii*) The initial robust location estimate is smoothed using a conventional low-pass lifter. The smoothed location estimate is given, offset by a second factor of 10, in the third curve from the bottom.

(*iii*) The central value in the spectrum estimate is compared to the robust local mean. This comparison is made within a window formed by the asymptotic extreme value distribution for distributions of exponential type. Denoting the raw estimate by $\hat{S}(\omega)$ and the smoothed "mean value function" by $\tilde{S}(\omega)$ this is accomplished by

$$r = \frac{\hat{S}(\omega)}{\tilde{S}(\omega)} \tag{4}$$

so that the window becomes

$$w = \exp\{-v_e e^{-r}\} \tag{5}$$

and the "roughened" estimate is given by

$$S_r(\omega) = w\hat{S}(\omega) + (1 - w)\tilde{S}(\omega) \tag{6}$$

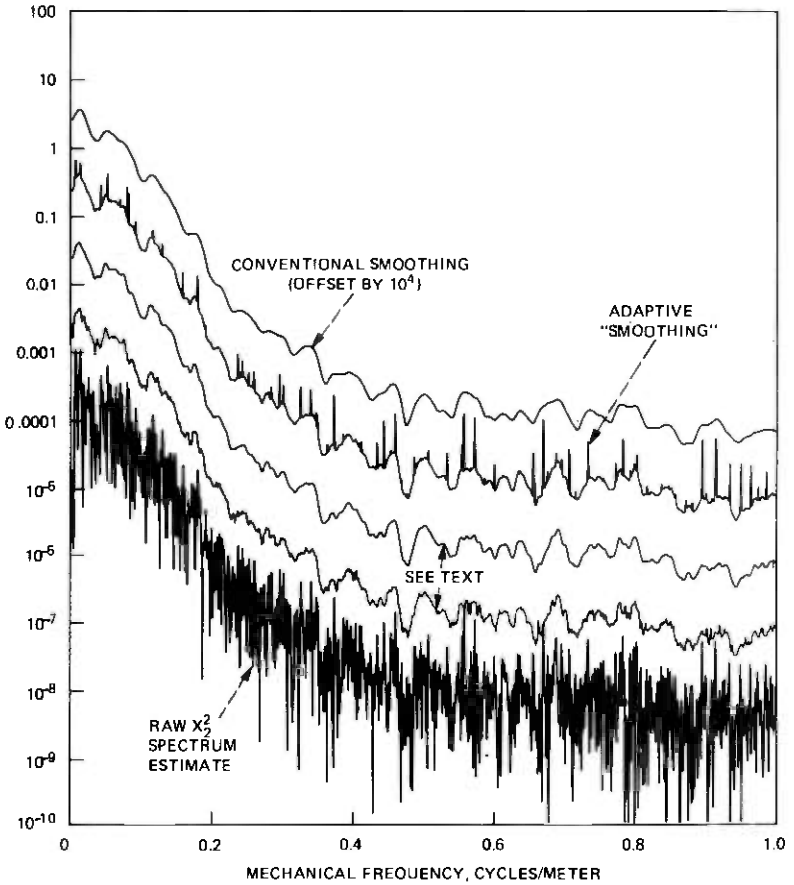

Fig. 11—Steps of a simple adaptive "smoothing" procedure applied to mode filter section 14 vertical curvature spectrum.

This estimate is shown as the fourth curve and the peaks are very evident. For comparison the top curve shows the results of conventional linear smoothing. Comparing the raw, conventional, and robust "smoothed" estimates it is clear that the nonlinear "smoothing" procedure is very helpful in identifying both the basic structure of the spectrum and also any potential periodic components.

VI. ROBUST FILTERING

In addition to the problems already mentioned, conventional estimates of spectra are not *robust,* that is, they are very sensitive to small amounts of erroneous or outlying data. This problem is of particular importance in data of the type obtained in millimeter waveguide problems because of the large range covered by the spectrum and the fact that we are often,

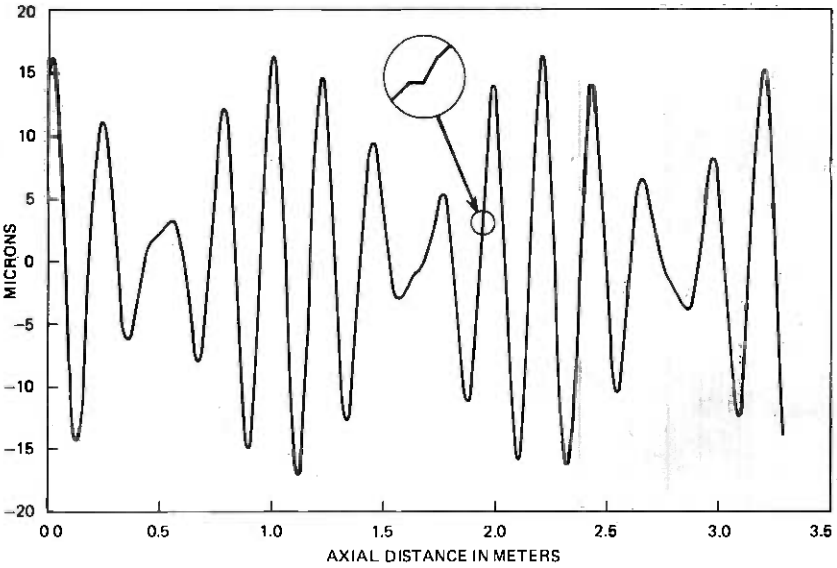

Fig. 12—Plot of the horizontal curvature gauge output for an experimental dielectric-lined waveguide. The insert shows one of two outliers in this data set.

for example in making TM_{11} and TE_{12} loss estimates, interested in the spectral density "at the bottom of a cliff." In this situation there is an aspect to robust estimation which does not appear in the usual situations, namely that an outlier does not have to be "large" to cause serious distortions of the spectral density estimate, but only large with respect to the process innovations variance. In many waveguide spectra, where the innovations variance is less than the process variance by a factor of 10^6 to 10^8 or more, this means that *outliers in time series may not be obvious.* As an example of this phenomena Fig. 12 shows a plot of the horizontal curvature gauge output from an early dielectric lined waveguide in which the outliers are almost invisible under normal plotting conditions but which can be seen when expanded. As will be shown later, such outliers can result in large errors in the estimated spectrum. Further examples are given in Kleiner et al.[16]

The solution which has been found to these problems is known as the *robust filter algorithm.* Basically this procedure uses approximate knowledge of the structure of the process to *predict* the process at the next time step. When the observed value of the process is close to that predicted, the filter simply copies the data. If, on the other hand, the data and prediction differ by a "large" amount, the filter output consists of the prediction. Prediction is used rather than interpolation because the predictor is based on *filtered* values of the process whereas interpolation requires use of data which itself may be contaminated. Also, in the usual

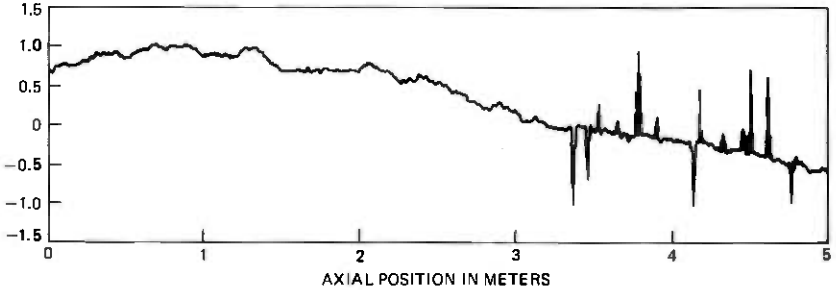

Fig. 13—Simulated waveguide curvature data with outliers. These data were generated using a 54th-order auto regression with a normal innovations sequence.

case where the procedure is combined with prewhitening, the predictive formulation has the important characteristic of having no zeroes in its transfer function on the real frequency axis.

This prediction is made using an autoregressive model of the process. Estimation of the parameters of such a model was described in Part I and further information is available in the recent works of Kailath, Morf, et al.[17,18,19,20]

To a large extent the behavior of the robust filtering algorithm depends on the weight function W and, because of the nonlinearities introduced, improper choice of weight functions can drastically alter the spectrum estimate. To illustrate the behavior of the different influence functions Fig. 13 shows a section of simulated curvature data with a burst of errors between 3 and 5 meters and in Fig. 14 the error sequence

$$\Delta_n = x_n - \hat{x}_n \tag{7}$$

between the original uncontaminated data, x_n and filtered series, $\hat{x}_n$ is shown. In this case the extreme value influence function (Part I, Section 7.7, $u_0 = 4.5$) was used and it can be seen that in the uncontaminated part

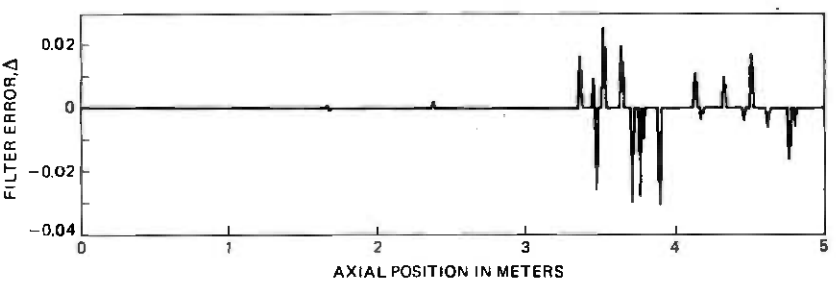

Fig. 14—The error, Δ, between the original uncontaminated data (The contaminated data is shown in Fig. 13) and the sequence obtained by robust filtering using an extreme value influence function with $u_0 = 4.5$. Note the difference in scale between Figs. 13 and 14.

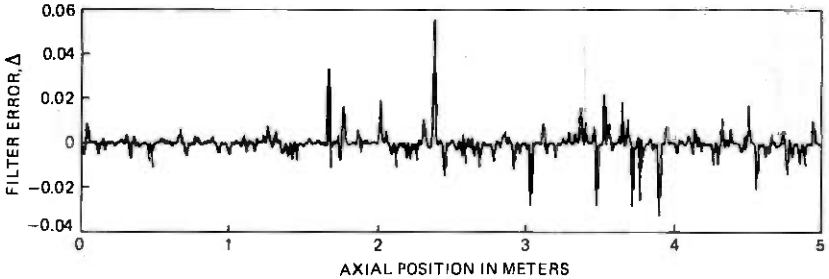

Fig. 15—Filtering error, Δ, between the original uncontaminated data and robust-filtered version using the bisquare influence function with $u_{bs} = 6$. Note the extensive errors occurring in the uncontaminated part of the series.

of the series the error is usually zero or very small. In the contaminated part of the series the errors correspond to the innovations sequence and error propagation is very limited. By contrast Fig. 15 shows the error sequence obtained when the common bisquare influence function

$$\Psi_{bs}(u) = \begin{cases} u[1 - (u/u_{bs})^2]^2 & |u| < u_{bs} \\ 0 & |u| \geq u_{bs} \end{cases} \tag{8}$$

with $u_{bs} = 6$. In this case the error is hardly ever zero, error propagation is general, and in many cases the errors are larger in the uncontaminated data than they are in the contaminated region. In the estimated spectrum these distortions result in spurious peaks and similar errors.

This behavior may be explained by considering the behavior of the filter on uncontaminated autoregressive data of order p so that the error sequence is given by

$$\Delta_n = [I - \Psi]\left(\xi_n + \sum_{k=1}^{p} \alpha_k \Delta_{n-k}\right) \tag{9}$$

where I represents the identity function, Ψ the influence function, and $\{\xi\}$ is the innovations sequence. Because ξ_n is independent of preceding values of Δ_n this equation may be used to compute the probability density function of the errors.

Figure 16 shows the probability density functions for the filter error sequences for three influence functions assuming an autoregressive process of order 1 with $\alpha = 0.9$ and Gaussian innovations. Here, in agreement with the examples shown above (which to simulate waveguide curvature data used an order-54 autoregressive representation), it can be seen that

(*i*) The density corresponding to the extreme value influence function has more than 99 percent of its mass concentrated near the origin and the continuous portion decays rapidly.

(*ii*) The density corresponding to the Huber influence function also

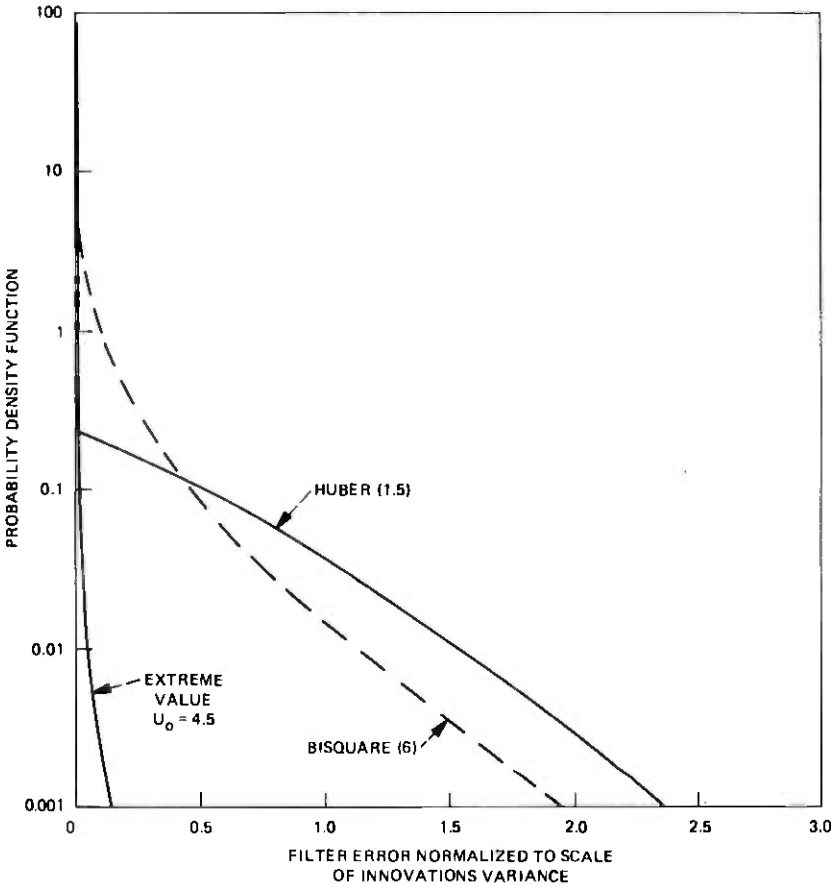

Fig. 16—Probability density functions for the error sequence of a robust filter operating on a first-order autoregressive process with $\alpha = 0.9$. For the extreme value case the density appears to be trimodal with the side modes at ± 6.5 and a level of about 10^{-5}.

has over 75 percent of its mass concentrated at the origin, but away from the origin the density decays more slowly than for the extreme value influence.

(iii) For the bisquare influence the density is large and peaked near the origin but is basically continuous and compares with the non-zero error process observed above.

VII. COMPARISON OF SPECTRUM ESTIMATES

Figure 17 shows the average, over 16 mode filter sections, vertical curvature gauge output spectrum from the Netcong WT4 field evaluation trial line computed using the methods described here. These calculations were made separately on each mode filter section and only a single it-

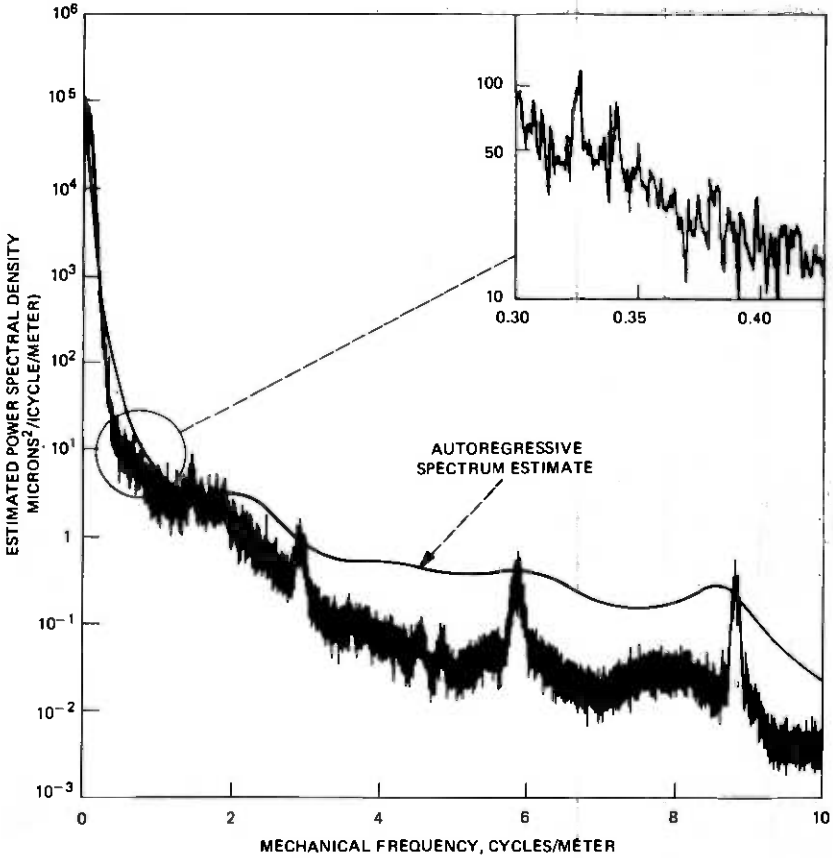

Fig. 17—The average vertical curvature gauge output for mode filter sections 1–10 and 12–17.

eration of the robust filtering procedure was used. The solid line in this plot is an "autoregressive spectrum estimate," the reciprocal of the power transfer function of the prediction error filter normalized by the estimated innovations variance. This particular example was obtained by fitting the averaged pilot estimates with an autoregression of order 54, the median value chosen by Parzen's criterion. It can be seen that the autoregression fits the gross shape of the spectrum fairly well but is completely useless as a description of the fine structure. As a particular example consider the two small peaks near 0.32 cycles per meter (see the expanded portion of the plot). These are completely absent in the autoregressive fit but show clearly in the nonparametric estimate. These peaks, one corresponding to harmonics of the 8.87 meter average tube length and the other to the ~60 foot sheath length were observed in 14 of the 16 mode filter spectra examined and account for considerable

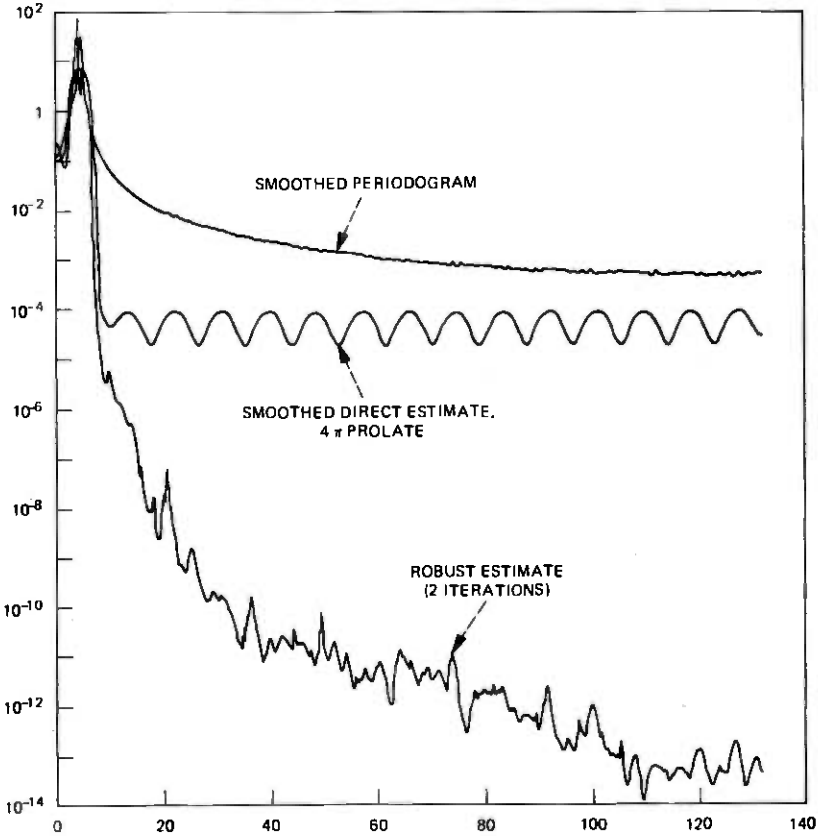

Fig. 18—Comparison of three estimates of spectrum for the data shown in Fig. 12. The systematic oscillations in the center curve are a result of interactions between the two outliers.

TM_{11} mode conversion loss which is confirmed by independent measurements (see Anderson et al.[7]). An even more significant failure of the autoregressive fit to reproduce details is evident at 8.8 cycles per meter. This peak, a result of the straightening operation used in the manufacture of the waveguides, exists in every waveguide tube and is detectable by simple techniques. In this region it can also be noted that, since the autoregressive fit is made to the pilot spectrum estimate, that the robust filtering procedure has improved the noise level by almost a decade and the spectrum estimated for the composite line is comparable with that expected on the basis of the measurements of the individual tubes.

As an example of how effective the robust filter algorithm can be for eliminating the effects of outliers in time series data Fig. 18 shows three different estimates of spectra for the curvature data shown in Fig. 12. The first estimate was computed using the simple extended periodogram;

this result is so badly biased as to be useless over 95 percent of the frequency domain. The second estimate was computed using the 4π prolate taper with the result that, depending on the frequency, the bias of the estimate is reduced by between 1 and 4 decades. While this result is still badly in error the cause of the error is the outliers mentioned earlier rather than limitations of the window. The third estimate uses both the prolate tapers *and* two iterations of the robust filter algorithm and again the estimate changes by *over eight decades* across much of the frequency range. In this estimate one can see details of the spectrum resulting from the manufacturing process rather than from artifacts of the measuring or analysis procedures.

VIII. CONCLUSIONS

Use of the adaptive and robust prewhitening technique in conjunction with data windows defined by prolate spheroidal wave functions has resulted in accurate estimates of spectra where conventional estimates fail. The bias of conventional estimates in situations commonly encountered in the WT4 development is so high that excessive levels of mode conversion are estimated if they are used. The high resolution and low bias properties of these estimates have proven extremely useful in understanding the measured field evaluation test loss data (see Anderson et al.,[7] Carlin and Moorthy[21]). In particular, since the high bias of conventional estimates would have resulted in much higher loss predictions for the TM_{11} and TE_{12} modes (higher in fact than the measured loss) these techniques must be considered a significant factor in the discovery of second-order TM_{21} mode conversion loss.

These procedures also allowed the identification of promising manufacturing techniques and were used extensively to develop, improve and control the manufacturing process. They were incorporated in the continuous monitoring of the waveguide tubing as it was being produced and were a major contributor to the high quality of the present WT4 waveguide.

IX. ACKNOWLEDGMENTS

It is my pleasure to acknowledge the contributions to this work resulting from conversations with B. Kleiner, C. L. Mallows, R. D. Martin, R. L. Pickholtz, D. Slepian, and T. J. West. The data on the individual tubes were supplied by V. J. Tarassov.

REFERENCES

1. D. J. Thomson, "Spectrum Estimation Techniques for Characterization and development of WT4 Waveguide—I," B.S.T.J., *56*, No. 9 (November 1977), pp. 1769–1816.
2. H. Rowe, and W. D. Warters, "Transmission in Multimode Waveguide with Random Imperfections," B.S.T.J., *41*, pp. 1031–1170.

3. J. A. Morrison, and J. McKenna, "Coupled Line Equations with Random Coupling," B.S.T.J., *51*, No. 2 (February 1972), pp. 209–228.
4. L. G. Pusey, *An Innovations Approach to Spectral Estimation and Wave Propagation*, D. S. Thesis, MIT (1975).
5. P. D. Welch, "The Use of the Fast Fourier Transform for Estimation of Spectra: A Method Based on Time Averaging Over Short, Modified Periodograms," IEEE Trans. Audio Electroacoustics, *AU-15* (1967), pp. 70–74.
6. D. Slepian and H. O. Pollak, "Prolate Spheroidal Wave Functions, Fourier Analysis and Uncertainty—I," B.S.T.J., *40*, No. 1 (January 1961), pp. 43–64.
7. J. C. Anderson, et al. "Field Evaluation Test—Transmission Medium Achievements," B.S.T.J., this issue.
8. H. J. Landau, and H. O. Pollak, "Prolate Spheroidal Wave Functions, Fourier Analysis and Uncertainty-II," B.S.T.J., *40*, No. 1 (January 1961), pp. 65–84.
9. D. Slepian, "Some Asymptotic Expansions for Prolate Spheroidal Wave functions," J. Math. Physics, *44*, pp. 99–104.
10. P. E. Fox, S. Harris, and D. J. Thomson, "Mechanical Gauging Techniques," B.S.T.J. this issue.
11. M. S. Bartlett, "Properties of Sufficiency and Statistical Tests," Proc. Roy. Soc., *A 160* (1937), pp. 268–282.
12. T. W. Anderson and D. A. Darling, "Asymptotic Theory of Certain "Goodness of Fit" Criteria Based on Stochastic Processes," Ann. Math. Stat., *23* (1952), pp. 193–212.
13. J. Durbin, *Distribution Theory for Tests Based on the Sample Distribution Function*, SIAM, 1973.
14. G. E. P. Box, "Non-Normality and Tests on Variances," Biometrika, *40* (1953), pp. 318–335.
15. D. J. Thomson, "A Test for Stationarity," in preparation.
16. B. Kleiner, R. D. Martin, and D. J. Thomson, "Robust Estimates of Spectra," in preparation.
17. T. Kailath, Some New Results and Insights in Linear Estimation Theory, Proc. of the IEEE–USSR Joint Workshop on Information Theory, 1975, pp. 97–104.
18. M. Morf, A. Viera, and D. Lee, Ladder Forms for Identification and Speech Processing, Proc. 1977 IEEE Conf. on Decision and Control.
19. M. Morf, A. Viera, D. Lee, and T. Kailath, Recursive Multichannel Maximum Entropy Method, Proc. 1977 Joint Automatic Control Conf., San Francisco, pp. 113–117.
20. M. Morf, D. T. Lee, and A. Viera, Ladder Forms for Detection for Estimation and Detection, presented at the 1977 Intl. Symp. on Information Theory.
21. J. W. Carlin and S. C. Moorthy, "TE_{01} Transmission in Waveguide with Axial Curvature," B.S.T.J., this issue.

THE BELL SYSTEM TECHNICAL JOURNAL
Vol. 56, No. 10, December 1977
Printed in U.S.A.

WT4 Millimeter Waveguide System:

Mechanical Gauging Techniques

By P. E. FOX, S. HARRIS, and D. J. THOMSON

(Manuscript received April 7, 1977)

For the WT4 waveguide system, mechanical measurements of the sheath, tubing, and waveguide were necessary before and after installation to ensure conformity to the manufacturing specifications, to verify the quality of installation techniques, and to acquire a better theoretical understanding of the effects of geometric imperfections on electrical loss. To fulfill these requirements a family of mechanical gauges or "mice" was developed. These include mice to measure individual lengths of sheath, tubing, and waveguide both in factory and laboratory environments and mice to measure long lengths of installed waveguide. The principles of mice are discussed in general and two particular mice are described in detail.

I. INTRODUCTION

During the development of the WT4 waveguide system, mechanical measurements of the various geometric distortions in the waveguide were used extensively

To monitor the manufacturing processes to ensure conformity to the specification.

To correlate mechanical distortions in the waveguide and the field evaluation test line with electrical loss measurements to improve manufacturing processes and installation techniques.

To acquire a better theoretical understanding of the relationship between mechanical distortions and electrical loss.

In many cases mechanical measurements are of greater value than direct electrical measurements. The problems associated with making accurate electrical measurements on long waveguide runs at millimeter wave frequencies are well known[1]; those of attempting to measure di-

rectly the mode conversion loss in a single section of steel waveguide tubing are better imagined! In fact, even if such measurements could be made, they would still be of limited utility in that they usually could not identify the cause of loss but only indicate its presence. To see this problem in the proper perspective it should be remembered that in the WT4 waveguide system a serious distortion[2] which results in losses of 0.1 dB/km corresponds to a single tube loss of 0.001 dB. Consequently measurements of most of the individual loss components on a single tube require accuracies on the order of 10^{-5} dB. Electrical measurements of this accuracy are currently impossible in the 40 to 110 GHz band. By comparison the mechanical measurements required to characterize such distortions are relatively undemanding.

To facilitate these mechanical measurements a family of gauges, popularly known as "mice", was developed. The members of this family are

(*i*) An external sheath mouse used to measure the curvature of individual lengths of sheath in the factory.

(*ii*) An internal sheath mouse used to measure installed sections of sheath up to 1.6 km in length prior to the installation of the waveguide.

(*iii*) A tubing mouse used to measure diameter and curvature of individual lengths of steel tubing at the factory.

(*iv*) A rotating-head mouse which is used to completely characterize individual tubes in a laboratory and also in quality control applications.

(*v*) A long-distance mouse used to measure the complete field evaluation test line.

This paper discusses the principles of the gauges and describes the last two in detail.

II. PRINCIPLES OF MECHANICAL MEASUREMENTS

In millimeter waveguide systems a significant fraction of the total loss is a result of power being coupled out of the signal mode into various spurious modes by geometric imperfections. To characterize these losses the departures from the nominal geometry of the guide are usually expressed in the form originated by Morgan,[3] where the radial distortion, δr, measured at an angle θ from a reference plane at some position, z, along the guide is given by

$$\delta r(z, \theta) = \tfrac{1}{2}a_0(z) + \sum_{n=1} a_n(z) \cos n\theta + b_n(z) \sin n\theta \qquad (1)$$

The Fourier coefficients $a_n(z)$ and $b_n(z)$ are then used to characterize the properties of the guide using techniques described in Rowe and

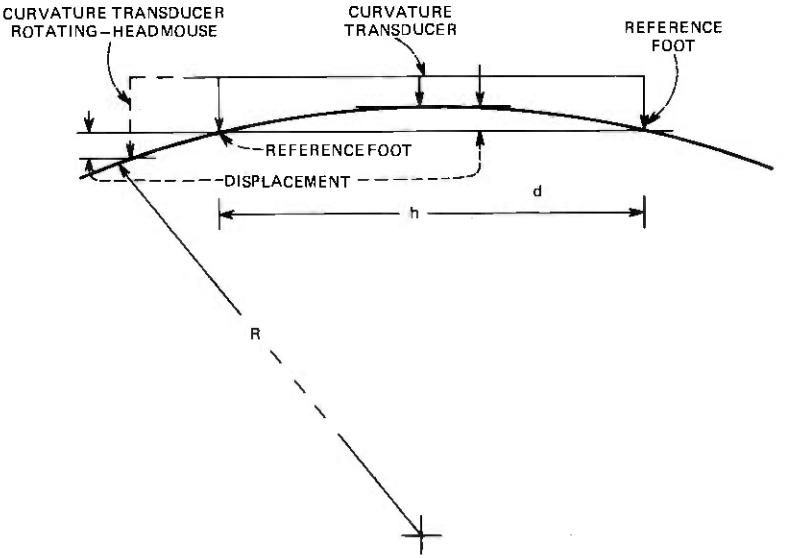

Fig. 1—Principle of measurement with three-point gauge.

Warters.[4] In this expression the a_0 coefficient represents the average radius, the a_1 and b_1 terms represent the offset of the guide axis from a straight line, and so on. Generally the summation index, n, is known as the *foil* and the associated distortion as n – *foil*. For describing the effects of offsets in the guide axis, it has been found that the *curvature* of the guide axis is a much more useful quantity than the offset itself. The primary reason for this choice is that curvature is insensitive to the exact position and orientation of the guide. For the simple gauge shown in Fig. 1 it can be seen that displacement of the movable probe with respect to the two fixed reference feet is a measure of the waveguide curvature or inverse bend radius and is equivalent to a second difference. If we assume for the moment that all distortions except the axis offset are negligible, the output of a mouse is the difference between a linear interpolation between its feet and the actual displacement of the probe. Denoting the distance between the fixed reference feet by h and the distance between the rear† reference foot and the probe by ph it is clear that the gauge curvature output in one plane is

$$x(z) = d(z) - p'd(z - ph) - pd(z + p'h) \tag{2}$$

where $p' = 1 - p$ and d is the axis displacement in that plane. It has been convenient to define the position of the gauge as that of its probe.

† We assume that the mouse is traveling in the positive z direction.

If such a mouse is used to measure a circular arc of radius R the output is approximately

$$x = \frac{h^2 pp'}{2R} \tag{3}$$

so that the sensitivity is proportional to h^2.

An alternative view of eq. (2) is to regard the mouse output as the result of a linear filtering operation on the displacement function and, if ω represents radian *mechanical* frequency, the transfer function of this filter is simply

$$H(\omega) = 1 - p'e^{i\omega ph} - pe^{-i\omega p'h} \tag{4}$$

The characteristics of the gauge when $p = 1/2$ are interesting, as this case corresponds to a classical symmetric second difference. In this case the transfer function reduces to $1 - \cos \omega h/2$ which has zeros at integer multiples of $2/h$. Since we are interested in curvature and not the direct gauge output, it is necessary to invert this transfer function. Consequently, the presence of zeros occurring in the frequency range of interest is undesirable. One possible solution is to make the length, h, of the gauge very short, but the associated loss of sensitivity makes this solution impractical. On the other hand, the only penalty to the alternative solution of making the gauge nonsymmetric is that direct interpretation of the gauge output is slightly more complicated. If one examines the position of zeros in the response function, it is found that a zero can only occur at frequencies where both ph and $p'h$ are integer multiples of the wavelength. One choice which has been used extensively is $p = 0.419$ which retains excellent sensitivity and also has no zeros out to 2000 cycles per meter. The power transfer function, $\omega^4/|H(\omega)|^2$, is shown in Fig. 2. The fact that this transfer function has a well-defined limit at $\omega = 0$ is a further consideration in favor of using curvature rather than offset.

III. THE ROTATING-HEAD MOUSE

The ability of the three-point gauges described above to recover curvature information was conditioned on the magnitudes of the other distortions in the guide being "small." If these distortions are not small the curvature gauge, while responding to them, cannot distinguish the nature of the distortion. To measure these coefficients unambiguously the *rotating-head mouse* was developed. This gauge operates primarily in a laboratory environment and, being intended to completely characterize the geometry of the guide, has been designed for exceptionally high angular resolution and sampling density.

The rotating-head mouse is shown in Fig. 3, in which its principal external features may be seen. There are two major sections, the "body,"

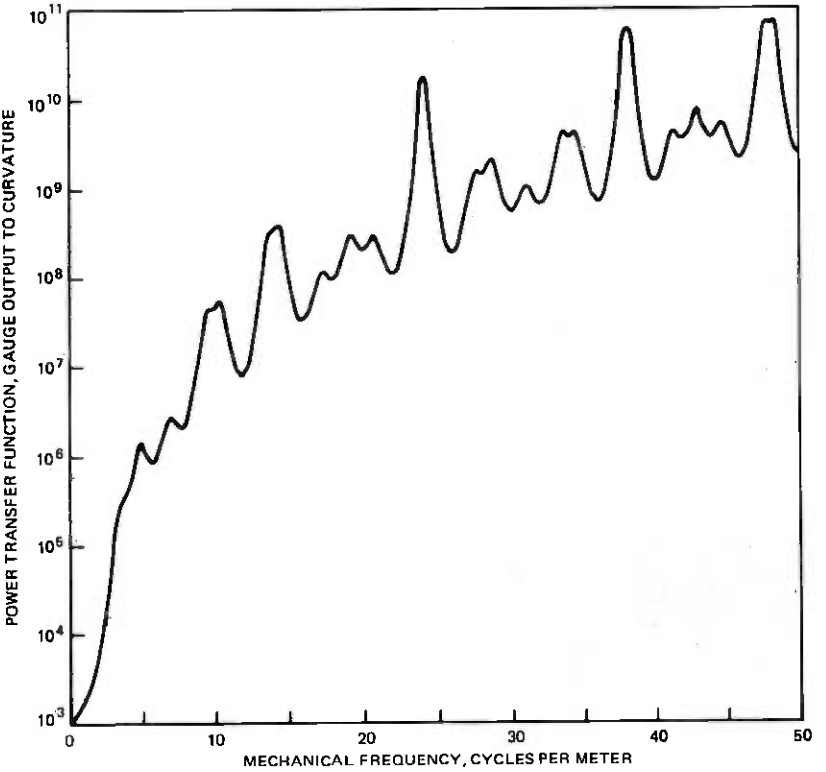

Fig. 2—Power transfer function for a three-point curvature gauge. Length $h = 0.5$ meter, offset $p = 0.419$.

and the "head." The body, like those of the curvature gauges described above, is supported by two pairs of carbide reference feet. These are positioned at ±45 deg from the vertical with one set at the rear of the gauge and the other close to the front. The head of the mouse contains a linear differential transformer and is supported by a precision needle bearing. The head is rotated by a small dc motor contained in the opposite end of the gauge housing. Signals from the differential transformer are brought out through slip rings and the angular orientation of the head is sensed by an optical encoder. Since the head is forward of both pairs of feet the parameter p is greater than 1 for this mouse, but the other considerations on its choice are identical.

The section of waveguide or tubing to be measured rests on two adjustable supports in line with a "measurements bench" and the mouse is moved through the tube by a push rod supported by the bench as suggested by the simplified block diagram, Fig. 4. The measurement and calibration procedures are controlled by a minicomputer. The mea-

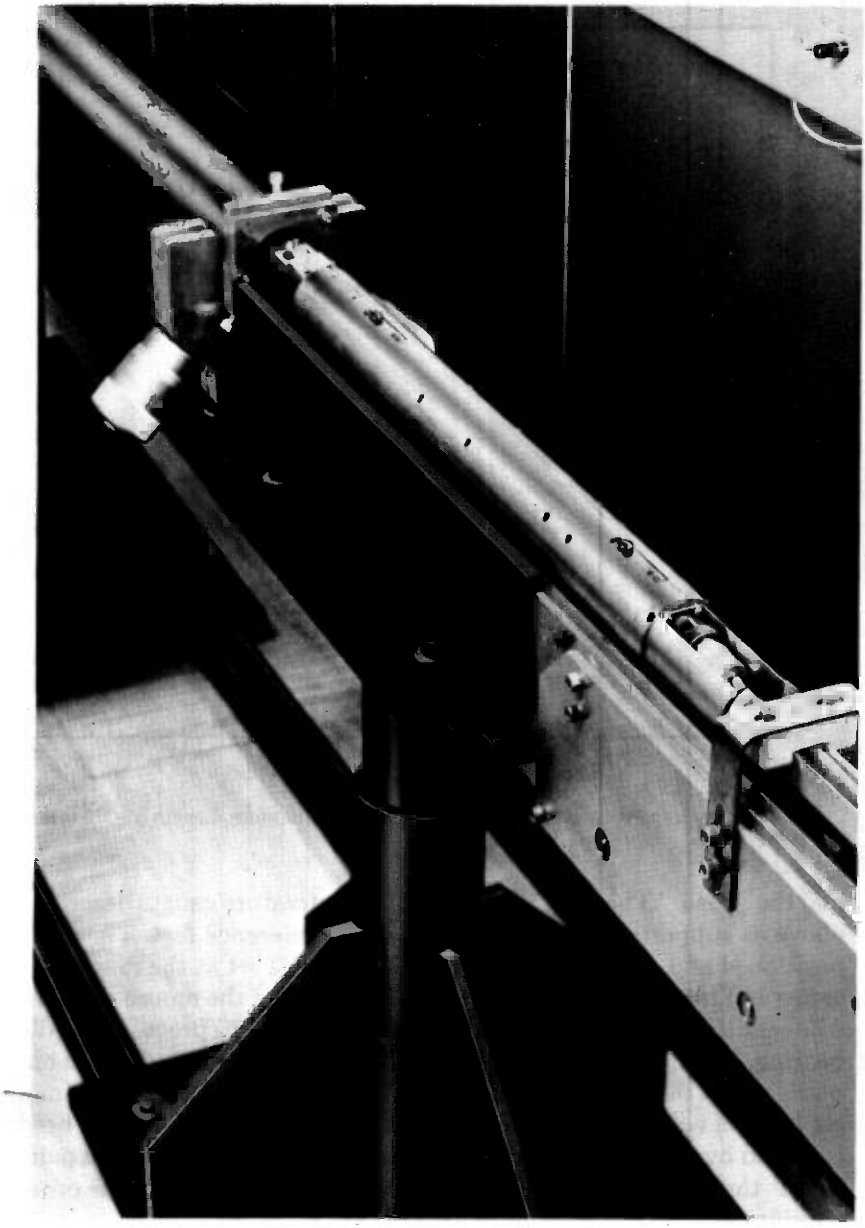

Fig. 3—Rotating-head mouse.

surement sequence which has been found most satisfactory is as follows:

(*i*) The section of tubing to be measured is supported at the "Airy"

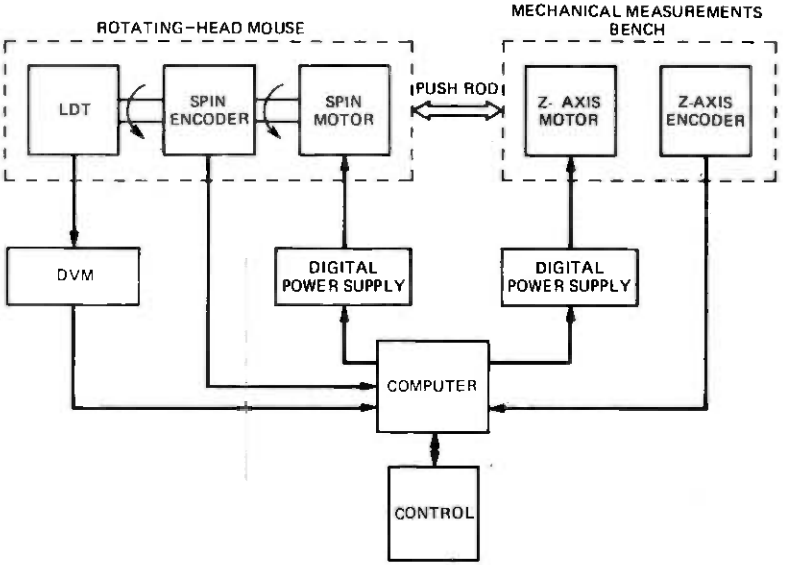

Fig. 4—Rotating-head mouse system block diagram.

points[5] so that there is zero curvature at the ends of the tube due to gravitational effects, and the gauge is positioned at the desired axial position.

(*ii*) The head is rotated for one revolution clockwise at a uniform speed. During this revolution measurements of the radial displacement are made at equally spaced angular increments (given by the optical encoder) using an integrating digital voltmeter.

(*iii*) The measurement is repeated at the same axial position with the head rotating counterclockwise.

(*iv*) The two sets of measurements are compared: if the agreement is good the average is recorded, but if either the mean square or maximum differences are larger than their respective limits, both measurements are repeated. The limit on the rms discrepancies between the two readings is typically less than 1 micron.

(*v*) The axial position is incremented and the process repeated.

The angular resolution and sampling requirements are determined primarily by the highest-order propagating mode and similarly the axial sampling interval is determined by the differential propagation constant or $\Delta\beta$ of this mode. For the electrical frequency range used in the WT4 system, 64 angular measurements per scan and a scan spacing of 2.5 mm have been commonly used. The accuracy requirements of this gauge are complex and, like the waveguides they measure, are specified in terms of the spectral density functions of the various Fourier coefficients. As

an example, the specification limit for the a_0 coefficient near *mechanical* frequencies of 1.3 cycles per meter is 6.5×10^{-2} microns^2/cycles/meter. The corresponding spectrum of steel tubing at this point is approximately 3×10^{-3} μ^2/c/m and the equivalent noise level of the gauge about 2×10^{-4} μ^2/c/m. (The equivalent noise level is obtained by measuring a precision ring gauge *without* changing the axial position and normalizing the spectral density estimates of the coefficients by the axial step size used in the actual measurements. The observed noise results primarily from imperfections in the bearing and differential transformer.)

As is the case with most conceptually simple measurements, the actual theory and implementation of the rotating-head mouse are quite complex. In part this complexity results from the fact that the gauge cannot be built to arbitrary precision. The primary reason, however, for the overall complexity of the system is that it is used for measurement and not for synthesis and, prior to the measurement, the origin of the desired coordinate system is unknown. The result is that the radial displacement measurements are made from the center of the gauge head rather than from the center of the guide. We define the center of the guide to be that point about which the radial expansion coefficients a_1 and b_1 are both zero when the measurement plane is perpendicular to the mean axis of the guide. The guide axis is the locus of the center of the guide.

Temporarily suppressing the z coordinate we assume that a set of measurements $a(\phi)$ have been taken as a function of the angle ϕ measured with respect to the center of head coordinates. We further assume that the head is located at a point (τ, ω) from the center of the guide. The expansion in terms of the coordinates (r, θ) about the center of the guide, is by definition

$$\alpha_n + i\beta_n = \frac{1}{2\pi} \int_{-\pi}^{\pi} r(\theta) e^{in\theta} d\theta \tag{5}$$

The two coordinate systems are related by the elementary identities. To simplify notation rotate both θ and ϕ by $-\omega$

$$a^2(\phi) = r^2(\theta) + \tau^2 - r(\theta)\tau \cos\theta \tag{6a}$$

$$a(\phi) \sin\phi = r(\theta) \sin\theta \tag{6b}$$

$$a(\phi) \cos\phi = r(\theta) \cos\theta - \tau \tag{6c}$$

These can be substituted into eq. (1) by straightforward but tedious algebra and, because the distortions tolerable in millimeter waveguide systems are small, the gauge head is always close to the guide center and a series expansion of the correction in terms of the offset, τ, can be made.

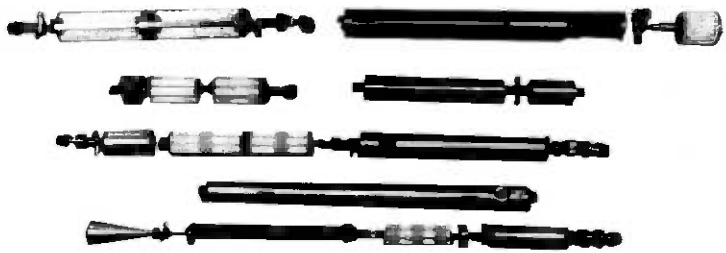

Fig. 5—Long-distance mouse.

The previous paragraph described the conversions between center of head and center of guide coordinate systems in the plane of the gauge head. To obtain meaningful curvature output from the gauge further corrections are necessary. The simplest of these corrections is a result of the gauge measuring a form of second difference of the guide axis displacement rather than an actual derivative and was discussed earlier. The present section is concerned with the influence of foils other than 1 on the apparent curvature.

Clearly the position of the gauge head depends on three distinct elements: the curvature of the guide axis and the positions of the two pairs of gauge feet. The positions of the feet depend on the distortions of the wall in the planes where the feet are located. In an idealized gauge the feet may be represented as vectors of length f_0 at angles of ± 45 degrees from vertical. Since both of these contact the guide wall they define the position of the center of the gauge body in the plane of the feet. Simple but tedious trigonometric equations then give the position of the center of the gauge body relative to the center of the guide in the plane where the feet are located. Extrapolating these differences from both the forward and the back pairs of feet to the plane of the head gives a correction for the influeneces of foils other than 1 on the indicated curvature.

IV. LONG-DISTANCE MOUSE

The long-distance mouse, shown in Fig. 5, is a battery-powered self-propelled gauge especially designed to measure the curvature and diameter of long lengths of installed waveguide. The mechanical data, along with certain status information, are digitally encoded and transmitted through the waveguide itself to a base station, which also controls the mouse. Most of the runs in the field test installation were made with a reflecting piston attached to the tractor so that mode conversion losses as a function of distance could be obtained[1] at the same time as diameter

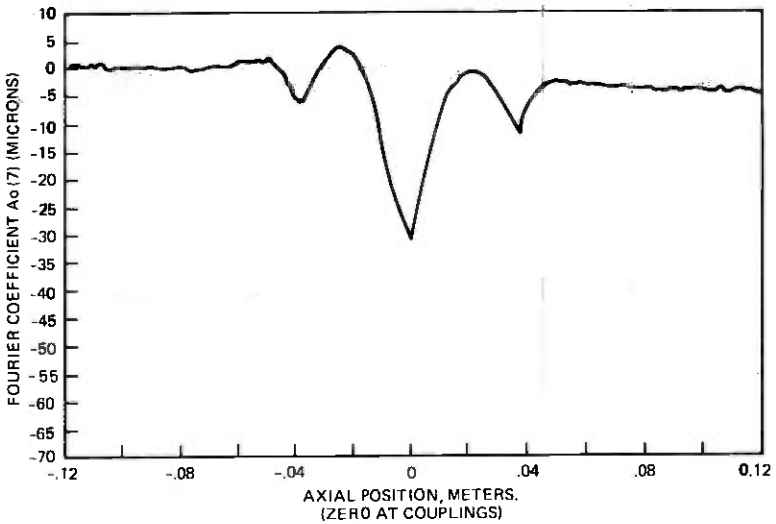

Fig. 6—Radius distortions in a welded coupling.

and curvature information. The data collected by the long-distance mouse contains information on both the placing and couplings, which cannot be present in measurements of individual tubes. Of these the distortions induced by welding the couplings, Fig. 6, contain the most detail, and to characterize this distortion a 1 cm sampling rate has been used for this gauge. While this sampling interval is much finer than required to characterize the placing operation, it provides sufficient redundancy to allow correction of occasional errors and to insure that unexpected high-frequency distortions that may be introduced by the installation procedure are detected.

The design represents a compromise between sensitivity, accuracy, and the necessities of fitting the equipment physically inside the waveguide. If the gauge is too short, eq. (3) implies that very high resolution is required, while if it is too long, one runs the risk of its becoming "stuck" in tight turns. An active length of 50 cm was chosen, representing a compromise allowing peak deflections of about ±1 mm, corresponding to a radius of curvature of about 27 meters and quantization errors of about 1 micron.

As was the case with the rotating-head mouse, the accuracy requirements of the long-distance mouse are complex. Figure 7 shows a set of measurements by the long-distance mouse of a coupling 2.2 km from one end of the field test. The data shown in the top frame, the vertical curvature output, are typical of a "tilt," or angular misalignment, at a coupling, while the data in the third frame, the horizontal curvature output, are typical of axial offset between the two guides. The second

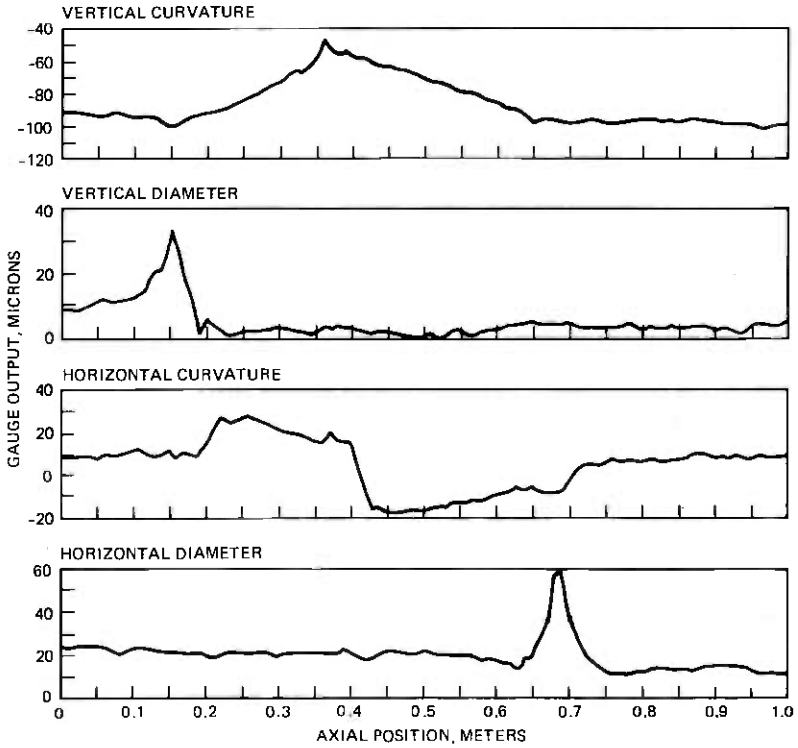

Fig. 7—Comparison of two long-range mouse measurements through a coupling. The apparent shift in location is a result of the transducer (see Fig. 10).

fourth frames represent the two diameter outputs. The long-term accuracy of the gauge is about 5 microns, while the short-term accuracy is much better, and details are reproduced with surprising accuracy. In these plots much of the low-amplitude "noise" is a result of the long-distance mouse running on wheels. Since the wheel noise is periodic at a known frequency, it is accounted for in the Fourier data analysis and, therefore, is of even less importance than it appears here.

As shown in the block diagram, Fig. 8, the long-distance mouse system consists of the following main components:

(*i*) Tractor
(*ii*) Stabilizer and torque isolator
(*iii*) Diameter and curvature gauge
(*iv*) Data encoder and command circuits
(*v*) Transmitter-receiver
(*vi*) Base station

These components will now be described in the above order.

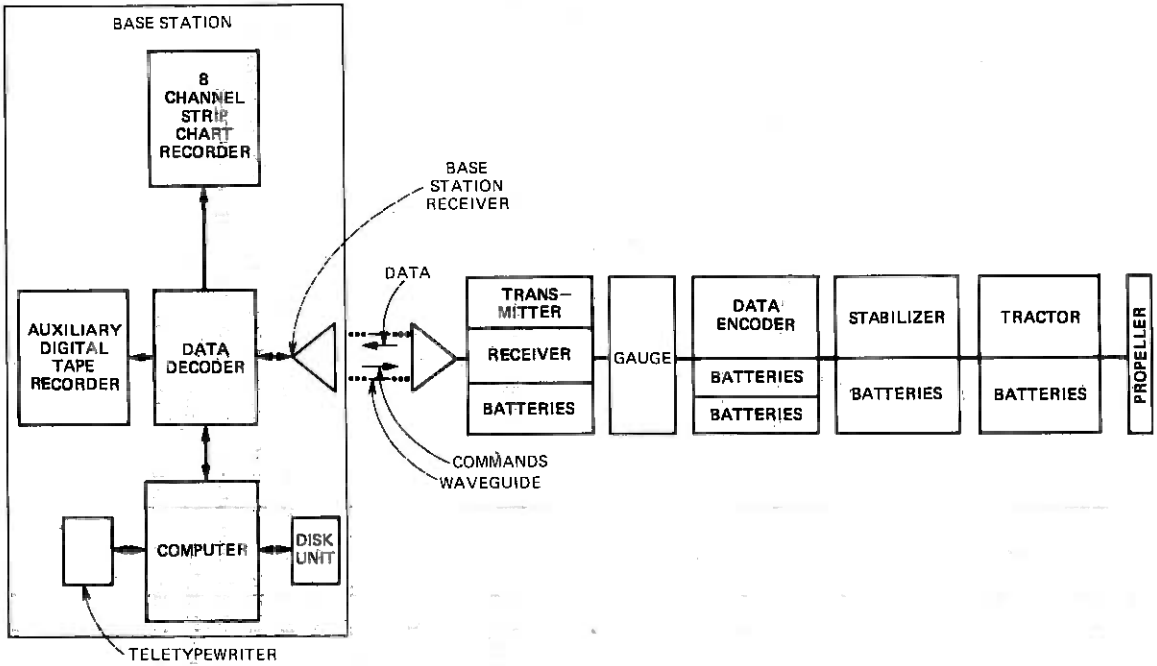

Fig. 8—Block diagram of field evaluation test mouse system.

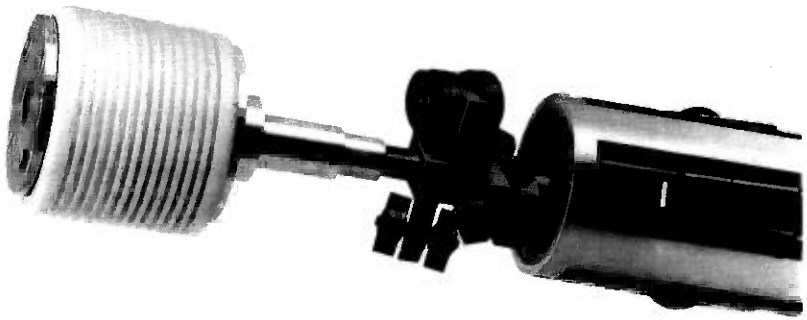

Fig. 9—Detail of propeller and pneumatic piston.

4.1 Tractor

The tractor comprises a tubular body provided with eight wheels and containing a dc motor and control circuitry. External to the body is a "propeller" driven by the motor and a pneumatic piston, as shown in Fig. 9. The propeller consists of four pairs of rubber-tired wheels set at an angle of 20 deg with respect to the axis of rotation of the propeller and bearing against the inner wall of the waveguide. As the propeller rotates, it pulls the tractor and its train through the waveguide. Counterrotation of the tractor is opposed by four rubber-tired wheels located at 90 deg around the forward end of the body. These wheels, and the propeller wheels, are spring-loaded against the inner wall of the waveguide to provide a constant adjustable frictional force essentially independent of variations in the inner diameter of the waveguide (such as those encountered when going from the dielectric-lined guide to the helix mode filters).

Power for the motor is supplied by two 12-volt nickel-cadmium battery packs each having a capacity of 3 ampere-hours. To reduce battery drain a nitrogen "boost" is applied to the mouse in the direction of travel, the force being developed essentially across the restriction provided by the pneumatic piston. Maximum range with a boost of 0.14 kg/cm^2 (2 psi) is about 10 kilometers at the nominal velocity of 30 cm/sec. For runs of less than 5 km only one battery pack is needed.

4.2 Stabilizer and torque isolator

Angular orientation of the mouse is maintained to within ±0.5 deg by a servo stabilizer. An electrolytic potentiometer, whose resistance varies

Fig. 10—Diameter and curvature gauge.

with tilt, is connected to form two arms of a phase-sensitive bridge. A rubber-tired spider, bearing against the inner wall of the waveguide, is attached to the shaft of a servo motor and, as the shaft turns in response to the error signal, the mouse assembly rotates as a unit to null the signal, thereby maintaining orientation. Since the torque restraining wheels on the tractor have a residual angular slippage, the tractor rotates at a low rate in a sense opposite to the rotation of the propeller. To avoid wasting battery power in correcting this rotation, a torque isolator is interposed between the tractor and the stabilizer to isolate rotationally the tractor from the rest of the assembly. Signals to the tractor are coupled through slip rings.

4.3 Diameter and curvature gauge

The diameter and curvature gauge, shown in Fig. 10, has four transducers so that the diameter and curvature can be measured simultaneously in both the vertical and horizontal planes. For diameter measurements a transducer is placed opposite a curvature reference foot. The level sensor for the stabilizer is mounted on one end of the body and a second sensor, having a greater range (±11 deg as compared to ±1.5 deg for the former), is mounted on the other end to provide information for telemetry regarding the orientation of the gauge and to indicate any malfunction of the stabilizer.

4.4 Data encoder

Eight analog channels are sampled sequentially every centimeter of gauge travel: the outputs of the four transducers, the gauge angle, the

ground reference, the drive motor supply voltage, and the 5-volt supply. These analog voltages are digitized and ordered into 16-bit bursts by the data encoder. The first bit of each bit is always a logical "one" for synchronization, the next three bits are the octal channel number, and the last 12 bits are the encoded data. The timing sequence for a complete data transmission is shown in Fig. 11. Also included are controls for gain

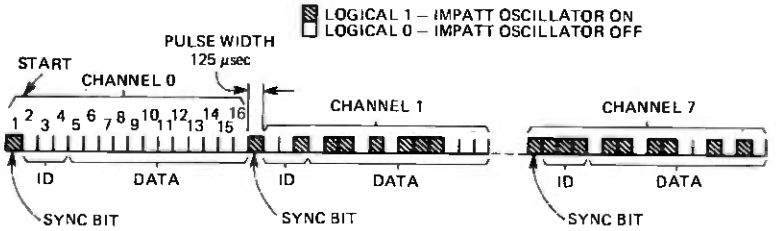

Fig. 11—Data burst timing diagram.

and offset and analog filters to prevent aliasing effects in the sampled data. Extensive use of CMOS integrated circuits reduces power consumption to a negligible level.

4.5. Transmitter-receiver

The transmitter-receiver unit includes the IMPATT oscillator, its driver-modulator, a Schottky diode receiver, a transmitting-receiving horn antenna, and associated millimeter-wave components. These include a directional coupler specially configured to fit in the restricted space available within the waveguide. The IMPATT oscillator operates at a frequency of 80 GHz and at an 8k bit per second rate.

4.6. Power supplies

The power supplies for the tractor and stabilizer have been described. The remaining supplies furnished regulated +5 volts and ±15 volts for the differential transformers and internal circuits. They are derived from nickel-cadmium batteries and have a capacity sufficient for 10 hours of operation. All supplies may be charged simultaneously without removal from the mouse. Power consumption of the mouse, excluding the tractor and stabilizer, is about 1 watt.

4.7. Miscellaneous features

The mouse assembly is over 5 meters long. A rigid assembly of this

length could not negotiate bends and would be impractical to transport and to insert into and remove from the waveguide. Each unit, therefore, is provided with universal couplings incorporating cable connectors with locking sleeves. To reduce the load on the stabilizer, all units following the torque isolator, except the gauge itself, are supported by spiders that allow the units to rotate freely about their common axis as well as to roll easily through the waveguide.

4.8. Base station

The base station has already been shown in block form in Fig. 8. It includes the base station receiver, the data decoder, and a minicomputer with peripheral equipment. Its purpose is to control the mouse and to monitor and record the received data.

The base station receiver employs conventional millimeter-wave circuitry to receive signals from the mouse and to transmit control signals to it. A received signal margin of 12 dB was obtained in measurements of the 14-km field test installation. As the waveguide loss at 80 GHz is about 0.5 dB/km or 7 dB for the entire installation, the loss margin implies that the receiver range is 38 km. Only minor improvements would be necessary to achieve adequate sensitivity for the expected repeater spacing of 50–60 km.

The data decoder has two basic functions: to convert the serially encoded data bursts into parallel format for the computer and to control the mouse. The mouse responds to seven commands; namely, start, stop, forward, reverse, power up, power down, and status. The commands are generated by pulsing an IMPATT oscillator at one of seven discrete frequencies between 25 and 68 kHz. The command signals are detected by the mouse receiver and used to operate bistable latching relays. The power down command turns off all circuits within the mouse except for the command receiver. The latter draws only 2 ma from a 0.45 ampere-hour battery so that the mouse may be left for extended periods in the power-down mode.

Meter displays indicate the distance travelled and velocity of the mouse.

4.9. Computer

The measurements are always made under computer control, although the computer may be overridden at will. The software selects the direction of motion of the mouse, the beginning and end points for the run, and performs certain housekeeping functions. As an example, the mouse is stopped when the data disk is filled. Malfunctions, such as failure of the mouse to respond to a command or lack of data from the mouse, are also indicated. Plots of the various data signals for any selected part of

the run may be obtained, but detailed analysis must be performed on a large computer.

V. CONCLUSIONS

The most convincing argument for the use of mechanical measurements in millimeter waveguide system development is provided by the *electrical* measurements of the completed installation. From these loss measurements[2] it is apparent that the mode conversion loss below 60 GHz is less than 0.05 dB/km.

This low level of mode conversion is primarily a result of process development and quality control[6] based on the use of mechanical measurements. Naturally this use depends on the ability to predict electrical losses from mechanical measurements. It is noteworthy that the theory of second order TM_{21} loss[7] was discovered largely as a result of discrepancies between the measured and predicted losses.

VI. ACKNOWLEDGMENTS

The development of the mice was a joint, intense effort on the part of many individuals. Among the many who deserve to be singled out are: T. J. West who conceived the idea of the propeller and supervised the design of several of the mice; E. Vignali, who designed the millimeter-wave sections of the long-distance mouse and the base station; E. Bochner, who wrote the software for the base station computer; K. R. Jones, who designed the external sheath mouse; E. Schultz, who contributed programs and control circuits for the rotating-head mouse; D. Olasin and D. R. Rutledge, who collaborated on the design of the internal sheath mouse; and L. W. Hinderks, who contributed greatly to the logic and software designs of several mice.

REFERENCES

1. M. A. Gerdine et al., "Electrical Transmission Measurement System," B.S.T.J., this issue.
2. J. C. Anderson et al., "Field Evaluation Test—Transmission Medium Achievements," B.S.T.J., this issue.
3. S. P. Morgan, "Mode Conversion Losses in Transmission of Circular Electric Waves Through Slightly Non-Cylindrical Guides," J. Appl. Phys., *21*, (1950), pp. 329–338.
4. H. E. Rowe and W. D. Warters, "Transmission in Multimode Waveguide with Random Imperfections," B.S.T.J., *41*, No. 5 (May 1962), pp. 1031–1170.
5. F. H. Rolt, *Gauges and Fine Measurements*, London: MacMillan, 1929.
6. R. J. Boyd, Jr. et al. "Waveguide Design and Fabrication," B.S.T.J., this issue.
7. J. C. Carlin and S. C. Moorthy, "TE_{01} Transmission in Waveguide with Axial Curvature," B.S.T.J., this issue.

THE BELL SYSTEM TECHNICAL JOURNAL
Vol. 56, No. 10, December 1977
Printed in U.S.A.

WT4 Millimeter Waveguide System:

Electrical Transmission Measurement System

By M. A. GERDINE, L. W. HINDERKS,
S. D. WILLIAMS, and D. T. YOUNG

(Manuscript received April 7, 1977)

An electrical transmission measurement system which measures the TE_{01} loss characteristics of the millimeter waveguide medium is described in this paper. This computer-controlled system operates from 33 to 117 GHz with fully automated measurements over 10-GHz frequency intervals after several preparatory manual adjustments. The measurement signal is a pulse which is reflected from the end of the test waveguide line and detected in a calibrated receiver. The transmitter and receiver are both located at one end of the test line. The measuring range is 50 dB and the systematic error and random uncertainty are less than ±0.3 dB and ±0.1 dB respectively for any test line longer than 100 meters. The minimum line length is determined by the spatial duration of the signal pulse. The system can also be used to measure the reflected signal from a piston moving in the waveguide. This technique is useful for measuring loss and mode conversion effects in a local region of the transmission medium.

I. INTRODUCTION

During 1975 and 1976 a field evaluation test of the WT4 millimeter waveguide transmission system was conducted jointly by AT&T Long Lines, Western Electric, and Bell Laboratories. A major component of this test was the installation and evaluation of 14 km of the buried waveguide transmission medium. This paper describes an electrical transmission measurement system which measures the TE_{01} circular mode transmission loss in the installed waveguide medium throughout the 33 to 117 GHz frequency band under consideration. This system has been used for evaluation of waveguide lines ranging from 0.1 to 14 km in length at frequency spacings as small as 50 MHz. The field evaluation

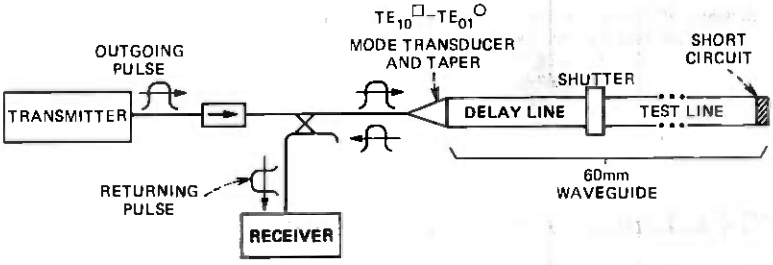

Fig. 1—Pulse reflection loss measurement arrangement.

test measuring system is the culmination of a test set development program which included systems for laboratory evaluation of dielectric and helix waveguide prototypes and final inspection of Western Electric waveguide product. Typically the loss is measured at as many as 1000 frequencies over the entire WT4 transmission band. A computer-controlled test set is required to make this number of measurements on a repeated basis with high accuracy. The computer system provides capability for automating the test set operation, fast signal averaging of the measured levels for more accurate and repeatable measurements, immediate Fourier transforms for data spectral analysis, and permanent data storage. These data can be displayed on a CRT moniter or plotted on hard copy for immediate evaluation. The performance capabilities of the measurement system are listed in Table I.

The electrical transmission measurements are made by a single-pulse reflection technique. The experimental arrangement is shown in Fig. 1. The transmitter sends a pulse down the delay line which is initially terminated by a closed short-circuiting shutter. This pulse is reflected back to the receiver where its amplitude is measured. Next, the shutter is opened and the pulse is reflected from a short circuit at the far end of the test line. The logarithmic amplitude difference between these pulses is the round-trip attenuation of the test line at the transmitter frequency.

Two manholes were installed in the test route for placing a short-circuiting shutter in the waveguide line. The delay line is 370 m in length to the first shutter location. Loss vs. frequency measurements were made on all the waveguide sections which were installed after this delay line. These sections were installed by the methods which are described by Baxter et al.[1] A detailed report on the electrical transmission data is given in Anderson, et al.[2]

Since the delay line and test line scatter energy from the TE_{01} signal mode into unwanted spurious modes, both lines should be terminated by ideal mode filters which cause infinite attenuation of the unwanted modes. This insures that: (*i*) the reference baseline obtained from the

round-trip pulse in the delay line is due solely to the TE_{01} mode incident on the test line when the shutter is opened and (*ii*) the one-way loss of the test line is one-half the measured round-trip attenuation. In practice, 9-meter lengths of helix mode filters, which were manufactured for the field evaluation test, were used to terminate the reference delay line and the test line.

The transmission measurement system is also used for measureihg the signal pulse reflected from a short-circuiting piston moving in the test waveguide. The shape of the received signal power plotted as a function of piston position is described by three main effects:

(*i*) The signal having propagated through a different length of guide for each piston position undergoes the TE_{01} mode round-trip attenuation of the traversed portion of the waveguide.

(*ii*) If the waveguide does not possess the ideal geometry of a right circular cylinder, some power in the TE_{01} mode is converted to power in unwanted spurious propagation modes. Power in the spurious modes is lost to the receiver since it only recovers the power in the TE_{01} mode.

(*iii*) If the waveguide attenuation for the converted spurious modes is not extremely large compared to the attenuation for the TE_{01} mode, some of the power in these spurious modes is reconverted into the TE_{01} mode by the same coupling mechanism which generated them initially, because the signal must propagate through the same waveguide geometry after being reflected from the piston. Since, in general, different modes have different phase propagation constants, this reconversion occurs in a manner varying from completely constructive to completely destructive, depending on the distance traveled and the difference in the phase propagation constants of the interfering modes.

The preceding discussion implies that increasing the test line length with a moving piston does not necessarily cause a monotonically decreasing signal level. In general, there is an average decrease due to the attenuation properties of the waveguide with superposed fluctuations caused by mode conversion and reconversion effects. The slope of the power level change versus test waveguide position is the average TE_{01} mode attenuation coefficient. The Fourier transform of the fluctuations over some section of the test waveguide is used to identify and obtain the average relative level of the spurious modes coupled in this section.[2]

In the following sections, we describe the important circuit and computer features and discuss the performance of the measurement system.

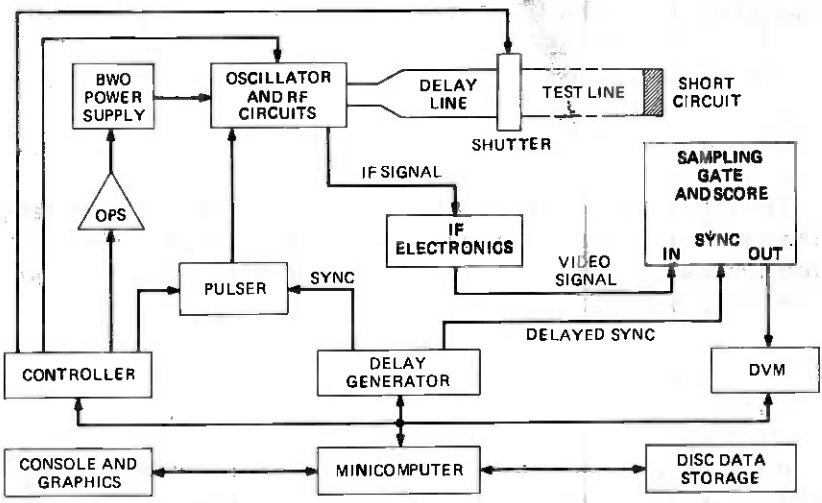

Fig. 2—Millimeter waveguide transmission measurement system.

II. CIRCUIT FEATURES

Figure 2 is a block diagram of the transmission loss set. The RF circuit consists of a single Backward-Wave Oscillator tube (BWO), which serves as the source of both the measurement signal and the Local Oscillator (LO), and rectangular waveguide components which operate in the dominant mode over the same frequency range as the BWO. The measurement signal is derived by shifting the BWO away from its quiescent operating frequency by 160 MHz for a short time (700 nsec). When this shifted frequency pulse returns from the test line, the BWO has returned to its quiescent frequency. The RF circuit (Fig. 3) directs a part of the transmitter signal to the test line and part, which serves as the LO, to the mixer diode. Signals returning from the test line are also directed to the mixer diode where they are down-converted to a fixed intermediate frequency of 160 MHz. Since the level of the LO signal remains constant regardless of the loss in the test line, the IF pulse amplitude is a measure of the signal returning from the test line. The level of the signal pulse is always maintained at least 20 dB below the LO. Therefore over the RF range of the set, the change in amplitude of the IF pulse is linearly related to the change in power of the RF signal. The calibrated IF substitution method is used to measure the signal level change. To provide measurement capability over the entire WT4 frequency band, three interchangeable RF circuits, each with its own BWO, are required. The three measurement bands are 33 to 50 GHz, 50 to 75 GHz, and 75 to 117 GHz.

BWO frequency control (Fig. 4) is accomplished using a high voltage (1000 volt) Operational Power Supply (OPS) inserted in series with the

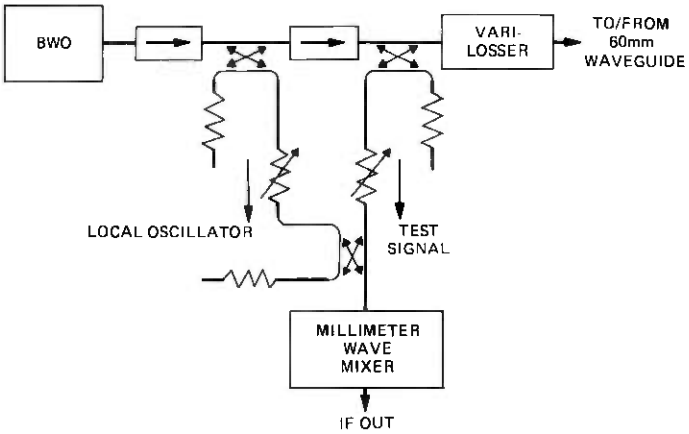

Fig. 3—RF millimeter-wave circuit arrangement.

output of a standard BWO power supply.[3] The combined voltage is applied to the cathode of the BWO, setting its quiescent operating frequency. The input to the OPS comes from a programmable 12-bit D/A converter located in the test set controller. Pulsed frequency modulation of the BWO is performed by superposing the output of a pulser on the anode of the BWO causing a momentary 160 MHz shift in the BWO output frequency. This burst of offset frequency provides the test signal in the waveguide line. The pulser is programmable because the amplitude of the pulse required to cause a 160 MHz offset is a rapidly varying function of the operating frequency of the BWO. Since the dynamic range of the

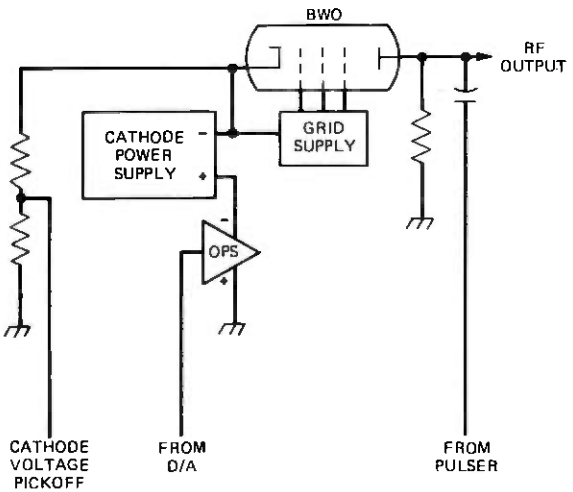

Fig. 4—BWO frequency-control circuit arrangement.

OPS and the programming range of the pulser are limited, the cathode voltage from the BWO power supply and the pulser voltage amplitude are manually adjusted 2 or 3 times for each RF circuit.

The IF electronics consist of a combined 160 MHz amplifier and video detector preceded by a calibrated precision step attenuator. The IF signal pulse is amplified and converted to a video pulse which is the input to the video instrumentation. The electronics and all succeeding measurement equipment are calibrated as a unit over a 25 dB range, by recording the output values as a function of 1 dB incremental settings of the attenuator. The IF calibration is restricted to 25 dB to assure an adequate signal-to-noise ratio that does not require time-consuming signal averaging to recover low-level video signals. In the measurement mode, measured values are converted to a relative dB value by exponential interpolation between the calibration points. Exponential interpolation is used since the video detector operates as a "square law" device.

All measurement data are obtained from video pulses. A sampling oscilloscope displays the pulse and provides a means for sampling the video signal at any point on the pulse and at some point outside of the pulse to serve as a base line reference for the pulse. The amplified output of the sampling gate is measured with a digital voltmeter, converted to a relative dB value and stored in memory. The delay generator controls the measurement cycle. This generator triggers the pulser causing a signal pulse from the BWO and after a programmable time interval, triggers the sampling gate enabling a measurement on the video representation of the returning delay line or test line pulse.

For long test lines the loss can be greater than the calibrated dynamic range (25 dB) of the IF signal. In this case, either the delay line pulse or the test line pulse will not be measurable. The range is extended by using the varilosser as a programmable precision RF attenuator over the full dominant mode waveguide bandwidth.[5] With the varilosser, a known amount of attenuation is automatically inserted when measuring the shutter pulse and removed when measuring the test line pulse. This added loss is accounted for in calculating the test line loss. A table of loss versus frequency for each of several fixed drive currents controlling the varilosser is generated by calibration with the precision IF attenuator. The currents are chosen to give nominal losses in 5-dB increments. This technique gives a repeatable varilosser calibration which is within 0.1 percent of the attenuation standard over a 25-dB range.

The test set controller operates the BWO frequency control circuit, varilosser, and shutter. A programmable current source is located in the controller for setting the varilosser attenuation. Relays in the controller operate the shutter which is located in a manhole where it intercepts a short span of the test installation.

III. COMPUTER FEATURES

The transmission loss set is almost completely automated. This automation is achieved by interfacing the programmable instrumentation to a minicomputer. The minicomputer system acquires, processes, displays, and stores the measurement data.

The computer's central processing unit (CPU) is equipped with 32k words of 16-bit memory. The real-time operating system, supplied by the computer manufacturer, requires 14k words of memory which leaves a user space of 18k. The system area of memory contains the operating system as well as the hardware interface drivers. These input-output (I/O) software routines are in part supplied by the computer manufacturer for use with their hardware. Other I/O drivers were designed especially for the test set. The CPU is equipped with special firmware for high-speed execution of many floating point operations. This increased computational speed allows almost all data reduction to be done in the CPU. The computer is equipped with two disk drives. The larger disk is capable of storing 5.0 megabytes of data, 2.5 megabytes on a fixed platter, and 2.5 megabytes on a removable cartridge. The fixed platter contains the absolute system programs and absolute user programs. The removable cartridge of the larger disk drive stores user source programs. The smaller drive has a 2.5-megabyte removable cartridge and stores measurement data files. As the removable pack of the small drive fills, an empty pack is easily inserted without disrupting the measurements if the operator does not want to halt the program. Additionally, the system has several terminals, a CRT display and hard-copy unit, and a line-printer.

Program development represented a large part of system development. To increase programmer efficiency a special software system, LOGON, was devised.[4] LOGON is a monitor system which provides an interface between the user and the computer vendor's operating system. The LOGON command structure is designed so that the user can perform the most often needed tasks of program development with relative ease. It allows for easy editing, high-level language programming and mass data storage such that software design modification is greatly simplified compared to previous minicomputer operating systems. LOGON can handle multiple users and time-share the CPU when multiple requests are made for the processor. Thus, LOGON enhances the real-time operating system to a multiprogramming time-sharing level.

The software development included I/O drivers; data acquisition programs; and data storage, manipulation, and display programs. The program space necessary to perform a complete task was generally too large for the limited CPU memory. Therefore, program modules, which performed individual functions, were chained together to accomplish the complete task. Each module performs its function, writes the results

Table 1 — Measurement system performance*

Frequency bands	33–50 GHz	50–75 GHz	75–117 GHz
Frequency uncertainty	±50 MHz	±50 MHz	±50 MHz
Frequency repeatability	±5 MHz	±5 MHz	±5 MHz
Reflection piston location uncertainty	±0.3 meters	±0.3 meters	±0.3 meters
Average measurement speed in 10-GHz subband	100 measurements/hour	100 measurements/hour	100 measurements/hour
Measuring range	50 dB	50 dB	50 dB
Relative error	±0.020 dB	±0.07 dB	±0.3 dB
Random error	±0.005 dB	±0.02 dB	±0.1 dB

* All experimental estimates are maximum values except the measuring range which is a minimum value.

on disk, and schedules the succeeding module from the user programs on the disk. The modules communicate with each other from a common CPU memory block.

IV. PERFORMANCE

With proper attention to details, the time domain technique of this measurement system virtually eliminates any sources of error due to millimeter wave component mismatches. The minimum length of reference delay line (370 meters) was chosen to allow reasonable transition times to obtain a well-defined signal pulse. Since this pulse is obtained by frequency offset of the single BWO source, it is extremely important that sufficient time (1 microsecond) is allowed for the BWO to stabilize at its quiescent point, which is the LO source, before the reflected signal arrives at the receiver. Since the shutter is rapidly operated, any errors due to amplitude fluctuations are also minimized. The signal levels in the calibrated IF section are chosen to minimize any errors from nonlinearities and noise.

If the mode filter at the end of the delay line does not provide sufficient attenuation of the unwanted modes which are converted from the forward TE_{01} signal pulse, there is a complex interaction between the forward and return trips of the pulse. This interaction leads to an error in the baseline measurement. The detailed base-line characteristic is a function of the round-trip length between mode conversion points on the forward trip and mode reconversion points on the return trip. This line length changes when the shutter opens, therefore the baseline reference at each measurement frequency can change from the measured value.

Since the transmission characteristics of the helix mode filters are strongly dependent on their installed axial curvature,[2] we performed an experiment which gave a worst-case estimate of the maximum baseline error. The loss characteristic was measured for a 710 m waveguide test line which was not terminated with a mode filter. The maximum

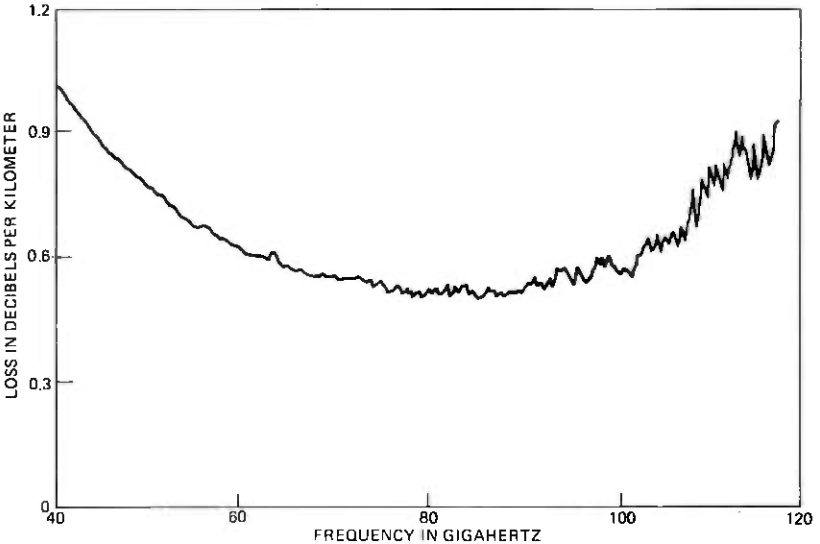

Fig. 5—Field evaluation test waveguide measured loss.

value of the peak-to-peak deviations from the average loss in each of the three RF circuit bands was scaled linearly to the 370 m length of the actual delay line. These estimates are given as the relative error in Table I. The random error (repeatability) values in Table I were obtained from continual experimental measurements on the buried field evaluation test waveguide line.

The measured loss for the 14 km field evaluation test route is shown in Fig. 5. The loss characteristic was measured at 250 MHz intervals from 40 to 75 GHz and at 100 MHz intervals from 75 to 117 GHz.

V. CONCLUSION

The computer-controlled system was developed to make TE_{01} circular mode transmission loss versus frequency and moving piston experiments on the field evaluation test waveguide medium. Accurate measurements are obtained for transmission loss up to 50 dB in the frequency range from 33 to 117 GHz.

VI. ACKNOWLEDGMENT

D. E. White generously discussed with us his initial work on computer control of millimeter-wave BWOs. E. Bochner developed much of the software support programs and E. B. Dunn was an important contributor to the mechanical design. D. R. Rutledge provided invaluable leadership in coordinating our loss measurements with the waveguide installation schedule. Numerous outside plant and station craftspersons at the Long

Lines Netcong main station were helpful during all phases of field evaluation test electrical measurements.

REFERENCES

1. H. A. Baxter, W. M. Hauser, and D. R. Rutledge, "Waveguide Installation," B.S.T.J., this issue.
2. J. C. Anderson, J. W. Carlin, D. J. Thomson, T. J. West, and D. T. Young, "Field Evaluation Trial-Transmission Medium Achievements," B.S.T.J., this issue.
3. D. E. White, "A Computer-operated Millimeter Wave Insertion-Loss and Return-Loss Measurement System," IEEE Trans. Instrum. Meas., *IM-25*, December 1976, pp. 419–424.
4. E. Bochner and L. Hinderks, unpublished work.
5. C. E. Barnes, "Broad-band Isolators and Variable Attenuators for Millimeter Wavelengths," IEEE Trans. Microw. Theory Tech., *MTT-9*, November 1961.

THE BELL SYSTEM TECHNICAL JOURNAL
Vol. 56, No. 10, December 1977
Printed in U.S.A.

WT4 Millimeter Waveguide System:

Reliability and Maintenance of the WT4 Transmission Medium

By R. P. GUENTHER and W. M. HAUSER

(Manuscript received April 7, 1977)

The reliability of the waveguide medium depends upon its resistance to damage from external forces, the restoral time in case it's damaged, its resistance to gradual deterioration, and the ability to move the location of the medium after it is installed. Trouble estimates, their causes, and restoration methods for the WT4 medium are discussed. This includes electrical and pneumatic fault location. Also discussed from both a systems design and operations viewpoint are maintenance systems designed to prevent deterioration of the WT4 medium (corrosion protection system and the nitrogen system) and the concepts for methods to change the location (route rearrangements) of the medium after it is installed.

I. INTRODUCTION

The maintenance plans for the WT4 transmission medium are unique when compared to other operational waveguide maintenance systems and conventional coaxial cable maintenance systems. Very high reliability and very low-cost on-going maintenance are achieved without high first-cost access points (manholes) and monitoring devices between the widely spaced repeater stations. Elimination of the access points and monitoring devices was made possible by developing techniques and methods to:

(*i*) Locate electrical faults in the waveguide with accuracy of a few meters when testing from repeater stations up to 20 miles from the fault.

(*ii*) Localize leaks in the waveguide sheath when testing from repeater station up to 20 miles from the leak.

(*iii*) Minimize water ingress into the waveguide in the event of a waveguide rupture.

(*iv*) Restore damaged waveguide to service very quickly.

The developments are part of a totally integrated maintenance plan which takes maximum advantage of the very rugged steel sheath to provide the reliability required for the high-capacity WT4 system. This paper discusses the WT4 transmission medium reliability and the steps that were taken to control medium outage.

II. RELIABILITY OF THE WT4 TRANSMISSION SYSTEM

2.1 General

For long-haul transmission systems, reliability is defined as the percent of time that a 4000-mile line is available for service. The reliability objective for the WT4 medium is 99.99 percent or service outage of less than 1 hour per year.

Outage on the WT4 transmission medium is determined by the number of service-affecting troubles, the restoration time for such troubles, and outage caused by the medium being unavailable for service due to operations such as route rearrangements.

2.2 Service-affecting troubles

Service-affecting troubles interrupt service on the waveguide medium by the introduction of transmission impairments. A 3 dB margin is allocated in the system loss budget so that minor transmission impairments in the medium do not become service-affecting. Therefore, incidents that cause less than 3-dB transmission impairments are considered to be routine troubles.

The causes of transmission impairments can be divided into three categories:

(*i*) Component failure
(*ii*) Corrosion
(*iii*) Mechanical damage

Component failures are controlled by the design of the medium, corrosion is controlled by design and by the maintenance systems, and mechanical damage is controlled by protection.

2.3 Component failure

The WT4 medium has several manufacturing and construction processes that are considered to be vital to the reliability of the medium. These are the bonding of the waveguide dielectric lining to the waveguide tube, the joining of the waveguide modules, and the termination of the

waveguide in building walls. Boyd et al.[1] discuss the dielectric bonding process. Gretter et al.[2] discuss the coupling design, and Liss et al.[3] discuss the termination of the waveguide in buildings.

During the design of the medium there was a conscious effort to eliminate components that could compromise reliability. As a result, the WT4 medium has no manholes, expansion joints (except inside buildings) or auxiliary cable for signaling.[4]

With the transmission impairment margin of 3 dB and the methods of locating and repairing routine troubles discussed later in this paper, it is expected that component failure will cause negligible outage.

2.4 Corrosion failures

The WT4 medium is buried and it can gradually deteriorate from corrosion. Continued corrosion could eventually lead to failures and service outages.

Early in the development of the WT4 medium it was recognized that the waveguide could not be effectively protected against corrosion if it were placed in a nonmetallic nonpressurizable sheath material such as PVC. The decision to use a steel sheath was heavily influenced by the need to protect the waveguide from corrosion. To minimize the corrosion of the steel sheath, a high-quality coating is used in conjunction with rectifier and sacrificial anode installations. The selection of coatings, and design and maintenance of cathodic protection systems is well covered in the literature.[5]

No economically justifiable corrosion control system can eliminate corrosion entirely and corrosion failures can be expected to occur. It is important that such failures do not cause service-affecting troubles. One function of the nitrogen pressurization system which is discussed later in this paper is to insure that corrosion sheath failures do not lead to service-affecting troubles. WT4 medium corrosion will cause negligible outage.

2.5 Failures caused by mechanical damage

Mechanical damage that causes transmission impairment is the main source of service-affecting troubles on coaxial cable systems. It is also expected to be the main source of service-affecting troubles for the WT4 medium which is installed on similar rights-of-ways.

The WT4 medium can be damaged in much the same way as coaxial cable, i.e., crushed, severed, etc. However, its susceptibility to such damage is drastically reduced due to the combined mechanical strength of the steel waveguide and its protective steel sheath.

The reliability information gathered on coaxial cable can be used to

predict the reliability of waveguide if the greater mechanical strength of the WT4 medium is considered.

Since 1969 the Long Lines Department of AT&T has been preparing detailed reports on all service-affecting coaxial cable troubles. Table I gives the trouble rate average for the years 1973 to 1975 for the major categories of trouble.

Analysis of the trouble reports shows that the Bell-associated troubles generally damage only a few coaxials in the cable and contribute very little to system outage. The WT4 medium will not be damaged by actions that cause only minor damage to coaxial cable because of the protective steel sheath. Bell-associated troubles will cause negligible WT4 medium outage.

Lightning entering the ground and jumping to the metallic sheath on coaxial cable produces an impact that can crush coaxial tubes. In only very rare occurrences are lightning damages severe enough to affect service on all coaxials in a 20-tube coaxial cable.

To determine how the WT4 medium would be affected by lightning, the sheath was subjected to lightning thermal and crushing tests. Tests with high-current energy depositions that were sufficient to crush all tubes in a 20-tube coaxial cable produced only small dents in the waveguide sheath. Lightning should therefore cause negligible WT4 medium outage.

2.6 Foreign Workers

"Foreign" workers (non-telephone-company related) cause the most severe damage to coaxial cables and are by far the biggest contributor to coaxial cable system outage. The damage occurs when construction equipment used by the workers accidently strikes the cable. Seventy percent of the foreign worker troubles in the years from 1973 to 1975 damaged all of the coaxials in the cable. Troubles caused by foreign workmen should be the only significant contributor to WT4 medium outage.

Table II shows the relative frequency with which various types of construction equipment damage coaxial cable. Backhoes and earth penetration devices such as drills, probes, and augers cause almost 70 percent of the troubles. A good measure of the reliability of the medium is its ability to withstand strikes from such equipment. Several field tests were conducted to determine the WT4 medium resistance to damage. The results are summarized below:

(*i*) Small backhoes (smaller than 3/4 yard) are not capable of causing service-affecting troubles with accidental hits on the medium. (Small backhoes most frequently damage coaxial cable.)

(*ii*) Large backhoes (3/4 yard and larger) can severely damage a buried

Table I — Coaxial cable troubles

Trouble category	Service-affecting troubles: Average number per year	Service-affecting troubles: Rate per 1000 miles per year
Bell associated (including engineering construction)	26	1.28
Lightning	25	1.25
"Foreign" Workers	19	.95

Table II — Construction machinery: relative frequency for damaging cable

Backhoe	40%
Drills	
Probes	29%
Earth augers	
Trencher	9%
Bulldozer	9%
Front-end loader	4%
Other	
Drag line	
Clam digger	
Plow	9%
Hand tools	

waveguide medium but only if the operator is determined to dig out an obvious foreign object. Most experienced operators would not damage the WT4 medium severely enough to cause outage.

(*iii*) Trenchers of moderately large size (30 inch width buckets, 8 foot diameter wheel) will not seriously damage the WT4 medium.

Although no specific tests have been conducted to determine the resistance of the WT4 medium to probes, drills, and augers, these tools are not likely to severely damage the medium because of the concentric design of the sheath and waveguide. The resistance of the WT4 medium to dig-ups by foreign workers is expected to be a factor of 10 to 100 better than coaxial cables. A factor of 25 is required to make the WT4 medium meet the reliability objective of 99.99 percent assuming a restoration time of 6 hours.

III. WT4 NITROGEN SYSTEM

3.1 General

The nitrogen system is the heart of the maintenance plan for the WT4 transmission medium. In addition to providing a low-loss medium for millimeter wave transmission, it is used in trouble prevention, corrosion protection, sheath fault location, and electrical fault location. It is designed for automated operation. The use of liquid nitrogen as the gas

source provides for high reliability with low on-going operational costs.

The nitrogen system was developed to meet the following requirements:

(*i*) Provide a low-loss transmission medium for the interior of the waveguide. Nitrogen is selected as the gas to pressurize the waveguide because it has no resonant frequencies in the bandwidth from 35 to 110 GHz as do oxygen and water vapor. The nitrogen used must contain no more than 25 ppm of O_2 and H_2O. With this specification the maximum loss due to the water vapor is 0.008 dB per mile at 110 GHz. The maximum loss due to oxygen is 0.005 dB per mile at 60 GHz.

(*ii*) Prevent corrosion of the waveguide exterior, roller supports, couplings, and sheath exterior. It is more cost-effective to provide corrosion protection for the annulus between the sheath and waveguide with nitrogen than with coating systems. Nitrogen is used instead of dry air because it is more economical, since a nitrogen system must be provided for the waveguide.

(*iii*) Prevent the entrance of contaminants into the waveguide and sheath when small leaks develop. If a small leak develops in the waveguide or sheath, the nitrogen flows out preventing the entrance of water or other contaminants. The operating pressures chosen for the waveguide and sheath are 25 psia and 23 psia respectively.

(*iv*) Minimize the entrance of contaminants into the waveguide in the unlikely event of waveguide and sheath rupture. Flooding of the waveguide with water could cause very long restoration times. To minimize the distance that water can contaminate the waveguide, the nitrogen system must be capable of providing a minimum of 25 scfm (standard cubic feet per minute) nitrogen flow at the rupture.

(*v*) Provide large volumes of nitrogen for purging waveguide during installation. A minimum of six volumes purge is required for the waveguide after installation and before electrical testing. Six volumes of nitrogen in a typical 25-mile repeater section is equivalent to approximately 25,000 scf of N_2.

(*vi*) Provide a nitrogen flow system that propels electrical measurement devices (pistons) through the waveguide bore. Electrical acceptance testing and fault location may use a piston that is propelled by a flow of nitrogen. Moving the piston at the desired speed of 1 m/second requires controlled flows in the range of 5 to 10 scfm.

(*vii*) Provide a stable absolute pressure source for the sheath to aid in leak localization. The sheath leak location method depends upon localizing a sheath leak to $\pm\frac{1}{2}$ mile using test sets at the repeater station. This operation requires stable sheath pressures.

(*viii*) Provide automatic sectionalization of leaks to a repeater span.

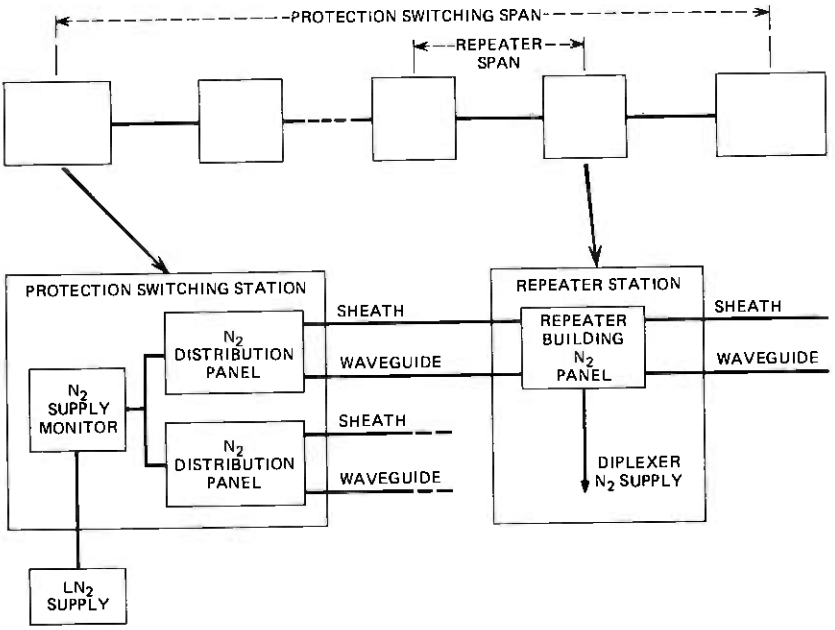

Fig. 1—WT4 nitrogen system maintenance area.

The nitrogen system must contain monitoring equipment that isolates leaks that develop in the waveguide or sheath to a particular repeater span.

(*ix*) Provide nitrogen for the diplexers located at the repeater stations. The diplexers and repeaters require a low-pressure dry nitrogen supply with a maximum usage of 100 cu ft per day. This nitrogen is most economically provided by the nitrogen system.

3.2 WT4 nitrogen system—description

The WT4 nitrogen system covers one protective switching span, a maximum distance of 250 to 300 miles (Fig. 1). At each protection switching station there is a nitrogen supply, monitor, and distribution system. Each repeater station has a monitor and control panel.

The nitrogen supply comes from a LN_2 storage system. The LN_2 storage system is commercially available and consists of a storage tank, evaporator, regulator circuit and economizer circuit. The tank is located outside of the station. The liquid nitrogen is delivered in tank trucks and is pumped into the LN_2 storage tank, which has a 900-gallon capacity.

The LN_2 is converted into a gas as needed in a heat exchanger or evaporator that is mounted on the outside of the tank. Heat transfer

through the walls of the superinsulated tank generates about 200 scfd of nitrogen. The economizer system uses this gas first to provide system needs. If the total system need is less than 200 scfd, the excess gas is vented to the atmosphere.

The gas from the supply system is piped into the station to the nitrogen supply monitor. The nitrogen, which is at a pressure of 50 to 100 psi, is checked for water vapor content and oxygen content. The supply monitor also measures the amount of nitrogen remaining in the supply tank and generates a warning alarm when it is 50 percent full and an action alarm when it drops to 20 percent full. A gross flow meter on the supply monitor is used by station craftspersons to determine usage rate of nitrogen. Nitrogen for the diplexers in this station is provided with a pressure-regulated source from the supply monitor.

Nitrogen from the supply monitor is piped to the nitrogen distribution panels. There is one nitrogen distribution panel for each WT4 waveguide run entering the building. The nitrogen distribution panel regulates the pressure and monitors the flow of nitrogen being supplied to the waveguide and sheath.

During normal operation all waveguide flow passes through a flow monitor which has insufficient flow capacity for purging or ruptures. The flow monitor is shunted by a normally closed, high-capacity valve which is opened either remotely or locally to enable large flows (up to 50 scfm to a leak in the first waveguide span outside a main station). A vent valve provides the means to depressurize the waveguide.

The sheath flow circuit is quite similar. It contains all features of the waveguide circuit with the addition of a two-level absolute pressure regulator. In normal operation, sheath pressure is maintained at 23 psi absolute, about 2 psi below waveguide pressure. Like the waveguide the sheath too contains a flow monitor and high-flow shunt. In addition the sheath pressure may be boosted to 35 psia by remote or local control. This higher sheath pressure is required in emergencies to assure adequate flow volume for line breaks.

The nitrogen from the distribution panel enters the sheath in the sheath end section and the waveguide through the nitrogen inlet section. It leaves the sheath and waveguide through like devices in each repeater station where it passes through the repeater station nitrogen panel. The repeater station panel monitors the flow rate in the waveguide and sheath and provides alarms at two flow levels. The repeater station nitrogen circuits also contain flow monitors of insufficient capacity for purging or ruptures. The monitors are shunted by normally closed, high-capacity valves which are opened either remotely or locally. An additional normally closed, high-capacity valve is used to interconnect the waveguide and sheath nitrogen circuits.

3.3 Operation

In the development of the WT4 system, a basic design philosophy was to integrate the maintenance of the repeater stations, electronics, and nitrogen system by using a common monitoring and control system.

The SCOTS (Surveillance and Control of Transmission Systems) system had been developed for transmission system maintenance and is used for WT4 maintenance. SCOTS has a computerized central control. Remote terminals are located in protection switching and repeater stations. The telemetry system for SCOTS is discussed by Bonomi et al.[4]

The alarms and status indications that the nitrogen panels generate will be transmitted to the SCOTS central control. The information will be continuously analyzed in the central computer and commands to operate the appropriate valves will be generated as needed for real-time control of the nitrogen system.

3.4 LEAK location methods

Although the WT4 waveguide and sheath have been designed to be mechanically rugged and corrosion resistant, methods must be available for locating the occasional leaks which may occur in order to prevent the gradual deterioration of the medium. A procedure for locating these leaks has been developed based on the following assumptions:

(*i*) Small sheath leaks are tolerable for an extended period and need not be located as rapidly as large leaks. Leaks under 200 scfd need not be located at all.

(*ii*) Large leaks which develop suddenly are most probably produced by large, easily visible causes, e.g., construction equipment or gross geological disturbances.

Leak location is envisioned as a three-stage process. The first stage identifies the repeater section in which the fault has occurred. The second stage produces a rough estimate of the leak's position accurate to within $\pm\frac{1}{2}$ mile. The third stage pinpoints the leak to within a few feet. The first stage of the leak location is accomplished by the nitrogen system flow alarms which were discussed previously.

For both large and small leaks, pinpointing leaks is a straightforward process. Massive leaks will generally be associated with highly visible indications of damage, caused by construction activity or natural disturbances. Equipment sufficiently massive to damage waveguide is not quickly deployed or concealed and can be visually located.

Small leaks can be pinpointed using a helium tracer gas method. At the projected location of the leak, the sheath is uncovered, it is then tapped and helium is injected into the tap hole. The helium flows to the leak where it escapes the sheath and rises to the surface in a funnel

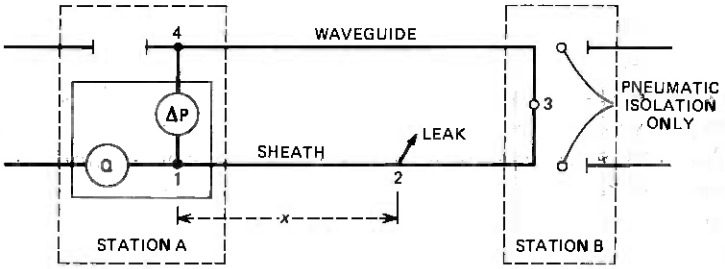

Fig. 2—Locating a leak.

pattern. Two-inch deep probe holes are made every 4 feet along the route, working away from the projected leak location. A simple thermal-conductivity gas monitor is used to sample gas from the probe holes immediately after they are made. When helium is detected the leak is located, usually within a couple of feet from the point where helium is detected. The third or pinpointing stage of leak location uses the helium tracer gas method or visual inspection.

3.5 Localizing small leaks

Since the helium method of leak pinpointing is impractical for the large repeater spans, which may be as long as 37 miles, a method of localizing leaks to within $\pm\frac{1}{2}$ mile was developed.

The leak localization system uses a test set which has a sensitive electronic manometer, an accurate flow transducer, and data recording equipment. The test set is installed at a repeated station only when a leak has been indicated by the flow monitors present in the station.

During normal operations sheath sections are interconnected at repeater stations by means of flow monitored channels. Waveguide sections are similarly joined. There is no normally open flow path between the sheath and the waveguide systems. The first step in the leak localization process is to pneumatically isolate the waveguide and sheath from the adjacent repeater spans. The waveguide and sheath are then joined together (Station B in Fig. 2) and the pressure is reduced by venting until it is equal to the sheath pressure in the adjacent repeater span. At the other end of the span (Station A in Fig. 2) the leak localization test set is installed. The flow meter in the test set monitors the flow from the adjacent sheath into the leaky sheath span. The electronic manometer is installed between the sheath and waveguide to measure the extremely small pressure between them.

There is a waiting period required for the sheath and waveguide to come to a common equilibrium. After equilibrium is achieved, there is no flow in the waveguide, and all flow to the leak passes through the

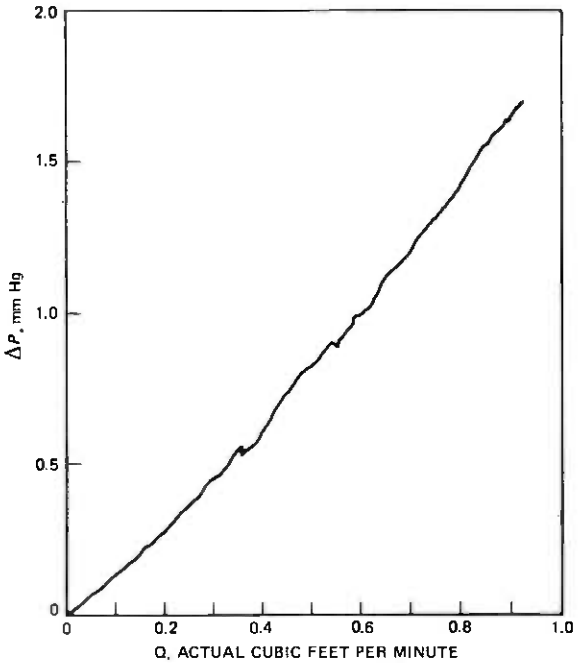

Fig. 3—Flow characteristics of WT4 sheath.

precision flow monitor in Station A. The estimated position of the leak, $\hat{x}$, is determined by application of a simple formula to the flow and differential pressure readings obtained with the test set:

$$\hat{x} = \Delta P / f(Q)$$

$$\Delta P = \text{Pressure drop measured by test set} \qquad (1)$$

$$Q = \text{flow measured by test set}$$

The differential pressure, ΔP, measured by the test set is the pressure drop caused by the flow to the leak because (*i*) the difference in absolute pressure between any two points in the waveguide-sheath circuit is quite small, (*ii*) the nitrogen temperature at any location is the same in both waveguide and sheath, and (*iii*) the use of a differential pressure manometer eliminates hydrostatic components.

The use of eq. (1) depends upon knowning $f(Q)$, the pressure gradient in the sheath as a function of volumetric flow. This function was determined experimentally during the field evaluation test and is plotted in Fig. 3.

The accuracy in projecting the location of a leak depends upon the stability of the sheath pressure and the accuracy of the test set. Esti-

Table III — Accuracy requirements for leak localization

Objective:	
Localize 200 scfd leak to within ±½ mile	
Requirements:	
Input Pressure Stability	±0.002 psi
Flow Measurement	±3 scfd
Differential Pressure	±0.0001 psi

Table IV — Leak localization test results

	Leak size	
	300 scfd	130 scfd
Known distance to leak	40,307 ft	20,147 ft
Projected distance to leak	40,641	21,240
Error	340 ft	1,093 ft

mating the position of a leak requires a precise knowledge of the leakage flow. What is measured by the leak localization test set is not the leakage flow, but the flow into the sheath under test. Because the nitrogen is compressible any small variation in applied pressure results in a corresponding change in flow into the sheath. The pressure variations are controlled in two ways: (*i*) by providing high-precision absolute pressure regulation in the distribution panel, and (*ii*) by having more than one repeater span between regulated pressure feed points. The latter method uses the sheath adjacent to the section under test as a "settling" tank.

The accuracy required for the test set was determined by analysis of the sheath annular flow data shown in Fig. 3. Table III gives the accuracy requirements for the leak localization procedure.

A leak localization test set was developed that exceeded the accuracy requirements listed in Table III. The test set, which was constructed of commercially available instruments, was used to locate two leaks that were introduced in the sheath at known locations. Table IV gives the results of these tests.

Both projections were well within the ±½ mile objective for leak localization accuracy.

IV. RESTORATION

4.1 Overview

The outage of the WT4 medium is directly proportional to the restoration time for failures. To meet the outage objective, a restoration time not exceeding 6 hours must be achieved. Four of the 6 hours are allocated for travel and trouble location and 2 hours are allocated for repair. The restoration of the WT4 medium proceeds as follows:

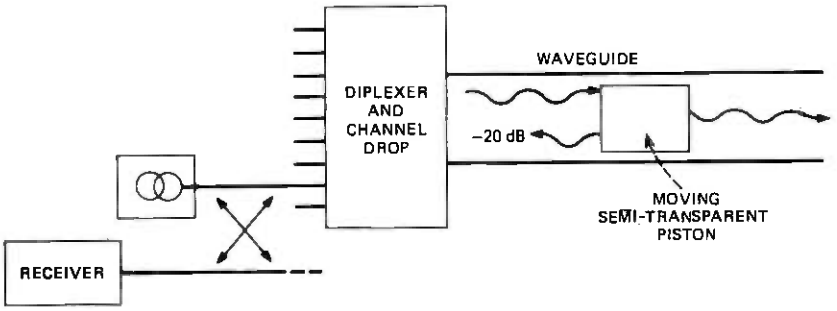

Fig. 4—Electrical fault location technique.

(*i*) A service outage occurs and the monitoring system detects the failure and determines the failed repeater span.

(*ii*) Simultaneous failure of many channels indicates a medium failure. When this happens (*a*) A crew with a portable electronic fault location test set is dispatched to the repeater station nearest the failure. (*b*) An immediate patrol of the route between repeater stations where the trouble occurred is initiated. The object of the patrol is to look for construction activity that might have damaged the waveguide. (*c*) Restoration equipment consisting of a small backhoe, a WT4 restoration trailer, and a cable restoration trailer is transported by the restoration crew from the maintenance center to a convenient location near the failed repeater section.

(*iii*) Upon location of the damaged waveguide by inspection or electrical or pneumatic fault location techniques, the restoration equipment is dispatched to the trouble site.

(*iv*) The damaged section is repaired with a temporary patch and service is restored.

After service is restored a permanent repair is engineered. A construction crew rather than a maintenance crew makes the permanent repair.

4.2 Waveguide electrical fault location

Waveguide faults such as delamination of the dielectric liner or rupture of a welded joint while the sheath is intact cannot be located with the gas pressure methods. A characteristic of these internal waveguide faults is that electromagnetic energy will be scattered from the TE_{01} mode into other modes causing a net forward propagation loss but little backscatter into the low-loss TE_{01} mode. Conventional reflectometers as used in cables for discontinuity detection are therefore not applicable here.

For internal waveguide fault location, therefore, a semitransparent dielectric piston (Fig. 4) is used in conjunction with a millimeter wave

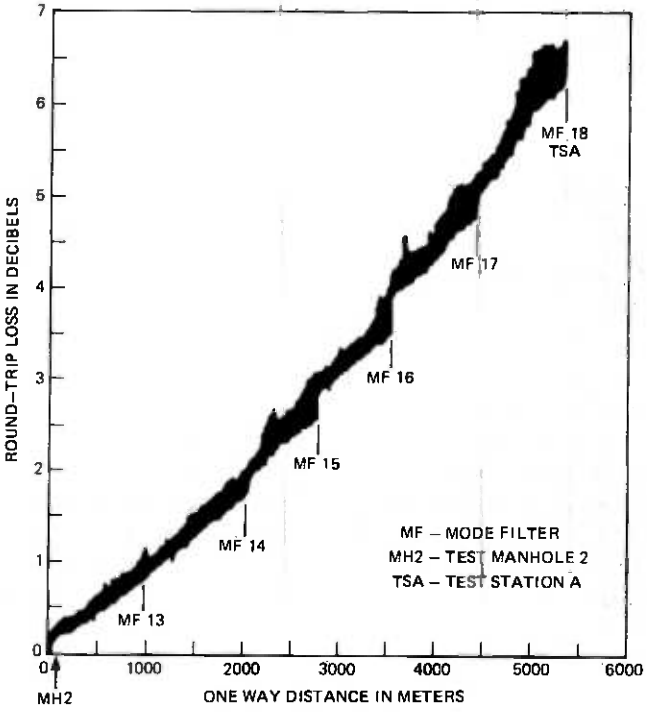

Fig. 5—Moving piston measurements, 95.8 GHz.

reflectometer operating for convenience in the vicinity of 80 GHz where the line loss has a minimum. A polystyrene foam piston normally is stored in the guide at one of the repeater stations where it causes only 0.1 dB forward loss and where the −20 dB discrete reflection has no significant effect on overall system performance. During routine maintenance testing or when a fault is suspected, the piston is propelled (by nitrogen flow) through the waveguide at a speed of about 1 to 2 meters per second until it hits an obstruction in the waveguide or arrives at the next repeater station. Throughout its journey through the guide, the piston is tracked by the reflectometer both in range and signal amplitude.[6] A typical loss versus distance trace of a 5.3-km-long piston run from the Netcong-Long Valley field evaluation installation is shown in Fig. 5. The waveguide line is characterized for its amplitude-versus-distance characteristics at the time of installation as part of the line acceptance test. The as-installed loss record is then compared with the newly taken record which then will reveal specific locations at which a fault in the line has increased the loss measurably as a result of one of the waveguide defects referred to initially.

Waveguide discontinuities with a very low reflection can also be de-

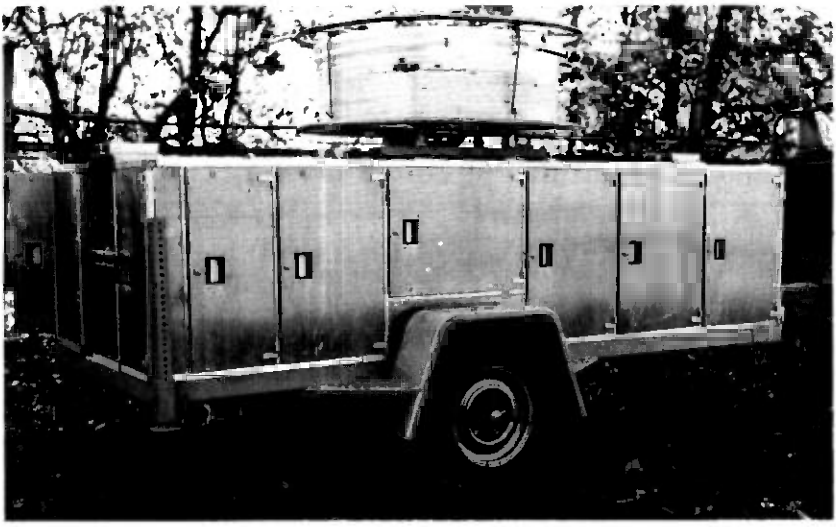

Fig. 6—Trailer for restoration equipment.

tected with a spatial resolution of 3 m using an adaptation of a reflectometer which uses coherent detection and was developed for the field evaluation test.[7] This set can measure reflected signals which have a combined reflection and line loss as high as 90 dB.

4.3 Repair methods for waveguide restoration

Repair of a damaged waveguide within the 2-hour objective requires special equipment and training. To minimize the training problem, the restoration operation is patterned after cable restoration techniques which are well understood. The equipment developed for restoration is simple, rugged, and is easily transportable by trailer or helicopter. All of the restoration equipment is carried on a specially designed trailer (Fig. 6). The tool and hardware cabinets on the trailer can be removed for transportation by helicopter to the trouble site.

Figure 7 illustrates the step-by-step restoration procedure, which is as follows:

Step 1. A small backhoe is used to uncover the damaged waveguide and expose undamaged sheath on each end.

Step 2. The restoration crew removes a length of the sheath on each side of the damaged section. The tools used for this operation consist of commercially available pipe cutters and abrasive disk saws.

Step 3. Waveguide sheath restrainers are installed to lock the waveguide to the sheath at each end. This is necessary because the waveguide will be in compression or tension and could move several feet if not restrained.

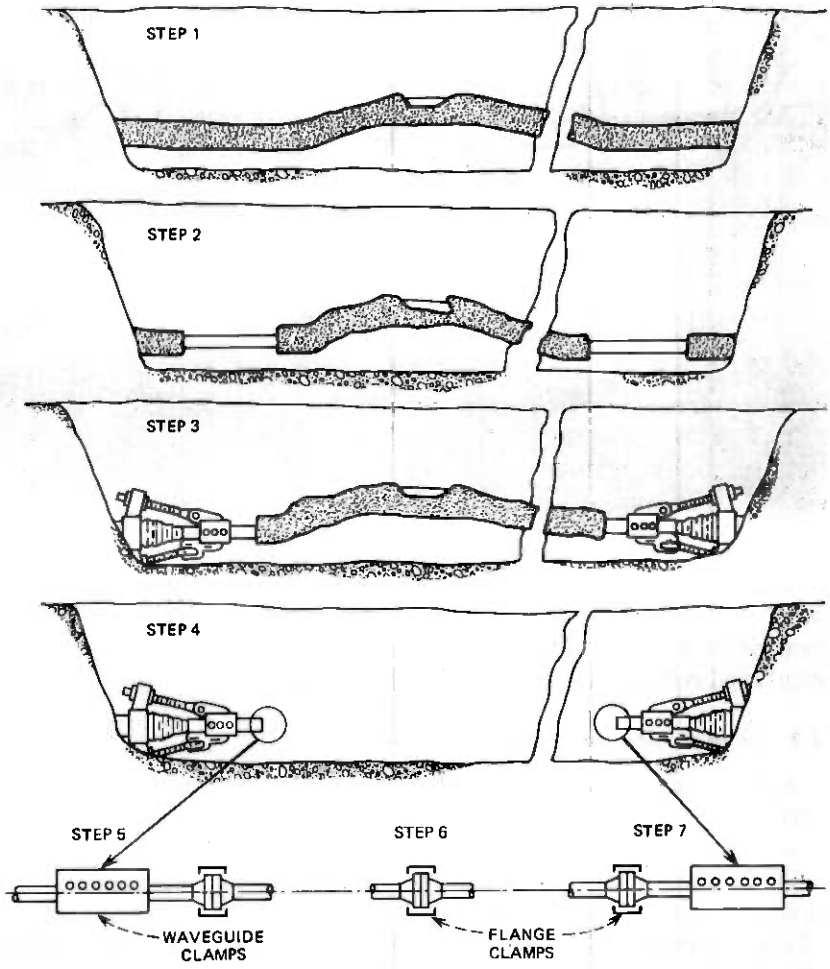

Fig. 7—Restoration concept.

Step 4. The waveguide is cut off at each end and pushed aside to make room for the patch waveguide sections.

Step 5. A patch waveguide section is joined to the end waveguide with a waveguide tube coupler

Step 6. Flange clamps are used to quick-connect waveguide patch sections until the patch spans the damaged area.

Step 7. The last patch section of waveguide is cut off and is joined to the waveguide end with a tube coupler. This completes the restoration and service can be resumed.

Field demonstrations of the repair methods and equipment have confirmed that the 2-hour objective is realistic.

V. Route rearrangements

It is sometimes necessary, despite the best planning efforts, to move or rearrange a right-of-way medium to allow for construction of roads, drainage ditches, etc. Route rearrangements can be divided into two categories: (*i*) rearrangements which do not require a break in the medium (generally a lowering operation) and (*ii*) rearrangements requiring the installation of new medium (generally a reroute).

Waveguide route rearrangements of the first category are similar to lowering operations for coaxial cables. Slack can be generated or removed for lowering operations by cutting the sheath but not the waveguide. The waveguide will stretch or compress to conform to the new profile.

Waveguide route rearrangements of the second category are very different from coaxial cable reroutes. With coaxial cables, service can be transferred from a working pair of coaxial tubes to a protection pair. The working pair is then cut and spliced into the new cable and service is then "rolled" back. Waveguide has only one transmission path so the rolling process is not possible.

To minimize service outage and to provide reroute capability, the concept of a "hot switch" was developed for the WT4 medium. The new waveguide and sheath are brought in parallel and above the in-service waveguide is prepared by removing a section of sheath and cutting coupling welds on each end. A series of synchronized "hot switch" machines then push the new section down displacing the old waveguide section to transfer service to the new waveguide. Fig. 8 shows the conceptual hot switch equipment.

The mechanical switch causes a transmission hit but will not drop service on the digital network provided the total outage is less than 140 milliseconds. Sixty milliseconds is needed for reframing the terminal equipment and 80 milliseconds is allocated to the hot switch.

The dynamics of the switch were analyzed and a machine was built to demonstrate feasibility and test critical subsystems. The results of the tests show that the hot switch is a practical concept to use for reroutes of the WT4 medium. The final machinery has not been designed.

VI. SUMMARY

In order to insure long life and low maintenance costs, the WT4 medium is designed with a steel sheath. The steel sheath provides excellent mechanical protection for the waveguide and it should eliminate all service-affecting troubles (lightning, Bell associated) except those caused by foreign workers. Considering the 3-dB repair margin, the service-affecting trouble rate due to foreign workers should be one to two orders of magnitude less than that for coaxial cable systems. With this low

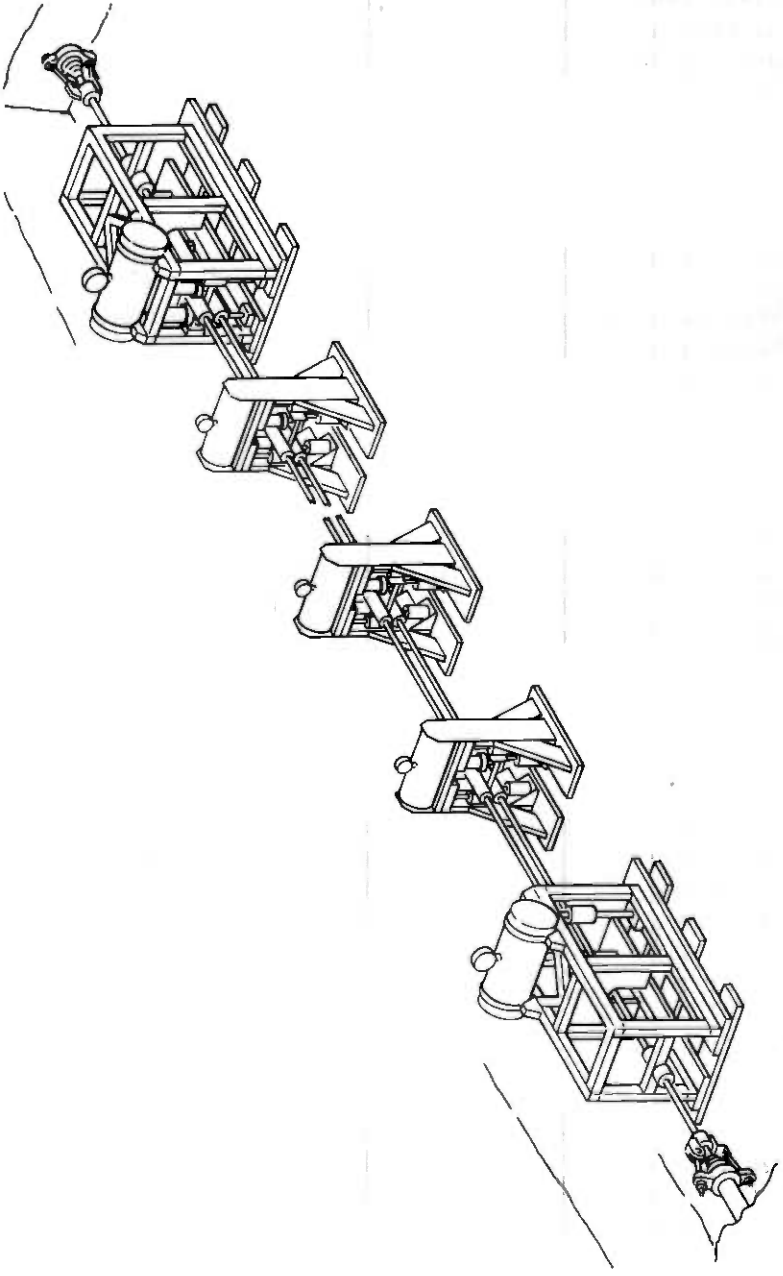

Fig. 8—Hot switch equipment.

trouble rate the overall reliability objective of 99.99% for a 4000-mile system is realizable.

The WT4 nitrogen system is designed to minimize the impact of service-affecting troubles by preventing contamination of long lengths of waveguide. It is also used for localization of leaks by pneumatic techniques and aids localization by electrical techniques by propelling transparent pistons through the line.

The pneumatic and electrical trouble-location methods insure the quick location of most troubles. Restoration is then accomplished using specialized equipment and methods.

VII. ACKNOWLEDGMENTS

Many individuals at Bell Laboratories and American Telephone and Telegraph Company, Long Lines Department, contributed to the development of the maintenance systems. Particular acknowledgment is due to C. J. Willis for development of the restoration methods and D. A. Alsberg for development of the electrical fault location concepts.

REFERENCES

1. R. J. Boyd et al., "Waveguide Design and Fabrication," B.S.T.J., this issue.
2. R. W. Gretter et al., "Waveguide Support and Protection System," B.S.T.J., this issue.
3. W. J. Liss, et al., "The Repeater Building," B.S.T.J., this issue.
4. M. J. Bonomi et al., "Protection Switching, Auxiliary Communications, and Maintenance," B.S.T.J., this issue.
5. A. W. Peabody, *Control of Pipeline Corrosion*, National Association of Corrosion Engineers, 1969.
6. D. A. Alsberg, U.S. Patent 4021731, May 3, 1977.
7. J. L. Doane, "Measurement of the Transfer Function of Long Lengths of 60-mm Waveguide with 1 MHz Resolution and High Dynamic Range," Digest of the Conference on Precision Electromagnetic Measurements, Boulder, Colorado, June 28 to July 1, 1976, pp. 153–155.

THE BELL SYSTEM TECHNICAL JOURNAL
Vol. 56, No. 10, December 1977
Printed in U.S.A.

WT4 Millimeter Waveguide System:

Regenerative Repeaters

By C. E. BARNES, P. BROSTRUP-JENSEN, E. T. HARKLESS, R. W. MUISE, and A. J. NARDI

(Manuscript received April 7, 1977)

The electronic circuitry and physical structure of 12 two-phase repeaters made for use in a field evaluation test are described. The repeaters consist of four kinds of circuitry; millimeter-wave circuits covering the 40 to 110 GHz range, IF circuits at 1.2 to 1.6 GHz, pulse circuits for the 274 Mb/sec pulse stream, and power supply circuits. All repeaters have been successfully operated over the trial repeater link in northern New Jersey. The results of this repeater development effort are the basis for an estimate of the performance obtainable in future four-phase repeater performance. This estimate has been used in the system repeater spacing calculations.

I. INTRODUCTION

A repeater design has been developed for the WT4 system which can regenerate a 274 megabit per second binary phase-modulated bit stream on mm-wave carriers in the 40 to 110 GHz range. These repeaters have sufficient gain to provide repeater spacing well in excess of the 45 km objective at an error rate of 1 in 10^9 bits when used with the transmission medium described in this issue of the B.S.T.J. This error rate is attained with a signal to noise ratio which is only a few decibels above the theoretical minimum. Twelve field evaluation test models have been constructed with three models each near 40, 54, 80, and 108 GHz. The models all have identical IF, baseband, and power supply circuitry, but differ in the construction and tuning of the frequency-sensitive millimeter-wave and equalizer circuits. There are four apparatus cases composing each repeater. These are the receiver, the line equalizer, the transmitter, and the power supply. The block diagram of Fig. 1 may be used to trace the signal flow through the repeater.

The modulated signal spectrum enters the receiver via a rectangular waveguide port, through a waveguide isolator into the mixer where the signal is converted to the IF signal centered at 1371 MHz. The IMPATT local oscillator is controlled at 1371 MHz below the incoming millimeter-wave spectrum by an AFC loop. The first IF amplifier has a maximum gain of 50 dB and a noise figure of 6 dB. The signal then leaves the receiver via a 50-ohm coaxial cable to the line equalizer which equalizes the differential delay slope caused by the transmission medium. Returning to the receiver case, the signal passes through the receiver equalizer, a bandpass filter which controls the width of the signal and noise spectra, more IF gain, and into the signal and AFC detector circuits. An error signal is fed back to the AFC circuit which varies the current through the local oscillator IMPATT to hold the IF signal centered at 1371

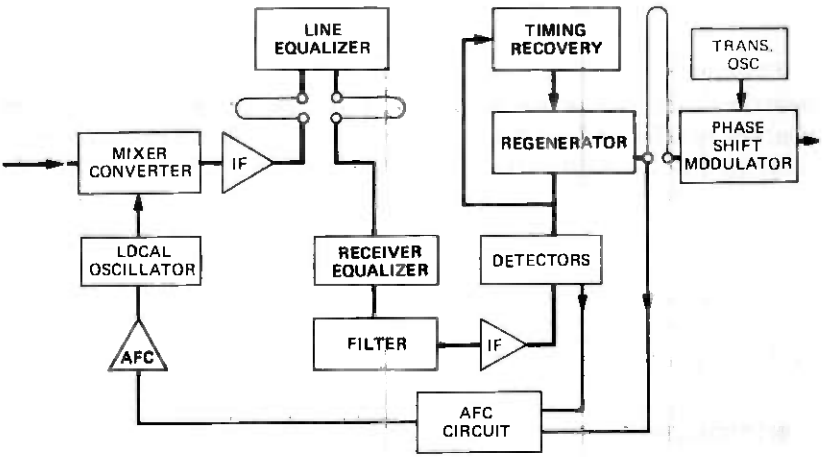

Fig. 1—WT4 repeater block diagram.

MHz ±1 MHz. The binary pulse stream from the signal detector is fed to the timing recovery circuit and the decision circuit in the regenerator. The regenerated pulses leave the receiver case via a coaxial cable (up to 30 feet long) over to the transmitter case. In the transmitter a high-power, cavity-stabilized IMPATT oscillator feeds a phase-shift modulator where a PIN diode reverses the phase of the millimeter-wave signal whenever a binary one is present on the incoming pulse stream. The output from the modulator then leaves the transmitter via a rectangular waveguide to a channel-dropping filter where it combines with all other transmitted spectra at that station and proceeds towards the next repeater. A short description of each of the major circuit blocks in the repeater will be given.

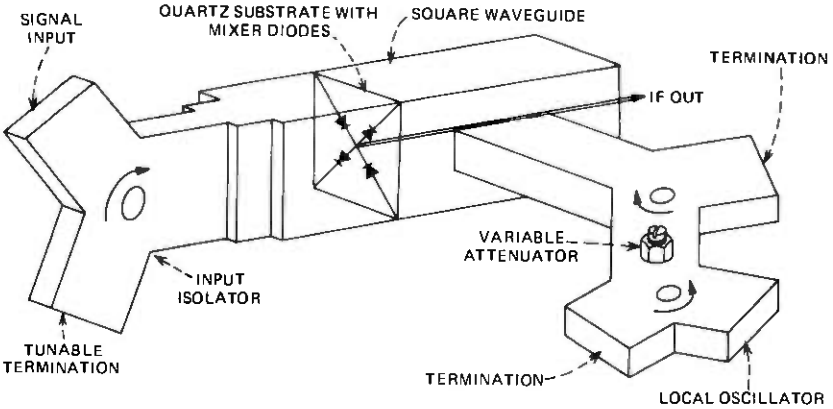

Fig. 2—Down-converter assembly.

II. DOWN CONVERTER

The down converter developed for the WT4 system is shown schematically in Fig. 2. It conists of an input isolator used primarily to reduce local oscillator leakage, a mixer circuit to shift the incoming millimeter-wave spectrum down to the IF passband centered at 1371 MHz, and an isolator-attenuator used to set the local oscillator drive level and prevent interaction between the mixer and the local oscillator (LO). The isolators are terminated circulators. The input isolator uses a single circulator and the isolator attenuator uses two terminated circulators.

The general format of the RF circulator designs is a waveguide, *H* plane, *Y* junction, with a simple cylinder of ferrite mounted on axis against one broad wall and a quarter-wave transformer with a central coaxial stub tuner on axis on the opposing wall. Adjustment of the stub penetration and the biasing field permits a peaking of the circulator characteristics at any frequency in a relatively wide tuning band. The typical instantaneous bandwidth characteristics are:

Return loss > 30 dB; BW 1 GHz
Return loss > 20 dB; BW 3 GHz
Insertion loss in 30 dB return loss band:
<0.2 dB at 40 GHz
<0.5 dB at 110 GHz

The isolator is required to provide low insertion loss, good input and output matches, and 20 dB of isolation over the signal band (~ 500 MHz) while providing 40 dB of isolation at the LO frequency, which is 1.37 GHz below the signal frequency. To meet these requirements the circulator is peaked at the signal frequency and is terminated in a tunable termination adjusted to conjugately match the circulator impedance at the LO frequency.

The isolator-attenuator between the receiver local oscillator and the mixer prevents pulling of the oscillator by the mixer and permits adjustment of the LO power to the mixer. It provides isolation in excess of 60 dB, a 20-dB attenuation range, and matches independent of attenuator setting. The insertion loss ranges from <0.5 dB at 40 GHz to <1.0 dB at 110 GHz.

Early in the development of the WT4 repeater a beam-lead mixer diode was selected for use in the down converter. Both theoretical studies and practical experience indicated that much greater lifetime should be attained with a beam-lead device than with wafer-type millimeter-wave diodes. It was also decided to try to avoid the use of resonant circuits to separate the signal and local oscillator frequencies. Since even an IF of 1371 MHz puts local oscillator and signal at 110 GHz fairly close together, sharp filter cutoffs are required and this may mean high transmission loss.

A double-balanced mixer configuration where the local oscillator and signal are in orthogonal polarizations in a square waveguide appeared to provide a straightforward development path. As shown in Figure 2, four beam-lead diodes are bonded to a gold thick-film pattern on a quartz substrate. The quartz substrate is clamped between two square waveguides so that the diodes run along the diagonals of the square. On one side of the substrate, the square waveguide is stepped down to rectangular waveguide for the signal input port. The square waveguide on the other side of the substrate has the IF lead brought out and also has a right-angle transition for the local oscillator waveguide port. Impedance matching elements are inserted in both the signal path and the local oscillator waveguide port. With about 1 milliampere diode bias, the IF impedance for the four diodes comes out fairly close to 50 ohms; however, an impedance matching transformation can be provided in the IF lead. Large gold pads on the quartz substrate provide return to ground for the IF currents on the outer beam leads. A sheet of 0.01-mm Mylar insulates these pads and each diode is provided with an adjustable dc bias current. Seven different basic designs (using seven different sizes of square waveguide) have been developed to cover the 40 to 110 GHz frequency range. Each design can be adjusted to cover any channel in one of the seven subbands[1] into which the WT4 spectrum is divided.

The major factor controlling the performance of the down converter is the quality of the mixer diodes used in the circuit. The important number for the WT4 system is the receiver noise figure, however, this number depends not only on the down-converter performance, but also on the IF amplifier noise figure and the matching network and/or isolator that is used between the down converter and IF amplifier.

$$\mathrm{NF} = L_c(\mathrm{NR} + \mathrm{NFI} - 1)$$

Where NF is the total single-sideband receiver noise figure
L_c is the down-converter conversion loss
NFI is the IF amplifier noise figure including any matching network or isolator
NR is the noise ratio of the mixer diodes

For the field evaluation test, the total receiver noise figure ranged from 12.2 dB at 40 GHz to 18.5 dB at 108 GHz. Laboratory tests with improved mixer diodes and a 3.5 dB noise figure for the IF amplifier, have yielded circuits which will produce repeaters with 7.5 dB noise figure at 40 GHz and 13.5 dB noise figure at 110 GHz.

III. IMPATT oscillators

One of the basic technological advances which permitted the development of a millimeter-wave repeater during the 1970s was the availability of IMPATT diodes operating up to 110 GHz. It was decided early in the repeater development that self-controlled oscillators would be employed in the repeater rather than have a low-frequency (about 100 MHz) crystal oscillator control the millimeter-wave frequencies. This implied that the receiver would have some form of AFC in order to track whatever drifts occurred in the transmitter or local oscillator frequency. With the omission of the many multiplier stages required to get to the millimeter-wave frequency range, the millimeter-wave circuitry occupies a relatively small percentage of the total volume in the receiver or transmitter case. The important parameters in the performance of the millimeter-wave oscillators are the frequency stability, the power output, the noise output, and the lifetime of the diodes.

The frequency stability of an IMPATT oscillator is very closely related to the physical and electrical structure in which the diode is embedded. For the transmitter, maximum frequency stability and minimum noise is required; both of these characteristics improve as the oscillator circuit Q is made larger. The major limitation on increasing Q is the increase in loss in the frequency-controlling resonant cavity. The WT4 transmitting oscillator designs have been planned to limit the resonant cavity loss to about 1 dB. This should yield an oscillator Q which is large enough to provide a transmitter frequency which drifts less than ± 25 MHz from all causes and also limit the oscillator output noise to an rms frequency fluctuation of less than 1000 Hz for a noise bandwidth of 1 kHz. The structure chosen for this design consists basically of three parts. First is a diode mount to place the diode package into a dominant-mode rectangular waveguide and provide a contact for dc bias of the diode, second is a damping resistor in the waveguide to stabilize the circuit and inhibit oscillations at undesired frequencies of oscillation. Third is a resonant cavity to provide accurate control of frequency and furnish high-Q,

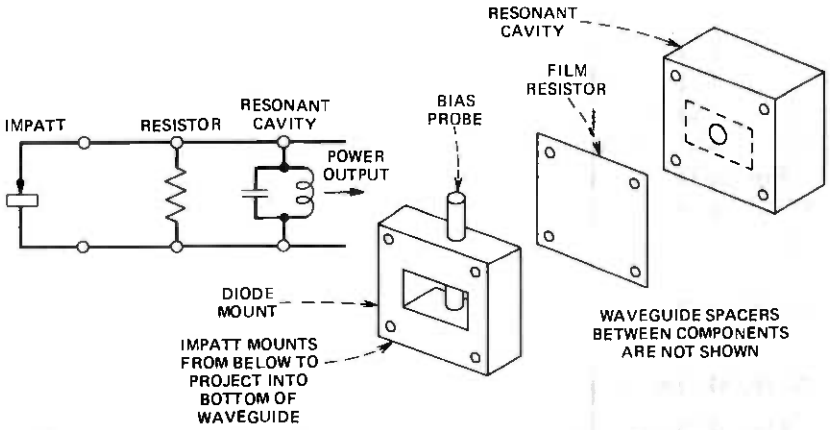

Fig. 3—Transmitting IMPATT oscillator.

low-noise performance. Figure 3 shows a physical and electrical schematic of the transmitting oscillator structure. Table I shows the electrical performance of the 12 models. All objectives were met except for the failure rate and slightly excessive frequency drift in a few cases. There have been five IMPATT device failures in about 2 years of field evaluation test operation. This rate is too high, however, and a new design of hermetically sealed devices has recently been made available. This improved device should provide a transmitting IMPATT with a FIT rate of 600 and also improve the frequency stability.

The local oscillator is a different design because of the AFC requirement that changes in bias current must produce a frequency shift of ±100 MHz or more. The resonant cavity for the local oscillator is formed as part of the dc bias line for the IMPATT. A movable coaxial short is part of the bias line, and the position of this short is the primary frequency-determining element in the oscillator. There is also a movable waveguide

Table I — Field evaluation trial transmitting oscillators

Frequency, GHz	Power, mW	FM noise, rms deviation, Hz/√kHz	Number of failures	Total drift, MHz	Months operating
40.235	145	238	0	+21	12
40.760	145	157	0	− 3	16
41.285	142	174	0	−27	12
53.910	75	147	0	+ 2	20
55.085	86	250	0	+ 6	20
55.610	83	217	0	+15	20
80.465	44	400	1	+14	11
80.990	43	234	0	−12	17
81.515	43	535	0	− 6	19
107.665	23	153	0	+38	18
108.190	26	230	1	+ 3	12
108.715	26	209	0	+ 6	14

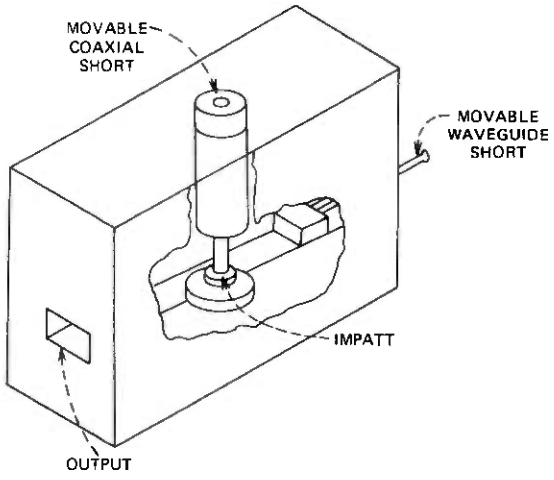

Fig. 4—Local oscillator.

short behind the diode, and this is varied to change the coupling from the diode to the waveguide. There are three basic designs to cover the 40 to 110 GHZ range for either the transmitting or local oscillators with different size bias probes available to provide complete frequency coverage and to accommodate diode variations. The local oscillator structure is shown on Fig. 4 and the field evaluation test performance is listed in Table II.

IV. IF AMPLIFERS AND VARIOLOSSERS

Several basic design preferences were established: (*i*) thin-film microstrip technology because the ground plane on the back of the substrates allows valid testing and trimming with enclosure covers removed;

Table II — Field evaluation trial local oscillators

Frequency, GHz	Power, mW	Modulation sensitivity, MHz/mA	FM noise, rms deviation, Hz/$\sqrt{\text{kHz}}$	Number of failures
38.868	20	24	1250	0
39.389	16	9	1000	0
39.914	16	13	800	0
52.538	31	11	1120	0
53.714	28	13	700	0
54.239	10	10	1000	0
79.096	32	10	880	0
79.620	31	10	880	1
80.145	32	13	640	0
106.295	35	30	1250	1
106.819	35	16	1150	0
107.344	20	17	800	0

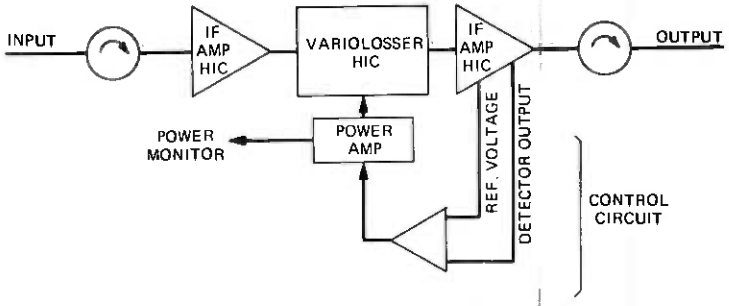

Fig. 5—Field evaluation test IF amplifier.

(*ii*) appliqued capacitors because the deposited capacitor technology is still evolving at these high frequencies; (*iii*) single string design for minimum transistor count with the resulting low input and output return losses masked by isolators; (*ii*) trim capability in order to accommodate any reasonable transistor parameter spread with one substrate design; (*v*) relatively little stress on miniaturization since the size of many repeater components excluded strong miniaturization in any event. Within these preferences, the design continued earlier work at Bell Laboratories.

The repeater requires a maximum IF gain of 100 dB in the band 1.15–1.60 GHz and an Automatic Gain Control (AGC) range of 40 dB. This gain is provided in two assemblies which contain two amplifer substrates each with 26 dB of gain and one variolosser substrate with a loss range from 2 dB to 22 dB. See Fig. 5. Lumped-element isolators provide 20 dB input and output return losses for the assembly.

4.1 IF amplifier substrates

A new beam-lead microwave transistor, developed at Bell Laboratories, has a maximum available gain of 11 dB at 1.6 GHz. Any resistance or inductance in the external circuit from emitters to ground must be kept to a minimum to avoid reducing the gain and the stability. Three transistors per substrate are sufficient for 26 dB of total gain. The gain rolls off at 6 dB per octave per transistor in the 1–2 GHz range; therefore the basic design approach is to use interstage networks (Fig. 6) to match the devices as tightly as possible at the top end of the band for highest gain and, in a controlled manner, mismatch the devices toward the low end of the band to obtain gain flatness. Input and output return losses are improved to the 10 dB level by two-element matching networks (Fig. 7). The 25-ohm resistors in the interstage networks serve to dissipate power at the lower frequencies where the devices are systematically mismatched. The design has great trim flexibility to meet batch-to-batch

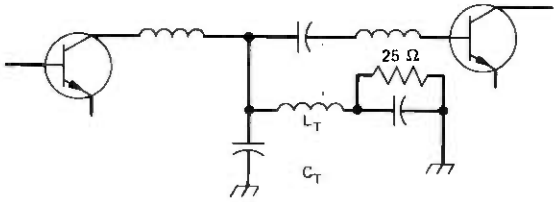

Fig. 6—Interstage network.

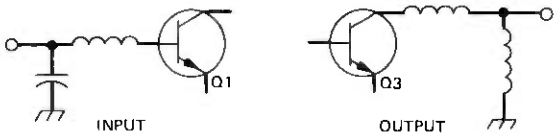

Fig. 7—Input/output matching networks.

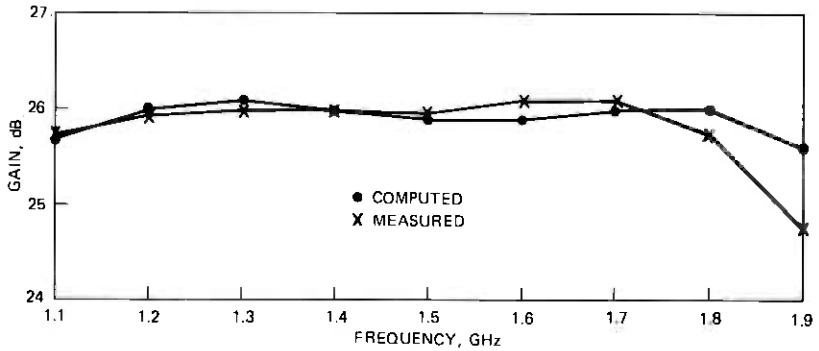

Fig. 8—Insertion gain vs. frequency.

variation in the transistor. All fixed capacitors are selectable; all inductors are 90-ohm transmission lines of varying length formed by laser cutting of rungs in a ladder-like layout; three capacitors are variable trimmer capacitors. The *S* parameters for a batch of similar transistors are measured and a computer program used to select a typical or nominal transistor for that batch. An optimization program is then used to select all fixed capacitors and determine all laser cuts for the inductors. After that, all transistors within the batch can be tuned with the variable capacitors to give the required flat gain. Figure 8 is an example; it also shows the close agreement between equivalent circuit computation and actual measurement.

4.2 IF variolosser substrate

The variolosser interconnects the two amplifier substrates. Its basic configuration is shown on Fig. 9. By having identical variable attenuator

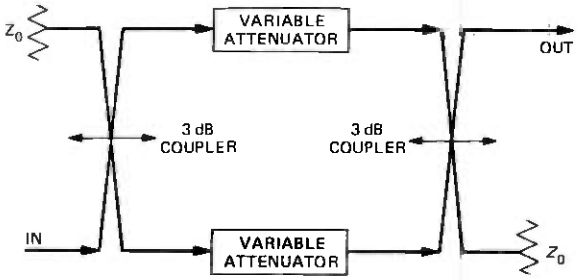

Fig. 9—Basic variolosser configuration.

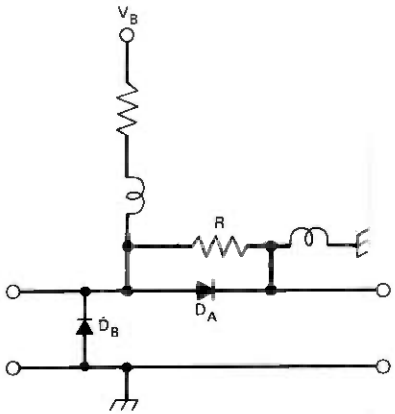

Fig. 10—Schematic of variable attenuator.

networks in both sides of the 3 dB couplers, good input and output return losses are assured even when the impedance of the attenuators deviates markedly from the 50-ohm characteristic impedance of the microstrip transmission lines and couplers. The schematic of the variable attenuator is also shown on Fig. 10. When the control voltage, V_B, is positive, D_A is forward-biased with low resistance and D_B is back-biased with high resistance resulting in little loss (approximately 2 dB) in transmission through the variolossers. As V_B is made less positive and, eventually, negative, D_B becomes forward-biased and D_A back-biased with a resulting high attenuation in the variolosser. The inductors (spiral structures in thin film) serve to isolate the IF paths from the bias circuitry. The final design exhibited about 1.5 dB of change in loss slope as the attenuation at midband changed from 2.0 to 22.5 dB; most of the change occurs in the last few dB of the attenuation range.

The driver for the variolosser gets its control voltage from the AGC detector on the amplifier substrate. The circuit can be adjusted to maintain a level of −12 dBm at the output of the first IF amplifier as-

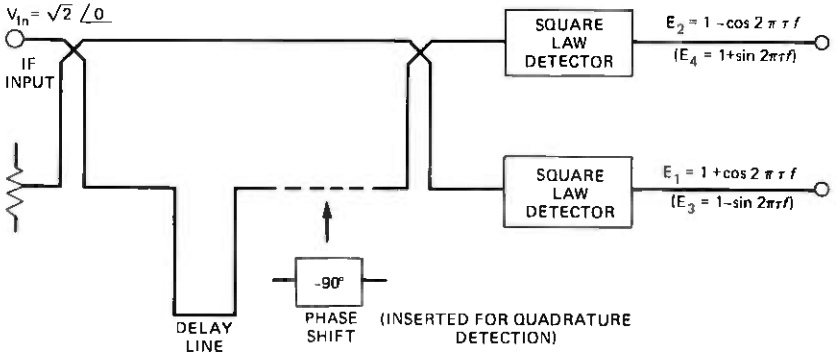

Fig. 11—Delay-line detector.

sembly and a level of +7 dBm at the output of the second IF amplifier assembly.

V. DETECTORS

Since two-phase differentially coherent phase-shift keying (DC PSK) can be demodulated with good performance by a very simple delay-line detector without the need for carrier recovery, it was decided to employ such a scheme in the initial WT4 system. Figure 11 shows the simple delay-line detector. In order to compare the phases of the successive pulses of IF signal, the delay line must be one time slot, $T = 3.65$ ns, in length, In addition, the delay line must be an integral number of half wavelengths at the IF to obtain maximum differential output voltage. For an integer of 10, this yields an IF of 1370.88 MHz. Thus the delay line is the IF-determining element.

Analysis shows that the differential output voltage from the detector, $D_s = E_i - E_2$, may be written:

$$D_s = -k \cdot A(t) \cdot A(t - T) \cos [\Delta\omega \cdot T + \phi(t) - \phi(t - T)]$$

where $A(t)$ and $\phi(t)$ are amplitude and phase, respectively, of the IF signal, $\Delta\omega$ is any deviation from correct IF center frequency, and k is a detector constant. At the sampling times, t_K, $A(t_K) = A(t_K - T) = A$ and $[\phi(t_K) - \phi(t_K - T)]$ is π for a binary "one" or 0 for a "zero." Therefore (for $\Delta\omega$ small):

$$\text{Binary "one": } D_s(1) = k \cdot A^2 \cdot \cos (\Delta\omega \cdot T + \pi) \approx +k \cdot A^2$$

$$\text{Binary "zero": } D_s(0) = k \cdot A^2 \cdot \cos (\Delta\omega \cdot T) \approx -k \cdot A^2$$

These are the desired type of demodulated outputs. However, $\Delta\omega$ must be kept small; a drift of 68.5 MHz, i.e., 0.1 percent at 75 GHz, makes $D_s(1) = D_s(0) = 0$. Thus automatic frequency control (AFC) is required.

The AFC detector differs from the signal detector only by having an additional $\pi/2$ phase shift in series with the delay line. The output, $D_Q = E_3 - E_4$, may be written:

$$D_Q = -k \cdot A(t) \cdot A(t - T) \cdot \sin [\Delta\omega \cdot T + \phi(t) - \phi(t - T)]$$

At the sampling times (for small $\Delta\omega$):

$$\text{Binary "one": } D_Q(1) = -k \cdot A^2 \cdot \sin (\Delta\omega \cdot T + \pi) \simeq +k \cdot A^2 \cdot \Delta\omega \cdot T$$

$$\text{Binary "zero": } D_Q(0) = k \cdot A^2 \cdot \sin (\Delta\omega T) \approx -k \cdot A^2 \cdot \Delta\omega \cdot T$$

Thus we get an output of magnitude proportional to the frequency error; however, the sign is positive or negative depending on the bit received and the signal averages to zero for a reasonable string of bits. If the product $D_{AFC} = D_S \cdot D_Q$ (at the sampling times) is formed, then:

$$\text{Binary "one": } D_{AFC}(1) = D_S(1) \cdot D_Q(1) = k^2 \cdot A^4 \cdot \Delta\omega \cdot T$$

$$\text{Binary "zero": } D_{AFC}(0) = D_S(0) \cdot D_Q(0) = k^2 \cdot A^4 \cdot \Delta\omega \cdot T$$

D_{AFC} consists of pulses of proper polarity and magnitude, occurring at the sampling times, and may be averaged to form a dc control voltage for the AFC circuit. This circuit is referred to as the "fast" AFC detector.

Unfortunately, the same operation may take place at frequencies which are half a baud frequency, 137.088 MHz, above and below the proper IF frequency. This can result in false lock-ups during turn-on of the repeater. The output from a simple discriminator, the "slow" detector, similar to Fig. 11 but with a short 5/4 λ IF delay line is used to override the output from the "fast" detector at these false operating points.

VI. AFC LOOP

The automatic frequency control (AFC) loop primarily responds to the "fast" detector which has a high sensitivity. In order to bring the local oscillator close to the correct null of the "fast" detector, however, the "slow" detector takes over control of the loop whenever the IF is more than 30 MHz in error. The slow detector has zero crossings separated by 600 MHz, but the local oscillator is set to vary by no more than ±150 MHz. Figure 12 shows a simplified block diagram of the AFC loop. When the slow detector and its instrumentation amplifier have an output larger than the breakdown voltage of the zener diodes, then it dominates the loop and the fast detector has no effect. However, when the IF is within 30 MHz of its correct value, the slow loop voltage does not breakdown the dead band diodes and the fast detector is in control. The fast detector has a sensitivity of about 1 mV per MHz and the local oscillator about

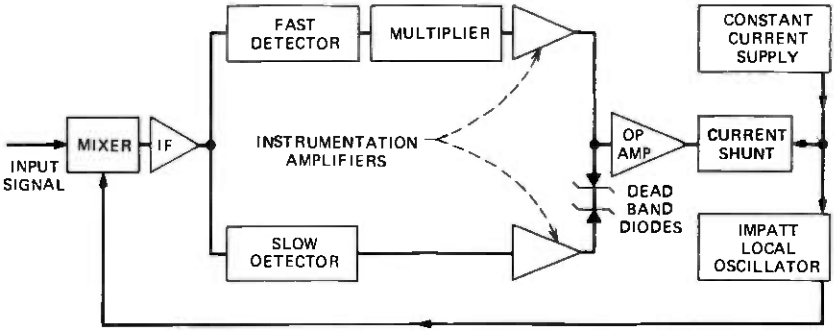

Fig. 12—AFC loop.

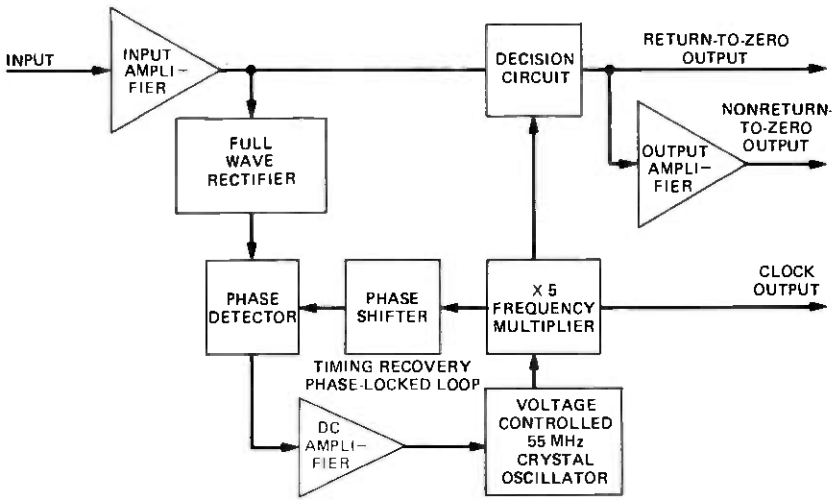

Fig. 13—Block diagram of WT4 regenerator.

10 MHz per mA. The gains of the amplifiers and the current-shunting transistor are adjusted to obtain a loop gain of greater than 100. All millimeter-wave oscillator frequency drifts are therefore reduced by a factor of 100 in the IF band. However, the AFC loop does not reduce any errors or drifts that occur in the fast detector zero crossing.

VII. REGENERATOR

An overall block diagram of the WT4 regenerator is shown in Fig. 13. The regenerator performs two basic functions, bit timing recovery and bit-by-bit binary decisions. The regenerator accepts a differential input signal of ±130 mV and amplifies this by 20 dB with a wideband amplifier before splitting the signal into two paths, one toward the decision circuit and one toward the timing recovery circuit.

The main signal path is toward the decision circuit where the binary decision is made as to where a "1" or a "0" was transmitted. Because of the high rate of transmission, 274.176 Mb/s, an emitter coupled logic (ECL) structure with microwave transistors was adopted for this circuit. The circuit consists of three stages of emitter-coupled transistor pairs. The first two stages provide amplification and the third stage is the sampling and decision-making stage. The third stage is shown in Fig. 14. The amplified baseband signal, V_{in}, to be sampled is applied to the bases of the transistors Q1 and Q2 in differential form.

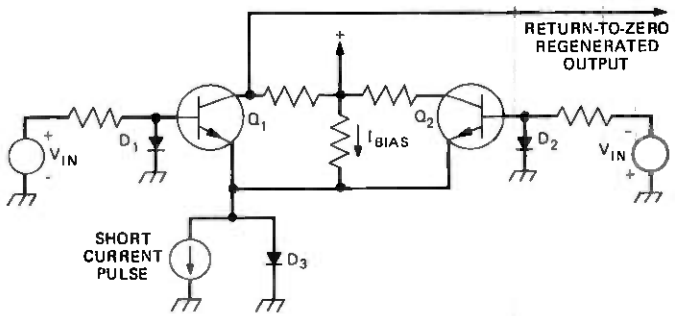

Fig. 14—Third stage of decision circuit.

If V_{in} is positive, then D1 will be forward-biased and D2 will be back-biased. A bias current flowing into D3 keeps it forward-biased. Therefore, under these conditions the biasing of diodes D1, D2, and D3 prevents either transistor from becoming active since the base-to-emitter voltages are either zero or negative. When a short pulse of current of sufficient magnitude is drawn from the node connecting the emitters of Q1 and Q2, the bias current flowing in D3 will be diverted and the additional current will be drawn from Q1, turning it on and producing a short voltage pulse at its collector. This voltage pulse is the return-to-zero (RZ) regenerated output signal. If V_{in} had been negative, then Q2 would have been turned on and no output at the collector of Q1 would have been produced. The RZ output of the regenerator is used to drive the phase shift modulator in the transmitter.

The time at which the short current pulse appears in the regenerator and, therefore, the time at which the baseband signal is sampled, is determined by the timing recovery circuit. The timing recovery circuit is a phase-locked loop (PLL) which is locked to the 274.176 MHz tone generated by full-wave-rectifying the incoming nonreturn-to-zero baseband signal. The PLL for the WT4 regeneration is a second-order loop to keep both phase offsets and phase jitter small. However, the second-order loop has a closed-loop characteristic which exhibits gain

over some frequency band. In order to avoid any large gain enhancement in a long chain of repeaters, the loop has been designed to be highly overdamped.

The regenerator by itself requires a baseband signal-to-noise ratio of 16.0 dB in order to achieve a 10^{-9} error rate. This is only 0.4 dB above the theoretical minimum of 15.6 dB. The timing recovery circuit has a hold-in range of ±40 kHz, operates over a 30 dB range of input signal levels, and produces less than 0.5 degree of phase jitter for a single repeater hop.

VIII. PHASE SHIFT MODULATOR

Each PSM is adjusted for operation at one of the 124 channel frequencies. It responds to each "1" in the bit stream from the regenerator by providing a differential phase shift of 180 deg ±5 deg. The switching time is approximately 0.5 nanosecond, and the timing jitter is less than 0.2 nanosecond. The insertion loss ranges approximately from 1.5 dB at 40 GHz to 3 dB at 110 GHz and differs in the two states by less than 0.25 dB. The PSM is designed to accommodate power levels up to 250 mW.

The PSM is of the basic type described by Clemetson, et al.[2] It consists of a PIN diode switch connected to one port of a Y-junction circulator and a terminated circulator used as an input isolator, all in a common integrated housing. The switch consists of the PIN diode[3] coupled to a standard rectangular waveguide. The coupling is through a short section of coaxial line parallel to the E plane of the guide. In a very loose approximation, the diode and its bias lead are seen as a short circuit on the waveguide for one bias state and as an open circuit for the other. In addition to the phase being reversed, the insertion loss of the modulator in the two bias states must be adjusted for a balance. The loss balance is achieved by adjustment of the length of coaxial line between the diode and the waveguide wall and between the choke filter and the waveguide wall.

The PSM bias driver switches the PIN diode between forward- and reverse-bias states in approximately 0.5 nanosecond. The forward current is 10 mA and the reverse-bias voltage is 10 volts. The driver responds to the pulse input from the regenerator. The driver consists of an input buffer amplifier, a flip-flop, an output amplifier, special circuits for adjusting the timing of the PLM output and temperature-compensated dc bias circuits. The pulse circuit and dc bias circuit are fabricated on two separate alumina substrates. Each substrate is approximately 1.1 × 1.3 × 0.025 inches. The circuits use thin-film tantalum nitride resistors, plated up gold conductors, beam-leaded transistors and diodes, and chip capacitors. The circuit cards are mounted on an aluminum drawer which

Table III — Power requirements for the WT4 repeater

INPUT:			
Nominal	−24		
Minimum	−20		
Maximum	−27		
Maximum transient	−30		
OUTPUTS:			
Constant voltage			
	No. 1	No. 2	No. 3
Voltage	−10	+10	−16
Regulation	±0.5%	±.5%	±.5%
Maximum load current	2.4 A	0.3 A	0.4 A
Dynamic load variation	±10%*	70–270 mA	195–370 mA
Ripple	<15 mV P-P	<15mV P-P	<15mV P-P
Constant current (two supplies)			
Current range	60–130 mA		
Voltage	15–50 V		
Regulation	±0.5 mA		
Ripple	<.05 mA P-P		
Noise	No tone > 4μA		
Output capacitance	<50 pF		
Maximum instantaneous current due to step change of input voltage	1.30 × set current or 120 mA, whichever is greater		

* At nonprotection switching repeaters, 1.25 A ± 10%. At protection switching repeaters, 2.10 A ± 10%.

in turn is mounted in the RF housing of the PSM. The average dissipation of the driver excited by a pseudorandom word is 3.8 watts.

IX. POWER SUPPLY

Power at the voltages required by the electronics is obtained via dc-dc converters. Constant-current and constant-voltage regulators are provided as necessary to power the repeater transmitter and receivers. Table III gives the power requirements for the field evaluation test repeaters. The power supply is mounted in its own housing with the current regulators located in the transmitter and receiver housings close to the IMPATT diodes which they feed. The converter portion of the supply uses a closed-loop frequency-controlled ferroresonant transformer whose fundamental switching frequency is 150 Hz. The choice of a low-frequency converter eases the problem of suppressing high-frequency noise. The voltage regulators were designed with a minimum input-output voltage differential to minimize wasted power. Regulator efficiencies of 82 percent and converter efficiencies of 68 percent were attained for the field evaluation test.

X. REPEATER PHYSICAL DESIGN

The WT4 field evaluation test repeater shown in Fig. 15 consists of four parts including a transmitter, receiver, line equalizer, and a dc–dc con-

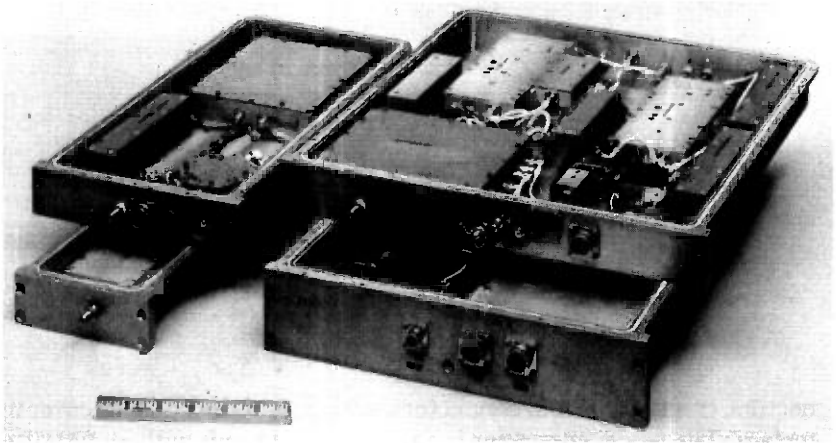

Fig. 15—Field evaluation test repeater.

verter. In an effort to reduce the loss within the channel multiplexer, the repeater was designed to make it as thin as possible to permit minimizing the distance between adjacent channel diplexer ports. To facilitate back-to-back testing of receivers and transmitters at the end of a span, separate housing are provided for receiver and transmitter circuits. The "line" equalizer circuits are closely associated with the transmission medium and the channelization networks, hence the fourth housing. Each of the four repeater housings consists of a cast aluminum structure resembling a frying pan with a flat aluminum cover. Subassemblies within each housing are bolted to the 0.3-inch-thick bottom plate allowing conductive heat transfer to the mounting surface of the housing which contacts a water-cooled channel attached to the repeater frame.

The repeater housings and covers form pressure-tight and RFI-shielded enclosures for the circuits. Dry nitrogen gas at 0.2 psig fills the housing thereby protecting a number of high-frequency devices which have not been encapsulated. The nitrogen is fed from the channel diplexer via the receiver and transmitter waveguide ports (Fig. 16). The line equalizer obtains dry nitrogen through tubing connected to the receiver. The receiver, transmitter and line equalizer have gas valves mounted on the rear of the housings to permit initial factory pressurization and purging during installation. The dc–dc converter has no shielding or pressurization requirement.

The RFI shielding is necessary because the intermediate frequency is in a prominent military radar band which could cause interference with the repeater signal. To maintain both RFI shielding and pressure sealing, dual-purpose seals are employed at the waveguide ports, power con-

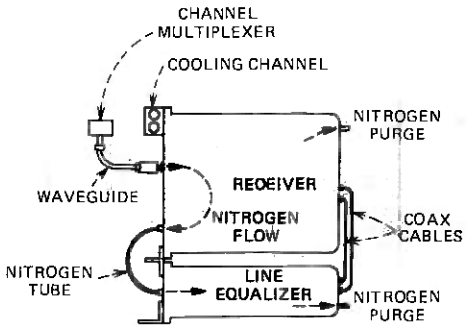

Fig. 16—Receiver and line equalizer.

nectors, IF and baseband connectors, and around the housing-cover interface. The power connector is a pressure tight unit with an RFI filter in series with each pin. Each lead in the power cable is shielded to minimize RFI pick-up. The IF and baseband connections to the repeater housings are pressure-tight and naturally shielded by the coaxial outer conducter.

10.1 Thermal considerations

Each WT4 field evaluation trial repeater dissipates 50 watts. The shielding requirement eliminated the option of removing the heat from critical circuits by convective means. The thermal question is further aggravated by the requirement that the IMPATT diode mounting stud be maintained at a temperature below 50°C. If a forced-air system were employed to maintain the required temperatures, the repeater frames would have been congested with large ducts, the audible noise level would be intolerable, and the system would not grow gracefully from a few repeaters to the full complement of 124. The best choice for the WT4 system was to remove the heat via a chilled water system. As shown in Fig. 17, heat is conducted from the IMPATT diode stud to the oscillator body and then to the repeater housing which is bolted directly to a channel filled with flowing cool (15°C) water. A companion article, "The Repeater Station," this issue, describes the features and reliability aspects of the chilled water system.[5]

10.2 IMPATT diode bias connections

One of the most serious mechanical problems was the design of reliable IMPATT diode bias contacts for the repeater. A bias rod is in contact with a quartz stand-off attached to the diode stud. A gold strap is bonded to both the stand-off and the diode. An attempt was made to minimize the mass in contact with the stand-off while providing a spring which could apply a force of between 60 and 100 grams over a 0.75-mm range of de-

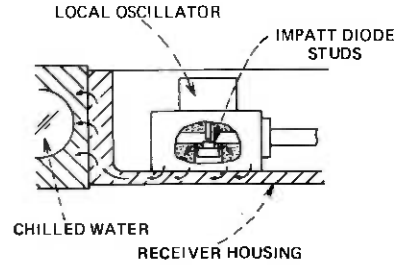

Fig. 17—Thermal path for receiving oscillator.

flection. In addition the natural frequency of the system had to be as high as possible to permit meeting stringent handling and shipping requirements. To minimize RF leakage, a close spacing (0.001 inch) between the bias line and oscillator walls was maintained. Insulation was formed by spraying a thin hard acroloid coating on the bias lines. It was necessary to develop separate designs (Fig. 18) for the transmitting and receiving oscillators.

10.3 Hybrid-integrated circuits

The WT4 field evaluation test repeater contains 21 codes of thin-film hybrid integrated circuits (HICs). The HICs that make up the baseband unit utilize standard bilevel thin-film technology. A number of IF circuits such as signal and AFC detectors, equalizers, and the IF filter require close tolerance ceramic thickness and dielectric properties. In addition, special metal and line delineation systems were developed especially for WT4 to meet the exacting line width requirements.

10.4 Circuit packaging

All WT4 thin-film substrates are housed in aluminum housings (Fig. 19). Spring clips are attached to each substrate and they are held in position when the housing cover is secured. Circuit interconnections are provided by gold straps bonded to gold lands on the top of the substrate.

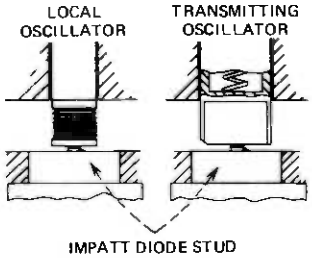

Fig. 18—Bias rods for WT4 oscillators.

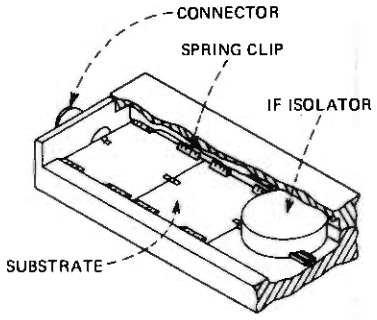

Fig. 19—Mounting of WT4 HICS.

Circuit ground continuity is provided by gold straps bonded to the ground planes on the bottom of the substrates. The metal housings serve only to support and shield the circuits. Filtered feed-throughs are provided for dc and monitoring connections. Circuit connections to the substrates are made through 50-ohm miniature coaxial connectors that clearly define both electrical and mechanical boundaries for each circuit package.

10.5 Repeater to channel diplexer connection

Figure 16 illustrates how a receiver or transmitter interfaces with the channelization network. Connections are made via a variable attenuator, a waveguide bend, and a short length of rectangular waveguide. For WR10 and WR15 these interconnection assemblies are flexible enough to permit small WG-WG misalignments. This is not the case for the WR22 assembly and a special short length of flexible WR22 waveguide is provided.

XI. SUMMARY

Twelve repeaters were manufactured at Bell Laboratories during 1974 and 1975 covering the frequency range 40 to 108 GHz. These repeaters were installed at the ends of the 14-km waveguide line in northern New Jersey and utilized in the systems test as described in the companion paper in this issue of the B.S.T.J. It is planned to continue operating the system test at least through 1977. While there are some known circuit changes which would improve repeater performance, the design described in this paper can be used to manufacture two-phase repeaters for a waveguide transmission system with very good performance.

Reference 4 gives the measured available gain* for the twelve field evaluation test repeaters. It ranged from 78.2 dB at 40 GHz to 64.6 dB at 109 GHz for these two-phase repeaters. Subsequent to fabrication of

* Available gain is defined for any channel as the dB ratio between the receiver input power required to attain an error rate of 1 in 10^9 and the transmitter output power.

the field-evaluation test repeaters, laboratory experiments have shown that considerable circuit performance improvement can be obtained, particularly in the IMPATT oscillators and down-converters. Based on these improved circuits, it is estimated that four-phase repeaters can be built to yield available gain ranging from 75 dB at 40 GHz to 58 dB at 110 GHz.

It is these projected four-phase repeater available gain numbers that have been used in system installation plans for repeater spacing.

XII. ACKNOWLEDGMENTS

The design of a millimeter-wave regenerative repeater is a mixture of a wide variety of electronic technologies and depends on the contributions of a large number of engineers. The authors would like to thank all those who contributed to the development of the repeaters.

In particular, contributors to the IF circuit development were: F. J. Peragine, H. F. Lenzig, J. J. Schottle, P. J. Tu, and M. D. Tremblay. To the baseband circuit development: W. E. Studdiford, A. F. Perks, M. J. Bonomi, S. Cheng, and A. F. Caruso. To the millimeter-wave circuit development: D. R. Gunderson, R. C. Ashenfelter, G. S. Axeling, T. F. McMaster, A. C. Chipaloski, and B. T. Verstegen. to the isolator and circulator development: B. Owen, D. J. Thibault, T. W. Mohr, J. J. Kostelnick, and R. D. Phillips. The contributions of C. B. Swan to the IF isolator design are especially noteworthy. G. M. Palmer was responsible for the physical design of the isolators and PSM. F. Bosch, M. J. Gabala, and R. W. Folojtar contributed to the PSM design. W. G. Thompson, J. J. Gainey, and H. H. Weinreich were responsible for the repeater physical design. Early work on the development of IF amplifiers in the 1 to 2 GHz frequency range was conducted by W. Kruppa. R. F. Lee, and K. F. Sodomsky.

The power supply development was carried out by Herb Stocker, and we are especially appreciative of his cooperation in the WT4 development.

REFERENCES

1. E. T. Harkless, A. J. Nardi, and H. C. Wang, "Channelization," B.S.T.J., this issue.
2. Clemetson, et al., "An Experimental MM-Wave Path Length Modulator," B.S.T.J., *50*, No. 9 (November 1971), pp. 2917–2946.
3. C. N. Dunn, O. G. Petersen, and D. C. Redline, "Semiconductor Devices for the WT4 Repeater," B.S.T.J., this issue.
4. S. S. Cheng, E. T. Harkless, R. W. Muise, W. E. Studdiford, and D. N. Zuckerman, "Field Evaluation Test System Performance," B.S.T.J., this issue.
5. W. J. Liss, D. Olasin, and S. Shapiro, "The WT4 Repeater Station," B.S.T.J., this issue.

THE BELL SYSTEM TECHNICAL JOURNAL
Vol. 56, No. 10, December 1977
Printed in U.S.A.

WT4 Millimeter Waveguide System:

Line and Repeater Equalization

By R. J. BROWN, P. BROSTRUP-JENSEN,
J. J. SCHOTTLE, and P. J. TU

(Manuscript received April 7, 1977)

The WT4 millimeter waveguide system requires equalization of the loss and delay of the line, which is made up of both the waveguide itself and the diplexer (waveguide channelizing filter) arrays. In the lower portion of the band (40 to 60 GHz) there is considerable linear delay (as much as 30.5 nsec per 400 MHz at 40 GHz), which is equalized by using a folded tape meander line delay equalizer. The remaining delay and amplitude deviation from the desired transfer characteristic is further reduced by field-adjustable trim equalizers. In this paper, we describe the equalization and measurement philosophy for the WT4 system and also the technologies used in achieving the resulting degree of equalization. We put special emphasis on the description of trim equalization because line equalization has been described in detail in a previous publication.[1]

I. INTRODUCTION

The WT4 millimeter waveguide system requires equalization of the loss and delay of the line which is made up of both the waveguide itself and the diplexer (waveguide channelizing filter) arrays.[2] Furthermore, the RF and IF portions of the WT4 receiver require equalization for optimum performance. In Fig. 1, we show a simplified block diagram of a repeater hop. In the WT4 system all equalization is performed about the IF of 1371 MHz. Theoretically, a single equalizer package could be designed to equalize simultaneously the line and the repeater. However, as a maintenance philosophy[3] evolved, it became desirable to separate the line equalizer and the repeater equalizer. The repeater equalizer equalizes only the RF and IF portions of the repeater and resides in the repeater package while the line equalizer is designed to equalize only the

Fig. 1—Repeater hop.

line and is mounted in a separate package apart from the repeater. The line equalizer is made up of a major delay equalizer and mop-up trim delay and amplitude equalizers. The repeater requires only trim equalization. Because passive devices are used for equalization, a very high degree of reliability as well as transfer function stability was obtained compared to the reliability and stability obtainable from active devices.

In order to determine the required characteristics for the various line equalizers, a line measurement is performed. A computer-controlled measurement of the line with utilization of time domain techniques is both feasible and attractive. Accuracy to within 0.1 dB rms for loss and 0.1 nsec rms for delay can be achieved using this method.

In this paper, we describe the equalization and measurement philosophy for the WT4 system and also the technologies used in achieving the resulting degree of equalization. We put special emphasis on the description of trim equalization because line equalization has been described previously.[1]

II. MAJOR DELAY EQUALIZATION OF THE WAVEGUIDE

The circular waveguide in the WT4 system has an inside diameter of 60 mm,[4] which corresponds to a cutoff frequency of 6.09 GHz. It can be shown that the waveguide introduces considerable dispersion in the WT4 signal. Although the dispersion introduced by the waveguide is an order of magnitude less harmful at the higher portion of the band than at 40 GHz, due to WT4's high transmission rate (274 Mb/s), long repeater spacing (up to 60 km) and tight performance requirement (error rate less than 10^{-9} per repeater hop), equalization over the entire WT4 band is essential. This may be seen by noting that a bit period is 3.6 ns and the linear delay distortion at the high end of the band is 1.5 ns per 400 Mhz which would cause considerable intersymbol interference if unequalized.

Part of the task in developing the major delay equalizer for the waveguide was the definition of the equalizer itself. This was especially important in the early stage of the repeater development, for the type of equalizer chosen could well influence the overall repeater configuration. For example, delay equalization could be carried out at the RF frequency band in the form of frequency frogging. This method, if adopted, would require that every other repeater be a linear repeater, as opposed to a regenerative repeater. The tight specifications that would

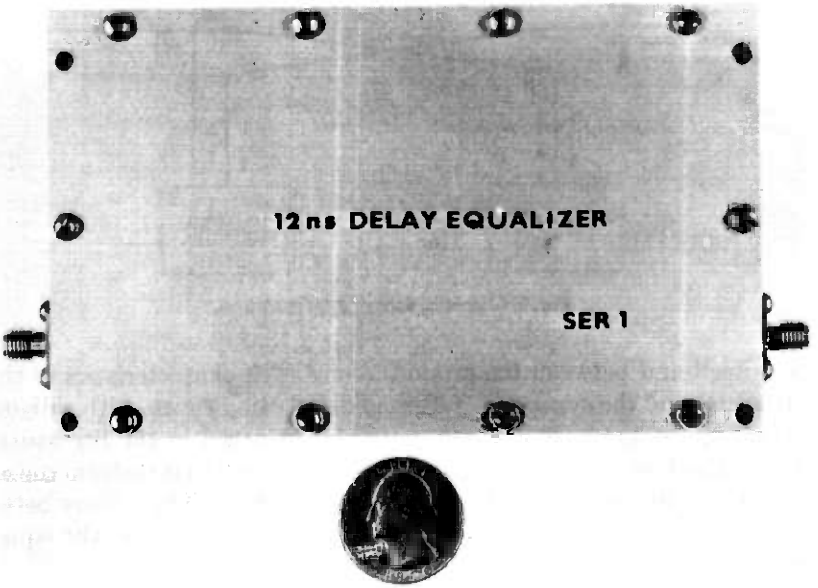

Fig. 2—FTML equalizer.

be required of the linear repeater design and the restrictions to be placed on adjacent repeater spacings, however, made this method undesirable.

Subsequent studies showed that it is best to equalize at IF frequency. Basically the reasons for this conclusion are that RF equalizers would be too costly, require more manufacturing codes (because of the numerous RF frequencies) and probably not perform as well as IF equalizers. In the IF equalization approach, the center frequency and the bandwidth of the equalizer are fixed for all channels. The IF band had been chosen to be from 1.15 to 1.57 GHz. The early objective, therefore, was to develop an L-band delay equalizer with 400 to 500 MHz of bandwidth.

The delay distortion of the waveguide, when measured in a 400 MHz window, is essentially linear. The magnitude of this linear delay varies from 30 ns at 40 GHz to 1.5 ns at 100 GHz. The amount of equalization required at each channel is different. The final configuration consists of seven codes of folded-tape meander-line (FTML) equalizers of fixed design to equalize the bulk of the waveguide delay.

2.1 Folded-tape meander-line equalizers

The FTML is a periodic structure, consisting of a conducting tape, perpendicular to two ground planes, folded back and forth to form a meander pattern. Dielectric material fills the space between the meander

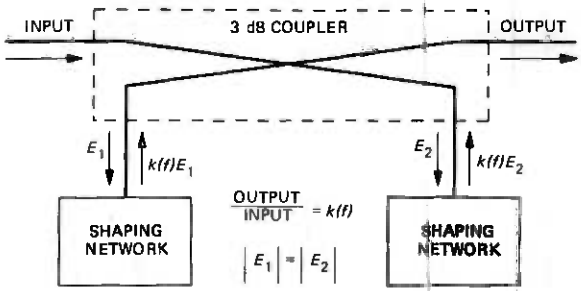

Fig. 3—Basic equalizer configuration.

line itself and between the ground planes. The characteristics of this structure and the synthesis of desired delay using FTML, with a digital computer program, have been described in detail in the literature.[1] Special techniques have also since been developed to transform the arbitrary FTML impedance to the desired 50 ohms. This allows better performance and a reduction in the physical dimensions of the equalizer.

In the final design, the FTML equalizer has an overall dimension of 5 by 3 by 0.5 inches. (See Fig. 2.) It provides linear delays at 4 ns (per bit rate frequency) increments up to a total of 20 ns. Above 20 ns, the increment is reduced to 3 ns. Typical insertion loss of the equalizer is approximately 0.15 dB per 1.0 ns of delay. The average return loss of the equalizer is better than 20 dB.

III. TRIM EQUALIZATION OF THE LINE AND REPEATER

The repeater and line trim equalizers are designed to compensate for relatively small amplitude and delay variations. The repeater equalizer compensates for distortions introduced between the input of the down-converter and the output of the final IF amplifier. The line trim equalizer is used to mop up after the meander line has removed the bulk of the transmission delay distortion. It also has an amplitude section which compensates more for amplitude distortions in the delay equalizers than for anything else.

3.1 Basic configuration

All equalization is accomplished in the IF band. Since the equalizer is in the transmission path it should present a good impedance match to connecting networks while at the same time shape the amplitude and delay characteristic of the signal. Consideration of these requirements along with other factors such as component availability and space limitation led to the selection of the network configuration shown in Fig. 3. The figure shows two identical shaping networks connected to the

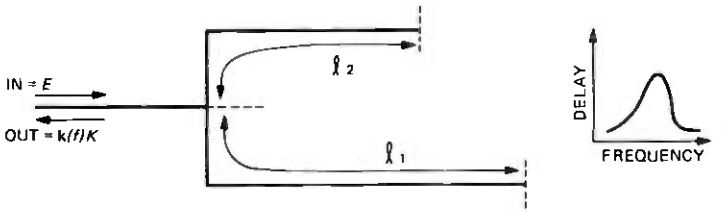

(a)

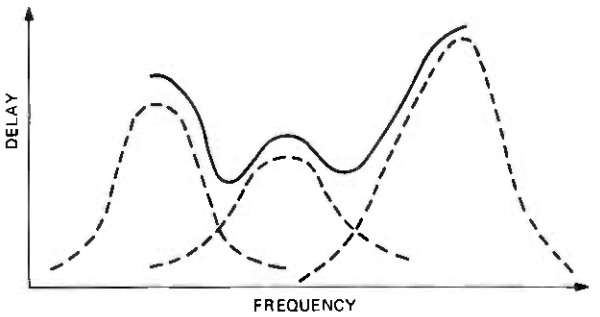

(b)

Fig. 4—(a) Delay reflection network. (b) Typical delay shape.

transmission ports of a 3 dB coupler. The input energy is divided evenly but 90 deg out of phase and sent to each network where the signal phase-frequency or loss-frequency characteristic is altered, and the energy is reflected back to the coupler. An additional 90 deg phase shift is introduced by the coupler, resulting in a cancellation of the reflected signals at the input port and the addition of signals at the output. The overall transfer characteristic is given by $k(f)$, the complex reflection coefficient of the shaping network.

3.2 Trim delay Equalization

The final version of the delay reflection network is shown in Fig. 4a. This network consists of two open circuit stubs forming a resonant circuit. The expression for delay, τ, is found by taking the derivative of the phase function of $k(f)$, and it is given by

$$\tau = \frac{1}{2f_0} \frac{(1-\delta)\cos^2\frac{\pi}{2}\frac{f}{f_0}(1+\delta) + (1+\delta)\cos^2\frac{\pi}{2}\frac{f}{f_0}(1-\delta)}{\cos^2\frac{\pi}{2}\frac{f}{f_0}(1-\delta)\cos^2\frac{\pi}{2}\frac{f}{f_0}(1+\delta) + \sin^2\pi\frac{f}{f_0}} \text{ nsec} \tag{1}$$

where ℓ_1 and ℓ_2 are the lengths of the open circuit stubs, f_0 is the frequency which makes $\ell_1 + \ell_2$ a half-wavelength long and $\delta = (\ell_1 - \ell_2)/(\ell_1 + \ell_2)$. When $f = f_0$ the delay expression reduces to

$$\tau|_{f=f_0} = \frac{2}{f_0} \frac{1}{(1 - \cos \pi\delta)} \tag{2}$$

Equation (2) is a very good approximation for the maximum delay given a value of δ. The expression is exact in the limit a $\delta \to 0$.

One complete network is fabricated on a 1 inch by 2 inch ceramic substrate, and it is configured as shown in Fig. 3 with two identical delay reflection networks. When a delay bump of a particular magnitude and center frequency is desired the stubs are laser-cut with δ proportional to $(\ell_1 - \ell_2)/(\ell_1 + \ell_2)$ and f_0 proportional to $\ell_1 + \ell_2$. Using this universal substrate a delay bump of any magnitude may be centered at any frequency between 1 GHz and 2 GHz. Fig. 4b indicates how three such delay bumps may be combined to yield a particular delay shape.

The synthesis procedure may be reduced to two major operations. The first is the specification of the delay requirement, after which the theoretical snythesis is performed using a computerized curve-fitting routine. The degree of accuracy for this procedure is completely dependent on the complexity of the delay requirement and the number of delay sections or bumps allowed to do the job. For the WT4 system three bumps have been used for all equalizers. Apart from this, the attractiveness of using the bump equalizer is that it allows the designer to estimate the closeness of fit and the location of bumps before any detailed synthesis is attempted. This cuts down on computation time since a trial-and-error technique is not required. Assuming that this first operation has provided a satisfactory curve fit, the second step is to specify the physical stub lengths on each of the substrates. The relationship between the electrical and physical length of the line is given as

$$\ell = \frac{c}{f\sqrt{\epsilon_e}} \tag{3}$$

where c is the free-space velocity of light, f is the frequency and ϵ_e is the effective dielectric constant of the microstrip line. Obviously the critical parameter is ϵ_e since c is a constant and f is specified by the synthesis. The value of the effective dielectric constant may be obtained from a theoretical analysis or it may be determined from a measurement made on the substrate. The latter approach has been used throughout the development due to the difficulty in determining the relative dielectric constant of the ceramic. The measurement technique will also compensate for junction effects and fringing capacitance which are an integral part of the network. The constant so determined is a function of the network layout; therefore it is not the value of effective dielectric

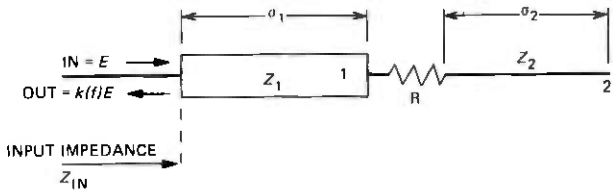

Fig. 5—Amplitude reflection network.

constant. In a mass-production environment, this characterization may be necessary only when a new batch of substrates is produced.

3.3 Trim amplitude equalization

The amplitude reflection network is shown in Fig. 5. This network consists of a low-impedance line, 1, a resistor R and a high impedance open circuit stub 2. As with the delay network, a bump loss shape is generated. The expression for the input impedance, z_{IN}, is easily derived and is given as

$$z_{IN} = z_1 \frac{(r + jz_2 ctn\sigma_2) + jz_1 \tan \sigma_1}{z_1 + j(r - jz_2 ctn\sigma_2) \tan \sigma_1} \tag{4}$$

where z_1, z_2 are the normalized impedances of the transmission lines, σ_1, σ_2 are the electrical lengths of the lines, r is the normalized resistance and z_{in} is the normalized input impedance. For the special case of $\sigma_1 = \sigma_2$, and the particular frequency, f_0, such that $\tan \sigma_1 = \tan \sigma_2 = \infty$, the input impedance is given as

$$|z_{IN}|_{f=f_0} = \frac{z_1^2}{r}. \tag{5}$$

The magnitude of the reflection coefficient for this case is

$$|k(f)|_{f=f_0} = \frac{1 - \dfrac{z_1^2}{r}}{1 + \dfrac{z_1^2}{r}} \qquad z_1^2 < r \tag{6}$$

and peak loss is given as

$$\text{Peak loss} = -20 \log |k(f)|_{f=f_0} \tag{7}$$

A maximum amplitude bump of 8 dB was deemed sufficient for amplitude equalization. Assuming also that the smallest practical resistor value available with thin-film technology is 10 ohms, the solution of eq. (6) leads to a value of $z_1 = 0.293$. For a 50 ohm system the line impedance is $z_1 \times 50 = 14.7$ ohms. To keep the flat loss to a minimum the skirts of the amplitude shape should drop off as rapidly as possible. To achieve

this, a very high impedance line is used to terminate the resistor. This line is 2 mils wide with an impedance $z_2 = 2.2343$. For the 50-ohm system, the 2-mil line has an impedance of $z_2 \times 50 = 112$ ohms.

One complete amplitude network is fabricated on a 1 inch by 2 inch ceramic substrate, and it is configured as shown in Fig. 3 with two identical amplitude reflection networks. The length ℓ_1 of the high-impedance line determines the center frequency and the resistance R determines the magnitude of the bump. As with the delay equalizer the bump shape may be moved across the IF band by laser trimming the high-impedance line and the magnitude adjusted by laser trimming the resistor. The bumps may be added to produce a general shape.

3.4 Equalizer synthesis

The amplitude and delay shape requirements are synthesized by adding three delay bump equalizers and three amplitude bump equalizers. To achieve the best possible fit, a least squares curve-fitting program is used to determine the equalizer parameters.

As indicated earlier, there is an interaction between the amplitude and delay equalizers. The amplitude equalizer has delay shape and the delay equalizer has loss.

An efficient technique was developed to determine the equalizer requirements and is illustrated in Figs. 6a and b. Fig. 6a shows the delay requirement plotted on the negative frequency axis and the amplitude requirement plotted for positive frequencies. The interaction components are plotted in Fig. 6b. The program is designed to optimize both amplitude and delay as though they were a single requirement. When the negative frequency region is used the program adds the delay of the delay equalizer to the delay of the amplitude equalizer. The positive frequency region computes and adds the loss of the amplitude equalizer to the loss of the delay equalizer. In this way the optimization procedure can fit the total equalizer requirement with all interaction components accounted for.

3.5 Equalizer fabrication

The individual networks are assembled in a single housing. The substrates may be connected in any order, with the equalizer normally consisting of three delay bumps and three amplitude bumps. However, any combination of amplitude and delay substrates totaling six may be used, depending on the equalizer desired. The substrates are bonded together with gold ribbon and the input and output ports are brought out through OSM-type connectors.

The line trim equalizer is designed to permit field equalization adjustments in conjunction with the equalization test set. Laser trimming

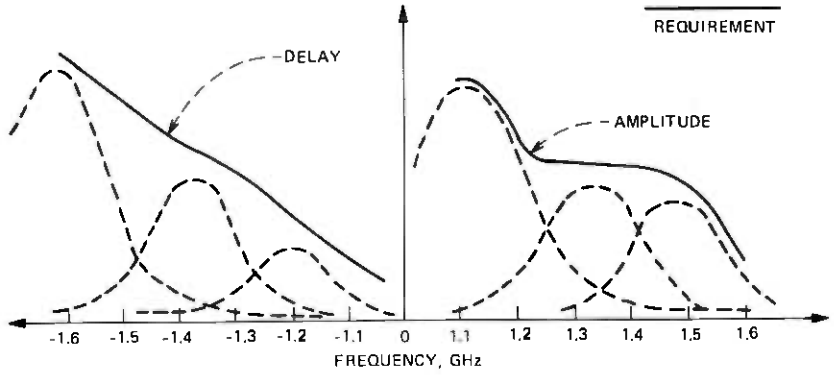

(a)

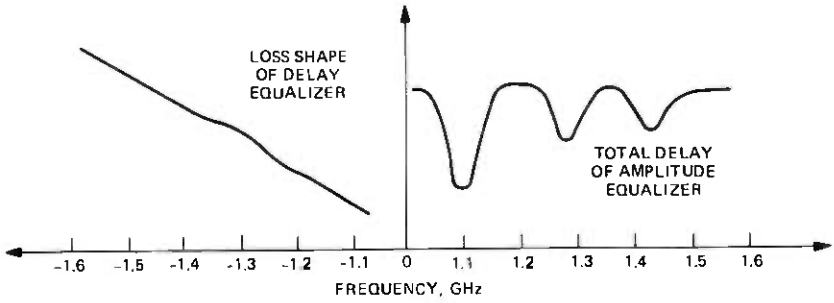

(b)

Fig. 6—(a) Delay and amplitude curve fitting. (b) Parasitic delay and loss.

was ruled out for field use so the repeater equalizer networks were modified to provide an acceptable tuning structure. The two basic reflection networks are shown in Fig. 7. The delay section is shown at the

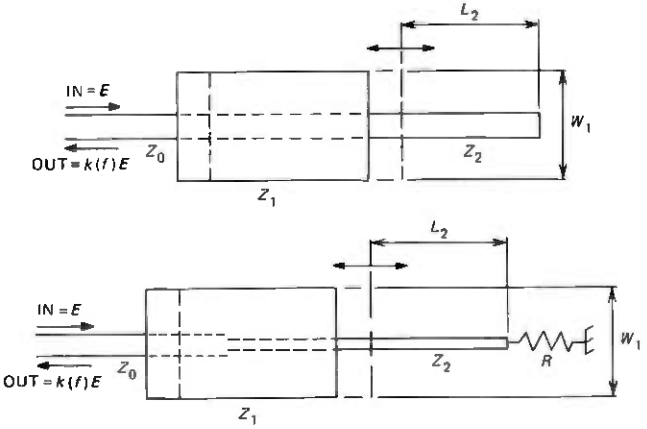

Fig. 7—Line trim equalizers.

top and the amplitude section below it. For each network the variable parameters are W_1, the width of the low impedance line, and L_2, the stub length from the open circuit or resistive termination. The magnitude of the delay (amplitude) bump is proportional to Z_2/Z_1 and the frequency at which the peak occurs is determined by L_2.

The tuning of this structure is accomplished by first selecting a preformed block which has the low-impedance line plated on and then positioning the block to set the center frequency. The blocks are fabricated to provide 0.5 nsec delay increments and 0.5 dB magnitude increments from 8 nsec (dB) down to 1 nsec (dB). When the adjustment is completed, the block is held in position by a spring-loaded cover and positioning bracket. The completed equalizer consists of six sections, three delay and three amplitude, housed in a metal case with miniature coaxial connectors to the outside.

IV. EQUALIZATION MEASUREMENT

In order to determine the transfer function of the required line and repeater equalizers some type of measurement must be performed. For the repeater equalizers it is simple to perform a swept-frequency measurement of the RF and IF portions of the repeater in the factory. The situation is quite different for the line equalizer, however.

It is clear that the required characteristics of the various line equalizers are not known in detail until the specific channel has been measured. Accurate measurement of loss and delay by well-established swept-frequency techniques requires that a suitable reference signal be supplied from the transmitter to the receiver while the measurements are being performed. For the waveguide system this is difficult to do because the two ends of any section to be measured up to 40 km apart. The total frequency range to be covered is also very wide (40 to 110 GHz). To provide full coverage would require at least three sets of wide-sweep millimeter-wave transmitters and receivers. Such test set bulk is of concern because the test set has to be transported from repeater station to repeater station throughout the country. These factors led to consideration of time domain measurement techniques. The basic procedure has been described in Ref. 5 and consists of digitally phase modulating the WT4 transmitter for a particular band and linearly detecting the pulse train received in the receiver IF. By using fast Fourier transform processing of the detected waveforms with the transmitter and receiver connected back-to-back and with transmission through the line, an accurate determination of the line transfer function can be made. This information is then used to synthesize and appropriate channel equalizer for the waveguide system. The above procedure is repeated each time a channel in the WT4 system is put into service for the first time. The complete operation is controlled by a PDP-11/05 minicomputer.

Table I — Typical equalization results

Frequency, GHz	Repeater delay, nsec	Equalizer delay, nsec	Total delay, nsec
1.21	1.01	−0.95	+0.05
1.25	0.55	−0.61	−0.06
1.29	0.14	−0.17	−0.03
1.33	−0.09	−0.01	−0.10
1.37	0.	0.	0.
1.41	0.23	−0.16	+0.07
1.45	0.67	−0.46	+0.21
1.49	1.23	−0.95	+0.28
1.53	1.82	−1.73	+0.09

Note: Delay figures are normalized to give 0 delay of 1.37 GHz.

V. EQUALIZATION RESULTS

5.1 Repeater equalization results

In Table I, we list the delay characteristic versus frequency of a typical repeater along with the corresponding delay characteristic of the repeater equalizer. Also included is the resultant delay of the repeater after equalization. Typically we have experienced ±0.2 ns in delay deviation after equalization and ±0.3 dB in amplitude deviation.

5.2 Line equalization results

The transfer characteristics of each broadband channel were measured using the equalization test set described in Section IV. Figure 8 shows the measured characteristics of a typical channel (solid curve) and the desired characteristics. For the line, the desired characteristic is the ideal shape of the waveguide channelizing filter which is shown with a dashed line in Fig. 8. The fast ripples in the transfer function are due mainly to the channelizing filters; the waveguide medium contributes small ripples. The equalizer is designed as described in previous sections to make up

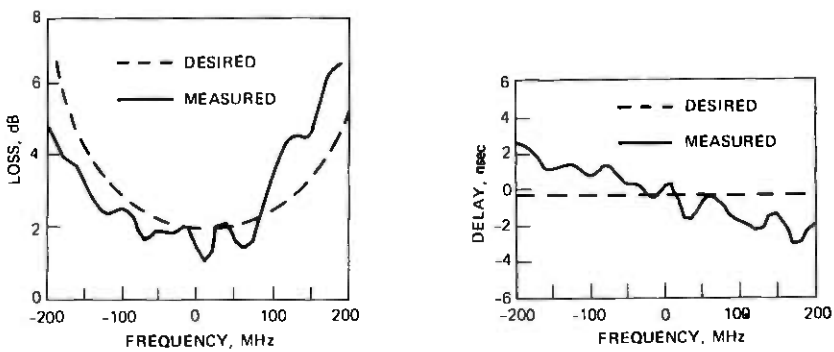

Fig. 8—Loss and delay in unequalized line.

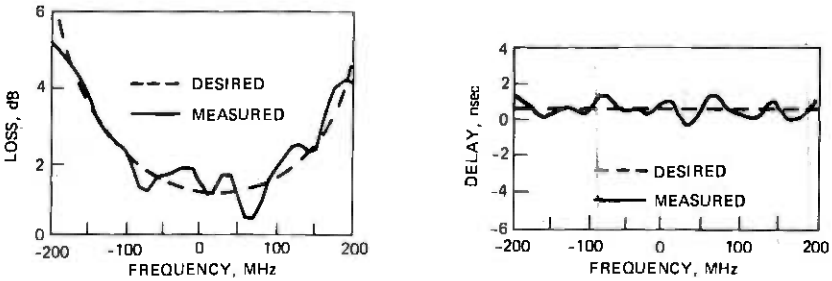

Fig. 9—Loss and delay in equalized line.

the difference between the curves. Our line equalizer is only capable of compensating for three "bumps" in amplitude and delay in addition to linear delay in the pass band; therefore, we are only attempting to equalize the slowly varying portion of the difference. The results of equalization are shown in Fig. 9. Note that the peak-to-peak variations in amplitude and delay after equalization are about ±0.5 dB and ±1.0 nsec and that essentially all of the slowly varying distortion has been removed.

VI. CONCLUSIONS

Line and repeater equalization techniques which have proved to be successful for the WT4 waveguide system have been described. The residual amplitude and delay shapes of the waveguide system transfer function after equalization is quite acceptable. Furthermore, an extension and modification of previous time-domain techniques to cover the millimeter-wave frequencies has been found to be both a feasible and attractive method for characterization of the waveguide line.

REFERENCES

1. P. J. Tu, "A Computer-Aided Design of a Microwave Delay Equalizer," IEEE Trans. Microw. Theory Tech., *MTT-17*, No. 8 (August 1969), pp. 626–634.
2. E. T. Harkles et al., "Channelization Plan and Networks," B.S.T.J., this issue.
3. M. J. Bonomi et al., "Protection Switching, Auxilliary Communication, and Maintenance," B.S.T.J., this issue.
4. D. A. Alsberg et al., "The WT4/WT4A Millimeter Wave Transmission System," B.S.T.J., this issue.
5. R. J. Brown and P. Brostrup-Jensen," Application of Time-Domain Techniques for Measurement and Equalization of a Millimeter Waveguide Line in the 40 to 110 GHz Band," IEEE Trans. Instrum. Meas., *IM-25*, December 1976 pp. 392–397.

THE BELL SYSTEM TECHNICAL JOURNAL
Vol. 56, No. 10, December 1977
Printed in U.S.A.

WT4 Millimeter Waveguide System:

Channelization

By E. T. HARKLESS, A. J. NARDI, and H. C. WANG

(Manuscript received April 7, 1977)

Waveguide networks operating in the millimeter wave region to separate the 62 transmitter and 62 receiver frequency spectra at each end of every waveguide transmission line are described. The overall loss of these networks for the various channels has been designed to complement the shape of the transmission medium loss in order to yield maximum repeater spacing. General descriptions of the design and performance of all filters used in the complete channelization array are given.

I. NETWORK LAYOUT

The main factors controlling the repeater spacing in the WT4 system are the available gain, the transmission medium loss, and the channelizing network loss. For each of the 124 channels, the available gain must exceed the sum of the transmission medium plus channelizing network losses. Both the transmission medium loss and the available gain are strong functions of frequency over the 40 to 110 GHz band. To obtain maximum repeater spacing and reduce systems costs, it is therefore necessary to plan the channelizing networks such that they will have minimum loss at the frequencies where the transmission medium loss is high and/or the available gain is low. Figure 1 plots the moderate terrain transmission medium loss and the projection of available gain for four-phase repeater development. (It is planned to set the repeater spacing such that four-phase repeaters can be introduced at some future date without change in repeater spacing or channelizing networks.) The plot clearly shows that the channelizing networks should be designed to minimize the loss at the edges of the band. In the early development of the system, it was projected that the medium loss at 40 GHz would be considerably higher than the loss at 110 GHz. Therefore, the chan-

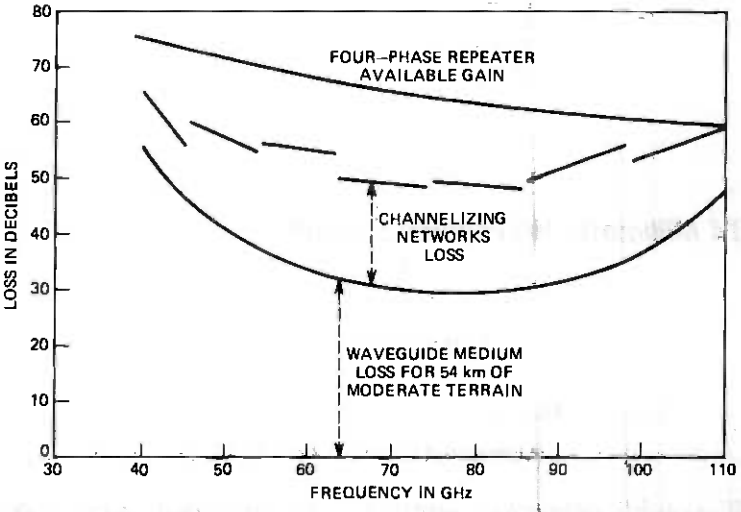

Fig. 1—Moderate-terrain transmission medium loss and projection of available gain.

nelization was laid out so that the lowest frequencies would be dropped first. A filter configuration to accomplish this and to separate all 124 mm-wave channels into individual ports is shown on Fig. 2. There are three types of filters used in this network; bandsplitting filters, channel dropping filters, and low-pass filters. The portion of the array closest to the transmission medium contains the six band-splitting filters and separates the 40 to 110 GHz frequency spectrum into seven subbands each about 15 percent wide. This portion of the array maintains the signals in the circular electric mode in 2-inch diameter waveguide so the losses are quite low. Each of the seven subband signals then goes through a taper transition to small semicircular waveguide. The semicircular waveguide runs have from 12 to 21 tandem connected channel-dropping filters. Each filter separates out one 475-MHz-wide channel via resonant cavities which couple from the flat wall of the semicircular waveguide to a dominant mode rectangular waveguide. When the band above 75 GHz is used for transmitters and the one below is used for reception, the low-pass filters prevent leakage of high-frequency transmitter signals into low-frequency receivers. The frequency assignments of the 124 channels are given in Table I.

The 40.2-GHz channel-dropping filter is connected closest to the band splitter so the 40.2-GHz signal passes through only one band splitter, one low-pass, and one channel-dropping filter. The other channel-dropping filters in subband 1 are connected in order of ascending frequency so that, as frequency increases, so does the number of filters traversed. In subband 7, the 109.8-GHz channel is dropped first in the string of channel-dropping filters so the loss and number of filters tra-

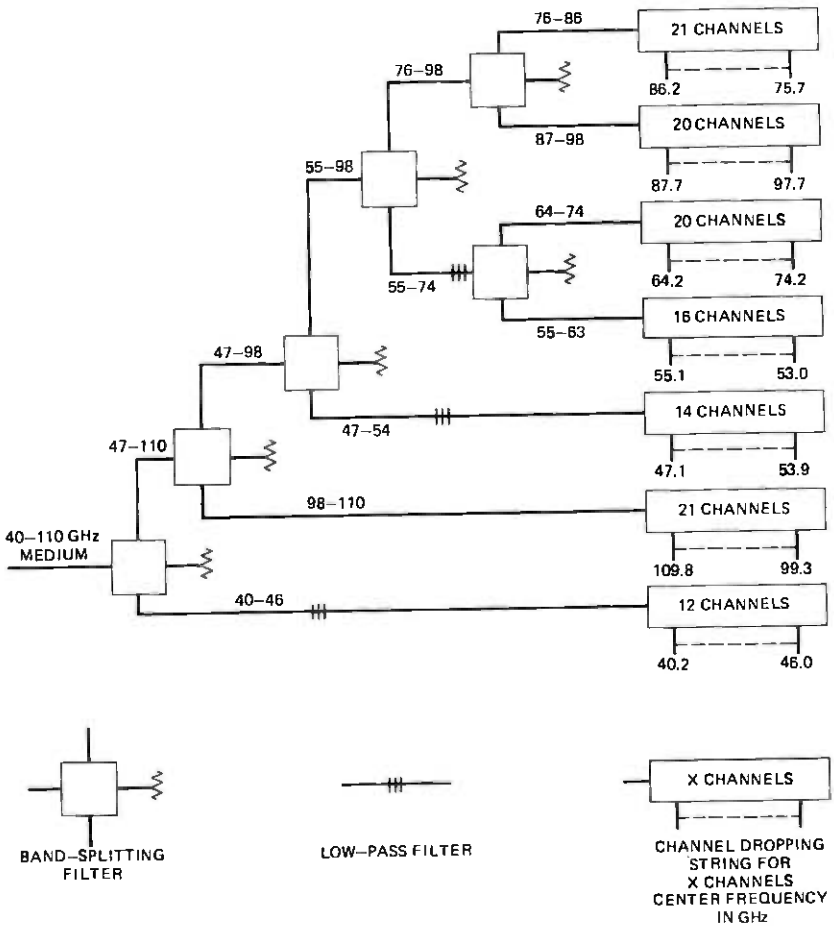

Fig. 2—Channelizing array.

versed increases as the frequency is lowered. The 109.8-GHz channel passes through two band splitters and one channel-dropping filter. This channelizing network layout, therefore, gives the lowest possible loss to the 40.2-GHz channel with slightly higher loss to the 109.8-GHz channel and increasing loss as frequency is moved toward the band center. This, of course, complements the shape of the transmission medium loss so as to obtain maximum repeater spacing.

The design of the individual filters will now be described.

II. BAND DIPLEXER

The band diplexer filters must separate subbands with low loss (at least near the band edges), and they also provide the means for physical

Table I — WT4 channel center frequencies

Subband	Channel	Frequency
1	1	40.235
	(12 channels)	
	12	46.010
2	13	47.085
	(14 channels)	
	26	53.910
3	27	55.085
	(16 channels)	
	42	62.960
4	43	64.235
	(20 channels)	
	62	74.210
5	63	75.740
	(21 channels)	
	83	86.240
6	84	87.715
	(20 channels)	
	103	97.690
7	104	99.265
	(21 channels)	
	124	109.765

All channels spaced 525 MHz within one subband.

separation of the groups of repeaters in the different subbands. In order to minimize loss both in the filters and the interconnecting waveguide it is advantageous to retain the low-loss circular-electric mode in oversized circular waveguide for the band diplexers. Figure 3 shows the Michelson interferometer diplexer[1] consisting of two hybrid junctions, two high-pass filters, four tapers, and two elbows. The function of the hybrid junction is to split the input signal equally between two output ports with no coupling to the fourth port. The high-pass filters provide the frequency separation with unit reflection below cutoff and very small reflection above cutoff. The tapers provide low reflection and low-mode conversion transitions between different diameters and the elbows are necessary to physically complete the structure.

2.1 Hybrid junction

The hybrid junctions used in the field evaluation test consist of the four port networks formed by the right-angle intersection of two oversized circular waveguides with a thin sheet of dielectric material with dielectric constant ϵ and thickness τ inclined at 45 deg across the junction. An ideal hybrid must (*i*) be lossless, (*ii*) have all ports matched, (*iii*) divide an input signal equally between two output ports, and (*iv*) have

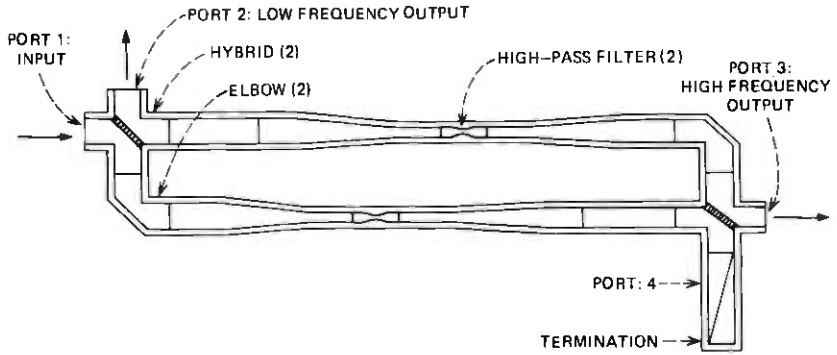

Fig. 3—Band-splitting filter.

phase quadrature between the output ports and have the fourth port decoupled. Since the waveguide is highly oversized, this structure can be analyzed as a quasioptical device, and properties (*ii*) and (*iv*) can be attained rather easily. The choice of ϵ and τ for each hybrid junction must be made to meet requirement (*iii*). If ϵ and τ are kept fixed across the junction for ease in manufacture, then there is a small (¼ dB) loss penalty associated with conversion of energy to other modes. Each band diplexer operates over a different frequency band depending on its position in the array, and the hybrids on each end of a band diplexer also operate over different frequency bands. The dielectric sheet (ϵ and τ) for each hybrid junction is chosen to optimize the return loss and insertion loss for each band diplexer. For the field evaluation test, the values of ϵ ranged from 6.5 to 8.7 and the thickness varied from 0.013 inches to 0.017 inches.

2.2 High-pass filters

The high-pass filter is a section of smoothly tapered waveguide whose diameter varies from 0.375 inch at both ends down to a diameter corresponding to the cutoff of the TE_{01}^0 mode at a subband edge frequency. The overall length is 6 inches. Six guard bands ranging from 600 MHz to 1100 MHz were allocated to separate the seven subbands. The filter must have an insertion loss greater than 25 dB for frequencies below the guard band and a return loss greater than 25 dB for frequencies above the guard band. In addition, the tapers must not exceed −40 dB mode conversion to the TE_{02}^0 mode over their operating band. In addition to the steep cutoff and low mode conversion, the design should be easily programmable to permit machining of the contour on a numerically controlled machine. Consequently, a satisfactory solution is one where analytical expression can be used to describe a contour and in which a good compromise can be made between the filter cutoff shape and mode

conversion. Literature[2] has established the theory of high-pass filter designs having a sharp cutoff and a good return loss in the pass band. However, this filter synthesis technique is strictly applicable to only single mode waveguide. Over portions of the WT4 band, the 0.375 inch diameter waveguide can propagate TE_{02}^0 and TE_{03}^0 and other higher-order modes. To include mode conversion coupling in a rigorous method of filter design would be very difficult. However, an adequate approximation can be obtained by the following procedure.

Several simple functions to describe impedance variation along the axis have been studied in the literature.[3] Among these the exponential function raised to the cosine nth power is of special interest. For $n = 2$, combined with proper parameters, the filter was shown to have an optimum return loss cutoff characteristic. However, the contour of this filter design has rather steep slope which in turn causes severe mode conversion. A larger value of n deviates from optimum cutoff but yields a design with better mode conversion. (Mode conversion was computed using an analysis program for a given contour.) By successive iterations, it is possible to determine a proper value of n to meet the requirement. The six pairs of high-pass filter design have their n value varying between 3 for the low-frequency band and 6 for the high-frequency band.

2.3 Tapers

The taper changes a 2-inch diameter waveguide to a 0.375-inch diameter and is designed to have less than −40 dB mode conversion to the TE_{02}^0 mode and 40 dB return loss over the 40 to 110 GHz band.[3] It has an inner layer of helically wound insulated wire and a lossy jacket on the outside. This suppresses all noncircular electric modes generated in the hybrid junction. The overall length is about 21 inches.

III. LOW-PASS FILTER

The low-pass filter structure used in the WT4 system consists of a parallel array of transverse dielectric disks in a section of circular TE_{01}^0 mode waveguide. If the material of each dielectric disk is homogeneous and isotropic there will be no mode conversion from TE_{01}^0 to any other modes, either propagating or nonpropagating. This yields the particularly simple equivalent circuit for the disk of simply a change in characteristic impedance for the TE_{01}^0 mode with no coupling to other modes and no discontinuity reactance at the disk boundaries. In addition, because the waveguide is highly oversized for most of the modes concerned in the design, the waveguide can be regarded as nondispersive. The stop band of the filter rejects not only the TE_{01}^0 mode but also most of the other modes which might exist in the system. This is a very desirable feature for components used in overmoded applications.

A detailed exact design procedure based on these simple transverse disks has been published elsewhere.[4] All known filter synthesis techniques are applicable. The image method will produce a simple structure if the desired pass band is far away from the cutoff frequency of the stop band. This design results in an array of uniformly spaced dielectric disks of identical thickness and, therefore, is economical for fabrication. In the case where the pass band is very close to the cutoff frequency, the image method may not yield sufficiently steep cutoff. Modern filter synthesis technique should then be used. However, the thickness of dielectric disks and their spacing will have more variations and the fabrication cost may be higher.

There are two codes of low-pass filters in the system. The first one has a pass band from 40 to 54 GHz and an insertion loss requirement of 80 dB from 76 to 110 GHz. The second code has a pass band from 55 to 74.5 GHz and a stop band from 76 to 110 GHz. The choice of dielectric material is mainly determined by the bandwidth of the stop band. In our cases, fused quartz was chosen. The first code uses 30 disks for the filter section and two 3-disk matching sections at the ends. The second code uses a 22-disk Chebyshev design. Excellent agreement between the theory and measurement was observed. The filter is constructed with two diameters of metallic rings (2.000 and 2.010 inch ID) stacked up alternately. Quartz disks of 2.010 inch diameter were inserted between rings. Although all parts require high precision on their thickness, they are readily manufactured due to their simple geometry. The pass band insertion loss was measured to be about 0.1 dB and pass band return loss was about 25 dB.

IV. CHANNEL DIPLEXER

Design of a millimeter-wave channel-dropping filter is, in principle, no different from the design of conventional waveguide filters except for an emphasis on low loss. At millimeter wave frequencies, filter structures designed in single mode rectangular waveguide have high loss for both the through channels and the dropped channel. Oversized semicircular waveguide has one-third the loss of single-mode rectangular waveguide, but mode cutoffs must be avoided in the passband. With an 18 percent bandwidth located between cutoffs of the TE^0_{12} and TM^0_{31} modes, seven sizes of semicircular waveguide are required to cover the 40 to 110 GHz band. Because of the nonzero longitudinal magnetic field along the axis of semicircular waveguide, circular electric modes (TE^0_{on}) can be discriminated from all other modes. Narrow rectangular apertures along the center axis provide convenient and practical couplings between the main guide and the resonant cavities (see Fig. 4). With the diameter chosen so that TE^0_{02} is below cutoff, theoretically, there is no moding problem at all.

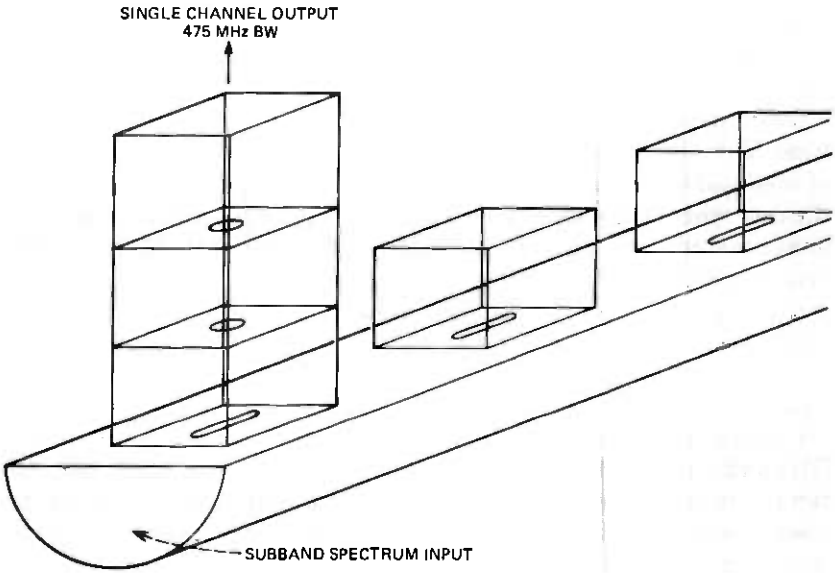

Fig. 4—Channel-dropping filter.

The channel diplexer used in WT4 is a two-pole design[5] with a 3-dB bandwidth of 475 MHz. There are seven sizes of semicircular waveguide, one for each subband. The dropped channel port is in rectangular waveguide. Only three sizes are used: WR22 covers 40 to 50 GHz, WR15 covers 50 to 75 GHz, and WR10 covers 75 to 110 GHz. For easy construction, the channel diplexer is divided into three main parts. A main guide block contains the semicircular channel. The coupling plate provides the top wall of the semicircular guide, three coupling holes and half of the four cavities. The tuning plate contains the other half of the four cavities and slots for tuning elements. There is a transducer block at the output port to provide a transition to the correct waveguide size. A sealing gasket, a protective cover and connecting hardware complete a channel diplexer. The coupling plate, the tuning plate, and the transducer block, which require a high degree of dimensional precision, are obtained by electroforming copper on permanent mandrels. The remaining parts are obtained by conventional machining. The mandrels are produced by high-precision, two-dimensional profile grinding operations. The use of permanent mandrels is a key to the manufacture of channel diplexers at a reasonable cost.

Thirty channel diplexers were built and tested for the field evaluation test. The input port return loss is about 20 dB over each subband. The dropped channel loss of the field evaluation test model at 108.7 GHz was about 0.8 dB above our objective of 2.8 dB.

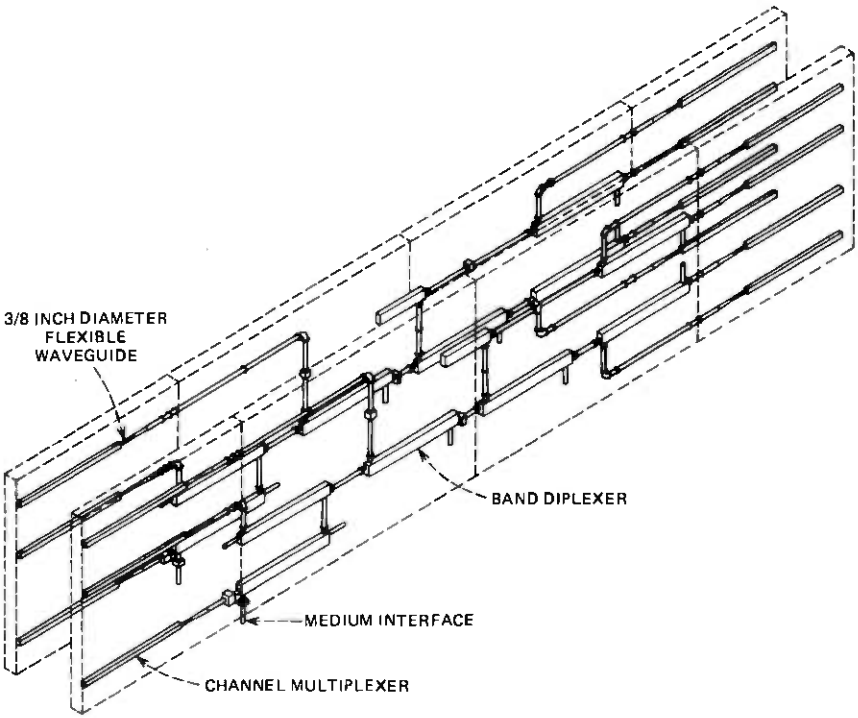

Fig. 5—WT4 channelizing networks.

V. CHANNELIZATION NETWORK PHYSICAL DESIGN

The band diplexers and channel filters that constitute the WT4 channelization networks are contained within two large frameworks each 43 feet long, 7.9 feet high and 1 foot deep (Fig. 5). Band-splitting elements and low-pass filters are mounted in the two center frames while the outer-frames contain the channel multiplexer assemblies and provide the mountings for repeaters and water-cooled channels. One network is provided at a repeater station for each waveguide medium direction. For each channel a receiver and line equalizer is mounted on one network framework while the associated transmitter is mounted on the second framework opposite the receiver (Fig. 6). Connections between the two are made at baseband frequencies via a coaxial cable. Figure 7 is a photograph of the field evaluation test band diplexer network.

5.1 Band diplexer assembly

The band diplexer assembly consists of the filters and interconnection sections of mode suppressing helix waveguide that split the waveguide bandwidth into seven subbands. The network components are mounted

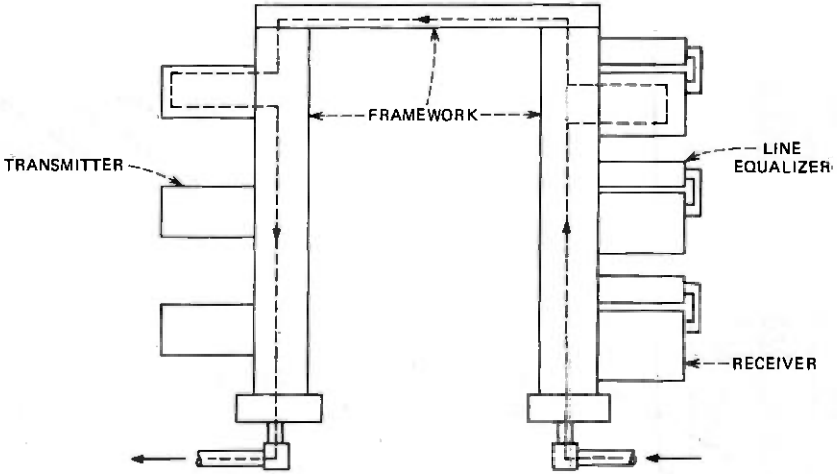

Fig. 6—End view of repeater mounting on channelization network frame.

on the frame starting with the component that interfaces with the medium. The band diplexer components are somewhat sensitive to mechanical stress so every effort is made to provide all connections as stress-free as possible. A large series of helix waveguide spacers are available to insure that the subband outputs are in the prescribed po-

Fig. 7—Band diplexer assembly.

sitions and that there is not an excessive tolerance buildup. Six-degree-of-freedom mounting brackets have been designed to simplify this process.

For shipping, the band diplexer assembly can be disassembled into four sections. As an option, the entire network can also be shipped as one unit. During the field evaluation test, the reassembly of the four sections in the Netcong station took less than one day.

5.2 Channel diplexer and repeater frames

The repeater and channel diplexer frames are installed in the repeater station at the same time as the band diplexer assembly. These frames include the fuse panels, patch panels, water-cooling channels, connectorized cables, and all mounting hardware for the individual channel multiplexers as well as the repeaters. The repeaters and channel multiplexers are installed as the system grows.

To take up the residual mechanical tolerances between the channel multiplexer and band diplexer subband port, a specially developed $\frac{3}{8}$-inch-diameter flexible waveguide section is provided. It consists of helix waveguide supported in a lossy flexible epoxy which allows offsets up to $\frac{1}{4}$ inch.

5.3 Channelization network environmental control

The entire channelization network is pressurized to $\frac{1}{6}$ psig with dry nitrogen. The gas is provided via a manifold mounted in the diplexer array. A waveguide window placed at the input to the network isolates the network from the higher pressure of the medium. The nitrogen supply system was designed to maintain the desired pressure relative to the local atmospheric situation. This was necessary because the low-pass filters are quite fragile and sudden changes in pressure across the quartz plates could cause a failure.

The water-cooling channels consist of rectangular extruded aluminum channels with two circular passages. Only one passage is required; the second is provided in the unlikely event that the first becomes clogged. Temperature monitors are mounted on the cooling channels, which are tied into the chilled water control and alarm system. The system has worked for over two years at Netcong without any malfunctions.

VI. CONCLUSION

Two channelization arrays have been constructed and one installed at each end of the field evaluation test waveguide run in northern New Jersey. Each end has a complete array of band-splitting filters to divide the 40 to 110 GHz spectrum into seven subbands. There were 18 channel-dropping filters installed at one end and 12 at the other end. The

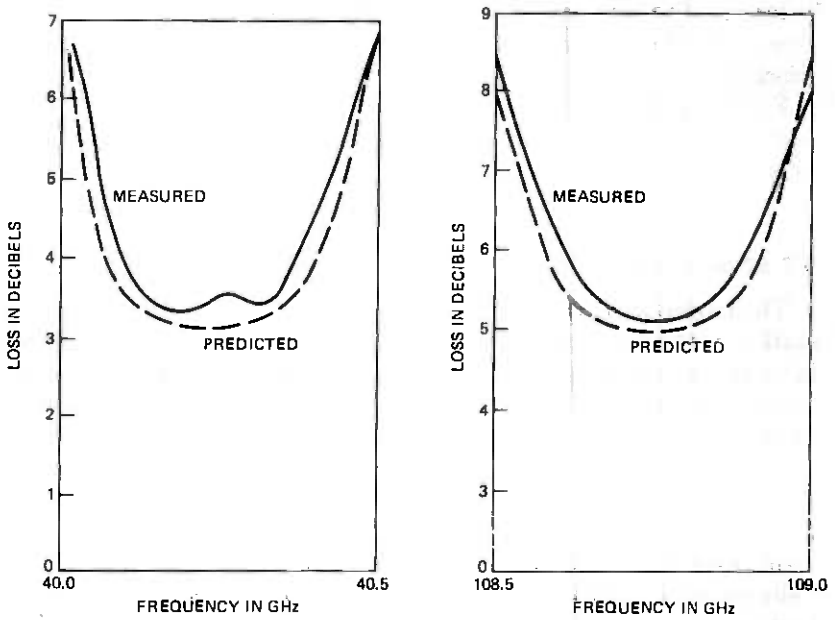

Fig. 8—Experimental measurement and prediction of channelizing network loss for channels at low end and near high end of spectrum.

transfer functions were measured for all 30 channels from the circular waveguide input port to each rectangular waveguide output port. Various leakages and return losses were also measured. The measured data agreed quite well with what would be expected from summing the performance of the individual filters. (See Fig. 8.) The performance of the two trial models indicated that a complete array for 124 channels would meet the performance requirements for either a two-phase or four-phase WT4 system.

The channelization filters described for the field evaluation trial operate in the 40 to 110 GHz range. However, measurements of the transmission medium[6] show that severe loss peaks could be avoided by shifting the highest WT4 channel to below 105 GHz. Simultaneous lowering of the bottom channel to 35 GHz would result in greatly increased medium loss for this lowest channel. If the number of millimeter-wave channels (124) is to be held fixed, then the only way to lower the top and not the bottom frequency is to move the channels closer together by reducing the guard bands. The field evaluation test measurements confirmed that 525-MHz spacing between adjacent channels was more than adequate to avoid appreciable adjacent channel interference. Studies have been made of the effect of changing the frequency assignments of Table I to a 500-MHz channel separation and also reducing the spacing between subbands slightly. The recommendation

resulting from these studies is to provide 124 WT4 channels in the frequency range of 38 to 104.5 GHz. The penalty associated with the reduced channel spacing is less than 1 dB in the repeater available gain.

ACKNOWLEDGMENTS

A large number of people contributed to the design, construction, testing, and installation of the channelizing networks. Some of these people are listed in the references, but the authors would like to extend their particular thanks to R. F. Wessling, C. L. Ren, R. P. Hecken, F. G. Joyal, G. M. Blair, P. W. Nield, P. A. Sakash, and N. K. Sharma for their work on the filters and to D. N. Zuckerman, W. G. Thompson, S. Shapiro, H. H. Weinreich, and B. T. Verstegen for their efforts in assembling and testing the channelizing array.

REFERENCES

1. E. A. J. Marcatili, D. L. Bisbee, "Band-Splitting Filter," B.S.T.J., *40*, No. 1 (January 1961), pp. 197–212.
2. C. C. H. Tang, "Nonuniform Waveguide High-Pass Filters with Extremely Steep Cut-off," IEEE Trans. Microw. Theory Tech., *MTT-12*, May 1964.
3. R. P. Hecken and A. Anuff, "On the Optimum Design of Tapered Waveguide Transactions," IEEE Trans. Microw. Theory Tech., *MTT-21*, June, 1973, pp. 374–380.
4. C. L. Ren and H. C. Wang, "A Class of Waveguide Filters for Over-Moded Applications," IEEE Trans. Microw. Theory Tech., *MTT-22*, December, 1974, pp. 1202–1209.
5. C. L. Ren, "Design of a Channel Diplexer for Millimeter-Wave Applications," IEEE Trans. Microw. Theory Tech., *MTT-20*, December, 1972, pp. 820–827.
6. J. C. Anderson, J. W. Carlin, D. J. Thomson, T. J. West, and D. T. Young, "Field Evaluation Test—Transmission Medium Objectives," B.S.T.J., this issue.

THE BELL SYSTEM TECHNICAL JOURNAL
Vol. 56, No. 10, December 1977
Printed in U.S.A.

WT4 Millimeter Waveguide System:

Protection Switching, Auxiliary Communication, and Maintenance

By M. J. BONOMI, P. BROSTRUP-JENSEN, D. R. MARCOTTE, R. W. MUISE, and P. J. TU

(Manuscript received April 7, 1977)

A statistical analysis shows two-way reliability of 99.98 percent or better for the WT4/WT4A system with two automatic protection channels and one manual patch channel for every 59 working channels and 20-year life expectancy for the repeaters. The feature of adding and dropping fully protected channels at intermediate repeater stations in a protection span is included. The equipment is divided into three bay arrangements: (i) span-terminating transmission bays which contain protection switches, performance monitors, and all interfaces with the high-speed communication signals as well as the auxiliary signals, (ii) the logic and control bays for the protection switching, and (iii) the order wire, telemetry, and fault locate bays. All auxiliary signals ride piggyback on special housekeeping bits in the broadband channels; double-ended access is therefore provided for the telemetry to ensure reliability. Fault locating is fully remoted and intended to operate with automated SCOTS systems. Typical, but partially equipped, bay arrangements were tested in the field evaluation test and were found completely satisfactory.

I. INTRODUCTION

The WT4/WT4A system[1] is intended to interconnect major traffic nodes in the toll transmission network. Figure 1 is a layout of such a span. Main repeater stations are located at the ends of the span and a number of important functions must be provided by span terminating bays at these locations. An obvious one is the interface with the rest of the Bell System. This function is performed by the cross-connect bays and the

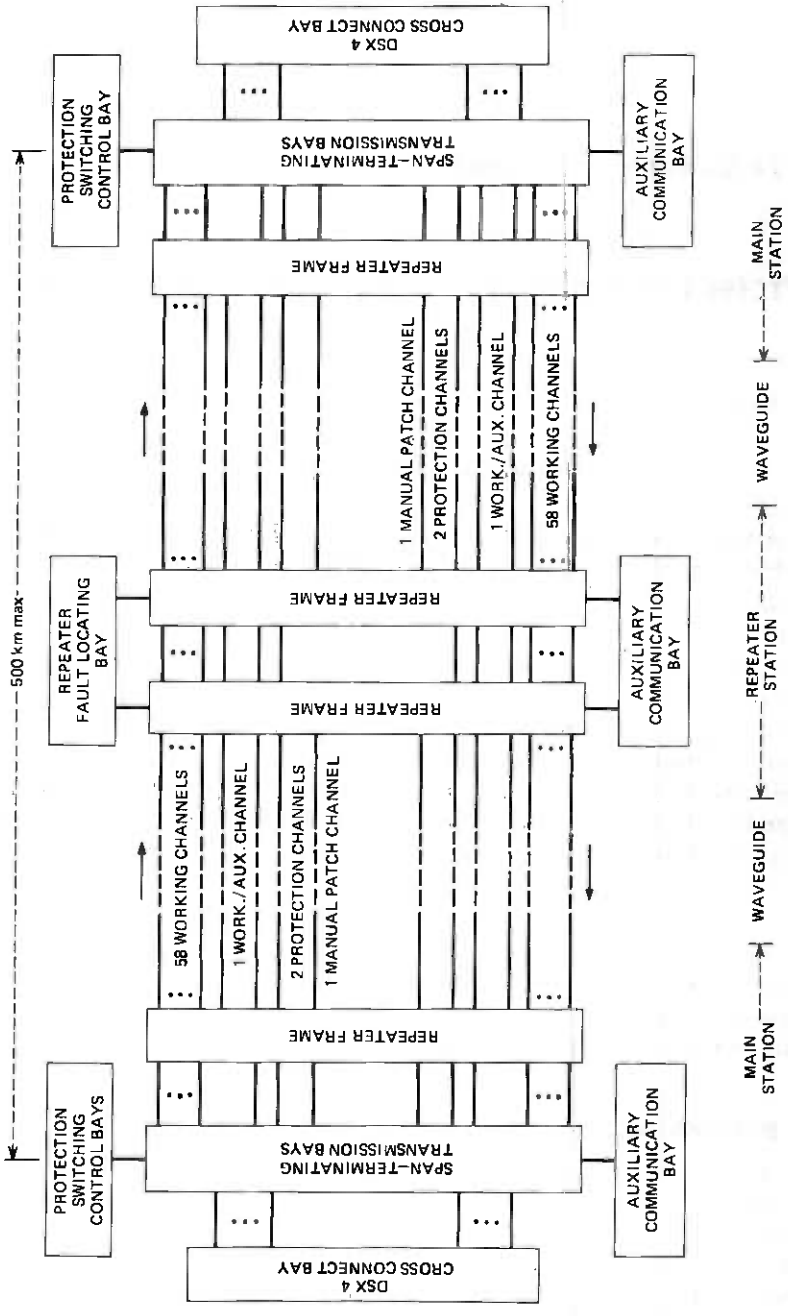

Fig. 1—Layout of protection span.

span-terminating transmission bays. The DSX-4 cross-connect bays are bays where all channels have baseband jack appearances; they serve to interconnect channels and route traffic in and out of the system.

Another function is protection switching. Protection switching must be provided at the ends of the span in order to keep the probability of service interruptions, or outages, on these important routes to a very small number. This is done by automatically transferring the traffic from any failed working channel to hot stand-by channels very rapidly ($\leq$100 ms).

In most other systems, all repeaters are identical and a reasonable number of spares can be strategically located to allow fast replacement of failed units and, thus, fast release of the protection channels. The WT4 system,[2] on the other hand, has 124 different repeater codes according to channel frequency; this calls for an impractically large number of local spares. Instead, WT4 is unique in using a manual patch channel. Unlike a protection channel which can be accessed only at the ends of the whole span and protect only one failure at a time, the patch channel is a hot stand-by channel which can be manually accessed at any intermediate repeater station within a span. It can be used to bridge any failed repeater in a hop by patching at the two ends of the hop at baseband where the signal format is the same in all repeaters. This temporary patch frees the protection channel, allows removal of the failed transmitter-receiver pair, and provides adequate time for a replacement pair to be sent from a large central spare depot. The power of a manual patch channel lies in the fact that pieces of it can be used to temporarily bridge many failed repeater hops as long as there is only one failure per hop. The statistics are such that two automatic protection channels and one manual patch channel in protection spans of 500 km will satisfy the Bell System objective of 99.98 percent availability per 6000 km of a fully loaded system. This assumes that the repeater has 20-year life, that it takes maintenance personnel 10 hours to establish a manual patch, and that it may take 300 hours before a permanent replacement repeater arrives and frees the patch channel. These numbers are operationally and economically reasonable.

There are also cases where it would be desirable to add and drop some of the traffic at points within a span. To meet this demand, the protection switching system allows for full protection switching of such add/drop channels at up to six add/drop stations within a span. Through-channels are completely unaffected; in fact, the entire topology is totally flexible.

Protection switching signaling, maintenance telemetry and commands, and operating personnel order-wire communication create a sizable need for auxiliary communications within a span. All these communications ride piggyback on some of the broadband channels by using special

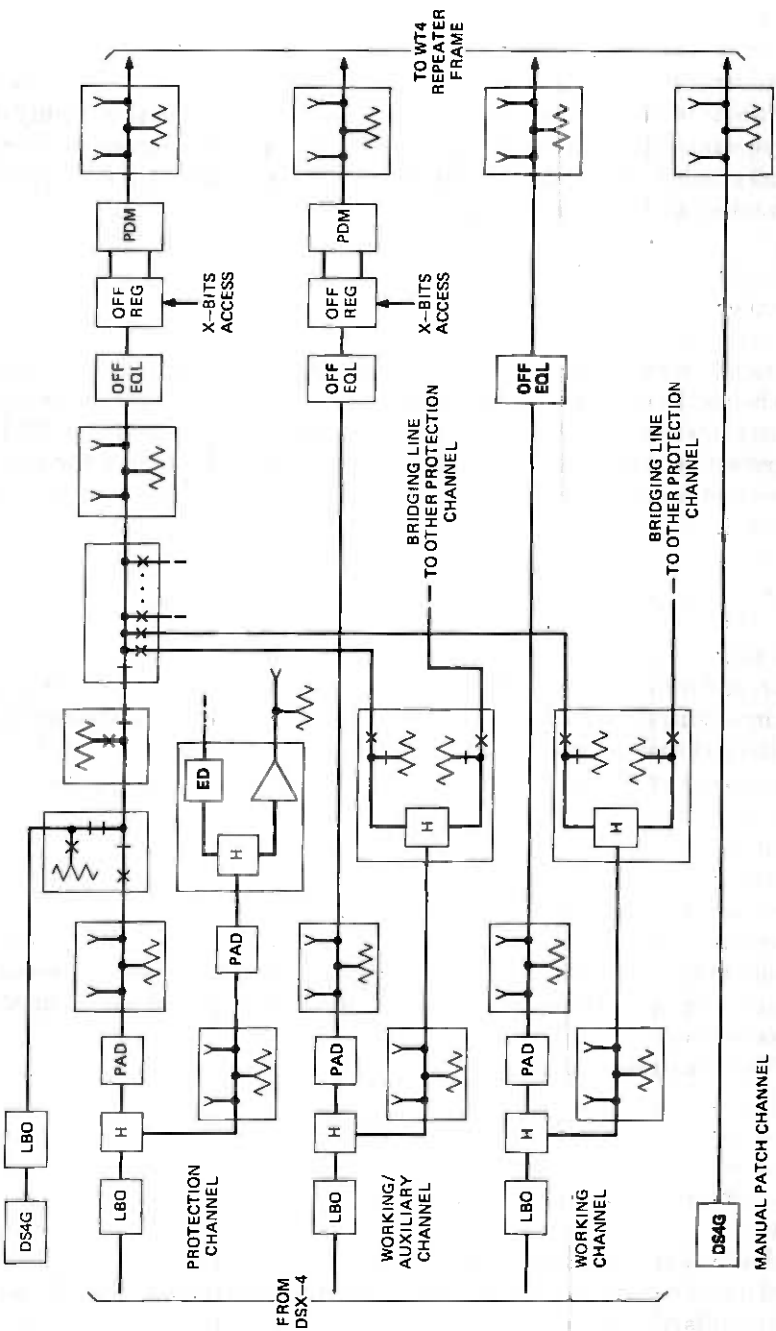

Fig. 2—Transmit section.

housekeeping bits supplied in the 274 Mb/s DS4 baseband format for just these kinds of purposes. This is an arrangement modeled after the T4M system.[3] For the WT4 system it provides inexpensive, fast, and highly reliable auxiliary communication because the signals travel inside the sheathed waveguide as opposed to a separate, repeatered multipair cable on the outside. The bits are referred to as X bits. They are used in triplets with majority decision and provide an extremely rugged bit stream with a total capacity of 58.3 kb/s per DS4 signal. The T4M system has developed a Protection Data Multiplex (PDM) unit which provides for insertion of the X bits and a Violation Monitor and Remover (VMR) which monitors the parity checks in the DS4 signal, removes any violations of the parity checks (but not the errors, themselves) and, as a by-product, extracts the X bits for reception. By inserting these units in the baseband portion of any WT4 channel, such as a channel can be used as a carrier of X bit auxiliary communication.

The protection switching system uses X bits on the protection channels in the opposite direction to carry the required signaling from the tail end of a span to the head end of the span and to any add/drop stations in between. The maintenance telemetry/command system and the order wire share the X bits on one of the broadband working channels, the working/auxiliary channel.

II. THE SPAN TERMINATING TRANSMISSION BAYS

The two-phase version of the WT4 system has 59 working channels. The two automatic protection channels serve most of the time as hot standby channels but on command may be accessed as additional working channels. When not carrying traffic, the protection channels (and the manual patch channel) are driven by a line drive signal consisting of a pseudorandom signal imbedded in a DS4 format.

Figure 2 shows the high-speed signal path through the transmit section for each type of channel. The DS4 signal first passes through a line build-out network (LBO) followed by a 3-dB splitting hybrid. The LBO is selected so that the total length from DSX-4 to LBO output is electrically equivalent to 50 m of 728A cable. The hybrid splits the signal into a through path and a bridging path that carries the signal through switches to the two protection channels. The signal in the through path is next passed through an equalizing network (OFF EQL) designed to restore the pulse shape in preparation for regeneration. For the working channel, the regeneration occurs in the transmitter located in the repeater frame, but for the protection and working/auxiliary channels the signal must pass through a regenerator-protection data multiplex (PDM) pair for X-bit access. The regenerator provides the data and clock levels required to drive the PDM. Jacks are provided to manually jump the bridging circuits in the event of a switch failure.

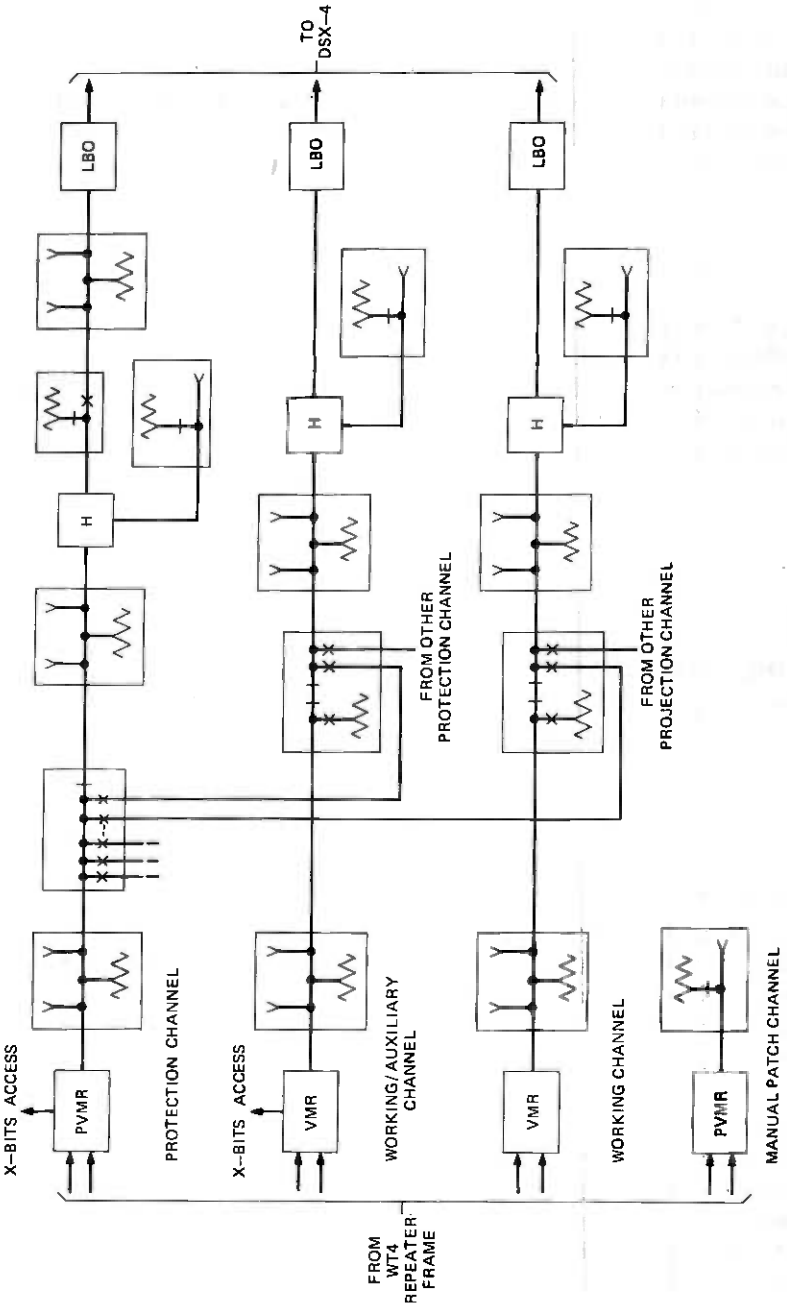

Fig. 3—Receive section.

In the receive section, Fig. 3, each channel passes through the violation monitor and remover (VMR) circuit for performance monitoring and X-bit access. The (P) signifies that the VMR also can detect the differences between a DS4 and a line drive signal. After monitoring, the DS4 signal passes through an LBO circuit similar to that in the transmit circuit. A hybrid and jack are provided at each output for maintenance purposes.

Four types of span-terminating transmission bays were designed: a 2×3 and a 0×10 bay for the protection switching station, and a 2×3 and a 0×10 bay for the add/drop station. The 2×3 bay contains the equipment associated with both the transmit and receive section for the two protection channels, the one working/auxiliary channel, two working channels, and the manual patch channel. The 0×10 bay contains ten working channels (transmit and receive section). Interbay cabling is necessary between these bays to complete the protection switching paths.

III. THE PROTECTION SWITCHING CONTROL BAYS

3.1 Overall system operation

A simplified block diagram of a typical one-way switching section using a typical protection switching arrangement is shown in Fig. 4. Transmission is from main station A to main station B over the 59 regular channels and protection channels X and Y. All of the switching in the section is done at baseband (DS4) by means of the reed switches located in the span terminating transmission bays. The head-end and receive-end switch networks are shown symbolically as single-pole, double-throw switches. The operations are similar to other 400-type protection switching systems.[4]

If the bit error rate of the incoming signal exceeds 10^{-6}, a switch request is generated for a working channel or a switch inhibit order for a protection channel. When a working channel VMR requests a switch, the receiving end logic determines whether a protection channel is available. If it is, a switch order is sent to the transmitting end, decoded, and the failed working channel bridged to the selected protection channel.

The transmitting end bridge provides transmission on the working as well as the protection channel simultaneously and also removes the DS4 line drive signal from the protection channel. The absence of this uniquely identifiable signal is a notification to the receiving end logic that the bridge at the transmitting end has been made. A receive end transfer is then made from the regular to the protection channel.

When the working channel again becomes good, the receiving end switch is restored to its normal state and a bridge release order is sent to the transmitting end. This reinserts the line drive signal on the pro-

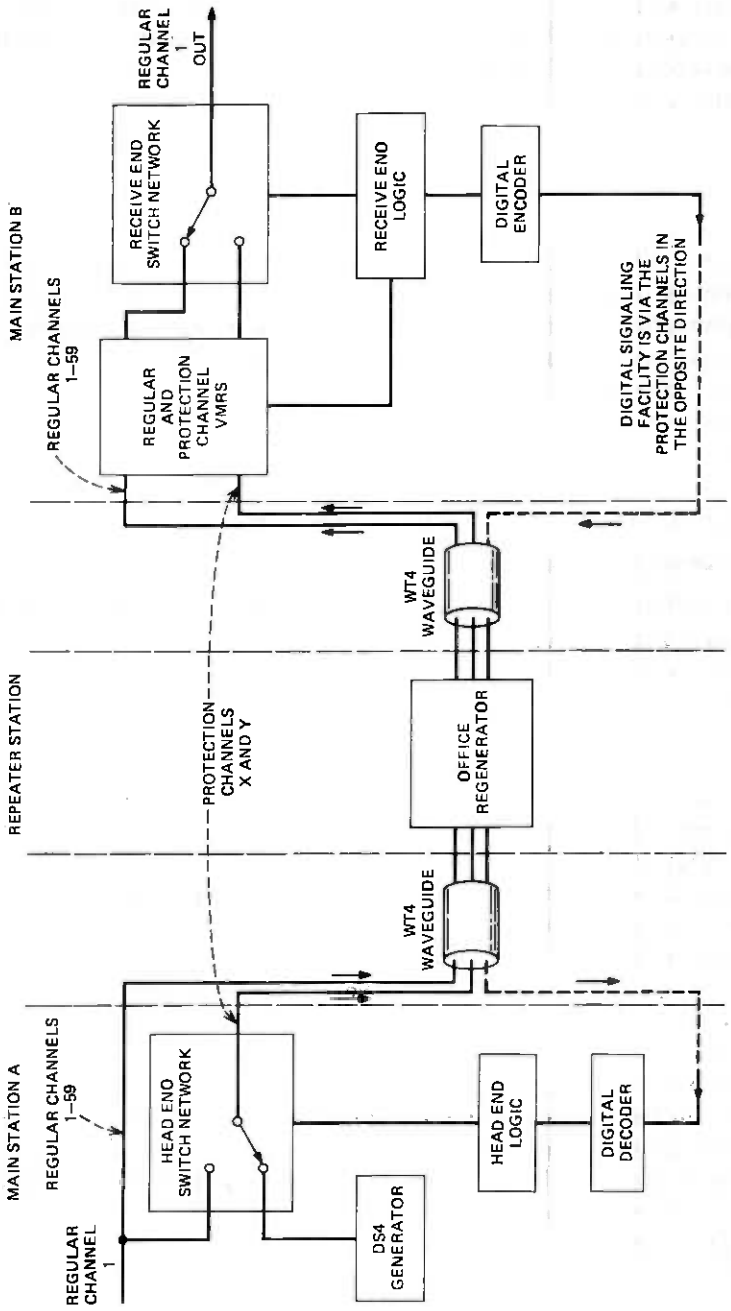

Fig. 4—Switching section—simplified block diagram.

tection channel and returns the system to its quiescent state. If the protection channels are accessed for use as additional service-carrying channels and such access service on protection channel X fails, an access switch request to protection channel Y is generated.

An actual operating test is the only effective way of checking for "quiet" failures. Once every 30 minutes, or on request, the 400A exerciser automatically tests all of the switching logic at both ends of the system and the signaling channel by a test sequence which includes head-end bridges from every channel to both protection channels. Operation of the receiving end switch is inhibited to prevent unnecessary transmission hits.

3.2 Signaling

The 400D signaling equipment is highly reliable since each switch order consists of a two-out-of-six codeword as well as three station address bits and a parity bit. Each station along the route is assigned a station address and within a station each channel is assigned a slot position in the bay. This switching topology is used with or without the add/drop feature. If the receiving end logic does not obtain verification that a switch operation is completed within a certain time interval, a switch order is originated to the second protection channel. If the second protection channel is not available, a service fail alarm is generated. Similarly, if an order to take down a switch is not carried out in the required time interval, the receiving end switch is held-operated and maintenance personnel are alerted. Any abnormal sequence of events, regardless of its origin, is processed, identified and translated to a warning to the maintenance personnel.

3.3 Manual control and alarms

Transmission through the WT4 system may be controlled by the operating personnel directly by operating the manual switch controls which are located at the receive end only. Manual control is used to set up access to the protection lines and to induce or lock-out switching as part of normal maintenance. An additional form of manual control independent of the logic operations is also used. It is called forced switching and places the transmit and receive switches under direct control of the operator. This is useful if the system malfunctions.

Since the major portion of the system control and logic is located at the receiving end of the system, most alarms are also initiated there. Forced switching is the only manual function performed at the transmitting end and there are only two alarms.

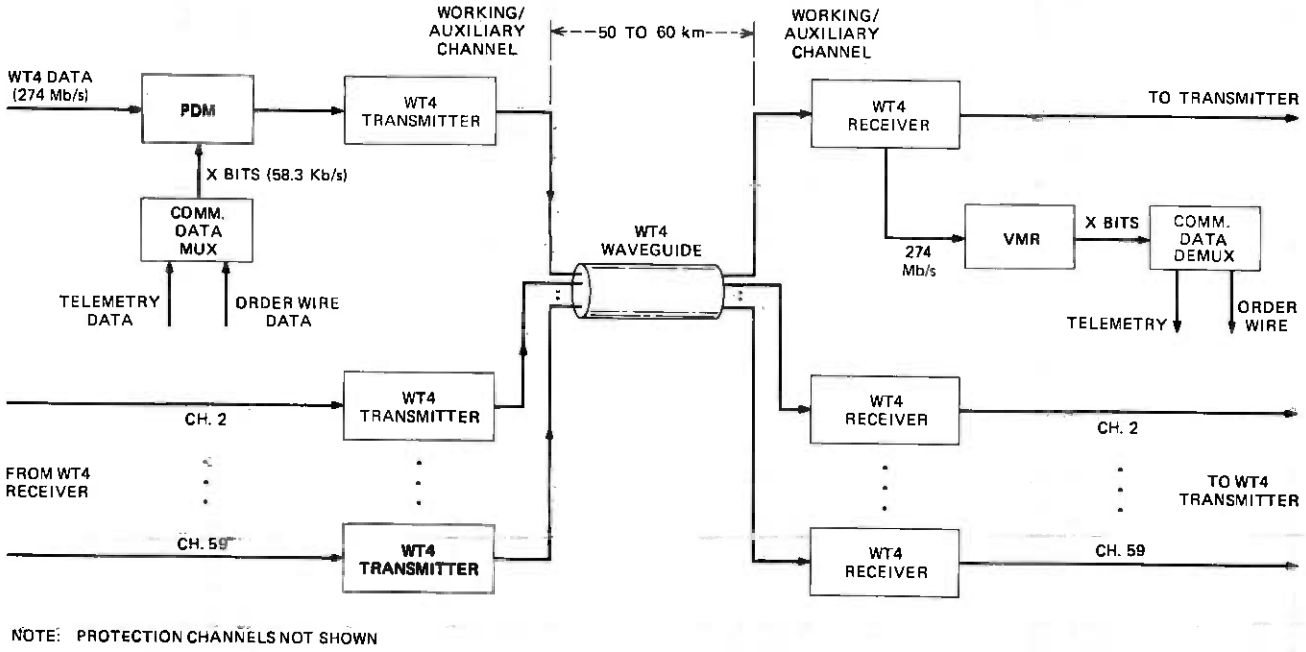

Fig. 5—Auxiliary communication via waveguide.

IV. THE AUXILIARY COMMUNICATION AND FAULT LOCATING BAYS

4.1 Telemetry and order-wire needs

WT4 electronics, waveguide pressurization equipment, power plant and converters, span terminating and protection equipments, building air conditioning and security must all be monitored and controlled by telemetry. Definite sequences of status polling and switch actions for fault locating and alternate telemetry access present further demands. All these functions can best be handled by a computerized control system such as SCOTS[5] (Surveillance and Control of Transmission Systems). The order-wire system interconnects all the WT4 stations in one maintenance area as well as the SCOTS central. Figure 5 illustrates the transmission of telemetry and order-wire data through one hop of WT4 waveguide. Every hop of the working/auxiliary channel is equipped this way. The two data signals are first time-division multiplexed in the CDM (Communication Data Multiplexer) to form the 58.3 kb/s X-bit data stream. At the receiving end of the hop, the high-speed data is amplified and detected by the WT4 receiver and sent to the VMR circuit, which extracts the X bits. Finally, the CDD (Communication Data Demultiplexer) separates the telemetry and the order wire circuits.

4.2 Telemetry network configuration

A typical WT4 telemetry network using E2A[6] remotes and a SCOTS central is shown in Fig. 6. The computerized SCOTS central interfaces with point-to-point private data lines to two WT4 protection switching stations via data sets. At the protection switching station, the received E2A format is converted to bits suitable for transmission via the X-bit format. The bits are received at all succeeding stations, converted back to the original E2A format, and sent to the local remote. The response data back to the central from the remotes go through the reverse process.

The central has the ability to poll the remotes cyclically for status or alarm indications and, when necessary, remotely operate switch relays.

4.3 Double access capability

The two data networks shown in Fig. 6 report to the same central computer, but are otherwise independent. The isolation switch at protection switching station B isolates one network from the other. Two remotes, however, are located at protection switching station B, and each is able to operate the isolation switch.

In the event of a transmission problem in either of the two networks, the computer reassigns the remotes beyond the trouble spot to the other

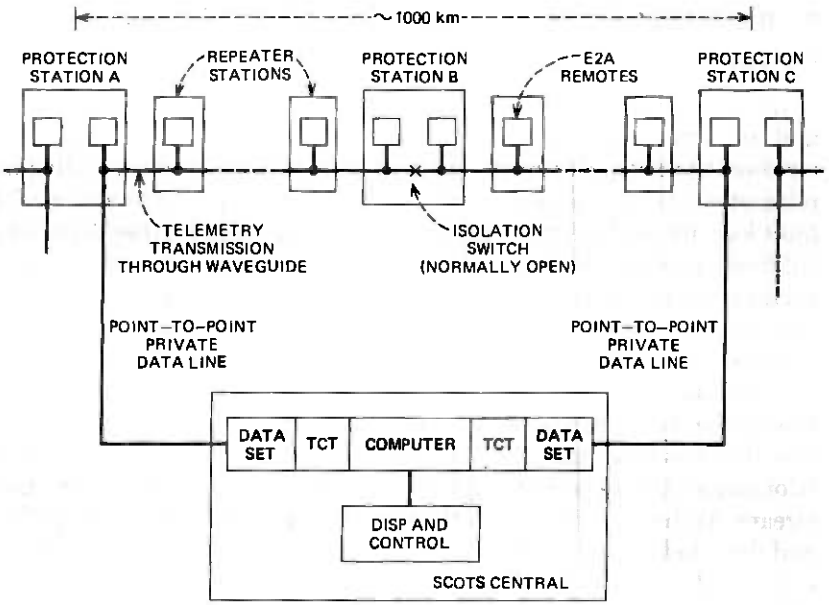

Fig. 6—Double access configuration.

network and sends a command through the trouble-free network to close the isolation switch. The closure of the isolation switch reestablishes communication between the central and the cut-off remotes.

4.4 Encoding of E2A signal

E2A uses 202T data sets which transmit asynchronous 1.2 kb/s, binary FSK (Frequency Shift Keying) signals with one tone for binary ones, another tone for binary zero, and no tone for idle.

The X bits have a transmission rate of 58.3 kb/s, but at least half of this capacity has to be allocated to order wire transmission. A maximum of 29.15 kb/s can be used for data bits. To provide the three types of data set line signals, and to avoid having to synchronize to a 1200 Hz clock, the following encoding rules were generated:

E2A data (1.2 kb/s)	WT4 data bits (≈ 29 kb/s)
1	1111 . . .
0	0101 . . .
Idle	0000 . . .

The data-bits are, therefore, a pseudo FSK signal with bit frequencies at approximately 29 KHz and 14.5 KHz.

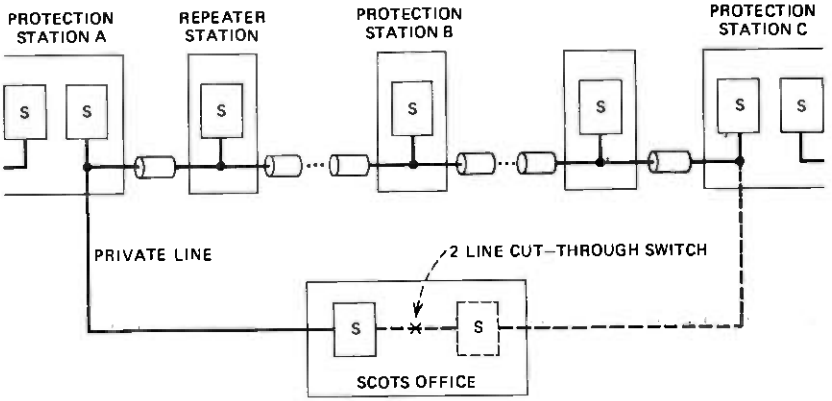

Fig. 7—Order-wire network with double access.

4.5 WT4 order-wire circuit

The WT4 order-wire network is configured in a manner similar to the telemetry network, see Fig. 7. Four-wire private lines connect the SCOTS office and the protection switching stations. Recently developed SS3 order-wire equipment with *TOUCH-TONE*® dialing is located in each station for signaling purposes. The dotted line in Fig. 7 is optional; it provides the ability to access all stations from the SCOTS office in the event of a single auxiliary network transmission failure. The two-line cut-through switch at the SCOTS office also enables stations to talk to each other despite a network cut. The cut-through switch is a special feature of the SS3 system and can be operated by dialing a special number.

Adaptive delta modulation is used to encode the voice signal into 29.15 kb/s digits. The quality of the voice signal is degraded each time it undergoes coding, and to avoid this the signal is sent through the delta modulator only when the local telephone handset is off-hook.

4.6 Repeater fault-locating bays

An important function of the telemetry in regular repeater stations is the locating of a faulty repeater.

From protection switching status information, the SCOTS central knows when a channel has failed; however, it does not know which repeater in the span has failed. It therefore issues an order to all repeater fault-locating bays to connect their Violation Monitor (VM) to the affected channel through a remotely controlled 124:1 switch array. The error rate of each repeater is reported. From this error rate profile, the central can deduce that the fault must have occurred either in the first

receiver showing poor performance or, possibly, in the preceding transmitter. Maintenance personnel is sent to perform the manual patch which frees these two failure candidates for repair. The fault locating bay can also be operated locally by the maintenance personnel to check the performance of the patch units and, later, the replacement units prior to restoring of the protection switch.

V. CONCLUSION

Representative assemblies of all the span-terminating bays were evaluated in the field trial[7] which was arranged as a "hairpin" system with Netcong "East" and Netcong "West" as protection switching stations and the trailer in Long Valley as an intermediate repeater station.

Two 2 × 3 span-terminating transmission bays were assembled and partially equipped. The PDM and VMR were identical to those used in the T4M system, but preceded by cards to align the data and clock inputs.

The protection switching control bays included primarily existing 400-type (400A and 400D) protection switching equipment and some newly designed interface circuitry. However, operationally, the system was typical of the expected final design. The system was equipped as a two-for-three system (two protection channels for three regular working channels) and although only sufficient transmission equipment for four one-way channels was available, the four channels were arranged in several different combinations in order to prove in all system criteria. The add/drop feature was not equipped on this field trial.

Four bays of auxiliary communication equipment were constructed. Two of the auxiliary communication bays were installed in the span terminating frames in the Netcong station, and one in the repeater station at Long Valley along with the fault locating bay. Implemented with double access feature for the telemetry network, the circuits in the bays were arranged according to the description given above.

The field trial results showed that all features of the span-terminating bays worked exactly as planned and the designs would be adequate to survey and maintain the WT4 system in good working order.

ACKNOWLEDGMENTS

Many people besides the authors were involved in the work described in this article. The authors particularly want to acknowledge the work in protection switching by H. D. Griffiths, C. R. Abbruscato, R. T. Cooney, F. H. Lanigan, and H. E. Menkes, and the work in sealed contact switches by R. M. Brownell, R. M. Arnold, and M. D. Tremblay. The latter was also very instrumental in repeater fault locating and auxiliary

communication along with S. H. Cureton; A. F. Caruso worked extensively on the span-terminating transmission Bays. J. J. Gainey was responsible for most of the physical design of the many different bays and plug-in units.

REFERENCES

1. D. A. Alsberg, J. C. Bankert, P. T. Hutchison, "WT4/WT4A millimeter Wave Transmission System," B.S.T.J., this issue.
2. C. E. Barnes, P. Brostrup-Jensen, E. T. Harkless, R. W. Muise, and A. J. Nardi, "Regenerative Repeaters," B.S.T.J., this issue.
3. J. M. Sipress, "T4M: New Super Highway for Metropolitan Communications," Bell Lab. Rec., October 1975.
4. H. D. Griffiths, "The 400A Microwave Radio Protection Switching Systems," Int. Conf. on Comm., ICC73, Seattle, Washington, June 1973, Conference Record, *II*, pp. 28.12–28.16.
5. Anthony Cuilwik, "Monitoring Remote Transmission Stations," Bell Lab. Rec., May 1976.
6. Robert J. Sanferrare, "E-Telemetry: Inside Story of Centralized Maintenance," Bell Lab. Rec., December 1974.
7. E. T. Harkless and R. W. Muise, "Field Evaluation Test System Performance," B.S.T.J., this issue.

THE BELL SYSTEM TECHNICAL JOURNAL
Vol. 56, No. 10, December 1977
Printed in U.S.A.

WT4 Millimeter Waveguide System:

Semiconductor Devices for the WT4 Repeater

By C. N. DUNN, O. G. PETERSEN, and D. C. REDLINE

(Manuscript received April 7, 1977)

Design, fabrication, performance, and reliability information is provided for three types of millimeter-wave diodes developed to operate over the 40–110 GHz WT4 band. A family of silicon IMPATT diodes generate the transmitter and local-oscillator power. These diodes use an ion-implanted double drift impurity profile. A hermetically sealed package was developed to achieve high reliability. A diamond heat sink provides a low thermal resistance. A silicon PIN subnanosecond switching diode phase modulates the transmitted power. The passivated mesa of the PIN diode chip is fabricated from thin, high-resistivity epitaxial material to achieve low capacitance and fast switching. A gallium arsenide Schottky-barrier mixer diode down-converts the signal in the receiver. The beam-lead Schottky diode is fabricated using molecular beam epitaxy, which provides a novel junction-isolation technique. Also, a brief description is given of the salient features of other active devices which operate in the IF (1.371 GHz) and baseband (dc to 300 MHz) circuitry. They consist of a family of both transistors and diodes (step recovery device, PIN variolosser, and Schottky mixer).

I. INTRODUCTION

Three new solid-state diodes were developed to generate, modulate, and down-convert millimeter-wave signals over the 40–110 GHz WT4 band. Silicon IMPATT diodes generate the transmitter and local oscillator power, a silicon PIN switching diode phase-modulates the transmitted power, and a gallium arsenide Schottky-barrier mixer diode down-converts the signal in the receiver.

Also, numerous other devices were either specifically developed for or found usage in WT4. These devices operate in the IF (1.371 GHz) or baseband (dc to 300 MHz) circuitry.

Table I—WT4 system requirements for IMPATT diodes

Frequency, GHz	Power output, mW		Efficiency,† percent		Figure of merit*		Thermal impedance, °C/W	Total capacitance, pF
	2-phase	4-phase	2-phase	4-phase	2-phase	4-phase		
43	170	340	4.3	6.4	173	86	30	0.41
50	130	260	4.1	6.1	173	86	40	0.35
59	100	200	4.0	5.8	173	86	55	0.30
70	75	150	3.8	5.5	173	86	70	0.25
80	55	110	3.6	5.2	86	43	84	0.21
90	45	90	3.3	4.9	86	43	97	0.19
105	35	70	2.9	4.5	86	43	112	0.17

* Local oscillator only: power output ≥ 16 mW.
† Junction temperature not to exceed 230°C at rated power output.

This paper provides a detailed description of the design, characterization, and performance of the three millimeter-wave diodes. The salient features of the most significant lower-frequency devices will be discussed briefly.

II. MILLIMETER-WAVE IMPATT DIODES

2.1 System requirements

The IMPATT diodes developed for the WT4 system are used to provide the local oscillator and the transmitter power. Several diode codes are necessary to cover the broad frequency range. In addition to providing power, these devices also must meet stringent requirements for noise, modulation sensitivity, and reliability. The system requirements were met by using double-drift silicon IMPATT diodes hermetically encapsulated using a novel packaging approach.

The device performance characteristics necessary to satisfy the two-phase and proposed four-phase WT4 system requirements are listed in Table I. The power output, efficiency, and thermal impedance pertain to the transmitting oscillator. The efficiency and thermal impedance requirements are those needed to provide the desired power output and reliability (junction temperature) and are compatible with the heat-removal designs. The figure of merit is defined as the ratio of noise ($Hz/\sqrt{KHz}$) to modulation sensitivity (MHz/mA). It is a measure of the diode noise performance and should be independent of the circuit characteristics. This requirement pertains to both the local oscillator and transmitter diodes to assure acceptable noise performance. The capacitance values listed are those required to provide the proper impedance match to the individual oscillator housings.

2.2 Device design

The design of the IMPATT diodes evolved through several different stages. Gallium arsenide and germanium IMPATT diodes were eliminated

because theoretical analysis indicated that these materials exhibited inadequate power-frequency products.[1] Silicon IMPATT diodes, however, do not display this shortcoming. For silicon IMPATTs there remained the choice of the design of the drift region and the physical configuration that the device would assume.

2.2.1 Avalanche-drift region

The design of the drift region for the avalanche and transit-time process represented an interesting series of technical considerations. Double-drift diodes were chosen instead of single-drift designs because the double-drift designs exhibit improved power, noise, efficiency, and thermal properties.[2,3]

Three different process techniques for obtaining the desired double-drift profiles were considered: (*i*) double-epitaxial growth, (*ii*) epitaxial growth followed by overcompensation using ion implantation, and (*iii*) a tailored ion-implanted doping profile into π-type epitaxy on p^+ substrates. The last was chosen since it represents the most controllable technique.[4] Because IMPATT diodes display a negative-admittance characteristic over a wide frequency range, three doping profile designs were adequate to provide oscillators covering the WT4 frequency range. These doping profiles provide devices with overlapping frequency bands.

The "all-implanted" double-drift n^+npp^+ structure was designed for use at 55, 75, and 105 GHz center frequencies. The design is shown in Fig. 1. The selection of a π on p^+ substrate structure takes advantage of boron's greater implant range compared with phosphorus or arsenic. Use of ν on n^+ substrates would require much higher implant energies.

The dose values were estimated empirically using previous experimental results and scaling laws. The ion dose is based upon a particular active number of carriers/cm^2 ($\int N\,dx$) establishing the desired drift width for the frequency of interest. An arsenic implant provides the high surface doping necessary to obtain an ohmic contact. The "all-implanted" design at all frequencies satisfied a system need for a single-polarity, single-process technology of IMPATT diodes.

To take advantage of the control inherent in ion implantation, it is necessary to carefully characterize the thin material used in this device. The most important parameter in the epitaxial concentration profile is the effective thickness, t_{eff}. This is the depth to which the active region is to be implanted and is measured by the spreading resistance (SR) technique.[5] After the dopant has been implanted and annealed, the slice is thinned, metallized, and separation-etched. Diodes are next bonded onto millimeter-wave bases and tailor-etched to the desired capacitance. Figure 2 shows the layout of the wafer, bonding tape, and package housing.

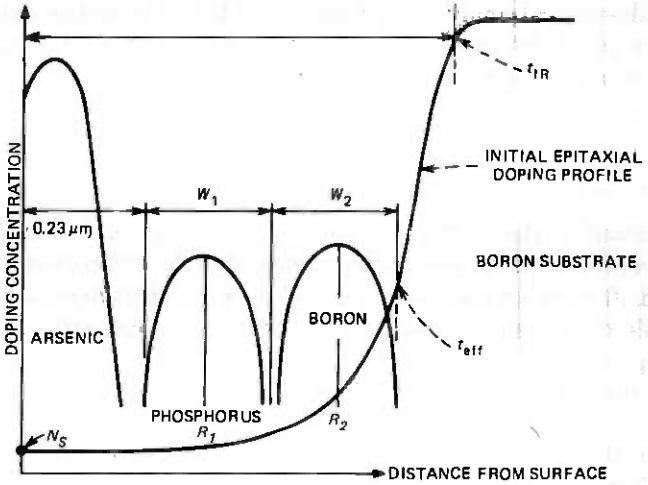

$W_{1,2}$ — DRIFT AND AVALANCHE, μm
R_1 — RANGE OF PHOSPHORUS IMPLANT, μm
R_2 — RANGE OF BORON IMPLANT, μm
t_{eff} — EFFECTIVE EPITAXIAL THICKNESS
t_{IR} — IR MEASUREMENT OF EPITAXIAL THICKNESS
0.23 μm — CONSTANT DEPTH INTRODUCED TO ACCOMMODATE SURFACE IMPLANT
N_S — SURFACE DOPING OF * LAYER

Fig. 1—Ion-implanted doping profile of millimeter-wave IMPATT.

2.2.2 Millimeter-wave IMPATT package

The package for the IMPATT diodes evolved to satisfy several needs that became apparent during the development of the diodes. These needs were to provide a controlled ambient for the surface of the silicon, protection for the wafer during handling, and a load bearing surface for the circuit probe contacting the top surface of the diode. The diamond heat sink was included to provide the low thermal impedance necessary to maintain sufficiently low operating temperatures to assure the desired reliability. It was embedded into the base to further reduce thermal impedance and to control the configuration of the diode base.

The package developed for the IMPATT diode applications provides low electrical parasitics and low thermal impedance. A package capacitance of 0.1 pF, inductance of 0.07 nH and the thermal impedance values listed in Table I were obtained.

The microminiature hermetic diode encapsulation shown in Fig. 2 is constructed on a metallized diamond embedded in a gold-plated copper base. The encapsulation is based on the use of a metallized quartz insulator having a hole in the center for the silicon wafer. The wafer is contacted and a top cover is thermocompression-bonded to the quartz, providing a hermetic package for the IMPATT chip.

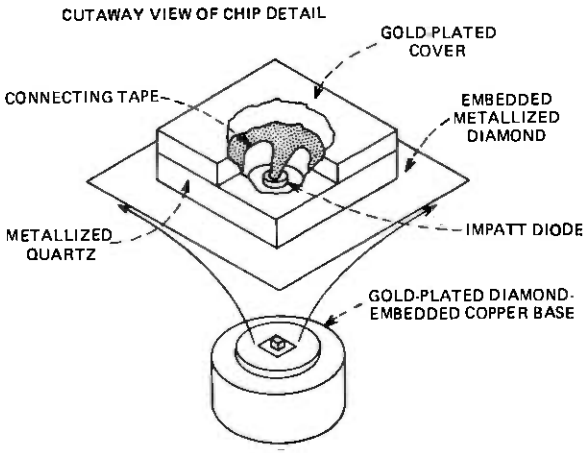

Fig. 2—IMPATT diode structure and package.

Since the package volume was too small to test hermeticity using conventional techniques the diodes were given an autoclave leakage test to evaluate both hermeticity and reliability.[6]

Instead of using a hermetic encapsulation to provide surface stability, we considered a passivated mesa approach. But calculations indicated that there were penalties in thermal impedance associated with the process. At 50 GHz the thermal impedance is 20 percent higher and would increase even more at higher frequencies. Also, the ability to tailor etch to obtain diodes for the desired frequency would be compromised and no mechanical protection would be provided.

2.3 System performance

The two-phase and four-phase power output requirements are plotted in Fig. 3. The dashed curve represents the median power output mea-

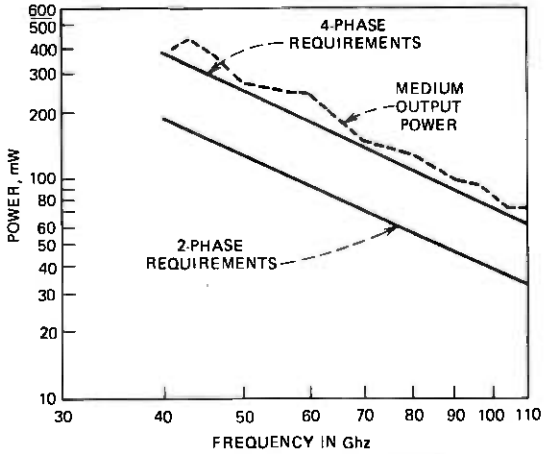

Fig. 3—IMPATT power output vs. frequency.

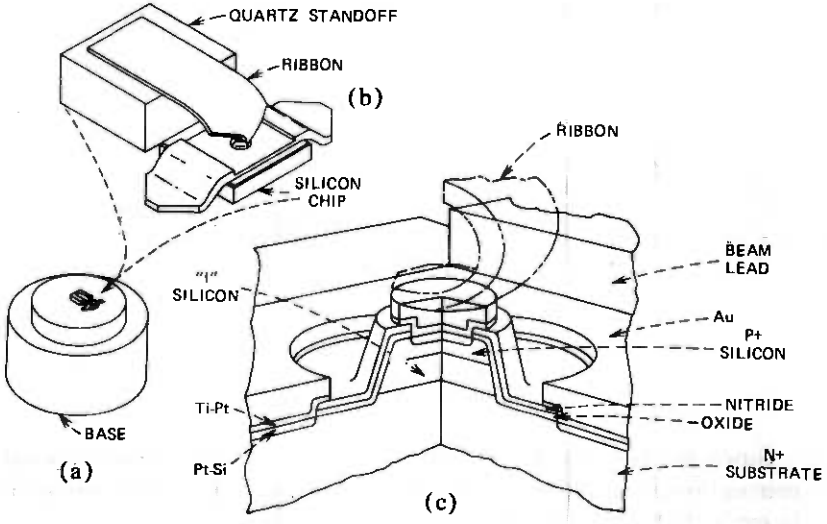

Fig. 4—Millimeter-wave PIN diode structure. (a) Assembled diode. (b) Diode chip, quartz standoff, and connecting gold ribbon. (c) Cut-away view of diode chip.

sured on groups of diodes at several of the WT4 design frequencies. The design has the ability to meet all two-phase requirements. However, to achieve a reasonable yield for the four-phase requirements the power output performance would have to be increased. Also, to meet the stringent noise and consequent figure-of-merit requirements of the local oscillator for the four-phase mode of operation, additional circuit/device/system evaluation is required.

III. PHASE SHIFT MODULATOR SWITCHING DIODE

3.1 Diode description and application

A low-loss, subnanosecond PIN switching diode was developed for WT4. It is used in the Phase Shift Modulator (PSM) of the transmitter over the 40–110 GHz frequency band. The quasi-beam-leaded (substrate only) diode chip is bonded on a gold-plated copper base as shown in Fig. 4a and 4b. A gold ribbon connects the oxide-nitride passivated mesa junction to the metallized top of an adjacent quartz standoff which is centered on the base. In the PSM the assembled diode terminates a coaxial line that couples into the waveguide. Switching the diode between forward- and reverse-bias states phase-modulates the incident waveguide signal.[7]

For proper circuit behavior a low and equal return loss is necessary in both bias states. The junction capacitance must be small to achieve the needed change in device impedance upon switching. Any parasitic

Table II—PIN diode electrical specification

Parameter	Condition	Limit	Typical
Balanced return loss	I_F = 10 mAdc V_R = 10 Vdc f = 54.2 GHz	≤1.2 dB	~0.7 dB @ 40 GHz ~1.0 dB @ 55 GHz ~1.5 dB @ 80 GHz ~2.5 dB @ 108 GHz
Total capacitance	V_R = 0 V	≤0.10 pF	0.06–0.08 pF
Total capacitance	V_R = 10 V	≤0.07 pF	0.04–0.05 pF
Breakdown voltage	10 μAdc	≥30 Vdc	~35 V
Storage time	$I_F = I_R$ = 10 mA	≤5.0 nsec	~4 nsec
Fall time		≤0.5 nsec	~0.4 nsec

reactive elements are present for both bias states and tend to mask the change in junction impedance, in addition to reducing the bandwidth. The time of switching between bias states must be short in comparison to the period of the modulating signal from the PSM driver. The stored charge injected during forward bias causes a delay in the switching action from the forward to reverse bias states and must be limited to avoid excessive timing errors.[8] The resulting electrical requirements that the PSM imposes on the PIN diode are shown in Table II.

At this time, it seems probable that two diode designs will be necessary to provide adequate circuit performance over the entire 40–110 GHz band. Different diode capacitances are needed for the low and high end of the frequency range. Further characterization is needed for frequencies >70 GHz, in particular, to firmly establish the diode loss as a function of frequency. The increased incident power of the four-phase system would not require any changes in diode design to meet either electrical or reliability specifications.

3.2 Device design

A thin-base epitaxial PIN diode fabricated using high resistivity ν-type silicon epitaxial material is most suitable for meeting the PSM switching diode specifications.[9] A "doping well" is formed by the shallow p^+ in-diffusion and steep doping tail from the n^+ substrate. This constitutes an optimum structure from the standpoint of maximum breakdown voltage, minimum capacitance per unit area, low resistance, and fast switching speed.

At very low reverse voltages (≲2 V) the junction depletion region extends completely to the substrate. The breakdown voltage is therefore essentially determined by the base width and the critical electric field at breakdown which for silicon is ~30V/μm. The base width was chosen to achieve a breakdown voltage of ~36 V. Similarly, the junction capacitance at −10 V can be determined in terms of a parallel plate capacitor model and was calculated to be 0.027 pF. The parasitic capacitance of the quartz standoff adds ~0.014 pF. The zero bias capacitance

specification is readily met due to the high resistivity of the base and is necessary to prevent varactor action and thereby undesirable modulation.

A mesa containing a plane junction was chosen to physically confine the stored charge injected during forward bias. During the forward-to-reverse bias switching transient, the majority of the charge is removed during a storage time interval before the device impedance switches to the high-impedance state. Switching occurs during the fall time interval when the residual stored charge is removed. In the usual planar diffused junction, part of the injected charge is distributed parallel to the surface. Removal of this charge component is diffusion-limited, and this results in slow switching speeds. The amount of stored charge injected during forward bias, is controlled by the mobile carrier lifetime. The lifetime is a direct function of base width and an inverse function of current density.[10] The exact functional relationship is processing dependent and must be established experimentally.

The forward-bias resistance of the base region is essentially fixed by the stored charge and its geometrical dimensions. The remaining diode series resistance is contributed by the metallurgical contacts and substrate. Spreading resistance from the small junction diameter and skin depth effects at millimeter-wave frequencies are important. To reduce these resistance contributions, a heavily doped n^+ substrate was used. The contact to the substrate was placed on the front of the chip, as close as possible to the base of the mesa—Fig. 4c. Beam leads for the substrate contact logically follow. The use of beam leads also permits the fabrication of a chip size sufficiently large to be manufacturable, while maintaining the small active diode region. The chip size, including beam leads, was determined by the minimum outer diameter of the coaxial line which the diode terminates.

3.3 Fabrication

Oxide-nitride passivation and a sealed-junction overlay PtSi-Ti-Pt-Au metallurgical contact was chosen for high reliability.[11] The low barrier height of PtSi (~0.25 eV) is needed to minimize the contact resistance of the small-diameter p^+ contact. The mesa height must be sufficient to assure that the substrate contact is made to material which has the bulk substrate resistivity. The epitaxial material was grown using chemical vapor deposition of $SiCl_4$. However, to achieve a sharp epitaxial-to-substrate doping profile, a heat treatment was performed after HCl *in situ* etching, but before deposition of the epitaxy.[12]

3.4 Characterization and results

Typical values achieved for the various electrical characteristics of the device are also listed in Table II. The storage time was within the

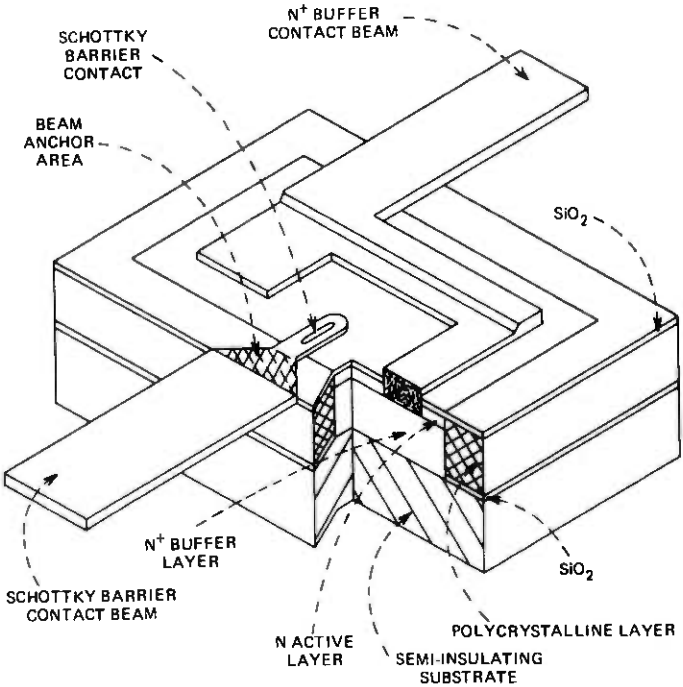

Fig. 5—Cross-sectional view of low parasitic capacitance Schottky-barrier mixer diode.

specification limit for the diode dimensions chosen, which were based upon breakdown voltage and capacitance requirements. If the storage time had been too high, the use of gold or platinum doping would have been considered. The fall time was found to be a function of the base width, the shape of the epi-to-substrate doping tail, and the junction depth. The first factor is basically a transit-time effect. The last two factors decrease the degree to which the stored charge is confined and are diffusion-limited. The switching path of the diode impedance was found to be close to resistive.[8] This permits a relaxation of transient and error timing requirements in the system.

IV. GALLIUM ARSENIDE MIXER DIODE

4.1 Device description and application

The WT4 receiver uses planar, isolated, gallium arsenide, beam-leaded diodes to down-convert the millimeter wave signal. One diode design is adequate to cover the entire 40–110 GHz WT4 frequency band and meet the two-phase receiver noise requirements. Low parasitic capacitance (~0.02 pF) between the Schottky-barrier beam and the n^+ epitaxial layer (see Fig. 5) is achieved by the simultaneous deposition of both

single-crystal and high-resistivity polycrystalline gallium arsenide by the Molecular Beam Epitaxy (MBE) technique.[14,15]

The diodes are thermocompression-bonded to millimeter-wave thin-film circuits in either the orthomode double balanced down-converter (four diodes)[16] or the half-frequency pumped down-converter (two diodes).[17–19] Typical diodes selected for these circuits have a total capacitance at zero volts less than 0.08 pF and an excess series resistance (R_{SF}), calculated from the dc forward-bias junction characteristics, less than 8 Ω. The final zero bias total capacitance and excess series resistance limits have not been established.

4.2 Diode Design

The diode design makes use of the majority-carrier current flow in a Schottky barrier to provide a nonlinear impedance at millimeter-wave frequencies for mixing the local oscillator and signal voltages in the WT4 receiver down-converter.

A major consideration in the design of the beam-lead diode was the overlay capacitance between the Schottky-barrier beam and the n^+ substrate—Fig. 5. This capacitance provides a shunt path for current across the Schottky barrier and lowers the local oscillator and signal voltage swing across the active metal-to-semiconductor junction.

The first diode design was a planar structure fabricated on an n-type epitaxial layer deposited on a heavily doped n^+ substrate. The performance of these diodes met the two-phase system conversion-loss requirements at the lower frequency end of the band, but the shunting capacitance degraded their high-frequency performance. The dielectric (deposited oxide) thickness could be increased to reduce the overlay capacitance. However, the definition of the junction window would deteriorate. Or the high-frequency performance could be improved by reducing the anchor area, but the diodes became mechanically fragile and difficult to handle and bond.

The development of MBE techniques, to produce simultaneously low-resistivity single crystal and high-resistivity polycrystalline gallium arsenide on semiinsulating substrates, provided the means whereby the overlay capacitance could be reduced. It was possible to simultaneously decrease the anchor area over the n^+ layer and to increase the dielectric isolation with respect to the remaining anchor area. In addition, the planar diode design was retained, along with adequate total anchor area.

For two-phase operation the planar polyisolated technique is capable of achieving the WT4 requirements over the complete frequency band. Further development is necessary to meet the four-phase objectives.

Table III—Typical diode characteristics for planar-isolated diodes

Parameter	Condition	Typical
Junction capacitance	$V = 0$ $f = 1$ MHz	0.04 to 0.06 pF
Parasitic overlay capacitance		~0.02 pF
Forward bias series resistance	$I_F = 5$ mAdc	4 to 8 Ω
Diode quality factor, n*		1.1 to 1.3
Reverse voltage	V_R @ 10 μAdc	5 to 12 Vdc
Reverse current	I_R @ −3.0 Vdc	$<1 \times 10^{-9}$ A

* $I_F = I_S$ [exp $(qV/nkT) - 1$]

4.3 Fabrication

Chromium doped semiinsulating substrates are polished and covered with a thin layer of deposited SiO_2 into which the isolation patterns are etched. The n^+ buffer and n active layers are deposited by MBE techniques and form into single-crystal gallium arsenide on the exposed gallium arsenide surface, and into high-resistivity polycrystalline gallium arsenide over the oxide-covered areas.

An n^+ ohmic contact pattern, centered in the single crystalline area, is defined in a second SiO_2 layer and etched to remove the n epitaxial layer down to the n^+ buffer layer. A low resistance ohmic contact to the n^+ buffer layer is formed by spike-alloying layers of gold, tin, and nickel.

After defining the junction window in the second SiO_2 layer, the Schottky barrier is formed by sequentially depositing titanium and platinum. The metallization pattern is Au plated and elsewhere the titanium and platinum are removed. Areas of the beam outside the active area of the diode and extending outside the region of the chip receive a heavy gold plate. The completed wafer is back-lapped, masked with photoresist, and etched to separate the diodes.

4.4 Characterization and results

Completed planar-isolated diodes are tested for 1-MHz zero-bias total capacitance, forward and reverse junction characteristics. The dc forward bias series resistance, R_S, is calculated from the forward bias characteristic. Diodes with typical characteristics as shown in Table III are suitable for mixer circuits.

The feasibility of using 1-MHz zero bias total capacitance and forward series resistance data to select diodes for mixer circuits is demonstrated by the curve shown in Fig. 6. Close agreement is found between the measured and calculated conversion loss plotted for a set of four diodes in a double-balanced down-converter.[16] In the original n/n^+ diode design the dc forward-bias series resistance was lower than the equivalent

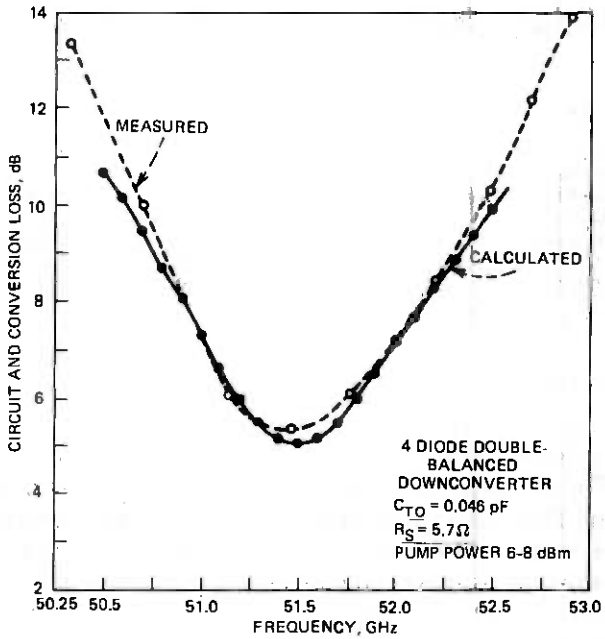

Fig. 6—Measured and computed conversion loss for a balanced mixer.

high-frequency resistance due to skin effects. This is not a major factor with the planar-isolated diode structure since the buffer layer is approximately the same thickness as the skin depth. Hence, the path along which both the dc and high-frequency currents must flow is approximately the same.

V. OTHER SEMICONDUCTOR DEVICES FOR WT4

5.1 Silicon surface PIN diode

A beam-lead PIN variolosser diode was developed for application in the AGC circuit of the receiver IF amplifier. The diode is fabricated from high resistivity n substrates using planar processing. The p^+ and n^+ regions were both formed on the front surface.[20] The diode features a low forward-bias resistance ($\leq 4\ \Omega$ at 20mA, 1.5 GHz) and low total reverse-bias capacitance (≤ 0.2 pF at -0.8V). A thick dielectric is used to reduce the parasitic junction beam capacitance.

5.2 Silicon step-recovery diode

A beam-lead step recovery diode is used at baseband frequencies in both the regenerator circuit and as a ×5 multiplier. The diode is fabricated from thin, high-resistivity ν on n^+ epitaxy, and is similar to the millimeter-wave PIN diode. Again, a passivated mesa junction confines

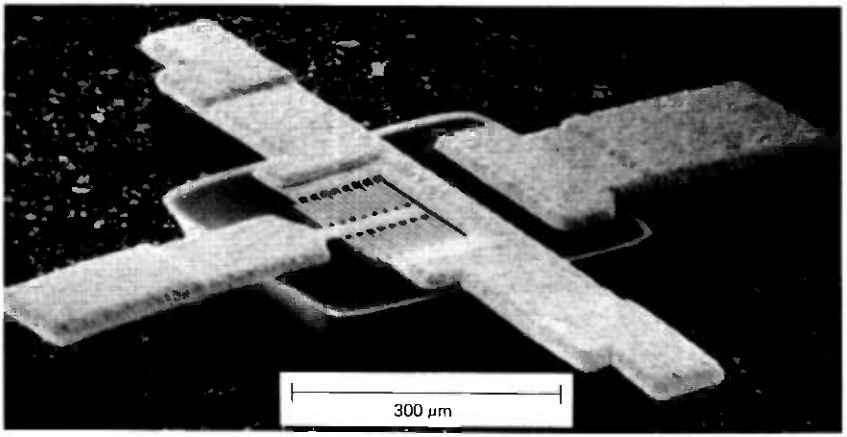

Fig. 7—Large area microwave transistor.

the stored charge to minimize the fall time ($\leq$0.7 nsec). The higher storage time of $\geq$7.0 nsec is met by increasing the junction diameter. The storage and fall times were measured for a drive condition of $I_F = I_R =$ 10 mA.

5.3 Gallium arsenide Schottky diode

A second beam-lead GaAs Schottky diode was developed for use in the IF detector and amplifier, PSM driver circuit, and various baseband circuits. This diode is fabricated using n on n^+ epitaxy and planar processing. The barrier metal is titanium. The diode has a zero bias capacitance of $\leq$0.5 pF and a series resistance of $\leq 3\Omega$.

5.4 Silicon microwave transistors

A family of beam-lead npn microwave transistors was developed for numerous applications in both the IF and baseband circuitry. The interdigitated emitter and base stripes have a 2.5 μm width and 2.5 μm separation between stripes. A 0.25 μm base width is achieved using ion implantation to introduce both the emitter and base dopants.[21] The transistor was designed to operate at a current level of $\sim$10 mA and has a typical collector-base capacitance of 2.5 pF at -3 V. One of the transistors must meet tight specifications on both magnitude and phase of all s parameters. In particular, the forward insertion gain is 9.7–11 dB at 1.4 GHz. Also, a transistor with four times the emitter area was also developed for the higher power needed in the PSM driver—Fig. 7.

VI. DEVICE RELIABILITY

Accelerated life tests were performed on all the devices developed for WT4 to establish their reliability. The median time to failure for each

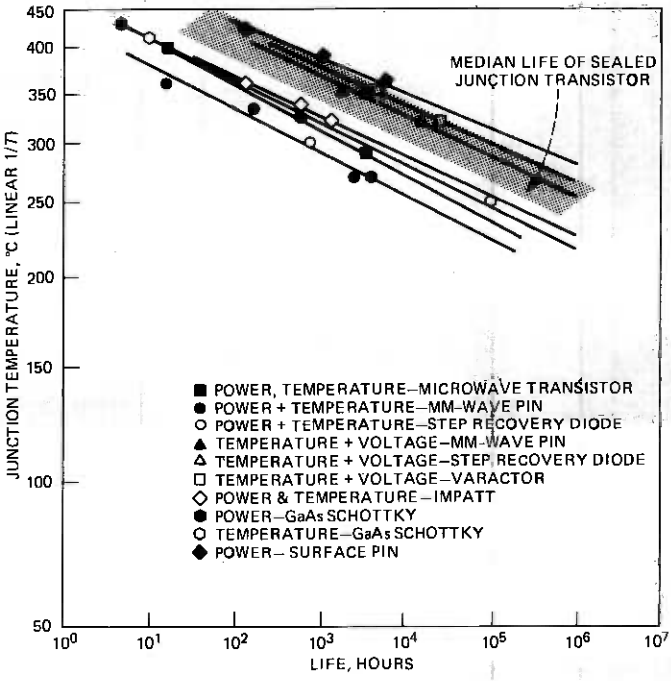

Fig. 8—Device reliability: median time to failure as a function of junction temperature.

device is shown plotted in Fig. 8 as a function of junction temperature. The shaded area on the figure represents extensive data of the median life of sealed-junction transistors as established by Peck.[22]

All the devices except the IMPATT have a projected reliability of less than 10 FIT when extrapolating the aging data to user condition. The IMPATT reliability is 600 FIT at the maximum operational junction temperature of 230°C.

The observed activation energies for the devices are characteristic of a metallurgical failure mechanism as opposed to a surface charge migration mechanism. The dominant failure mode was a degradation of the reverse characteristic and excessive leakage current, with some catastrophic failures showing evidence of contact metal alloying into the silicon.

Temperature aging at 350°C, with and without reverse bias, and dc forward-bias power aging were performed on the millimeter-wave PIN diode. Bias had little effect on the mean time to failure. Power dissipation was the more severe aging condition. Data for the step-recovery diode matches that of the PIN diode quite well. Both devices have a thermal impedance of approximately 600°C/Watt. An activation energy of 1.7 eV was calculated for the regression curve of the aging data.

For the beam-leaded millimeter-wave GaAs Schottky both ac power aging and temperature aging fit the same regression line. The beam-leaded microwave GaAs Schottky data also fell on this regression line. This was equally true for a third device, a packaged GaAs chip, not reported on in this paper. All three devices use titanium as the barrier metal and have an activation energy of 1.8 eV.

The beam-leaded surface PIN diode was subjected to forward-bias dc power aging at elevated temperature. A 2.3 eV activation energy was established. Temperature aging with reverse bias data was also available for a silicon beam-leaded varactor diode used in WT4. It has an activation energy of 1.9 eV.

DC and 50-GHz power aging at elevated temperature was performed on the millimeter-wave IMPATT diode. For the microwave transistor both temperature and power aging data fit the same regression curve. Activation energies of 1.9 eV and 1.6 eV, respectively, were calculated.

VII. SUMMARY

Three unique devices were developed to generate the millimeter-wave power, phase-modulate the carrier, and down-convert the signal of the WT4 system. These devices represent a wide application of state-of-the-art materials and fabrication development and millimeter-wave characterization. Reliable devices were provided that meet the two-phase requirements of the WT4 system over the frequency band 40–110 GHz. To meet the four-phase system objectives would require further device and circuit development. Numerous other devices were also developed for operation in the IF and baseband circuitry.

ACKNOWLEDGMENTS

Many people contributed to the development effort described in this paper. In particular, we wish to thank W. C. Ballamy, J. L. Boyle, W. L. Buchanan, C. A. Goodwin, C. M. Hsieh, B. C. Lewis, R. Morales, K. H. Olson, D. C. Potteiger, A. W. Rhoads, and L. J. Smith.

REFERENCES

1. D. L. Scharfetter, "Power-Impedance-Frequency Limitations of IMPATT Oscillators Calculated from a Scaling Approximation," IEEE Trans. Electron Dev., *ED-18*, No. 8 (August 1971), pp. 536–543.
2. T. E., Seidel, R. E. Davis, and D. E. Iglesias, "Double-Drift-Region Ion-Implated Millimeter-Wave IMPATT Diodes," Proc. IEEE, *50*, No. 8 (August 1971), pp. 1222–1228.
3. R. L. Kuvâs and D. R. Gunderson, unpublished results.
4. C. N. Dunn, B. L. Morris, C. L. Paulnack, T. E. Seidel, and L. J. Smith, "Improved Fabrication and Noise Performance of Silicon Double-Drift Millimeter-Wave IMPATT Diodes," IEEE International Electron Device Meeting Digest, IEDM Digest 1973, December 1973, pp. 486–488.
5. B. L. Morris, "Some Device Applications of Spreading Resistance Measurements on Epitaxial Silicon," J. Electrochem. Soc., *121*, March 1974, pp. 422–426.

6. H. M. Olson, "A Mechanism for Catastrophic Failure of Avalanche Diodes," IEEE Trans. Electron Dev., *ED-22*, No. 10, October 1975, pp. 842–849.
7. C. E. Barnes, P. Brostrup-Jensen, E. T. Harkless, P. T. Hutchison, R. W. Muise, and A. J. Nardi, "Regenerative Repeaters," B.S.T.J., this issue.
8. F. Bosch and O. G. Petersen, "MM-Wave PIN Diodes for Ultra High Data Rates," IEEE MTT-S International Microwave Symposium, San Diego, June 1977.
9. W. J. Clemetson, N. D. Kenyon, K. Kurokawa, B. Owen, and W. O. Schlosser, "An Experimental MM-Wave Path Length Modulator," B.S.T.J., *50*, No. 9 (November 1971), pp. 2917–2946.
10. R. C. Curby and L. J. Nevin, "Low Resistance, Low-Bias Current PIN Diodes," IEEE International Solid-State Circuits Conference, Philadelphia, February 1976.
11. M. P. Lepselter, "Beam-Lead Technology," B.S.T.J., 45, No. 2 (February 1966), pp. 233–253.
12. T. Ishii, K. Takahashi, A. Kondo, and K. Shirahata, "Silicon Epitaxial Wafer with Abrupt Inferface by Two-Step Epitaxial Growth Technique," J. Electrochem. Soc., *122*, November 1975, pp. 1523–1531.
13. O. G. Petersen, C. E. Bradford and R. V. Cranmer, "Impedance Measurements at Millimeter Wave Frequencies (54.2 GHz)," IEEE International Solid-State Circuits Conference, Philadelphia, February, 1977.
14. W. C. Ballamy and A. Y. Cho, "Planar Isolated GaAs Devices Produced by Molecular Beam Epitaxy," IEEE Trans. Electron Dev., April 1976, pp. 481–484.
15. A. Y. Cho, and W. C. Ballamy, "GaAs Planar Technology by Molecular Beam Epitaxy (MBE)," J. Appl. Phys., *46*, No. 2 (February 1975).
16. G. S. Axeling, private communication.
17. M. V. Schneider, and W. W. Snell, Jr., "Stripline Downconverter with Subharmonic Pump," B.S.T.J., *53*, No. 6 (July–August 1974), pp. 1179–1183.
18. M. V. Schneider and W. W. Snell, Jr., "Harmonically Pumped Stripline Down-Converter," IEEE Trans. Microw. Theory Tech., *MTT-21*, No. 3 (March 1975), pp. 271–275.
19. T. F. McMasters, M. V. Schneider, and W. W. Snell, Jr., "Millimeter-Wave Receivers with Subharmonic Pump," IEEE Trans. Microw. Theory Tech., *MTT-24*, December 1976.
20. B. W. Battershell, and S. P. Emmons, "Optimization of Diode Structures for Monolithic Integrated Microwave Circuits," IEEE J. Solid State Circuits, *SC-3* (1968), p. 107.
21. R. S. Payne, R. J. Scayuzzo, K. H. Olson, J. M. Nacci, and R. A. Moline, "Fully Ion-Implanted Bipolar Transistors," IEEE Transactions on Electron Devices, *ED-21*, April 1974, pp. 273–278.
22. D. S. Peck, "Reliability of Beam-Lead Sealed-Junction Devices," Proceedings of Annual Symposium on Reliability, Chicago, January 1969.

THE BELL SYSTEM TECHNICAL JOURNAL
Vol. 56, No. 10, December 1977
Printed in U.S.A.

The WT4 Millimeter Waveguide System: The WT4 Repeater Station

By W. J. LISS, D. OLASIN, J. W. OSMUN, and S. SHAPIRO

(Manuscript received April 7, 1977)

The WT4 repeater station is discussed from outside plant construction, building construction, Western Electric installation, and operations viewpoints. Unique properties of the waveguide medium have necessitated the development of a utility tunnel for interfacing the waveguide with the diplexer array. The utility tunnel and associated waveguide hardware for termination are discussed. The diplexer array assembly and water-cooled repeaters placed further requirements on the above-ground portion of the building. A method of incorporating these requirements, as well as providing ancillary support equipment for the repeaters, is also presented. Future areas to be investigated, notably the use of a modular prefabricated building, are also explored.

I. INTRODUCTION

Repeater stations for the WT4 system are spaced at intervals of up to 60 kilometers and perform the function of interfacing the waveguide medium with the repeaters. Each station—including the structure, land, and access roads—contains waveguide and sheath terminating hardware, channelizing networks, repeaters, power and environmental control systems, and maintenance electronics.

Design and construction of a repeater station requires the coordination of many groups including Long Lines Outside Plant engineering and construction, Long Lines Buildings Group and Western Electric Engineering and Installation (Fig. 1). In developing the WT4 repeater station concept, an attempt was made to define the interfaces between these groups and minimize their interdependence where possible. This was achieved by allowing for parallel rather than serial construction in many stages of the station construction, and also by incorporating flexibility

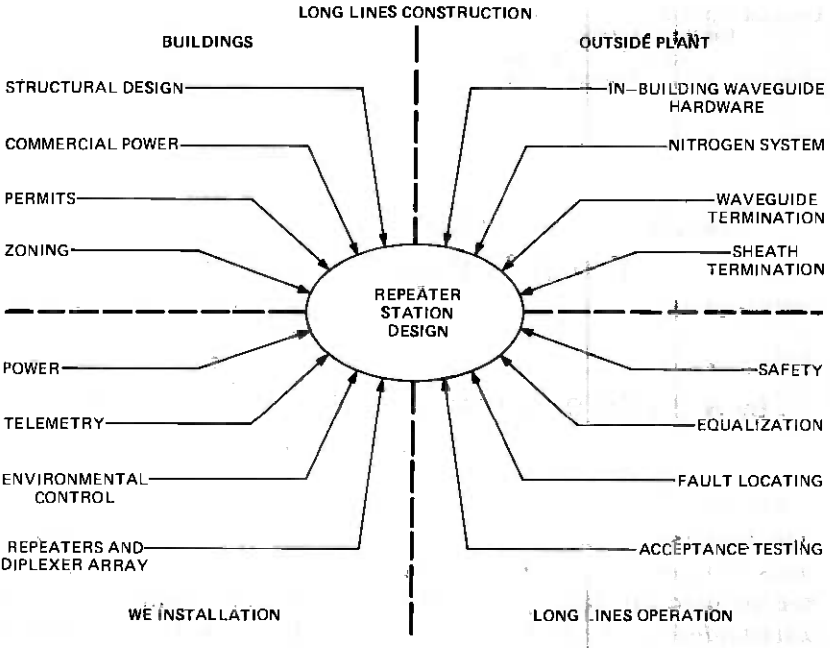

Fig. 1—Influences on repeater station design.

in the overall station layout. The net result is reduced lead time from construction authorization to service turn-up.

II. REPEATER STATION DESCRIPTION

2.1 Background

Early designs of the WT4 repeater station envisioned both hardened underground and partially above-ground structures. The diplexer arrays were to be horizontally mounted either above or below the vertical repeater bays—a method certain to cause problems in the central office environment.

These proposals also failed to address the problems of sheath termination, waveguide medium access, and the building/outside plant construction interface. For example, the building would have to be constructed in its entirety before the sheath could be terminated. Building planning would have to start well in advance of medium route engineering, a concept not compatible with WT4 route engineering.[1] To avoid these difficulties a station concept was developed in which the building construction is decoupled from the sheath and waveguide installation through the station site.

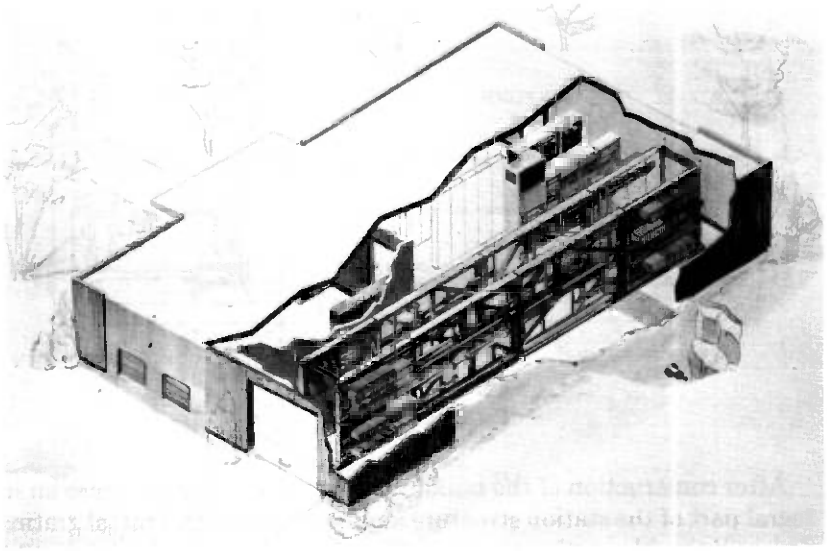

Fig. 2—Artist's rendition of repeater station.

2.2 Current design

The current repeater station, shown in Fig. 2, is a composite of two largely independent structures. The below-grade portion, or utility tunnel, accommodates the sheath/waveguide entry and nitrogen pressurization requirements. The tunnel is a precast concrete structure which is placed well in advance of the repeater building. It is installed by the sheath installation crew and provides final termination for the sheath. In addition, it provides access to the sheath for mechanical inspection, cleaning, drying, and leak-testing.

The millimeter-wave signal path proceeds through the tunnel waveguide, passes through a right-angle bend and enters the diplexer assembly from below. The diplexer assembly, or channelizing network, then allows the wideband signal to be separated into 124 millimeter-wave channels and delivered to the repeaters. The reverse path allows all the signals from the various repeaters to be combined and transmitted through the outgoing waveguide.

The above-ground portion, or repeater building, is approximately 48 feet long × 23 feet wide × 10 feet high, and houses the channelizing networks, repeaters, and support equipment. The length of the building is determined by the overall length of the channelizing assemblies which terminate each waveguide entry into the station. The building may be either of conventional on-site construction or of field-assembled, preinstalled modular construction.

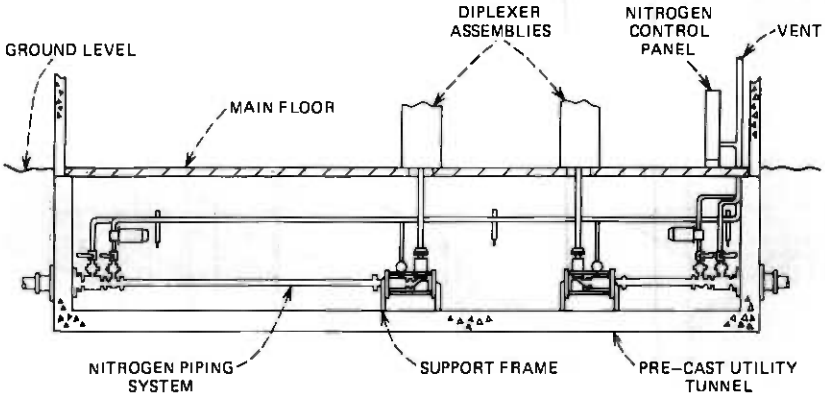

Fig. 3—Utility tunnel.

After construction of the building, the utility tunnel becomes an integral part of the station structure and is covered with a metal grating. This will provide continuous ventilation, which is required since possible nitrogen leaks into a closed area can cause oxygen deficiency. The open construction eliminates the need for expensive and trouble-prone oxygen monitoring equipment.

III. BELOW-GROUND STRUCTURE

The utility tunnel is designed to be as small in volume as possible, yet provide reasonable working space for the installation and maintenance of the waveguide and sheath termination hardware. The transverse cross-sectional dimensions of the tunnel are approximately 5 feet deep by 3 feet wide, with the sheath being no closer than 1 foot from either side wall. Figure 3 shows a cross section of the utility tunnel with the termination hardware installed. The tunnel axis is normally perpendicular to the plane of the diplexer assemblies, to facilitate in-line waveguide installation, but may vary slightly from 90 degrees to provide flexibility in building orientation for zoning purposes.

3.1 Medium termination requirements

The unique design of the waveguide medium necessitated the development of new hardware for the waveguide and sheath termination in a repeater station. The requirements for such terminations are as follows:

(*i*) The tunnel wall and hardware must be capable of sustaining a 30,000-lb thermal-stress load from the sheath. The small cross-sectional area of the tunnel entrance wall is ideal for this requirement.

(*ii*) The waveguide entering the building must be in line with and

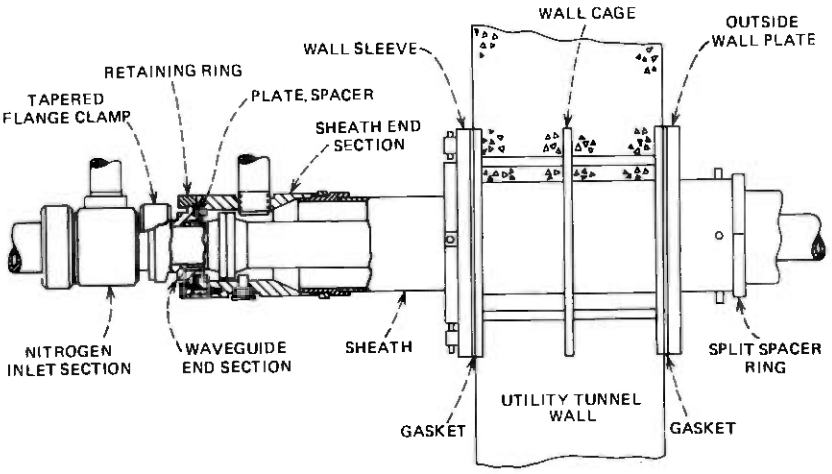

Fig. 4—Special entrance hardware.

at right angles to the vertical axis of the diplexer entry port. This requirement also applies to the sheath because of the concentric design of the waveguide medium.

(*iii*) The waveguide termination must be compatible with the insertion method of installation[2] and must be capable of sustaining a 10,000-lb thermal load.

(*iv*) Electrical arc welding is not to be permitted for any of the wall terminations, as this poses a safety hazard in closed environments.

(*v*) The termination hardware must pneumatically isolate the sheath annulus from the waveguide bore.[3]

(*vi*) The termination must provide access to the full bore of the sheath for mechanical inspection, cleaning and drying operations.

(*vii*) Waveguide in the repeater station cannot be subjected to axial forces. Because temperature variations are expected within the utility tunnel, expansion joints are required in the tunnel waveguide runs.

(*viii*) The diplexer must be protected from overpressure in the event of a pressure window failure in the waveguide line.

3.2 Medium-termination hardware description

The medium-termination hardware includes all waveguide components installed by the construction crews. Figure 3 shows these components installed in a utility tunnel. The sheath and waveguide termination and the nitrogen inlet section are shown in Fig. 4. The wall sleeve assembly is designed to provide angular adjustment of the sheath for alignment with the axis of the diplexer entry port.

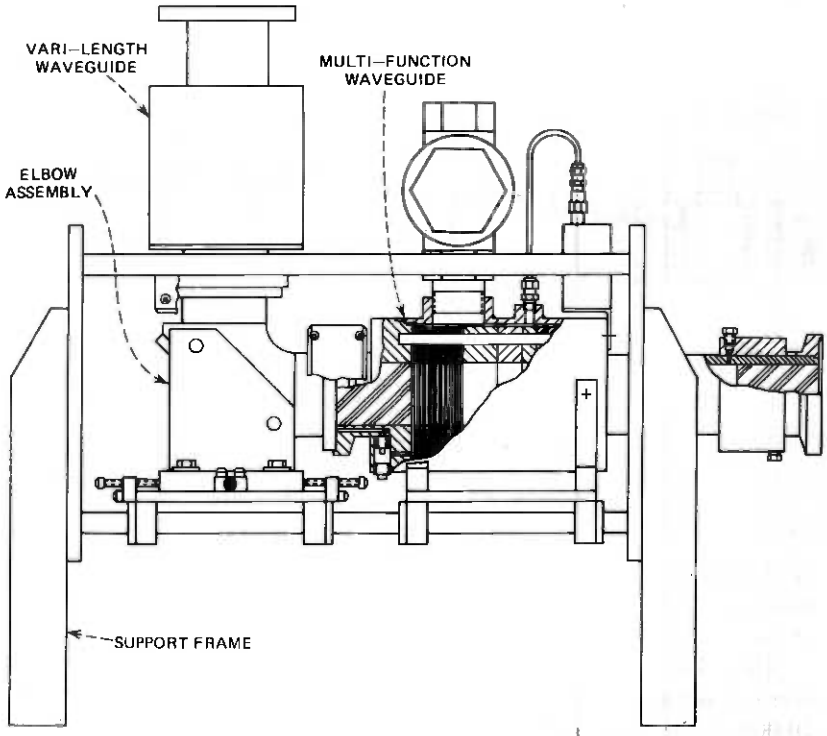

Fig. 5—Support structure assembly.

A benchmark installed in the tunnel floor allows the sheath end section to be installed before the diplexer array. An optical device is attached to the sheath end section and is used to align the end section with a plumb line aligned with the benchmark. When the diplexer is installed the benchmark is again used for proper placement.

The waveguide end section (Fig. 4) is installed as the waveguide is inserted into the repeater station. The remainder of the hardware is generally installed after the diplexer is in place because final adjustment can only be made at that time.

The support frame holds the multifunction waveguide, the elbow assembly, and the vari-length waveguide (Fig. 5). The assembly also provides the adjustment capability needed to connect the medium to the diplexer.

The multifunction waveguide (Fig. 6) contains several unique features that allow a number of operations to be performed:

(*i*) Primary and secondary pressure windows isolate the high pressure of the waveguide run from the low pressure of the diplexer array (25 psig maximum vs 0.25 psig, respectively).

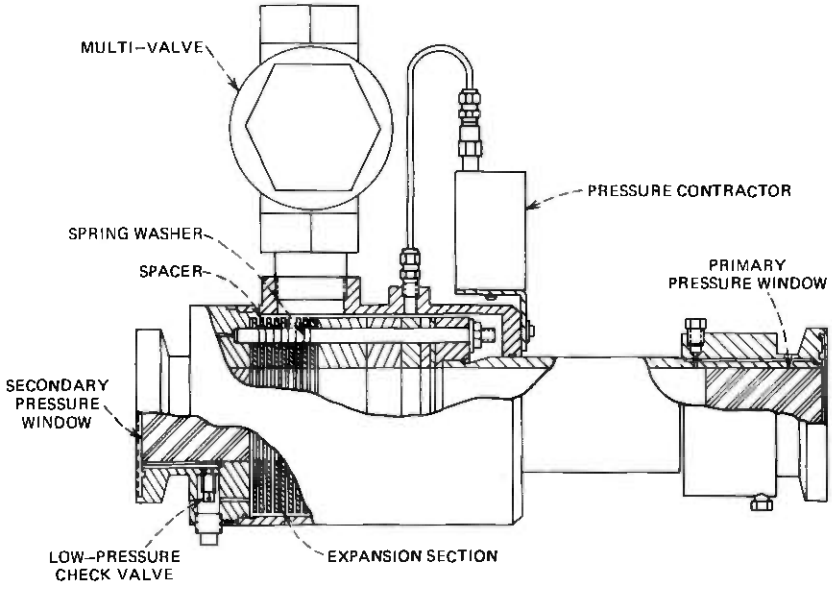

Fig. 6—Multifunction waveguide.

(*ii*) A sensitive check valve provides low, positive pressure from the diplexer array to the assembly, while preventing high pressure exposure to the diplexer components.

(*iii*) A series of spring-washer loaded discs allows for expansion and contraction of the waveguide within the utility tunnel due to temperature variations without affecting the transmission path.

(*iv*) A set of disks of varied thickness provides a means of adjusting the overall length of the assembly by up to 3 inches to accommodate any installation tolerances.

(*v*) A low pressure vent valve allows for the venting of large quantities of nitrogen in the event of primary pressure window failure, while a pressure contactor will detect leakage of the same window and activate an alarm through the telemetry system.

The vari-length waveguide provides a 2-inch length adjustment and an expansion feature similar to that of the multifunction waveguide.

IV. ABOVEGROUND BUILDING

The aboveground building houses the repeaters, channelizing networks, repeater frames, and power and telemetry systems and provides environmental control for both portions of the system. The channelizing networks, we recall, are required to separate out the 124 individual millimeter-wave channels. The building is partitioned into an electronics

room, housing the diplexers and electronics, and an equipment room, which houses the noisy, massive support items.

4.1 Repeater/diplexer assembly

As shown in Fig. 7, the dominant features of the building are the two back-to-back channelizing network assemblies. Stringent requirements on the physical layout of these arrays[4] have led to the elongated planar arrays shown. Each array, measuring 41.5 feet in length, is a modular assembly of eight rigid aluminum frameworks. Front and rear access is required for each assembly, as shown, for both installation and maintenance functions. For personnel or test equipment movement from front to rear, 3 feet of clearance is provided at each end of both arrays. The modules can either be individually shipped to existing underground stations or new conventionally constructed buildings or delivered as an assembled unit within a transportable building.

4.2 Environmental control

4.2.1 Repeater cooling

Repeaters for the WT4 system are cooled by the passage of chilled water (at 60°F) through the repeater mounting surfaces to ensure reliability and increased life of the IMPATT diodes.[5] Specially designed water chillers, mounted in the equipment room are used to perform this function. Due to the critical nature of the cooling requirement, redundant chillers are utilized, each unit having a dual pump and compressor arrangement. In addition there is a dc-powered pump which continues to circulate the water through the repeater frames in the event of complete ac power failure.

4.2.2 Ambient control

Dimensional stability of the channel diplexers, as well as the high-pass filter components of the band diplexers, require that the repeater station ambient be restricted to a ±20°F temperature variation. This regulation is achieved by utilizing a process cooler, mounted in the electronics room and fed by the water chillers mentioned above. At the same time this unit regulates the room humidity, and prevents condensation on the chilled repeater-mounting surfaces.

4.2.3 Nitrogen supply system

The need to maintain low levels of oxygen and moisture exists within the band and channel diplexer assemblies as well as the waveguide. However, due to the presence of several delicate components within the

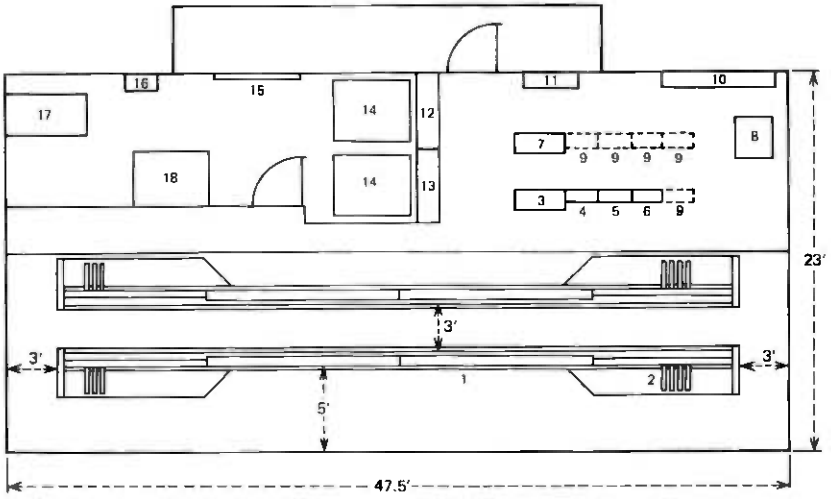

1 DIPLEXER ARRAY
2 REPEATERS
3 PROCESS COOLER
4 LOW PRESS. NITROGEN BAY
5 FAULT LOCATION BAY
6 AUX COMMUNICATION BAY
7 150/151 POWER PLANT
8 NITROGEN CONTROL PANEL
9 FUTURE
10 48V BATTERY
11, 12, 13 AC SWITCHING (POWER DISTRIBUTION)
14 WATER CHILLER
15 FILTER
16 TURBINE CONTROLS
17 TURBINE
18 TOILET

Fig. 7—Floor plan layout.

band diplexer array, these units can be pressurized to only ¼ psi (6 inches H_2O). A nitrogen control panel regulates the high-pressure nitrogen coming from the waveguide and provides both major and minor alarms based on flow rates to the diplexers and pressure levels within the array. The system also feeds dry nitrogen to the individual repeater units, thereby protecting the unencapsulated thin-film devices.

4.3 Station power

Power for each repeater station is obtained from local commercial ac service. The use of a separate power cable buried along with the waveguide, with either high-voltage ac or dc fed from the main stations, was considered as an alternative to the local commercial ac power feed but it was rejected due to the higher cost. As shown in Fig. 8, for normal operation the commercial ac power is fed to the charging equipment in a conventional −48 volt battery plant and directly to the utilities, which include the lights, pumps, fans, and water chillers. The −48 volt battery, which is engineered for a 3-hour reserve, in turn provides power for the repeater dc-dc converters and for the converters that power other station electronics. Long-term ac reserve is provided by a 60-kW turbine-al-

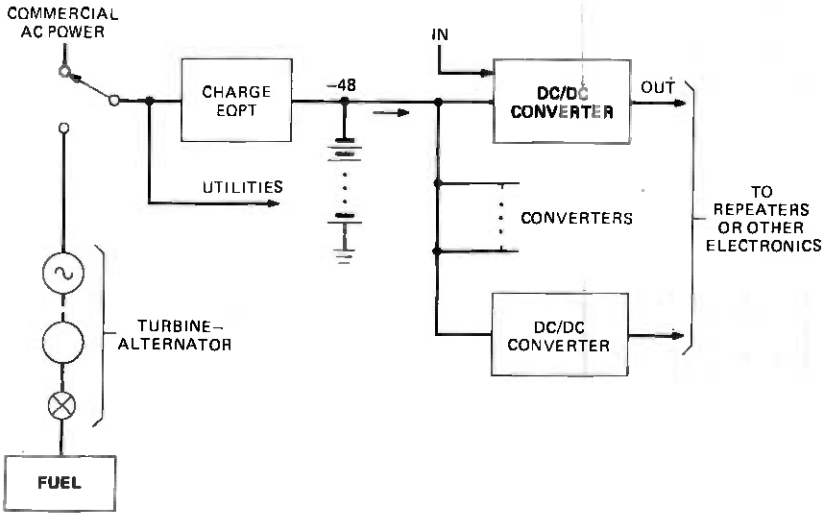

Fig. 8—Local powering arrangement for WT4 repeaters.

ternator for extended commercial ac power failures. The dc power required from the −48 volt battery to power the station electronics is 7500 watts. The dc pump motor for the frame chilled-water system will require an additional 1500 watts. The total ac power required for these two load elements, allowing for rectifier inefficiencies, is 10.3 kW. To this must be added 30.1-kW ac power for the utilities, water chillers, and other environmental control equipment for a total of 40.4 kW required from the turbine-alternator.

4.4 Auxiliary electronics

In addition to the above, each regular repeater station requires an auxiliary communications bay and fault location bay.[5] These units are shown on the floor plan layout in close proximity to the repeater bays to which they interconnect. Space is also reserved for any future equipment necessary for add/drop features.

4.5 Equipment interconnections

Equipment installation is completed by providing the wiring, cabling, and piping between the bays. For the WT4 repeater station, these interconnections include—beyond the standard power and cable runs—stainless steel piping between the water chillers and the process cooler or repeater frames, and copper tubing for both nitrogen control systems. With conventional construction, this effort would be coordinated with and logically follow the on-site equipment installation. With modular buildings, the task is a more complicated one. The extent of the prein-

stalled wiring and piping is dependent on a number of factors. These include the location of the module parting line, the amount of intermodule activity, and the effort required to reconnect any terminated conduits. A final decision on this matter will be made at a later date.

V. FUTURE WORK

Although much design effort and model building have gone into the items described, no actual WT4 repeater station has been built. As a result, details of several items have not been finalized. The two main areas requiring significant work are the modular building concept and the construction details of the utility tunnel.

5.1 Modular buildings

The experience of the field evaluation trial demonstrated that assembled diplexer arrays can survive shipment in a transportable or modular building. However, this fact alone does not answer all the questions of the modular building approach. A standard repeater station requires two modules, with a possible parting line shown in Fig. 7. A KS-specification, detailing the architectural and structural requirements for each module, is required. In addition, procedures for on-site placement of each module as well as interfacing and joining of the modules are required.

5.2 Utility tunnel details

A mock-up of the proposed utility tunnel has been constructed and used to validate the feasibility of the concept. The interfacing of the tunnel with the building, however, has yet to be implemented. Since the tunnel is structurally independent of the upper structure, some means must be developed to tie the two structures together. Utilization of modular buildings will require integration of a slab foundation with the utility tunnel as well as the transportable shelter. Provisions must also be made for the more complicated interface arising from an angular orientation of the utility tunnel with respect to the building.

VI. SUMMARY

Although additional work remains for final implementation of the proposed WT4 repeater station, sufficient groundwork has been laid to give reasonable confidence in its design. The proposed station answers the basic questions of construction and installation flexibility, and safe operation. Implementation of the proposed station should result in a highly reliable segment of the overall WT4 system.

VII. ACKNOWLEDGMENT

The authors express their thanks to R. P. Guenther for his helpful contributions on the utility tunnel concept.

REFERENCES

1. J. C. Anderson, R. W. Gretter, and T. J. West, "Route Engineering and Sheath Installation," B.S.T.J., this issue.
2. H. A. Baxter, W. M. Hauser, D. R. Rutledge, "Waveguide Installation," B.S.T.J., this issue.
3. R. P. Guenther and W. M. Hauser, "Reliability and Maintenance of the WT4 Transmission Medium," B.S.T.J., this issue.
4. E. T. Harkless, A. J. Nardi, and H. C. Wang, "Channelization Plan and Networks," B.S.T.J., this issue.
5. C. E. Barnes et al., "Regenerative Repeaters," B.S.T.J., this issue.
6. M. J. Bonomi et al., "Protection Switching, Auxiliary Communication, and Maintenance," B.S.T.J., this issue.

THE BELL SYSTEM TECHNICAL JOURNAL
Vol. 56, No. 10, December 1977
Printed in U.S.A.

WT4 Millimeter Waveguide System:

Field Evaluation Test System Performance

By S. S. CHENG, E. T. HARKLESS, R. W. MUISE, W. E. STUDDIFORD, and D. N. ZUCKERMAN

(Manuscript received April 7, 1977)

The WT4 waveguide transmission system is a long-haul digital transmission system operating at 274 Mbaud. Field tests have been carried out on a trial WT4 system including span terminating equipment, repeaters, channelizing networks, and a 14-km waveguide line from Netcong to Long Valley, New Jersey. In this paper the configuration and the principal results of the trial are described. Channelizing networks and repeaters were installed and equalized at 12 different frequencies from 40 to 108 GHz. The principal results include loss and delay measurements of the waveguide and the channelizing networks, and error-rate measurements of two-phase repeaters transmitting 180 ° phase-shift keyed pulses over the WT4 waveguide line. Extrapolation of the 14-km waveguide loss and the gain and error rate performance of the installed two-phase repeaters indicates that a system with four-phase repeaters operating at the same symbol rate could have spacings as large as 50–60 km.

I. INTRODUCTION

The WT4 waveguide transmission system is a long-haul, high-capacity digital transmission system. The system frequency multiplexes 124 high-frequency carriers into the band 40–110 GHz with each carrier phase-modulated by a 274-Mbaud digital bit stream.[1]

A field evaluation test was carried out in order to obtain a measure of the overall system performance of the WT4 waveguide transmission system. This test included all the elements of a complete operating system such as protection switching, span terminating, fault locating, auxiliary communications, and maintenance, in addition to 12 operating

repeaters, channelizing networks, and 14 km of field-installed waveguide.

In this paper the emphasis will be placed on the combined performance of the repeaters, line equalizers, channelizing networks, and the waveguide medium. Companion papers[2–5] discuss the design of each of these individual elements in detail. Similarly, the span terminating, protection switching, auxiliary communications, and maintenance subsystems are discussed in an additional companion paper.[6]

For the field evaluation test, 14 km of waveguide was installed from a metropolitan junction station at Netcong, New Jersey, to a temporary equipment shelter at Long Valley, New Jersey. At each end of the waveguide a complete band diplexer array was installed along with enough channel diplexers to allow the testing of the 12 repeaters that were built for the field evaluation test.* The repeaters were divided into four groups, each of three repeaters centered near 40, 55, 80, and 110 GHz. Since six of the repeaters operate below 75 GHz and transmit in one direction while the other six transmit in the opposite direction, this arrangement could be used to connect up to 12 repeaters in tandem by looping back at baseband. The repeater frequencies were carefully chosen so that adjacent channel interference and interferences from harmonically related frequencies could be evaluated; for example, 40-GHz repeaters interfering with 80-GHz repeaters. Because the waveguide run is short, attenuation was provided in the rectangular waveguide portion of the system to adjust the power levels to approximate the loss of 40 km or more of waveguide. This loss was provided in the form of both fixed and variable attenuators and could be placed at either the transmitting or receiving end or could be divided between them.

The main objective of the tests was to measure repeater performance in the field where we would encounter degradations due to transmission deficiencies of the line (the waveguide and the channelizing networks), misequalization, interchannel interference, interactions between the repeaters and the channelizing networks, baseline wander and bit timing recovery phase jitter. The results of the tests were then used to predict system performance and repeater spacing for an advanced system using four-phase repeaters. The repeaters used in the test were two-phase repeaters using a differentially coherent phase shift keying (DCPSK) digital modulation scheme to transmit 274 Mb/s. The advanced four-phase repeater would use a coherent PSK scheme to transmit 548 Mb/s.

II. CHANNELIZING NETWORK

The array of filters to be used to connect individual channels to the

* For a detailed discussion of the millimeter-wave channel diplexers, band diplexers, and channelizing network, the reader is directed to Reference 4.

Table I — Midband insertion loss for channelizing networks

Frequency, GHz	Insertion loss	
	Netcong, dB	Long Valley dB
40.235	3.4	3.5
40.760	3.6	3.6
41.285	3.6	3.6
53.910	5.3	5.7
55.085	9.4	9.8
55.610	9.5	9.4
80.465	8.2	8.8
80.990	8.0	9.0
81.515	8.2	8.8
107.665	5.9	6.4
108.190	6.0	6.4
108.715	5.3	5.1

waveguide medium has been described in Ref. 4. Two complete band-splitting filter arrays were constructed and installed at Netcong and Long Valley. Five of the seven subbands at each location were partially equipped with channel-dropping filters; i.e., filters for all 12 field evaluation test frequencies were installed at both ends and in addition, Long Valley had six additional filters in the 80-GHz subband for a total of nine channel filters connected in tandem. The insertion loss and differential delay were measured from the circular waveguide connection port to each of the 12 or 18 rectangular waveguide connection ports. The circular waveguide medium is connected to the circular port and the repeaters are connected to the rectangular ports. Each of these loss measurements was compared with the sum of the individual filter losses which had been previously measured in the laboratory. The average disagreement between measurement of the assembly and the sum of the pieces was 0.2 dB. The worst interaction between filters occurred in the subband near 55 GHz where return loss and mode conversion echoes created fast transmission ripples. Table I gives the midband insertion loss measured for each of the field evaluation test channels at Netcong and Long Valley. It is seen that the lowest-frequency channel has a channelizing network loss of about 3.5 dB and the highest frequency about 5.2 dB. These values correspond to the system objective of obtaining lowest channelizing-network loss at the lowest frequency and fairly low loss at the highest frequency so as to complement the loss shape of the medium.

III. LINE EQUALIZATION

The equipment and techniques for equalization of the field evaluation test system are described in a companion article.[3] Each transmitter-receiver pair, connected back-to-back through a flat precision attenuator, was measured first in the laboratory and then again at intervals of several months, after shipment to the field. The largest changes ever observed

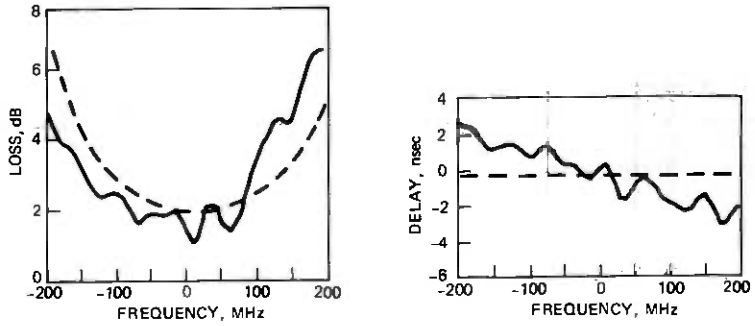

Fig. 1—Unequalized loss and delay characteristics.

in the back-to-back response were ±0.2 dB and ±0.2 ns with typical changes being ±0.1 dB and ±0.1 ns, which compares favorably with the measurement accuracy of ±0.1 dB and ±0.1 ns.

The characteristic of a line is the difference between the back-to-back response and the response with the channelizing networks and waveguide inserted between the transmitter and the receiver. Since all measurements are stored on tapes in the test set, differences are immediately available. A comparison with the desired optimum response for the channel established the required equalizer shape. Equalizers with the appropriate shape were laser-trimmed and assembled typically within one week by using a synthesis program available at Bell Labs, Holmdel.

Figure 1 shows the measured characteristics of a channel in the 80-GHz subband (solid curve) and the desired characteristics (dashed curve). The fast ripples in the transfer function are due mainly to the channelizing filters; the waveguide medium contributes negligibly to the ripples. The results of equalization are shown in Fig. 2. Note that the peak-to-peak variations in amplitude and delay after equalization are about ±0.5 dB and ±1.0 ns and that the line equalizer has removed all of the slowly varying distortion. This amount of residual variation is well within our conservative allocation of up to ±2.5 dB and ±2.7 nsec.

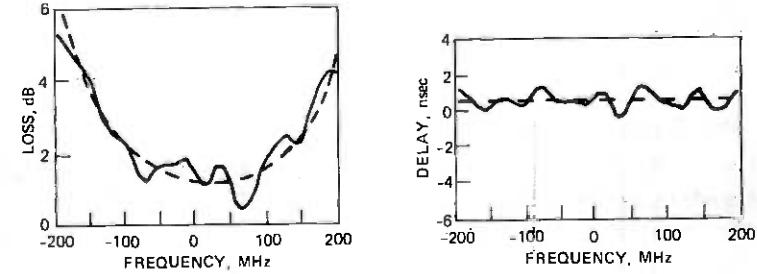

Fig. 2—Equalized loss and delay characteristics.

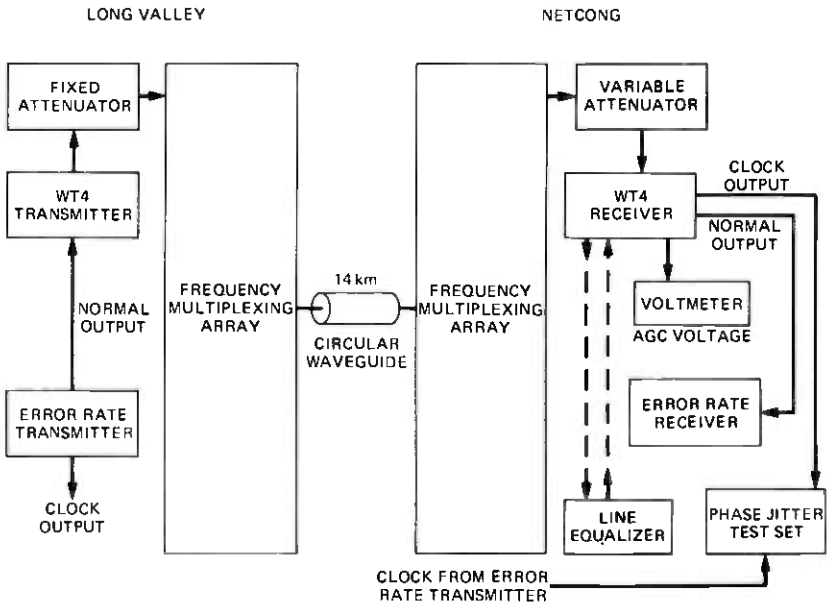

Fig. 3—Equipment arrangement for field measurements.

The line equalizer is a separate unit. It is unique to the particular location and particular line and is independent of the transmitter-receiver pair. Since the equalizer package is passive, it is not prone to fail; should it fail, a duplicate can be made based on the original test data. Therefore, the equalization test set is needed only during initial installation; it is not required as part of any maintenance and repair procedure.

IV. ERROR RATE MEASUREMENTS

Since the WT4 system is a digital transmission system, the degradation that it introduces becomes apparent in the form of bit errors. An error-rate measurement is, therefore, an overall measure of system performance and is of paramount importance. For this reason, error rate measurements were made for a number of different system configurations using an error-rate test set. A typical arrangement is shown in Fig. 3. At the transmitter the error-rate test set can generate a pseudorandom pulse sequence of either length $(2^{11}-1)$ or $(2^{15}-1)$ and at the receiver the test set can synchronize to either of these signals and detect any line errors. With sequences of these lengths we can measure the effects of intersymbol interference spread over as much as five to seven time slots. The fixed attenuator after the transmitter and the variable attenuator ahead of the receiver provided a means of varying the received power so that error rate versus received power or versus signal-to-noise ratio

could be measured. As indicated by the dashed line, the performance with or without the line equalizer could be measured.

Other arrangements were to measure the error-rate performance of one channel while sending data over an adjacent channel or a harmonically related channel to determine the amount of adjacent and interchannel interference. Tests were also run with repeaters connected in tandem to insure that electrical interfaces had been satisfactorily engineered.

An error-rate objective of 10^{-9} or less per repeater hop was set to insure that a long-haul system encompassing as many as 200 repeaters would have a very small probability of having an error rate which exceeded 10^{-6}, 10^{-6} being the long-haul error rate objective.

From these measurements the available gain of the repeater (G_A) and the required relative carrier power (RCP) for an error rate of 10^{-9} could be determined. G_A is an overall measurement of the repeater performance and is given by

$$G_A = P_T - P_R \quad \text{dB}$$

where P_T is the output power of the transmiter and P_R is the minimum receiver input power in dBm for an error rate of 10^{-9}. That is, G_A is the maximum attenuation that can be placed between the transmitter and the receiver and still have the repeater operate at an acceptable error rate. Since G_A is defined in this manner it inherently encompasses all sources of degradation and all noise contributions and is the single most important measure of repeater performance. G_A is defined for each broadband channel and is, therefore, a function of frequency.

The minimum receiver input power P_R for a 10^{-9} error rate can be written in a simplified manner as

$$P_R = N_T + \text{NF} + \text{RCP} \quad \text{dBm}$$

where N_T is the thermal noise, at room temperature, in a bandwidth equal to the signaling rate of 274.176 Mbaud and NF is the noise figure of the receiver. RCP, the relative carrier power, is a comparative measure of how large the carrier power must be relative to the actual noise level in the signaling rate bandwidth, so that the repeater will operate at an error rate of 10^{-9}.

RCP is made up of two parts. The first part, "theoretical minimum," is the RCP that would be required for an optimum transmission and detection scheme. The second part, known as the "degradation," is the additional power that is required because none of the system elements, such as the transmitter, channelizing networks, waveguide medium, or receiver are ideal.

Table II is a summary of our measurements of required RCP. There are three sets of measurements: (*i*) back-to-back in the laboratory, (*ii*)

Table II — Relative carrier power measurements

Frequency, GHz	Back-to-back, dB	Line unequalized, dB	ΔRCP, dB	Line equalized, dB	ΔRCP, dB	Objective, dB	RCP margin, dB
40.235	15.8	—	—	17.4	1.6	22	4.6
40.760	14.7	—	—	16.8	2.1	22	5.2
41.285	15.1	—	—	16.1	1.0	22	5.9
53.910	15.6	17.6	2.0	16.4	0.8	22	5.6
55.085	15.4	20.2	4.8	18.3	2.9	22	3.7
55.610	14.7	19.7	5.0	18.2	3.5	22	3.8
80.465	16.0	17.8	1.8	17.9	1.9	22	4.1
80.990	14.6	17.0	2.4	16.9	2.3	22	5.1
81.515	15.7	16.4	0.7	17.1	1.4	22	4.9
107.665	14.6	16.7	2.1	17.1	2.5	22	4.9
108.190	15.8	18.7	2.9	18.5	2.7	22	3.5
108.715	15.3	16.9	1.6	16.9	1.6	22	5.1

over the line without equalization, and (*iii*) over the line with equalization. The ΔRCP columns are the increases in RCP above the laboratory back-to-back measurements. For the lowest frequency channels there are no "unequalized" measurements because the large amount of linear delay distortion at these low frequencies precluded error rate measurements without equalization. Note that the average RCP in the back-to-back mode is about 15.2 dB which is 2.2 dB above the theoretical minimum for DCPSK of 13.0 dB at an error rate of 10^{-9}. After equalization, the average RCP is 17.3 dB for an average penalty of 2.1 dB above back-to-back. Furthermore, even the worst channel (18.5 dB) is well below our system design objective of 22 dB. Note that the line equalizer is most effective for low frequencies where there is a large amount of linear delay distortion and becomes less effective as the frequency increases.

In a similar manner, Table III presents results of the error rate measurements in terms of available gain. Here we show the transmitter power (P_T) and the minimum receiver power (P_R) for 10^{-9} error rate. The available gain is G_A. Note that in only one case, 107.665 GHz, are we below our objective, and then only by 0.1 dB. This was due to higher-than-expected loss in both the mixer and the phase shift modulator. Note in general that we tend to have more margin at the lower frequencies due to better mixer and phase shift modulator performance.

V. LEAKAGE AND INTERFERENCE

With 62 transmitters and 62 receivers connected to each end of every transmission span, there are many opportunities for leakage and interference. The millimeter-wave channelizing filter two-pole response is such that the adjacent channel leakage is only 14 dB down at the center of the pass band. However, several field evaluation tests have shown no

Table III — Available gain measurements

Frequency, GHz	P_T, dBm	P_R, dBm	G_A measured, dB	G_A objective, dB	G_A margin, dB
40.235	19.5	−59.1	78.6	72.6	6.0
40.760	19.9	−60.4	80.3	72.6	7.7
41.285	19.3	−59.3	78.6	72.6	6.0
53.910	17.2	−56.8	74.0	69.7	4.3
55.085	17.4	−54.5	71.9	69.5	2.4
55.610	16.9	−58.4	75.3	69.5	5.8
80.465	13.7	−54.0	67.7	65.2	2.5
80.990	13.1	−53.7	66.8	65.2	1.6
81.515	13.6	−56.2	69.8	65.2	4.6
107.665	10.3	−51.0	61.3	61.4	−0.1
108.190	11.0	−52.4	63.4	61.4	2.0
108.715	9.7	−54.9	64.6	61.4	3.2

P_T = transmitter power, dBm
P_R = received power for 10^{-9} error rate, dBm
G_A = available gain, dB
$G_A = P_T - P_R$

measurable degradation due to the presence of an adjacent channel signal. It is expected that a change to four-phase modulation will result in only a small (less than 0.1 dB) increase in this degradation. Attempts have been made to measure second harmonic output from field evaluation test transmitters, but no energy has been detected with systems capable of measuring to −65 dBm. Similarly, the field evaluation tests have shown no measurable second harmonics. A series of nine different field tests looking for image response and receiver response to the local oscillator second harmonic has yielded only one detectable interfering tone and no measurable degradations of the system response at a 10^{-9} error rate.

VI. BASELINE WANDER AND TIMING RECOVERY PHASE JITTER

The investigation of two phenomena, baseline wander and timing recovery phase jitter, required a slight modification of the test setup as shown in Fig. 3. Baseline wander is a term used to describe the degrading effect of removing the low-frequency portion of the baseband signal by utilizing ac coupling in the regenerator, a technique which greatly simplifies the circuit design. The ac coupling used had a 3-dB cutoff frequency of about 10 kHz and since a pseudorandom sequence of length equal to $2^{15}-1$ at a signaling rate of 274 Mbaud has frequency components spaced every 8.4 kHz, a longer sequence was required to measure the degrading effects. Similarly, the closed loop bandwidth of the timing recovering phase-locked loop is also about 10 kHz and, therefore, again required a longer sequence in order to test the degrading effects of bit timing recovery phase jitter. A longer sequence was generated by cascading two pseudorandom word generators, one of length $2^{11}-1$, and the

other of length $2^{15}-1$ to form a word of length $(2^{15}-1)(2^{11}-1)$ which is approximately 2^{26} and which has frequency components spaced every 4.1 Hz. Error rate measurements using first the short sequence $(2^{15}-1)$ and later the long sequence (2^{26}) indicated that neither baseline wander nor phase jitter introduced any measurable degradation (less than 0.1 dB). Using the long sequence, the measured rms phase jitter was about 0.5 deg for a single repeater and was about 1.4 deg for a cascade of 10 repeaters. The phase jitter was measured by comparing the relative phase of the clock output of a repeater and a highly stable reference clock in the error rate transmitter. This phase jitter performance was very close to what was anticipated and an extrapolation of this data indicates that for a complete system of about 200 repeaters the rms phase jitter should be less than 10°. This is quite acceptable considering the fact that the digital multiplexers can easily handle phase jitter in excess of several hundred degrees.

VII. SUMMARY

In determining overall system performance, the available gain, G_A, of the repeater, both in the laboratory and again in the field after installing the repeater, has been measured. Also, the relative carrier power RCP (an important component in determining available gain) has been measured under both conditions. The relative carrier power and, of course, the available gain is a function of the measurement conditions; i.e., if interfering tones or distortions of the transfer function shape are present, then greater RCP is required to attain the error-rate objective. Table II shows the measured RCP for the two conditions. The required RCP for a 10^{-9} error rate changed from about 15 dB to 18 dB primarily due to distortion in the transfer function shape introduced by the channelizing networks and the transmission medium. The available gain would, of course, be correspondingly reduced by 3 dB.

In order to understand the significance of the measured available gain of the repeater and the loss of the waveguide medium, we can make the following calculation. At 40 GHz, 78 dB of available repeater gain was measured in the laboratory. When the repeater was installed in the field, there was a 2-dB reduction in available gain. Furthermore, when the repeater was installed in the field, the RCP was about 17 dB. In our system design we have assumed an RCP of 22 dB, which means a safety margin of 5 dB above the measured value of 17 dB. This is more than sufficient to take care of aging and additional interference that might occur when all 124 channels are operating. Therefore, the available gain that we should use for an installed two-phase repeater at 40 GHz is 71 dB. This was arrived at by taking the laboratory measurement of 78 dB and subtracting the 2-dB reduction actually observed in field installation and also subtracting the additional margin of 5 dB.

This available gain must overcome the loss of the channelizing networks at each end, the loss of the waveguide medium, and the additional loss that might be incurred during a waveguide repair. At 40 GHz the loss of the channelizing networks is 7 dB and we have allowed 3 dB of additional loss during the time the waveguide medium is being repaired if it has been damaged and for route rearrangements.[8] These two components sum to 10 dB and when subtracted from the available gain of 71 dB mean that 61 dB of loss is allowed for the medium at 40 GHz. The medium loss as measured is 1.0 dB/km at 40 GHz.[7] Therefore, 61 dB of loss is equivalent to a repeater spacing of 61 km. A similar calculation at 109 GHz yields a 62-km repeater spacing. Thus, we can conclude that the field evaluation test system performance is more than adequate to insure very large (in excess of 60 km) two-phase repeater spacing.

For future development of a commercial four-phase system, as discussed in Alsberg et al.,[1] the operating frequency band is being shifted to 38–104.5 GHz. Laboratory tests of improved repeater circuitry indicate that available gains ranging from 75 dB at 38 GHz to 59 dB at 104.5 GHz can be expected. This estimate of four-phase repeater available gain means that we could expect a four-phase system to have a repeater spacing of 50–60 km.

VIII. ACKNOWLEDGMENTS

The success of the field evaluation test was due to the efforts and cooperation of many individuals. In particular, P. Brostrup-Jensen, R. J. Brown, J. J. Schottle, and P. J. Tu provided the line equalization test set, the line measurements and the line equalizers. Their results were reported on in this paper and in a companion paper in this issue of the B.S.T.J. B. T. Verstegen assisted in performing the channelizing network measurements. A. F. Caruso and A. C. Chipaloski assisted in performing the repeater measurements. And last but not least a great deal of physical design support was provided by A. J. Nardi, S. Shapiro, W. G. Thompson, and H. H. Weinreich.

REFERENCES

1. D. A. Alsberg, J. C. Bankert, and P. T. Hutchison, "The WT4 Millimeter-Wave Transmission System," B.S.T.J., this issue.
2. C. E. Barnes, P. Brostrup-Jensen, E. T. Harkless, R. W. Muise, and A. J. Nardi, "Regenerative Repeaters," B.S.T.J., this issue.
3. P. Brostrup-Jensen, R. J. Brown, J. J. Schottle, and P. J. Tu, "Line and Repeater Equalization," B.S.T.J., this issue.
4. E. T. Harkless, A. J. Nardi, and H. C. Wang, "Channelization Plan and Networks," B.S.T.J., this issue.
5. R. J. Boyd, W. E. Cohen, W. P. Doran, and R. D. Tuminaro, "Waveguide Design and Fabrication," B.S.T.J., this issue.
6. M. J. Bonomi, P. Brostrup-Jensen, D. R. Marcotte, R. W. Muise, and P. J. Tu, "Protection Switching, Auxiliary Communication, and Maintenance," B.S.T.J., this issue.
7. J. C. Anderson, J. W. Carlin, D. J. Thompson, and T. J. West, "Field Evaluation Trial—Transmission Medium Achievements," B.S.T.J., this issue.
8. R. P. Guenther and W. M. Hauser, "Medium Reliability and Maintenance," B.S.T.J., this issue.

THE BELL SYSTEM TECHNICAL JOURNAL
Vol. 56, No. 10, December 1977
Printed in U.S.A.

WT4 Millimeter Waveguide System:

Field Evaluation Test—Transmission Medium Achievements

By J. C. ANDERSON, J. W. CARLIN, D. J. THOMSON, and T. J. WEST

(Manuscript received April 7, 1977)

A 14 km length of WT4 millimeter waveguide, designed to operate from 40 to 110 GHz, was installed in northern New Jersey and tested during the AT&T WT4 field evaluation test. The waveguide transmission medium has characteristics and requirements which are quite different from those for existing Bell System facilities, such as coaxial cable or microwave radio. Thus, a significant part of the field evaluation test effort was devoted to the installation and characterization of the waveguide transmission medium. The most significant transmission medium achievements of the field test were: (i) demonstration of the practicality of sheath and waveguide installation with standard construction methods, (ii) low transmission medium losses which allow a repeater spacing in excess of 50 km, (iii) theoretical prediction of electrical losses from mechanical measurements of waveguide curvatures, and (iv) development of an experience and data base from which losses for future waveguide routes were projected. The measured loss of the 14-km-long field evaluation test waveguide line was approximately 1 dB/km or less across the 70 GHz band—the lowest losses for a waveguide system yet reported in the world—which confirms that the installation methods used result in curvatures acceptable for a commercial WT4 system.

I. INTRODUCTION

The WT4 millimeter waveguide transmission system is a long-haul, high-capacity digital transmission system. In order to prove-in the various manufacturing, installation, and maintenance procedures of the

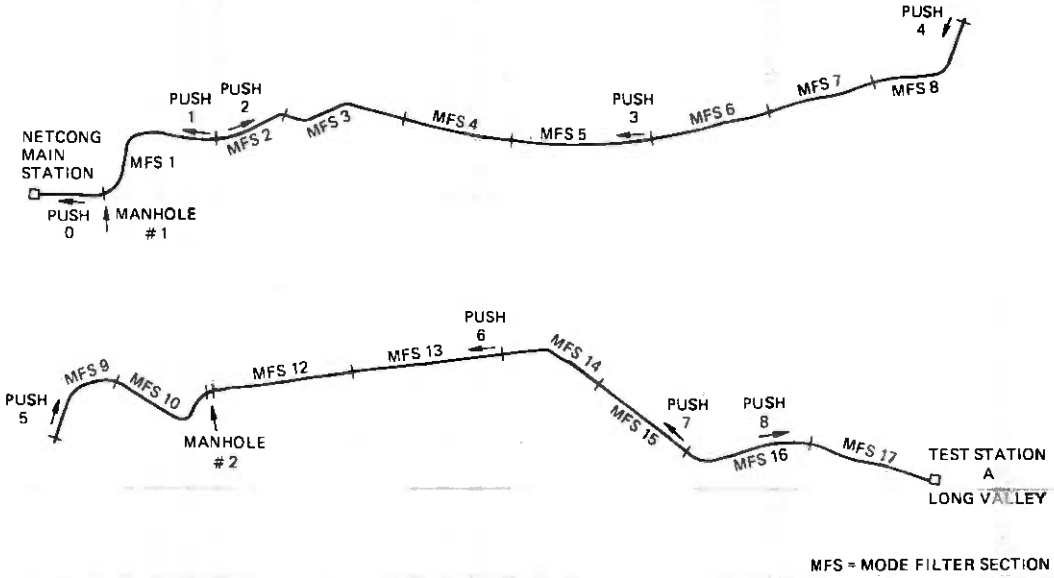

Fig. 1—WT4 field evaluation test between Netcong and Long Valley.

WT4 system, a 14-km length of WT4 millimeter waveguide was installed in Northern New Jersey and tested during the WT4 AT&T field evaluation test. The waveguide is supported on spring supports inside a protective sheath. The waveguide was inserted into the previously installed sheath in several sections, called "pushes." [1] The route, as shown in Fig. 1, began at the Long Lines main station in Netcong and terminated at a temporary facility, Test Station A, in Long Valley, N.J. Two intermediate manholes, which were required to support the transmission medium measurements, were located at approximately 0.4 km and 8.6 km from the Netcong main station. The manholes would not be required for a commercial WT4 system. A variety of route features, typical of those expected for future installations, were encountered along the right-of-way, some of which are listed below:

Push 1, mode filter section 1—steep grade and plan bends.

Push 4, mode filter section 6—Route 206 road crossing.

Pushes 4 and 5, mode filter sections 8 and 9—plan bends and swampy areas.

Push 7, mode filter section 14—severe profile bends in part due to a stream crossing.

Push 8, mode filter section 17—wet area and plan bends.

The installed WT4 transmission medium consists of 60 mm diameter dielectric-lined circular waveguide with one 9-m-long helix waveguide mode filter for approximately every 800 m of dielectric-lined waveguide. Thus the field evaluation test waveguide line consists of 17 mode filter sections each of approximately 800 m in length. The location of each helix waveguide mode filter and each push are shown on Fig. 1.

The field test has proved-in the sheath and waveguide installation procedures for future WT4 commercial applications. The most significant transmission medium result of the field test was the realization of low waveguide losses of approximately 1 dB/km or less across the band, which allow a repeater spacing in excess of 50 km for a commercial WT4 system. The electrically measured transmission medium losses are discussed in Section III. The importance of being able to predict electrical losses from mechanical measurements of the in-place waveguide curvature was recognized early in the WT4 development. The results of the field test mechanical measurements are given in Section IV. Loss calculations and their agreement with electrically measured losses are discussed in Section V. Lastly, the field test has provided data and experience which further our ability to project losses for future waveguide routes. Using field test curvature data and basic statistical models for vertical and horizontal waveguide curvatures, a Monte Carlo computer study was initiated. The initial results from this study for expected losses and loss fluctuations of what is referred to in this paper as nominally

"straight" waveguide sections are discussed in Section VI. In nominally "straight" waveguide mode filter sections, the waveguide has random curvatures due to manufacturing deviations and trench bottom roughness. However, there are no curvatures due to plan bends or grade changes in nominally "straight" mode filter sections.

II. TRANSMISSION MEDIUM INSTALLATION

The field evaluation test transmission medium was constructed in two basic steps. First, the protective steel sheath was constructed along the right-of-way and buried, using methods similar to those used in ordinary pipeline laying. Long Lines Northeastern Area craftspersons supervised the sheath construction which was done by a pipeline contractor. The waveguide was then inserted into the sheath in sections, referred to as "pushes," which ranged in length from 0.5 km to 2.5 km. The push points are indicated on Fig. 1 along with the direction of each push. The Long Lines Northeastern Area craftspersons operated the specially designed waveguide insertion equipment. Thus, the sheath and waveguide installation procedures have been demonstrated to be practical for WT4 commercial applications.[2–4] The field test has also proved-in the WT4 transmission medium reliability and maintenance methods.[5]

III. ELECTRICAL RESULTS

Electrical loss measurements were made from the Netcong main station as each push was completed and for the entire 14 km length of the test.[6] Briefly, a shutter in manhole 1 was used as the reference point for the loss measurements of pushes 1–3, 1–4, 1–5, and 1–8 as described in Ref. 6. Manhole 2 was the reference point for loss measurements for pushes 6, 6–7, and 6–8. The accuracy of the loss measurement at 110 GHz for the entire test length, pushes 1–8, is within 2 percent.[6]

Measured losses of individual pushes are desirable in order to compare them with loss calculations and to determine the dependence of individual push losses on the number and severity of route bends and grade changes. Since the loss measurements are made in a field environment, it is necessary to obtain them with minimum relocation of test equipment. The individual push losses can be obtained from the loss measurements on pushes 1–3, 1–4, 1–5, etc., as follows. The losses of separate mode filter sections can be considered independent of one another because of the helix mode filters between sections. Thus, the loss at any one frequency for individual pushes can be obtained from the above measurements by subtraction. That is, the loss for push 4 is given by the difference between the loss measurements of pushes 1–3 and those of pushes 1–4.

The error associated with the measured loss at 110 GHz for individual pushes is higher than the 2 percent loss measurement error quoted for

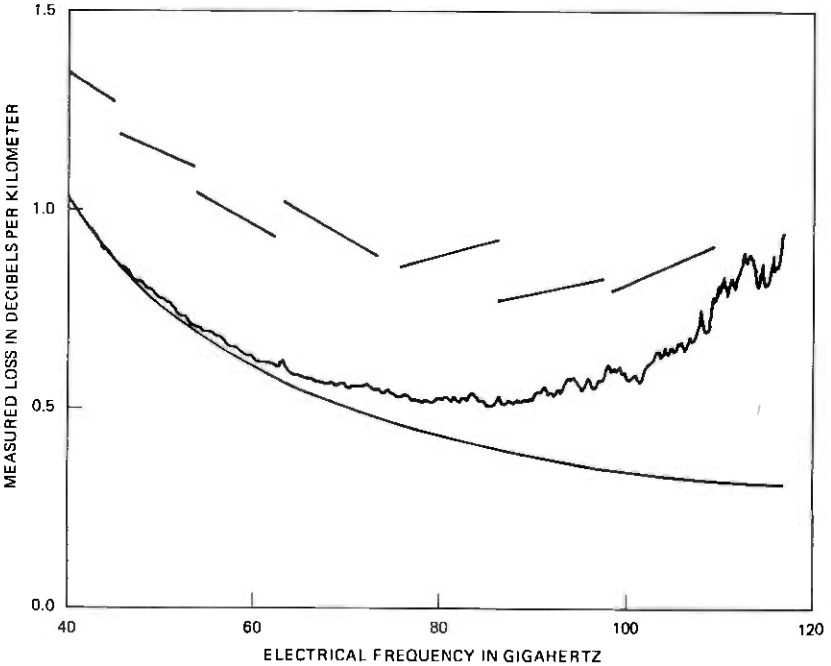

Fig. 2—WT4 field test measured loss; 50-km loss ceilings.

the entire test length, pushes 1–8. The two primary contributors to the error are the loss measurement test set error, as discussed in Ref. 6, and the error incurred by the subtraction process described above. The error in the measured losses at 110 GHz for pushes 5, 6, and 7 is estimated to be about 10–15 percent. This figure is based on both the test set errors and a comparison between the push 6 measured losses with the reference short circuit in manhole 1 and manhole 2.

The measured loss for pushes 1–8, which is approximately 13.6 km long, was approximately 1 dB/km or less across the 70 GHz band from 40–110 GHz. This overall field test loss measurement is shown in Fig. 2 along with the estimated transmission medium heat loss. The medium loss ceilings, also shown in Fig. 2 for a 50-km repeater spacing, depend on the channelizing network loss and on the available gain for the repeater as discussed in Refs. 7 and 8. Several notable observations can be made from this figure. First, the transmission medium losses allow a repeater spacing of 50 km or more across the entire 40–110 GHz band. The losses of approximately 1 dB/km or less across the 70 GHz band are the lowest losses for a waveguide system yet reported in the world.[9,10] These low system losses are the result of concentrated efforts to manufacture, with economical processes, very high quality waveguide, reduce the curvatures which result from installation, and minimize the number

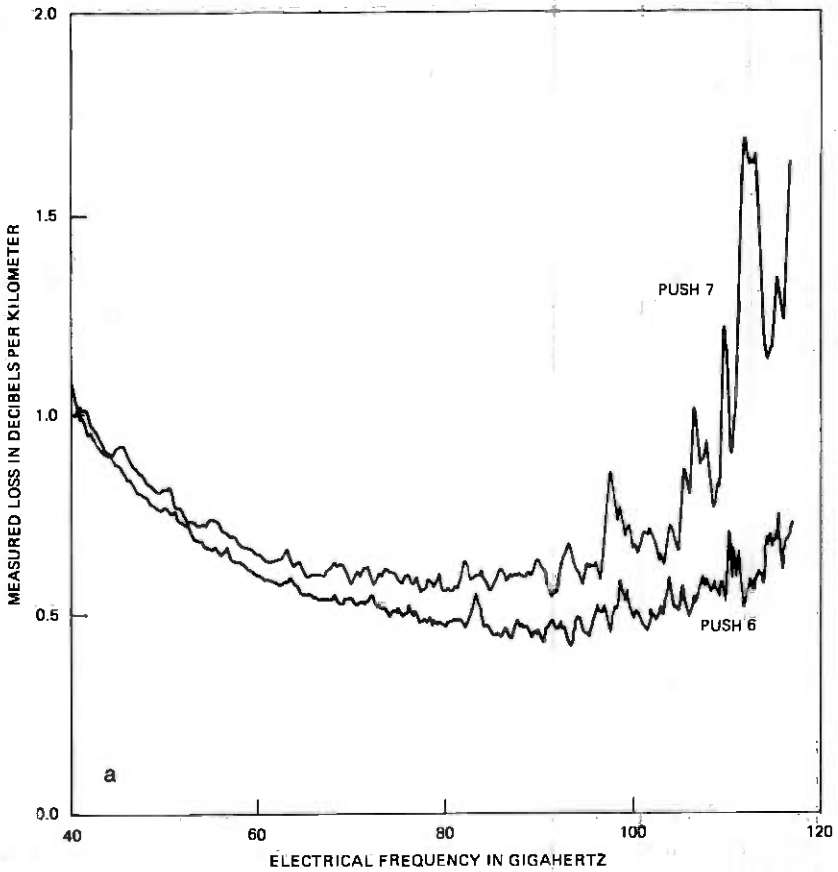

Fig. 3—Measured loss for (a) push 6 and push 7, (b) push 6 and push 5.

of helix mode filters needed for spurious mode suppression.[1,11] The high quality of the manufactured waveguide is particularly reflected in the fact that there is essentially *no* mode conversion loss at the low end of the band. In fact, for all loss measurements made, the transmission medium loss at the low end of the band consisted predominately of heat loss as discussed further in Section V. Thus, the transmission medium loss at the low end of the band is predictable.

The characteristics of the transmission medium loss at the high end of the band are different. At 110 GHz, there is extensive mode conversion loss both in dielectric-lined waveguide and in helix mode filters. At high frequencies, the helix waveguide has much higher loss than the dielectric-lined waveguide and, therefore, contributes significantly to the total loss at 110 GHz. Mode conversion losses at the high end of the band are sensitive to trench bottom roughness and route bends with the second

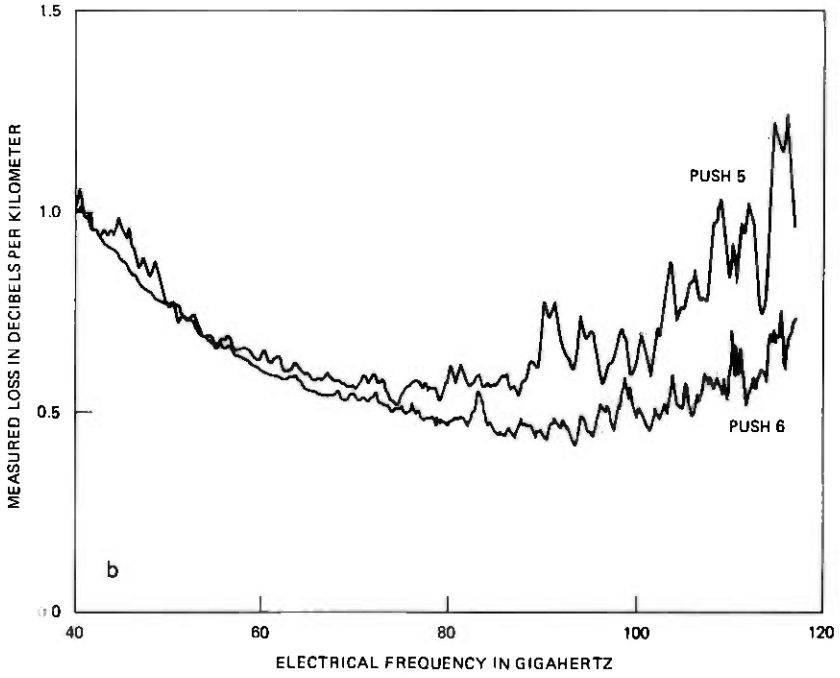

Fig. 3 (*continued*)

order TM_{21} losses being especially sensitive.[12] Consequently, the transmission medium loss at 110 GHz varied considerably from push to push depending on the amount of trench roughness and the type of route bends present. Since second-order TM_{21} mode conversion losses had not been anticipated prior to the field test, the overall loss margin at 110 GHz was smaller than that at 40 GHz. Notice also that this overall loss margin at 110 GHz could be quite different for another route, depending on the number and type of route bends present. Mode conversion losses are discussed further in Section V.

The sensitivity of second-order mode conversion losses to route bends is clearly illustrated in Fig. 3a, which compares the measured losses for pushes 6 and 7. The measured loss for push 6, with only trench bottom roughness and no plan or profile bends, is very low (about 0.6 dB/km at 110 GHz). On the other hand, push 7 had one plan bend and two severe profile bends. The high push 7 loss (over 1 dB/km at the high end of the band) reflects the large second-order mode conversion losses caused by the severe profile curvatures.[12] Figure 3b compares the loss measurements for pushes 5 and 6. Push 5 had several plan bends and also has significant second-order mode conversion losses.

Over the two-year period since the field test was installed, many measurements of loss have been made both on the entire line and on

shorter sections. Comparison of these measurements confirms the stability of the transmission medium losses as a function of time. The losses measured at 40 GHz vary by less than 0.01 dB/km after correcting for temperature variations. At 110 GHz, the variation is less than 0.02 dB/km.

IV. MECHANICAL RESULTS

Mechanical measurements of the installed field test waveguide geometry were also obtained and losses calculated from them. Power spectral densities were calculated from the measured vertical and horizontal curvatures, as a function of length along the waveguide axis.[13] The power spectral density (PSD) of the curvature in the horizontal or vertical plane of a given length of waveguide is the magnitude squared of the Fourier transform of the horizontal or vertical curvature divided by the total length of the waveguide. Each component of mode conversion loss listed below is directly related to either the mean-squared curvature or to the mechanical PSD of curvature or of functions of horizontal and vertical curvatures as given below:

(*i*) Helix loss: mean-squared horizontal and vertical curvature.[14]

(*ii*) TM_{11}, TE_{12} loss: S_{C_h} = PSD of horizontal curvature, $C_h(z)$, and S_{C_v} = PSD of vertical curvature, $C_v(z)$.[15]

(*iii*) TM_{21} loss: $S_{C_h^2-C_v^2}$ = PSD of the function $C_h^2(z) - C_v^2(z)$ and $S_{C_hC_v}$ = PSD of the function $C_h(z)C_v(z)$.[12]

The individual loss components are discussed in greater detail in Section V. The power spectral densities (S_{C_h}, S_{C_v}, $S_{C_h^2-C_v^2}$, $S_{C_hC_v}$) were computed for each mode filter section in the field test and then averaged to obtain average power spectral densities for the entire test length. Figures 4 to 7 show the average power spectral densities, S_{C_v}, S_{C_h}, $S_{C_h^2-C_v^2}$ and $S_{C_hC_v}$, of the installed waveguide for the 14-km-long test. The mechanical frequency ranges which determine the most significant losses in the WT4 band are indicated on each figure. These ranges, for the appropriate spectra, are

0.33 c/m (110 GHz) to 0.51 c/m (51 GHz) for TM_{11}
0.50 c/m (110 GHz) to 1.5 c/m (40 GHz) for TE_{12}
0.04 c/m (110 GHz) to 0.80 c/m (40 GHz) for TM_{21}

The average vertical spectrum in Fig. 4 is relatively flat out to about 0.1 c/m where it drops off rapidly. This low-frequency vertical curvature (below 0.1 c/m) is due primarily to trench bottom roughness and the cutoff is due to the mechanical filter of the waveguide support system.[1] Vertical curvatures at higher mechanical frequencies are associated with manufacturing curvatures in the waveguide and distortions at couplings.[11] The low, 10^{-8} $1/m^2/c/m$ level of the vertical spectrum above

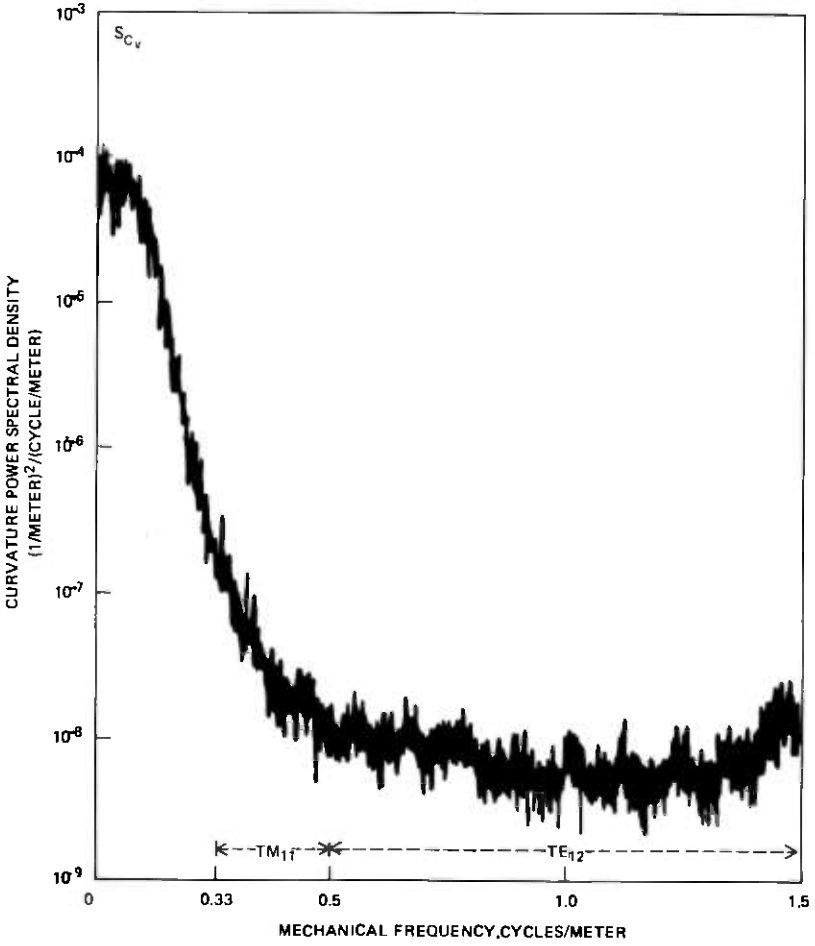

Fig. 4—Average field test vertical curvature spectrum.

0.5 c/m confirms the high quality of the manufacturing and couplings of the waveguide. A vertical spectrum level of 10^{-8} $1/m^2/c/m$ at 0.5 c/m corresponds to a loss of only 0.022 dB/km at 110 GHz due to TE_{12} mode conversion.

The shapes and levels of the spectra are directly related to route features. Profile curves have short arc lengths (less than 30 m) which tend to increase the level of the entire vertical spectrum. However, the waveguide support system filters out most of the increased curvature above 0.1 c/m. To illustrate, Fig. 8 compares the vertical spectra from mode filter section 12 and mode filter section 14. Mode filter section 12 is in push 6, which is "straight," while mode filter section 14 is in push 7, which had severe profile curves. Notice a difference in the vertical

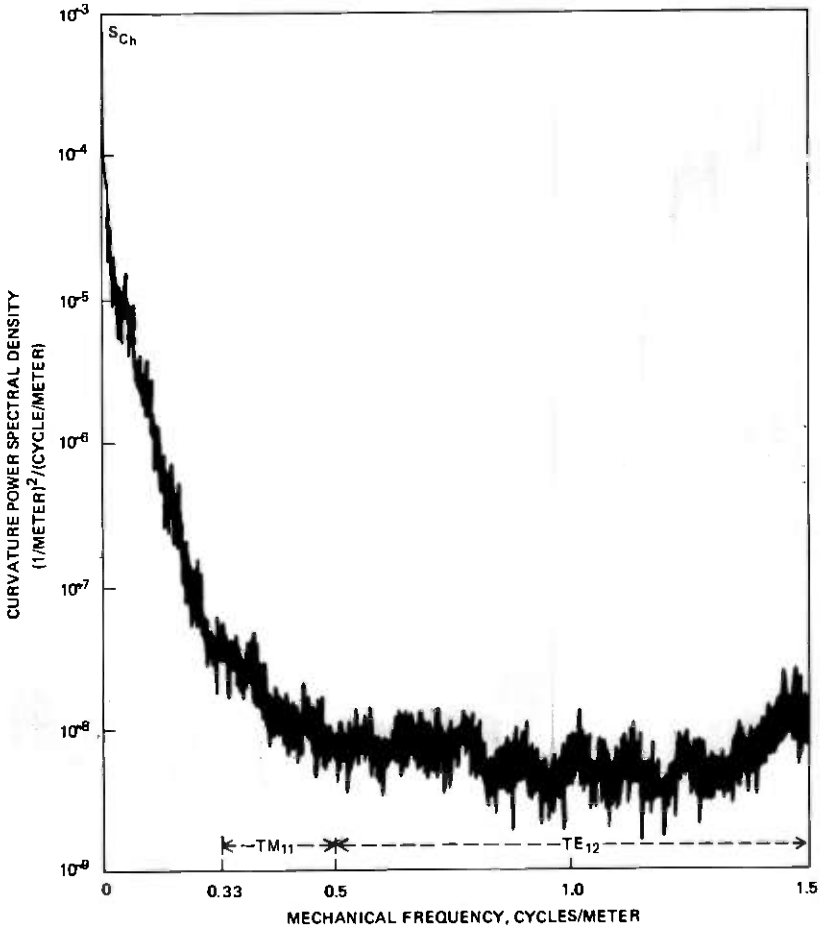

Fig. 5—Average field test horizontal curvature spectrum.

spectra of at least one-half a decade at mechanical frequencies below 0.1 c/m. The difference between these spectra is clearly demonstrated by their respective rms curvatures. Mode filter section 12 has a rms curvature corresponding to a 326 m radius of curvature, whereas the rms curvature for mode filter section 14 corresponds to a 170 m radius of curvature.

Horizontal power spectral densities are affected by plan bends. Unlike profile bends, plan bends usually have long arc lengths (100–200 m) with gradually tapered curvatures into and out of the bends. Therefore, in the horizontal spectrum, a plan bend appears as a narrow peak, much like a delta function, with most of the energy below 0.02 c/m. Figure 9 compares the horizontal spectra for push 5, which had several plan bends,

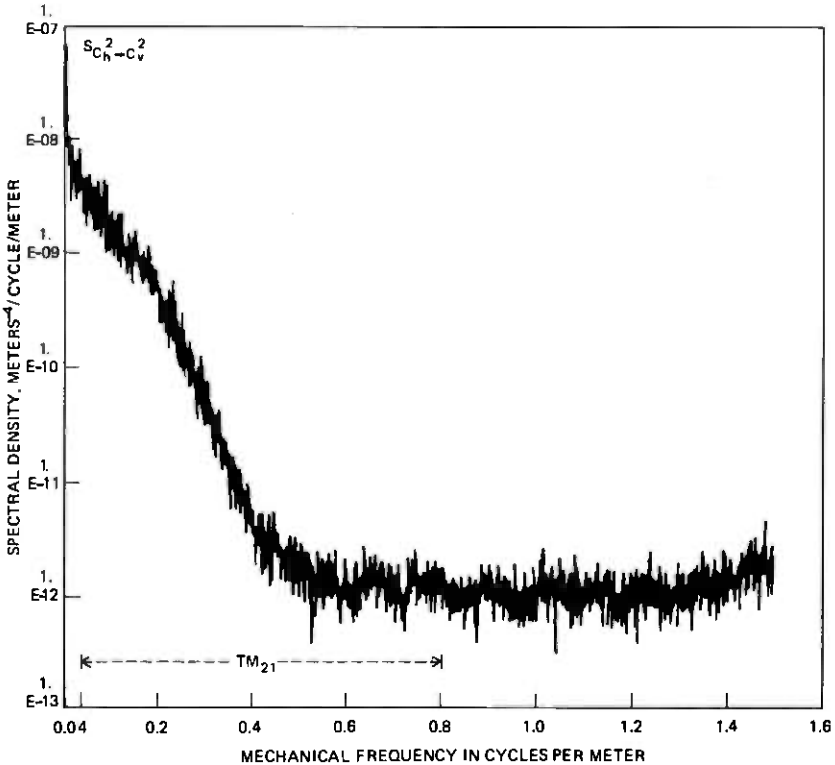

Fig. 6—Average field test $C_h^2 - C_v^2$ spectrum.

with that for push 6 with no plan bends. Notice the high peak (about 5×10^{-3} 1/m^2/c/m at about 0.002 c/m in the push 5 horizontal spectrum.

V. LOSS CALCULATIONS

The WT4 transmission medium losses for the test route have been calculated from mechanical measurements of the in-place waveguide curvatures. Comparison of loss calculations and measured losses for the entire test length and most individual pushes has yielded good agreement. The transmission medium loss calculations include the following loss components:

(*i*) Heat loss
(*ii*) Additional attenuation due to helix mode filters
(*iii*) First-order mode conversion losses (TM_{11} and TE_{12} modes)
(*iv*) Second-order mode conversion losses (TM_{21} mode).

Mode conversion losses to other modes have been calculated from ge-

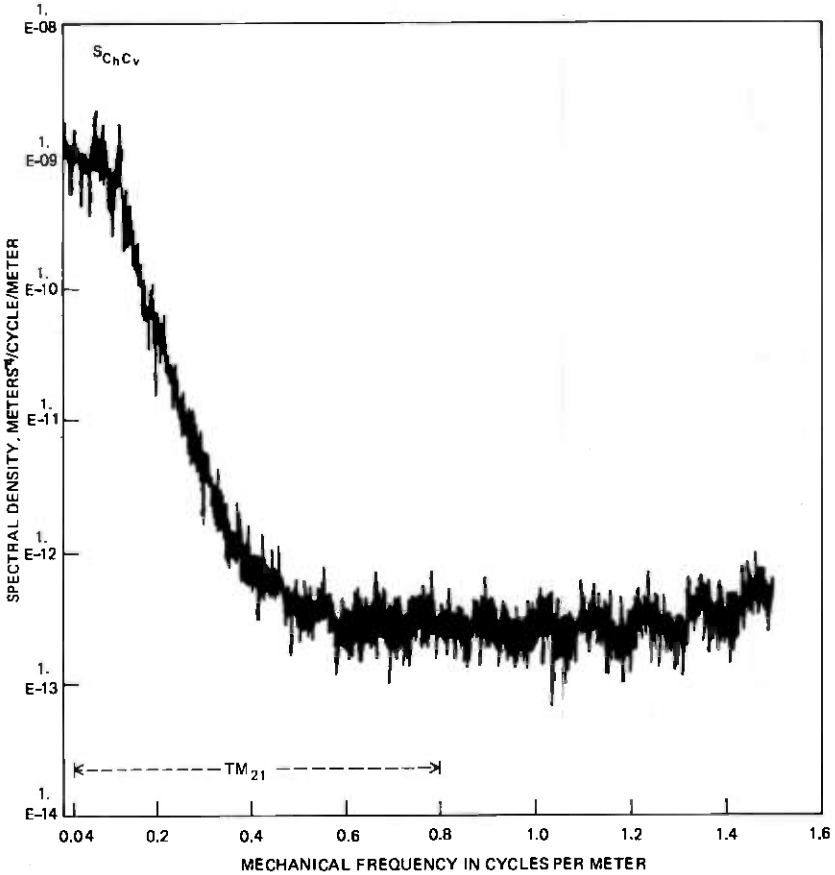

Fig. 7—Average field test C_hC_v product spectrum.

ometry data of manufactured waveguide and found to contribute less than about 3 percent of the total loss and are therefore omitted from the loss calculations. Each loss component is discussed below and is shown on the estimated field test loss curves on Fig. 10.

The transmission medium heat loss is estimated by the formula

$$\alpha + \alpha \times 0.20(f/100)^{1.5}$$

where α is the theoretical ohmic loss, f is the electrical frequency in GHz, and the second term represents additional loss due to copper roughness or surface imperfections. The transmission medium heat loss estimate agrees with laboratory measurements at both the low and high ends of the band. The heat loss estimate of .32 dB/km at 110 GHz may be high by, at worst, 10 percent due to mode conversion losses which may have been included in the laboratory measurements. The heat loss estimate

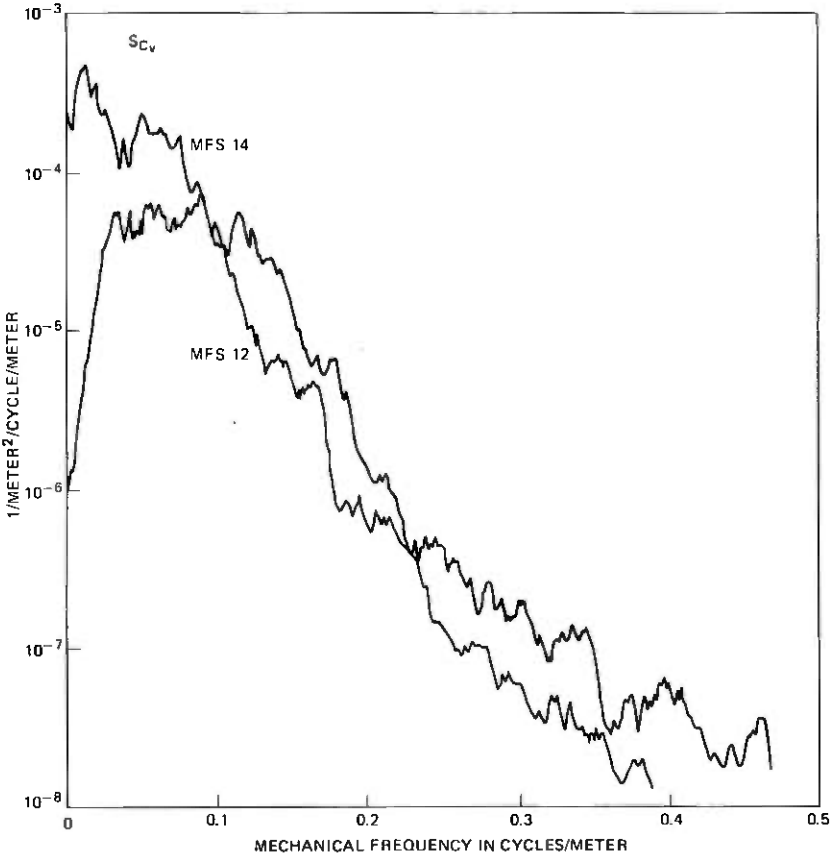

Fig. 8—Vertical curvature spectra.

of 1.03 dB/km at 40 GHz has been confirmed by the field test loss measurements and, notably, is significantly lower than had been anticipated at the beginning of the WT4 development. The measured heat loss at 40 GHz is only 6 percent above the theoretical limit for copper and is confirmation of the high-quality copper plating process.

A direct loss estimate for each helix mode filter in the test from its measured curvature is difficult since the mode filter is only 9 meters long and because the curvatures at its ends are nonzero. Therefore, known methods of calculating loss in helix waveguide are not applicable, necessitating the use of an approximate estimate of the mode filter losses. The helix mode filter loss estimates include loss due to both manufacturing curvatures and curvatures associated with placing.

The helix manufacturing loss was estimated from loss calculations, using the results of Young,[16] and measurements of a string of six precisely

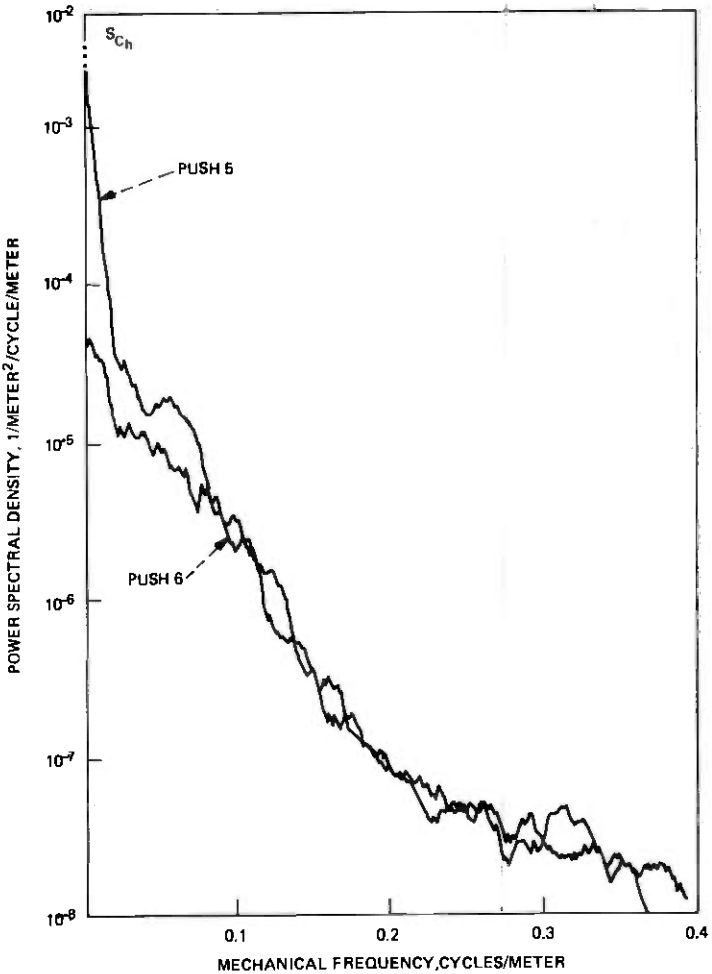

Fig. 9—Horizontal curvature spectra.

aligned, 4.5-meter-long helices which are representative of the test helices. The resulting average helix manufacturing loss was 3.6 dB/km at 110 GHz. Further measurements of field test helices has indicated a possible range of manufacturing loss from 2 dB/km to 10 dB/km at 110 GHz. The source of the large variation in the manufacturing loss for helix waveguide has been identified and will be corrected for the commercial WT4 system.

Helix placing losses were estimated from the mean-squared curvatures measured for each mode filter.[14] The estimated helix placing losses varied from 2 to 20 dB/km at 110 GHz for the test mode filters. The total helix mode filter loss was then estimated by the sum of the average helix

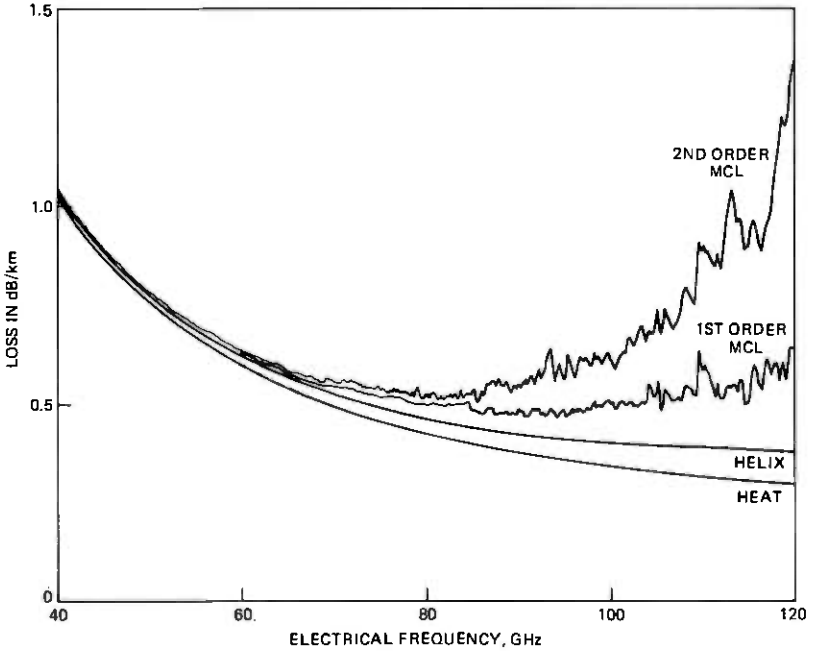

Fig. 10—WT4 field evaluation test estimated loss.

manufacturing loss (3.6 dB/km at 110 GHz) and the helix placing loss derived from the measured mean-squared curvature for each mode filter. Therefore, the total helix losses represent our best estimate of the mode filter losses but may be in error by as much as 50 percent for any one mode filter. A large part of this 50 percent error is due to the fixed 3.6 dB/km estimate of helix manufacturing loss at 110 GHz for each mode filter. However, the predicted helix loss for the entire field test is better and is estimated to have an error of 20 percent or less.

First-order mode conversion losses are directly proportional to the vertical and horizontal power spectral densities, which are calculated from mechanical measurements.[13,15] Modes in circular waveguide can be generated in two polarizations depending on the plane of curvature, as discussed by Carlin and Moorthy.[12] The symbols ↑ and → represent the horizontal and vertical polarizations, respectively. The largest proportion of the first-order losses is usually due to the TM_{11}→ (generated by vertical curvature) mode. The error in the first-order loss calculations is estimated at less than 10 percent, based on comparisons of these first order loss calculations and direct numerical solutions of the coupled-line equations. Second-order TM_{21}↑ and TM_{21}→ losses are approximated by expressions which are proportional to the power spectral densities of $C_h^2(z) - C_v^2(z)$ and $C_h(z)$-$C_v(z)$.[12] Some TM_{21} second-order loss results

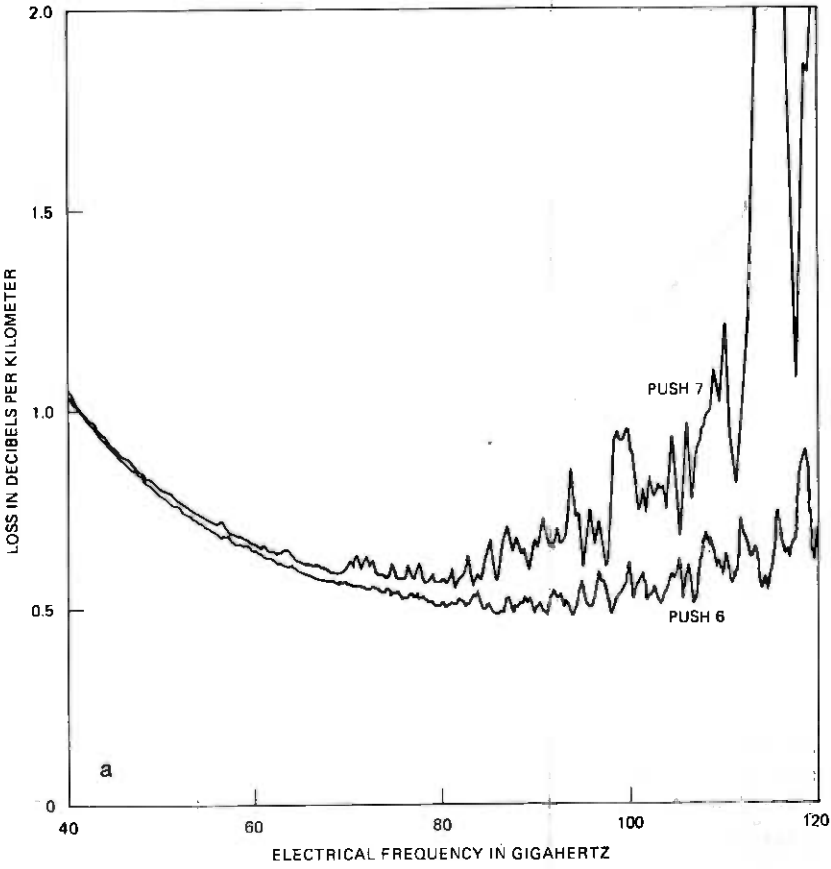

Fig. 11—Netcong curvature loss for (a) push 6 and push 7, (b) push 6 and push 5.

from trench bottom curvatures, but plan or profile bends increase the TM_{21} losses dramatically, as was seen in Fig. 3. These second-order TM_{21} loss calculations are estimated to be accurate to about 20–25 percent except at very high loss peaks as in push 7 at 113 GHz. Comparisons of second-order mode conversion loss calculations to exact solutions are discussed by Carlin and Moorthy.[12]

Figure 10 gives the upward cumulative loss break-down calculation for the 14 km long test with each curve labeled according to the components listed above. Notice that the steeply rising second-order TM_{21} losses comprise about $\frac{2}{3}$ of the total mode conversion loss at the high end of the band. This loss calculation agrees well with the electrically measured test losses shown in Fig. 2. The error between estimated and measured losses for the entire test length increases from about 0.02 dB/km at 85 GHz to about 0.09 dB/km at 117 GHz. The rate of increase

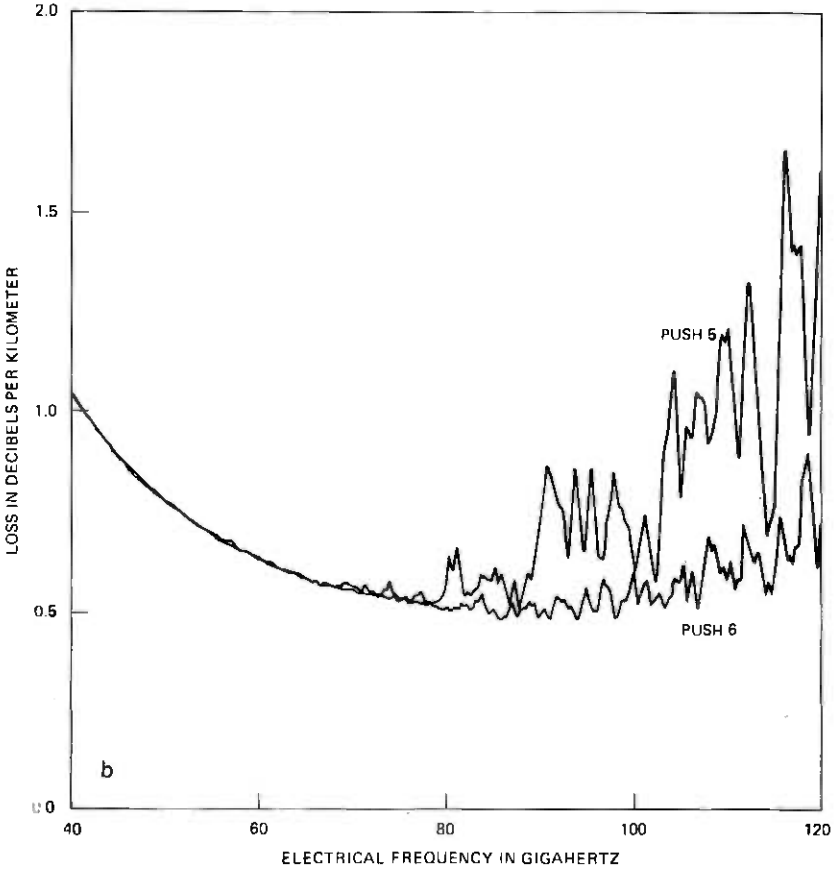

Fig. 11 (*continued*)

for this error is roughly proportional to the fifth power of frequency, indicating that the majority of the error is in the perturbation loss calculations rather than in the helix loss estimate.

Figure 11a compares the estimated losses for pushes 6 and 7. Push 6 has no plan or profile bends but push 7 has two severe profile bends and therefore has significant second-order mode conversion loss. The push 7 loss estimate compares favorably to the measured losses in Fig. 3 except at peaks at the high end of the band and especially at the very high loss peak at 113 GHz. The error between peaks in the estimated and measured losses for push 7 is probably due to the overestimation of the TM_{21} loss.[12] The shape of the push 6 loss estimate agrees with that of the measured losses but is higher than the measurement by about 0.03 dB/km at 60 GHz to about 0.05 dB/km at 110 GHz. This difference may be due to an overestimate of the helix loss or to the errors associated with

the measured losses for a single push as discussed in Section III. Figure 11b compares the loss calculations for pushes 5 and 6. The shape of the estimated loss for push 5, which has several plan bends, agrees well, over most of the band, with the measured loss shown in Figure 3b. Again the estimated loss is higher than the measured loss at loss peaks for push 5, which is probably due to an overestimation of the TM_{21} losses. In general, the rest of the pushes showed similar agreement between calculated and measured losses, as does the overall loss estimate for the entire test length.

VI. STATISTICS OF SPECTRA AND LOSSES

The field test transmission medium curvature measurements have also established a data base for projecting waveguide losses of future WT4 routes. Field test mechanical curvature measurements of in-place waveguide, combined with basic statistical models of curvature, were employed to perform a Monte Carlo computer simulation of waveguide losses. The statistical models used and details of the study are discussed below. The results of the study were estimates of expected losses and loss fluctuations from the TM_{11}, TE_{12}, and TM_{21} modes in dielectric-lined waveguide for a nominally "straight" mode filter section.

For a nominally "straight" waveguide right of way, the curvatures in the horizontal and vertical planes are stationary Gaussian random processes.[13] Thus, their vertical and horizontal curvature spectra, at each mechanical frequency, are each distributed as Chi-Squared random variables with two degrees of freedom. Since first-order mode conversion losses are directly proportional to the vertical and horizontal spectra, the Chi-Squared model for these spectra yields estimates of their loss fluctuations. However, the second-order mode conversion losses are approximately proportional to $S_{C_h^2 - C_v^2}$ and $S_{C_h C_v}$. The distributions of the spectra of $C_h^2(z) - C_v^2(z)$ and $C_h(z)C_v(z)$ do not readily lend themselves to analysis since neither $C_h^2(z) - C_v^2(z)$ nor $C_h(z)C_v(z)$ can be assumed to be Gaussian random variables. To estimate the magnitude of loss fluctuations for second-order mode conversion losses, a Monte Carlo computer study was performed. The horizontal and vertical spectra from seven nominally "straight" mode filter sections of the test were separately averaged to obtain an average S_{C_h} and an average S_{C_v} for "straight" mode filter sections. From these averaged spectra and a pseudorandom number generator, sets of vertical and horizontal curvatures were obtained.

The results of this study of nominally "straight" mode filter sections, were that the $S_{C_h^2 - C_v^2}$ and $S_{C_h C_v}$ were each approximately distributed as a Chi-Squared random variable with two degrees of freedom. A typical quantile-quantile plot of the quantiles of the 140 samples of $S_{C_h^2 - C_v^2}$ vs. the Chi-Squared-2 quantiles is shown in Fig. 12.[17] This particular QQ

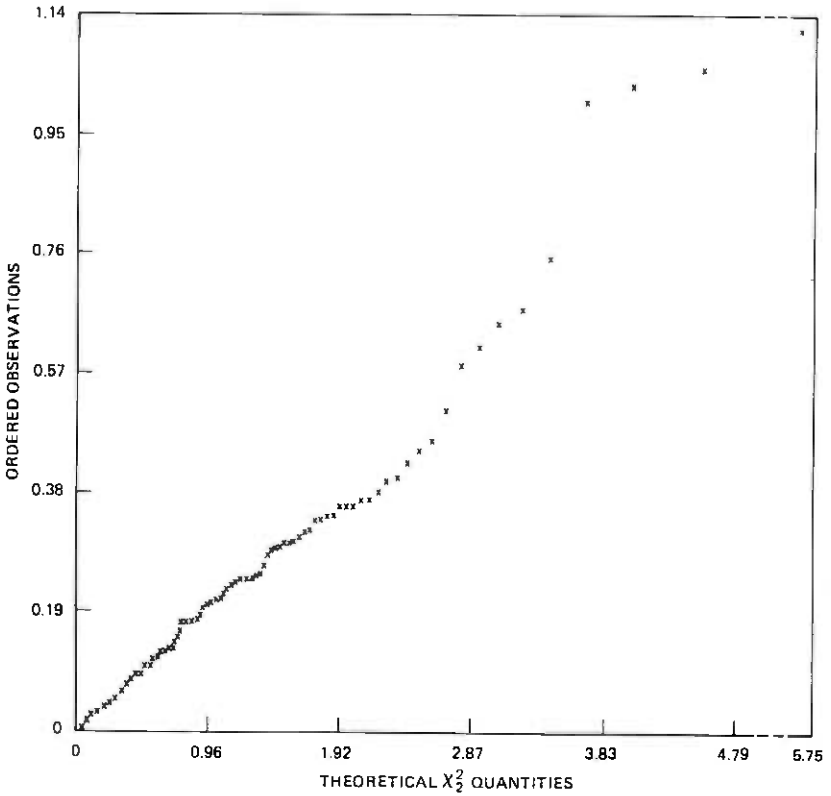

Fig. 12—QQ plot of TM_{21} losses at 110.22 GHz vs. χ_2^2 quantiles.

plot shows the distribution of the $S_{C_h^2-C_v^2}$'s at 0.04 c/m mechanical frequency, which corresponds to 110.22 GHz for the TM_{21} mode.

In addition to ascertaining the approximate distributions of the second-order mode conversion losses, estimates of the total expected losses and loss fluctuations were obtained. The results of the Monte Carlo study for nominally "straight" mode filter sections indicate that almost all the mode conversion loss in dielectric-lined waveguide is due to the $TM_{11}\rightarrow$ mode (generated by vertical curvature) and the $TM_{21}\uparrow$ mode which is generated by the curvature function $C_h^2 - C_v^2$. The estimated expected values of these losses at 110 GHz are about 0.2 dB/km for $TM_{11}\rightarrow$ and 0.16 dB/km for $TM_{21}\uparrow$. The other modes ($TE_{12}\uparrow$, $TE_{12}\rightarrow$, $TM_{11}\uparrow$, and $TM_{21}\rightarrow$) yield a combined mode conversion loss of about 0.05 dB/km at 110 GHz. The expected losses for each mode from 100–110 GHz are shown on Fig. 13. As shown in Fig. 13, there is a $TM_{11}\rightarrow$ loss peak of about 0.1 dB/km at 110 GHz. This loss peak is due to a peak in the vertical spectrum at 0.33 c/m and is also evident in the measured losses discussed in Section III. The peak occurs in the vertical spectra of most

mode filter sections and is believed to be a harmonic of either the tube length or the sheath length. The loss peak at 106 GHz is also due to a harmonic of the tube or sheath length.

Loss fluctuations are also important parameters for future WT4 systems. The distribution of loss for a 50-km-long repeater span has more than 100 degrees of freedom since it consists of more than 60 independent mode filter sections each with at least two degrees of freedom. Therefore, a 3σ repeater span loss is, approximately, at the 99.9 percent confidence level where σ is the standard deviation of loss at any one frequency. Also shown on Fig. 13 is the "3σ" loss based on the loss fluctuations of the Monte Carlo study and a 50-km repeater span consisting of sixty-two 800-m-long, nominally "straight" mode filter sections. This "3σ" loss includes empirical fluctuations from both polarizations of the TM_{11}, TE_{12}, and TM_{21} modes in dielectric-lined waveguide and is about 0.53 dB/km at 110 GHz. Any practical route would contain both plan bends and grade changes along with their associated increases in loss and loss fluctuations. Therefore, Monte Carlo studies for mode filter sections containing plan and profile bends are currently in progress.

Preliminary results for mode filter sections containing a single 90 degree, 81 m radius-of-curvature plan bend indicate an added loss of 0.23 dB at 110 GHz for the plan bend. The Monte Carlo results also showed that the added loss for the plan bend is a rapidly increasing function of frequency which increases about as frequency to the seventh power. The distribution of the total mode conversion loss in a mode filter section with a plan bend differs from that of a nominally "straight" mode filter section in that the loss is now primarily due to three polarizations: $TM_{11}{\rightarrow}$ and both polarizations of the TM_{21} mode. In nominally "straight" mode filter sections, the loss is primarily due to only two polarizations, $TM_{11}{\rightarrow}$ and $TM_{21}{\uparrow}$. However, the loss in each particular polarization is still approximately distributed as a Chi-Squared random variable with two degrees of freedom, as were the individual polarization losses in nominally "straight" mode filter sections.

VII. SUMMARY

The field evaluation test results discussed in this paper have led to an increased understanding of the characteristics and requirements of the transmission medium for a commercial WT4 system. The WT4 field evaluation test has:

(*i*) Demonstrated the practicality of sheath and waveguide installation procedures.

(*ii*) Achieved a transmission medium loss which allows a repeater spacing in excess of 50 km.

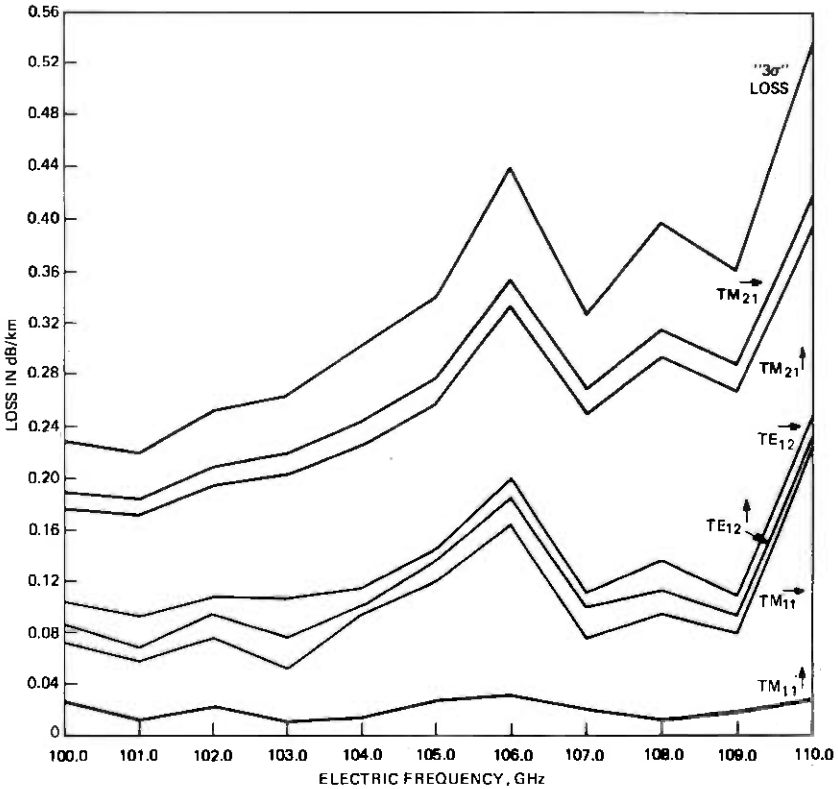

Fig. 13—Expected loss and "3σ" loss for nominally "straight" mode filter sections.

(*iii*) Successfully predicted electrical losses from mechanical measurements of in-place waveguide curvatures.

(*iv*) Established an experience and data base from which to project transmission medium losses for future waveguide routes.

Monte Carlo studies for mode filter sections with no route bends have established a statistical model for waveguide losses in these nominally "straight" sections. The higher losses and loss fluctuations associated with route bends affect repeater spacings, and are therefore also being evaluated using Monte Carlo techniques. A statistical model for waveguide losses has been established for mode filter sections with a single plan bend. Additional Monte Carlo studies are underway to determine expected losses and loss fluctuations for waveguide routes which have both plan and profile bends.

ACKNOWLEDGMENT

The successful field evaluation test transmission medium achievements reported here represent the long-term efforts of many people

involved in the WT4 development, in addition to the authors. D. T. Young and S. D. Williams provided the field evaluation test electrical loss measurements and participated in many discussions on the interpretation of loss data. Particular thanks are also due to J. Aagesen for transmission medium heat-loss measurements, P. M. Synefakis for her estimates of field evaluation test helix losses, and to S. C. Moorthy for his second-order perturbation loss calculation and helpful discussions concerning the Monte Carlo studies. Finally, J. M. Landwehr is acknowledged for his considerable aid in analyzing and interpreting the statistics of the Monte Carlo results.

References

1. R. W. Gretter, R. P. Guenther, M. Lutchansky, D. Olasin, and A. B. Watrous, "Mechanical Design of Sheathed Waveguide Medium," B.S.T.J., this issue.
2. D. A. Alsberg, J. C. Bankert, and P. T. Hutchinson, "The WT4/WT4A Millimeter-Wave Transmission System," B.S.T.J., this issue.
3. H. A. Baxter, W. M. Hauser, and D. R. Rutledge, "Waveguide Installation," B.S.T.J., this issue.
4. J. C. Anderson, R. W. Gretter, and T. J. West, "Route Engineering and Sheath Installation," B.S.T.J., this issue.
5. R. P. Guenther and W. M. Hauser, "Reliability and Maintenance of the WT4 Transmission Medium," B.S.T.J., this issue.
6. M. A. Gerdine, L. W. Hinderks, S. D. Williams, and D. T. Young, "Electrical Transmission Measurement Systems," B.S.T.J., this issue.
7. E. T. Harkless, A. J. Nardi, and H. C. Wang, "Channelization," B.S.T.J., this issue.
8. E. T. Harkless and R. W. Muise, "Field Evaluation Test System Performance," B.S.T.J., this issue.
9. P. A. Trudgett and G. H. L. Childs, "The Dimensional Measurement and the Interpretation of the Transmission Performance of the United Kingdom Post Office Field Trial Waveguide," International Conference on Millimetric Waveguide Systems, November 9–12, 1976.
10. K. Noda, K. Miyauchi, S. Shimada, F. Ishihara, and S. Seki, "Research and Development of Guided Millimeter-Wave Transmission Systems in Japan," International Conference on Millimetric Waveguide Systems, November 9–12, 1976.
11. W. E. Cohen, W. P. Doran, and R. D. Tuminaro, "Waveguide Design and Fabrication," B.S.T.J., this issue.
12. J. W. Carlin and S. C. Moorthy, "Waveguide Transmission Theory," B.S.T.J., this issue.
13. D. J. Thomson, "Spectrum Estimation Techniques for Characterization and Development of WT4 Waveguide–II," B.S.T.J., this issue.
14. H. G. Unger, "Noncylindrical Helix Waveguide," B.S.T.J., *40*, No. 1, (January 1961), pp. 233–254.
15. H. E. Rowe and W. D. Warters, "Transmission in Multimode Waveguide with Random Imperfections," B.S.T.J., *41*, No. 5 (May 1962), pp. 1031–1170.
16. D. T. Young, "Effect of Differential Loss on Approximate Solutions to the Coupled Line Equations," B.S.T.J., *42*, No. 9 (November 1963), pp. 2787–2793.
17. M. B. Wilk and R. Gnanadesikan, "Probability Plotting Methods for the Analysis of Data," Biometrika, *55*, 1968, pp. 1–17.

THE BELL SYSTEM TECHNICAL JOURNAL
Vol. 56, No. 10, December 1977
Printed in U.S.A.

WT4 Millimeter Waveguide System:

Waveguide Medium Manufacturing Process Research and Development

By M. P. ELEFTHERION

(Manuscript received July 15, 1977)

The Western Electric Engineering Research Center (ERC) conducted the research and development effort necessary to establish the waveguide medium manufacturing process technology. The Forsgate Laboratory staff was involved in product design, process research and development, facility development, setting up a pilot plant, and gaining valuable manufacturing experience. The development of a low-loss transmission medium was a key part in establishing the overall WT4 system capabilities.

I. INTRODUCTION

1.1 Project objectives

Full-scale development of the WT4 millimeter waveguide system was authorized in 1969. Bell Laboratories, charged with overall system responsibility, requested that the Western Electric Company participate in a joint program to develop the waveguide medium technology. Western Electric involvement was deemed extremely important because it was impossible to separate the design and processing problems and because the overall system economics was tied directly to the manufacturing process capability of the medium.

The Western Electric Engineering Research Center (ERC) initiated project involvement late in 1969 and outlined the major objectives:

(*i*) To develop the manufacturing process technology for fabricating waveguide both economically and reliably,

(*ii*) To fabricate the waveguide for various Bell Labs evaluations and the field evaluation test.

With the major objectives defined, effort initially was directed toward solving the problems of organizing a staff and providing the space and facilities for conducting the research and development effort. The goal of a system trial planned for 1974 posed a formidable challenge for the ERC technical staff both in technology development as well as waveguide fabrication. The project would involve product design, process R&D, facility development, setting up a pilot plant, and gaining valuable experience in manufacturing. Essentially, the ERC had the responsibility of a Product Engineering Control Center (PECC) and was totally accountable for shipped product.

1.2 Organization

The overall waveguide effort was assigned to an assistant director at the ERC. The initial organization of a waveguide R&D staff involved the selection of personnel with both extensive academic experience and manufacturing process development from previous Western Electric plant experience. It was anticipated that the blending of both types of personnel would permit the developments to move at a more rapid pace.

An initial staff of 7 in 1969 grew to 27 by 1971. This period was directed toward highlighting the technical problems, setting up experimental facilities, and starting the initial research and development effort. By 1973, the staff increased to 42 with the addition of some personnel from the Western Electric–Kearny Works. The Kearny Works had been given the waveguide medium allocation through the planned field evaluation test. The period from 1973 included the final process development, pilot plant equipment development, and the preparation for pilot plant production. The addition of plant development engineers from Kearny was planned to provide an orderly transition of responsibility from development to high-volume manufacture.

1.3 Forsgate Laboratory considerations

The next step in the overall planning involved obtaining adequate and suitable space for the medium research and development. Initial space studies indicated that approximately 50,000 ft^2 of floor space would be required to provide for process research and development and waveguide fabrication. Considerations on space included:

Process flow	Waste disposal
Facility requirements	Support services
Personnel requirements	Transportation needs
Plant services	Duration of project
Building height	Geographic location

Fig. 1—Forsgate Laboratory.

Since space was not available at ERC, other alternatives were necessary. Investigations covered possible space at Western Electric locations such as Kearny and Baltimore. In addition, several leased facilities were also investigated. After considerable effort, it was determined that a leased site, approximately 18 miles from ERC in Monroe Township, New Jersey, offered the most flexibility relative to both project and geographic considerations.

The location designated as the Forsgate Laboratory was leased and initially occupied during mid-1970. The building as shown in Fig. 1 included only the basic structure which allowed for the layout of the facilities for the most reasonable processing sequence. The ultimate layout of 44,000 ft^2 allowed for separate helix and dielectric-lined waveguide areas and for a separate measurement area. While this space satisfied the processing needs, an additional 16,000 ft^2 was subsequently required for waveguide electrical testing, packaging for sheath insertion and shipment to the field. This space was leased from the Kearny Works.

II. TECHNICAL EFFORT

2.1 Overall dielectric waveguide processing

As noted in a previous article,[1,2] the waveguide system will use two types of waveguide, namely, helix and dielectric-lined. Since the dielectric-lined waveguide is to be used as the main transmission path (~99 percent), the major portion of the technical discussion will cover only

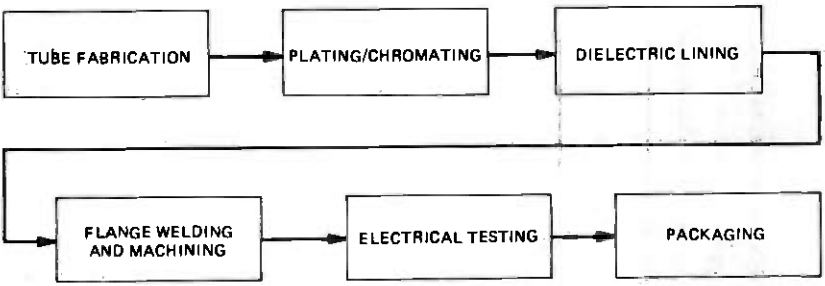

Fig. 2—Dielectric-lined waveguide processing.

developments in this area. The processing steps that evolved relative to dielectric-lined waveguide are outlined in Fig. 2.

At the start of the project, the major manufacturing processing problems included:

(*i*) Need for precision tube and measurement technology.
(*ii*) Need for precision copper plating and surface preparation.
(*iii*) Need for low loss/reliable dielectric lining process.
(*iv*) Need for low loss/reliable method for flange attachment and machining.

Considerable effort for each item shown in Fig. 2 has been expended relative to design, process, and facility feasibility. For example, the tube fabrication program advanced the state of the art of tubing manufacturing, yielding tubes of much higher geometric precision than available in the general trade. The in-house development of copper plating technology demonstrated the precise control over long lengths. The melt bonding process of dielectric lining included two stages of development. The first stage required the development of thin-walled precision dielectric tubing using low-loss pellets of high-purity polyethylene materials. The second stage required the development of a reliable method of bonding. Methods for flange attachment resulted in the selection of electron beam welding to provide low distortion, highly reliable fusion joints. The evolution of precision machining methods resulted in waveguide sections that exhibited very low mode conversion losses. This was mainly due to the excellent section-to-section tilt and offset alignment. The extensive development of mechanical and electrical measurement concepts resulted in facilities for on-site tube measurements and low-loss guide testing. The packaging effort resulted in concepts that provided for ease of waveguide shipment and installation. All of the Forsgate developments contributed to the successful processing of low-loss waveguide. Due to the space limitations, only two of the areas noted will be discussed. The main consideration in the subsequent

TUBE PARAMETERS	COMMERICAL TOLERANCE, mm	INITIAL SPECIFICATION, mm
Inside diameter	8.8×10^{-2}	1.3×10^{-2}
Ellipticity	3.5×10^{-1}	2.0×10^{-3}
Minimum radius of curvature	$2.1 \times 10^{+5}$	$7.6 \times 10^{+5}$

Fig. 3—Initial tube tolerances (51 mm).

technical discussion is to note the detailed method of technology research and development and the associated results.

2.2 Tube development

The need for a precision tube with extremely close control of curvature, diameter, ellipticity and other forms of geometric distortions is highlighted in another article of this issue.[2] Prior to the involvement of the ERC, it was recognized that domestic tube mills did not possess the technology to manufacture waveguide tubes with requirements as noted in Fig. 3.

ERC staff members visited various tube mills aimed at evaluating the tube-making capability as well as the technical capability of the tube fabricator. As a result, a tube fabricator was selected for on-site evaluations. An extensive analysis of the tube processing operations showed that the final operation of roller straightening was the most critical element in controlling the geometric tolerances. As a result, a roller straightener was completely overhauled, installed and dedicated solely for the waveguide project at the tube mill. Detailed studies on this facility showed that the roller shape was one of the dominant machine parameters controlling the final tube geometry.

In the straightening process as shown in Fig. 4, a tube passes through three sets of rollers rotating around its center line. The first and last set of rollers are in a fixed position with respect to the reference axis of the tube. The center pair of rollers is vertically offset from the reference axis. As the tube passes through the three sets of rollers, each element of the tube undergoes a complex pattern of bending stress reversals producing the desired straightening. During the process the tube is driven forward and turned by the rotation of the rollers which are at an angle to the tube axis.

As outlined, the rotary straightening operation has inherent difficulties that produce undesirable distortions in the cross-section of the tube. Conventional rollers, designed to work over a wide range of tubing sizes, do not distribute the load evenly over the contacted tubing, producing load concentrations at the tubing surface. The high load concentrations propogate through the tube wall producing a helical pattern of deformation on the inner surface of the tube.

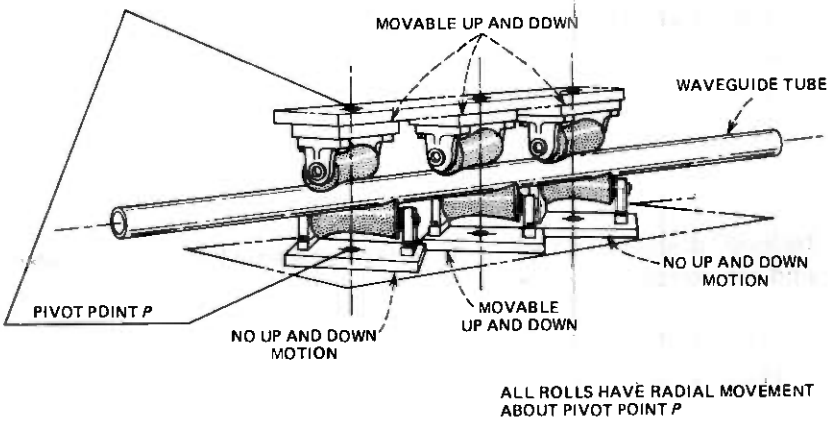

Fig. 4—Roller straightener.

The roller-tube interaction shown in Fig. 5 was studied by P. F. Lilienthal, ERC, in order to mathematically describe a roller geometry having a line of contact over which the applied load could be distributed. The objective of the effort was to develop a roller contour which would allow uniform load distribution over the length of the roller.

An examination of the geometry of the horizontal plane at distance z_0 from the center of the roller denotes the elliptical cross section of a tube having center coordinates of x_0,y_0,z_0. Tangent to this ellipse is the undetermined radius R of the corresponding roller cross section. The coordinates of the tangency point are x,y,z_0. The center of the elliptical tube section is located at

$$x_0 = R_1 + R_2 \tag{1}$$

$$y_0 = \frac{z_0}{\tan\theta}$$

The equation of the circular cross section of the roller at plane $z = z_0$ is

$$x^2 + y^2 = R^2 \tag{2}$$

and the corresponding expression for the ellipse is

$$\frac{(x - x_0)^2}{a^2} + \frac{(y - y_0)^2}{b^2} = 1 \tag{3}$$

where $a = R_1$ and $b = R_1/\sin\theta$. As is shown in Fig. 6, both the circle and the ellipse have a common tangent at point (x,y,z_0). Therefore,

$$\left.\frac{dy}{dx}\right|_{x,y,z_0}^{\text{circle}} = \left.\frac{dy}{dx}\right|_{x,y,z_0}^{\text{ellipse}} \tag{4}$$

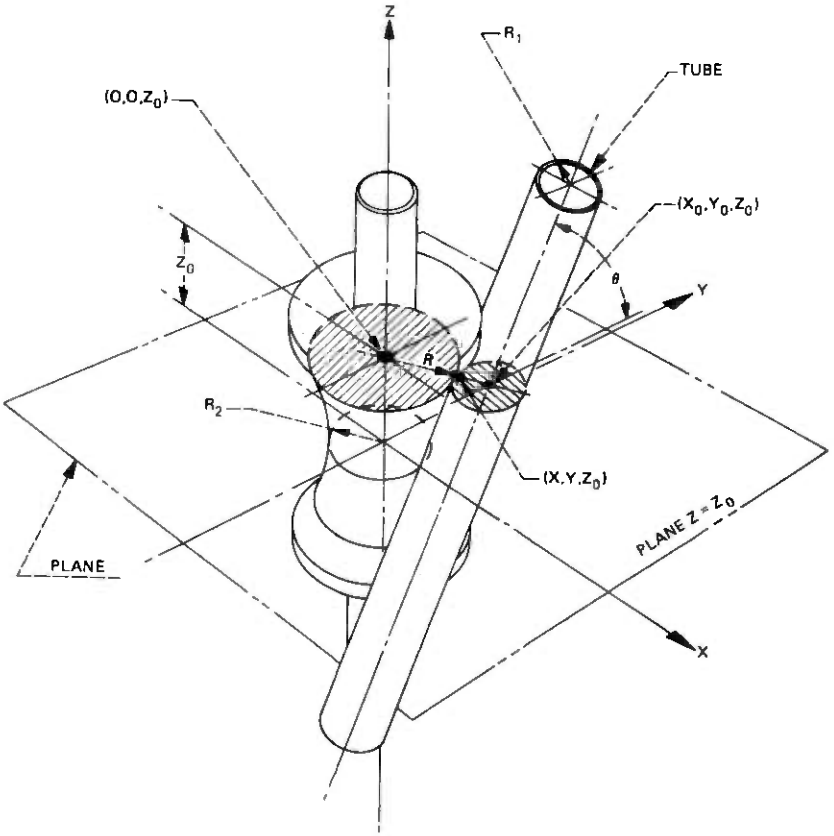

Fig. 5—Roller-tube interaction.

or

$$\frac{x}{y} = \frac{(x - x_0)b^2}{(y - y_0)a^2} \tag{5}$$

When solved for x, eq. (5) yields

$$x = \frac{x_0 y b^2}{y(b^2 - a^2) + y_0 a^2} \tag{6}$$

Substituting (6) into (3), we get

$$x_0 a^2 \left[\frac{y - y_0}{y(b^2 - a^2) + y_0 a^2}\right]^2 + \frac{(y - y_0)^2}{b^2} = 1 \tag{7}$$

which, in turn, can be expressed as

$$Ay^4 + By^3 + Cy^2 + Dy + E = 0 \tag{8}$$

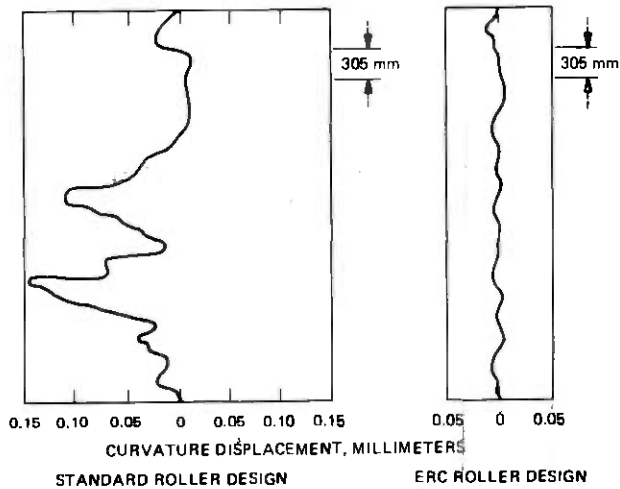

Fig. 6—Curvature results.

where A, B, C, D, and E are coefficients determined by the known parameters such as x_0, y_0, θ. The coordinate of the tangency point is y.

Equation (8) yields four roots when solved for y, two of which are complex.

One of the two real roots, only the one at point (x,y,z_0), Fig. 6, where the ellipse and the circle have a common tangent, is used. Solving eq. (3) for x, the result is:

$$x = x_0 - a\sqrt{1 - \left(\frac{y - y_0}{b}\right)^2} \tag{9}$$

In this manner, the tangent point coordinates x,y,z_0 are determined, and the radius of the roller at the given plane is computed by eq. (2). The longitudinal cross section of the roller is obtained by computing a series of R values for incremental distances from the origin of the coordinate system (0,0,0). A computer program is used to calculate the coordinates. The roller contour is then described by closely spaced points whose coordinates comprise arbitrarily chosen z_0 values and their corresponding R distances from the z axis.

The roller contour was computed for the straightener and N/C tapes were made at the ERC using the coordinates as input for the program routine.

The validity of the concept and the accuracy of the method were verified on small scale aluminum rollers and a full-size wooden roller. Six rollers of the ERC design were produced for experiments and use at the tube mill. The rollers were successful in producing tubes with greatly improved straigh tness by heavily suppressing the amplitude of the he-

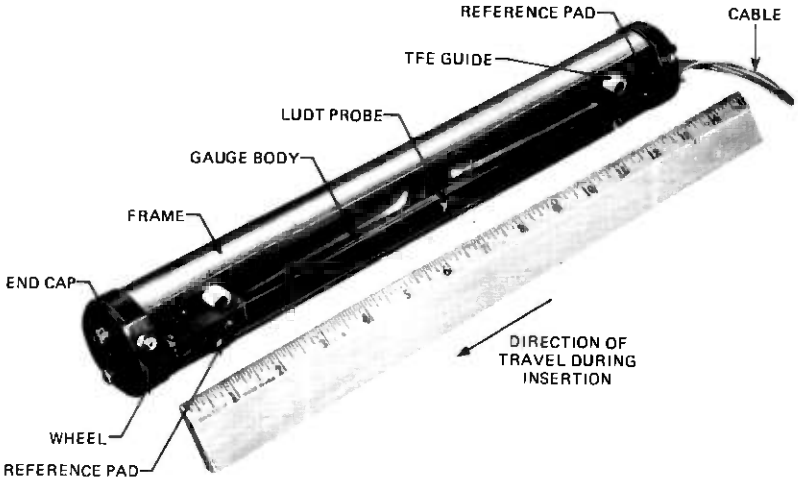

Fig. 7—Curvature gauge.

lical indentations normally introduced by the straightener process. Figure 6 compares early curvature measurements taken on waveguide tubing during trial runs using the standard roller designs in conjunction with a straightener which had not yet been optimized for waveguide tubing. The tubes typically had large helical impressions and poor straightness. The tubes processed on the specially designed rollers had no trace of helical deformations and showed an order of magnitude improvement in straightness. In addition, improvements in diameter control were also achieved over the same period. This was in part a response to the new roller design and also a result of improved methods of tube fabrication preceding the final rotary straightening operation.

The critical importance of tube geometry to transmission performance makes extremely accurate measurements as essential part of the waveguide medium evaluation program. A second aspect of the tube evaluation program involved the development of precision measurement facilities for use at the tube mill or at the waveguide fabrication plant. Gauges for measuring both the curvature and diameter of the tubing were developed.

The following discussion will center only on the curvature gauge.

The basic curvature gauge shown in Fig. 7 consists of a rigid frame maintaining two reference points and a displacement probe in fixed positions with respect to one another. In operation the curvature gauge is inserted into the waveguide tube contacting the inner tube on diametrically opposed lines by means of the two 3-point structures. All three points contact the surface but during measurement the middle point, which contains a linear variable differential transformer (LVDT), is

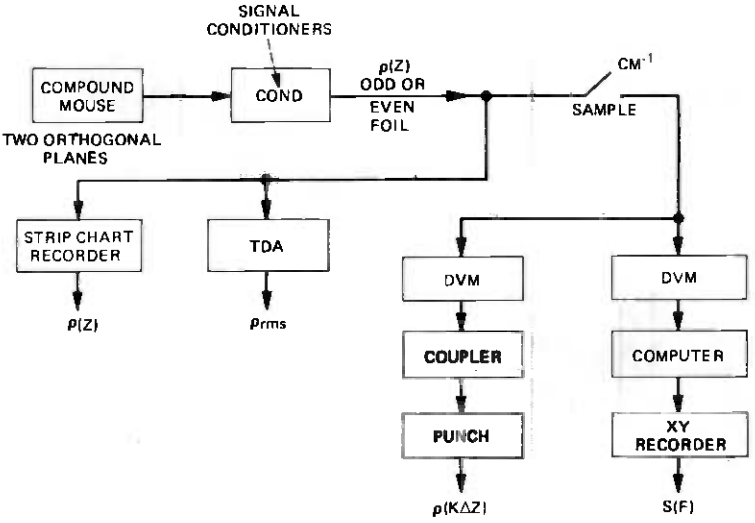

Fig. 8—Measurement system.

displaced with respect to the other two points. This displacement of the probe is proportional to the curvature of the tracked path.

The curvature gauge was incorporated into a system consisting of the gauge, drive mechanisms, and the control system. The system signal flow is shown in Fig. 8. The LVDT displacement probe generates a modulated ac signal which is demodulated, amplified, and directly recorded. The time-domain analyzer is used to compute root-mean-square curvature. The data acquisition system records curvature behavior for use in predicting transmission losses. The program and hardware for the system as noted were supplied by Bell Laboratories. The sequence of data gathering and analysis is as follows:

(*i*) Acquire and store curvature data to a maximum of 1024 points (one data word per centimeter of gauge displacement).
(*ii*) Compensate data record by means of a cosine taper.
(*iii*) Perform statistical detrending and filtering of the record.
(*iv*) Perform 1024-point fast Fourier transform on data record.
(*v*) Convert corrected transform to power spectral density (PSD).
(*vi*) Output curvature power spectral density to x–y recorder, plotting the PSD from 0 to 50 cycles per meter.

Figure 9 shows a comparison of the output curvature PSD before and after the roller-straightening operation.

The roller straightener effort and the development of very precise measuring equipment resulted in optimizing the overall tube processing at the tube mill. This combined effort resulted in a tube yield improve-

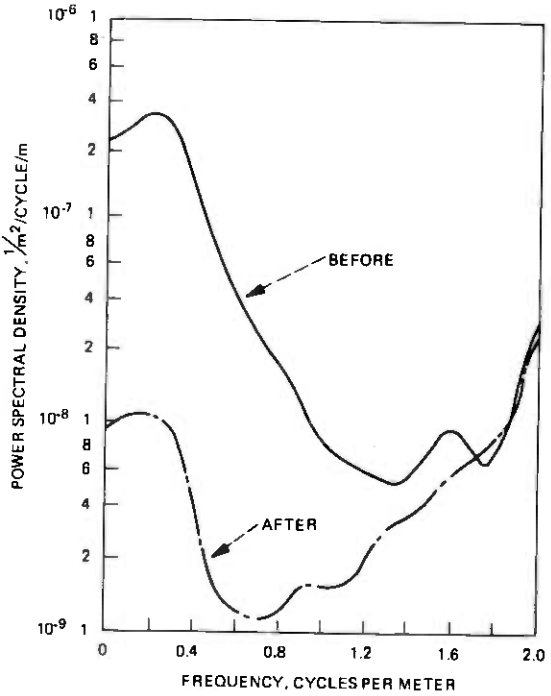

Fig. 9—PSD (before and after straightening).

ment from less than 50 percent to approximately 90 percent by the end of the field evaluation test.

2.3 Electrodeposition of copper for waveguide tubes

A second key development area involved the electrodeposition of copper on the interior surface of the millimeter waveguide tubes. The use of copper as a conducting surface is based primarily on achieving low ohmic losses, while achieving a high degree of reliability. The objectives of the effort were outlined as follows:

(*i*) Control average diameter variation within extremely tight tolerances.

(*ii*) Maintain the plated surface finish to less than 35 microinches rms.

(*iii*) Deposit a continuous, nonporous, high-conductivity copper layer.

(*iv*) Provide a deposition with excellent adhesion to the steel.

(*v*) Establish technical feasibility of plating long lengths.

(*vi*) Develop process suitable for future high volume production with low cost and high reliability.

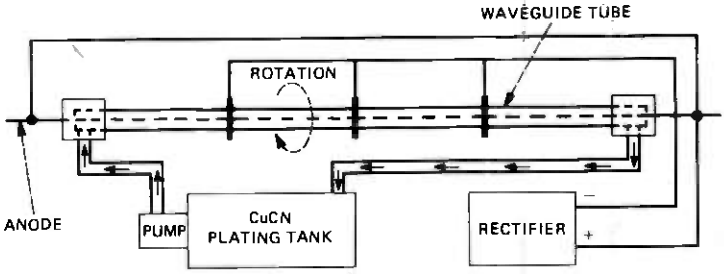

Fig. 10—Horizontal plating system.

Initial effort was directed toward obtaining plated tubes from outside suppliers. It was quickly determined that the technical capability for meeting the above requirements did not exist. As a result, the ERC proceeded at an accelerated pace to develop an in-house capability. The overall technology in this area was developed by D. J. Fineberg, R. Haynes, and W. E. Rapp.

Initial effort directed at vertical plating was followed by the development of a horizontal plating system. The horizontal system shown in Fig. 10 consists of a hollow stationary copper anode inserted into the steel tube. In operation, the electrolyte is circulated through the annulus between the tube (cathode) and the anode while the tube rotates. To prevent short-circuiting, the stationary copper anode and rotating cathode are separated by an insulating rod helically wound around the anode. The ends of the spacer are positioned in grooves in the stationary components of the head and tail stock assemblies, thus preventing rotation of the spaces. The tube is inserted into a sleeve fastened to the drive motor pulley.

Electrical connections between the rectifier and the exterior tube are made through copper blocks contoured to the outer diameter of the tube. Under operating conditions, 90 percent of the current is consumed for copper deposition. The 10 percent current loss is a result of a side reaction which evolves hydrogen gas at the cathode.

To ensure permanent adhesion of the deposited copper, the steel tube must be thoroughly cleaned and the surface chemically activated before plating. The cleaning solution must be compatible with the metal being processed. A cleaning process that does an excellent job of oil removal but severely attacks or even slightly etches the metal surface is undesirable. The millimeter waveguide bore requires a surface finish of less than 35 μin. rms. To maintain this preplating finish, the cleaning processes should not etch the steel substrate. Inspection of the tube after the cleaning operation is made more difficult by the fact that no visual observation of the surface is possible since the solutions are circulated through a closed system.

The first step is a soak cleaning in an alkaline solution at 160°F for 10 minutes to remove the oils and lubricants applied at the tube mill. This step is followed by draining and rinsing. Since the steel tubes are not heavily oxidized, a mild acid is sufficient to neutralize the residual alkaline chemicals from the preceding step and to remove any light oxide film from the steel substrate. After the pickling operation, the tube is drained and rinsed.

The final step is a sodium cyanide rinse for 3 minutes at room temperature. This accomplishes two things:

(*i*) It inhibits tarnishing of the activated steel substrate resulting from an inadvertently long dwell time between cleaning and plating.

(*ii*) It neutralizes the residual acid salts and, as a result, prevents their carryover into the plating solution.

The copper anode with its insulating spacer is inserted into the cleaned, wet tube and both are loaded into the plating machine. The end connections are fastened and the hot copper cyanide plating solution is pumped through the rotating tube at a flow rate of 25 gpm. When the tube reaches the operating temperature of the plating solution, the rectifier is turned on. Upon completion of the specified plating cycle, the rectifier automatically shuts off, the electrolyte is drained, and the tube rinsed in cold and hot water. After unloading the plated tube from the plating machine, the anode and spiral are removed. To dissolve residual plating salts, the waveguide tube is again cleaned with a sodium cyanide solution for 3 minutes at room temperature. The tube is then rinsed and dried.

The uniform current density distribution and therefore uniform plating is assured through the rotation of the tube and uniform mixing of the solution throughout the tube. The rotational speed, spiral dimensions, and the plating time (12 minutes for a 10-micron thickness) tend to minimize the periodicity. This occurs from the mechanical action of the insulator on the copper plate. The current density, fluid flow pattern, and temperature are coupled process parameters to insure a minimum effect of secondary current distribution on the copper thickness control.

The cathodic deposition efficiency is greater than 90 percent. The anode, which is a copper tube (25 microns in diameter), is dissolved at close to 100 percent efficiency and is used to plate an average of 75 steel tubes. The cathode-to-anode ratio begins at 5.58 and decreases to 14.29.

Waveguide tubes plated with this system showed uniform thickness with no significant diameter variations. Figure 11 shows the thickness results of the horizontal plating facilities at 0°, 90°, 180° and 270° positions around the diameter. The average thickness was controlled to

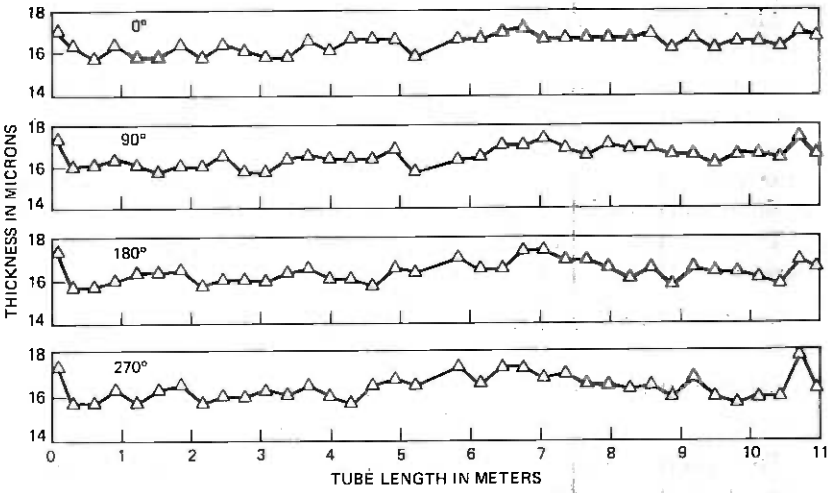

Fig. 11—Plating thickness results.

approximately 16 microns with a variation of ±2 microns. The developments in the copper plating and surface preparation prior to dielectric lining contributed significantly to the low ohmic loss characteristics of the dielectric-lined waveguide. Figure 12 shows the plating area during the pilot production period.

III. PILOT PLANT OPERATION

3.1 Operating strategy

The previous section of the paper discussed some aspects of the first objective, namely, the research and development of the manufacturing process technology. The second project objective—the fabrication of the waveguide for Bell Labs evaluations and the major field evaluation test—proved to be an equally challenging objective. During the period from 1970 through early 1972, effort was directed toward prototype facilities and providing approximately 2.3 kilometers of 51 millimeter waveguide for Bell Labs evaluations. During the period from late 1972 through 1973, effort was directed toward finalizing designs, establishing prototype production facilities, and adding operating personnel. This period essentially represented the "design, build, and prove-in" stages. By early 1974, Forsgate was producing approximately 2.3 kilometers of 60-mm waveguide per month.

As the waveguide installation designs and procedures were more clearly defined, it became apparent that additional space would be required for waveguide assembly, sheath preparation, and packaging for field installation. Discussions with Western Electric–Kearny resulted in the addition of approximately 25,000 ft^2 of space in the merchandise

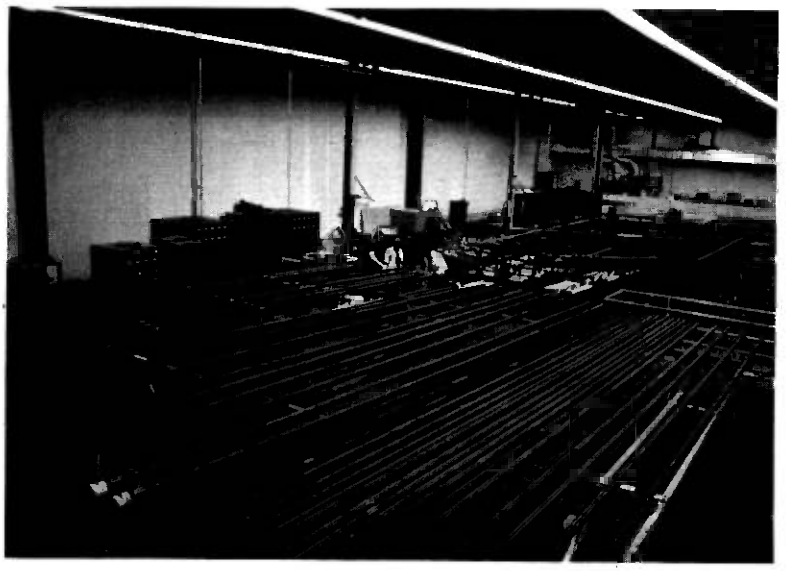

Fig. 12—Plating areas.

building at the Kearny Tract. A subsequent decision by Bell Labs to separate the sheath installation from the waveguide installation resulted in a reduction in space requirements to approximately 16,000 ft^2. This space was prepared in 1973 and early 1974 to include the following operations:

(*i*) Receive waveguide from Forsgate.
(*ii*) Test coupled waveguide sections (~6–9 meter lengths).
(*iii*) Purge with nitrogen and cap waveguide ends.
(*iv*) Install the waveguide roller supports.
(*v*) Construct shipping package.
(*vi*) Insert and package waveguide.
(*vii*) Ship to field installation.

With the space and processing considerations established, effort was directed toward staffing the operating (shop) organization. It was projected that 35 shop personnel would be required to staff the facilities for fabricating, testing, and packaging the waveguide medium. Arrangements were made with Western Electric–Kearny to provide both the shop supervision and direct work force. The consideration for shop operators involved establishing proper job classifications, personnel selection, and training. The overall training involved the rotation of shop operators on process facilities to provide the flexibility of moving personnel to various facilities for maximizing the efficiency of the shop operation.

The operating personnel, while reporting to the Forsgate management, were retained on the Kearny personnel roll. The shop experience was provided from Kearny in order to minimize the start-up of pilot plant production facilities. In addition, this arrangement provided ERC with the unique position of having both engineering and operating responsibility.

3.2 Scheduling

The scheduling of waveguide fabrication was closely coordinated with the projected Bell Labs installation plans for the field evaluation test.[4] The original schedule was to provide 13.5 km in 1974 and 16.5 km in 1975 for a total of 30.0 km. The revised schedule provided 12 km in 1974 and 2 km in 1975 for a total of 14.0 km. The schedule was such that initial fabrication began during the first quarter of 1974 and reached a peak of 2.3 km per month during the third quarter of 1974. This output represented an average daily processing rate of 20 waveguide tubes.

3.3 Process and reliability control

The waveguide installation for the field evaluation test initially was planned to be part of a commercial route in New Jersey. As such, the fabricated waveguide required a quality level consistent with long-term reliability. Considerable effort by both Bell Labs and Western Electric was directed toward meeting this goal. The Forsgate Laboratory quality control included the following plans:

(*i*) Develop a quality control program for the waveguide processing and testing areas for:

In-coming material inspection
Facility inspection
In-process checking at all operations
Overall quality survey prior to shipment

(*ii*) Establish inspection procedures and personnel training.

(*iii*) Document key waveguide processing data for design and specification purposes.

A complete history of dielectric-lined waveguides was kept through the field evaluation test production. The information included:

(*i*) Steel melt, tube run, tube geometry.
(*ii*) Process data, date, parameters, material.
(*iii*) Inspection and reliability data.

The detailed information was compiled for data analysis, fault analysis, and determining the process capability at each step of the assembly operations. The 1974–1975 field evaluation test waveguide fabrication

had an overall process yield of 77 percent during the peak operating period. During the final months of operation, the overall yield exceeded 90 percent. This overall improvement in process yield was mainly due to two factors:

(*i*) The valuable manufacturing experience gained throughout the field evaluation test.

(*ii*) The improvements on the individual process parameters and the implementation of quality control procedures.

The two technologies discussed earlier, namely the tube and plating developments, were indicative of such improvements as noted below:

Field evaluation test production yield

Process step	*Initial 1/3 prod.*	*Next 1/3 prod.*	*Final 1/3 prod.*
Tube Processing	96.9%	99.1%	99.7%
Copper Plating	86.6%	97.2%	98.9%

The waveguide tube mill improved inspection allowed for few tube rejects at the fabrication plant, and as a result provided the capability for a very high overall process yield. One of the key factors in the increased copper plating yield was the reduction in thickness to 12 microns nominal.

The improvements made during the field evaluation test fabrication definitely demonstrated the capability of expanding the process technology to a factory producing 750 km to 1500 km per year.

IV. OVERALL SUMMARY

The Western Electric Company utilizing the ERC technical capability established the Forsgate Laboratory. This laboratory very successfully met the objectives for the research and development of manufacturing process technology for waveguide fabrication. The waveguide medium as developed exhibited extremely low-loss transmission characteristics. This represented a key development in proving that a reliable and cost-competitive waveguide system could become a reality.

The technology and facility developments at the Forsgate Laboratory demonstrated the manufacturing process feasibility for high-volume factory production.

ACKNOWLEDGMENT

The highly successful manufacturing process research and development was mainly attributed to the dedicated, aggressive, and hard-working Forsgate staff. This staff combined in a team effort to overcome tremendous technical challenges in a very short period of time.

The author would like to thank the Forsgate management staff, namely, A. E. Dugan, F. J. Jannett, of ERC, and W. P. Doran, R. L. Hull and W. Kollman, from Kearny. The factory plant experience from the Kearny staff was an important aspect of the project success. Special thanks are also due to H. E. Kapp and the Plant Engineering organization at ERC for the excellent services provided.

REFERENCES

1. D. A. Alsberg, J. C. Bankert, and P. T. Hutchison, "The WT4/WT4A Millimeter Wave Transmission System," B.S.T.J., this issue.
2. R. J. Boyd, W. E. Cohen, W. P. Doran, and R. D. Tuminaro, "Waveguide Design and Fabrication," B.S.T.J. this issue.
3. P. E. Fox, S. Harris, and D. J. Thomson, "Mechanical Gauging Techniques," B.S.T.J., this issue.
4. J. C. Anderson, J. W. Carlin, D. J. Thomson, and T. J. West, "Field Evaluation Test—Transmission Medium Achievements," B.S.T.J., this issue.

Contributors to This Issue

Dietrich A. Alsberg, B.S.E.E., 1938, Techniche Hochschule, Stuttgart, Germany; graduate school 1939–1940, Case School of Applied Science; development engineer with several companies in Ohio, 1940–1942; U. S. Army, 1942–1945; Bell Laboratories, 1945—. While with Bell Labs he has been active in precision high-frequency and microwave transmission measurements, early transistor characterization, Thor and Titan ballistic missile radio-inertial guidance systems for military and space missions, Nike-X, Sentinel, and Safeguard phased-array radars, nuclear hardening, Electromagnetic effects of nuclear weapons, and millimeter waveguide transmission. He currently is head of the Microwave Transmission Department where, in addition to the millimeter waveguide system, he is responsible for microwave radio remote surveillance systems and small satellite antennas. Senior member, IEEE.

Janis C. Anderson, B.S. (mathematics), 1967, Carnegie Institute of Technology; M.S. (mathematics), 1971, and M.S. (electrical engineering), 1976, Stevens Institute of Technology; Bell Laboratories 1967—. Ms. Anderson has been engaged in the development of the WT4 waveguide system, doing measurement analysis, route engineering, and statistical and system studies. Currently, she is involved in designing the system architecture for a computer-based remote microprocessor measurement system for the AR6A radio system.

Jon C. Bankert, B.S.M.E., 1958, Duke University; M. Engr., 1962, Yale University; Bell Laboratories, 1963—. At Bell Laboratories, Mr. Bankert was first engaged in the development of ocean cables and other equipment for sonar systems. He was later concerned with the design of automotive and construction equipment for outside plant craftpersons. He participated in the development of installation and maintenance techniques for the millimeter waveguide system. Currently, he is head, L-Carrier Systems Department. Member, Tau Beta Pi, Pi Tau Sigma.

C. E. Barnes, was born in Tuscola County, Michigan on October 24, 1929. He received his B.S. (physics), 1956, Michigan State University;

Bell Laboratories, 1956—. Mr. Barnes became a technical group supervisor in 1965. He has been involved in the development of microwave and millimeter-wave ferrite devices and circuits, phased-array radar receivers, and lightwave transmitters for fiber optic systems. He is currently supervisor of the Millimeter-Wave and Fiber Optics Group at Bell Labs in Allentown, Pennsylvania.

H. A. Baxter, B.S.M.E., Iowa State University, 1937. At Bell Telephone Laboratories from 1937 to 1950, he worked principally on mechanical design of radar antennas, servomechanisms, and electromechanical components. From 1950 to 1965, Mr. Baxter worked for Hughes Aircraft Company, American Machine and Foundry Company, Norma Hoffman Bearings Company, and Regent Controls, Inc. He returned to Bell Laboratories in 1965, working principally on development and field evaluation of ocean bottom survey systems and Sea Plows I, II, and III and on development of waveguide installation machinery. He is presently supervisor, Feeder Distribution Interface Design Group.

Marco J. Bonomi, B.E.E., 1960, Polytechnic Institute of Brooklyn, M.E.E., 1961, New York University, Bell Laboratories, 1960—. Mr. Bonomi worked on the design of digital and analog microwave transmission systems, and also satellite transmission systems including the Telstar experiment. He worked on both the system design and the span terminating equipment design for the WT4 project. He is currently working on the design of a Time Assignment Speech Interpolation (TASI) terminal for international use.

R. J. Boyd, Jr., B.S., 1954, U.S. Coast Guard Academy, M.S. (engineering mechanics), 1960, New York University; Bell Laboratories 1958—. He has been primarily involved in the manufacture of steel tubes for waveguide use. Prior to working on waveguide, he was in the Outside Plant Development Laboratory working on cable gas pressure systems and the underground installation of cables.

P. Brostrup-Jensen, M.S.E.E., 1956, New York University; Bell Laboratories 1956—. Mr. Brostrup-Jensen has developed test equipment for laboratory use and locating of failures in submarine cables, including diver-operated probes and corona investigations. He has also developed protection switching equipment and other maintenance equipment for digital systems, and developed the IF circuits and equalization techniques

for the WT4 millimeter waveguide system. He is presently supervisor of the Satellite Applications Group.

R. J. Brown, B.S.E.E., 1968, M.S.E.E., 1969, Ph.D.E.E. 1971 Georgia Institute of Technology; Bell Laboratories, 1971—. Mr. Brown has been engaged in time-domain test set development for equalization for the WT4 millimeter waveguide system. More recently he has been doing systems studies for advanced satellite communications. He is presently supervisor of the Satellite Technology Group.

James W. Carlin, B.S.E.E., 1962, Illinois Institute of Technology; M.S. 1964, Ph.D., 1967, electrical engineering, University of Illinois; Bell Laboratories, 1968—. From 1968 to 1969 Mr. Carlin was involved with work on electromagnetic pulse effects on Bell System facilities. During the WT4 development he participated in analytical and experimental studies of coupling in multimode media, normal mode characteristics for circular waveguide, helix mode filter design and manufacturing methods, and electrical and mechanical measurements on installed waveguide. Mr. Carlin is presently supervisor of a group responsible for L5/L5E office circuits.

Steven Shui-uh Cheng, B.S., 1963, National Taiwan University; M.S., 1967, Tufts University; Ph.D., 1970 California Institute of Technology, all in fields of physics. Between 1970–1971, Mr. Cheng participated in the first U.S. electron-positron colliding-beam experiment at Harvard University. Since joining Bell Laboratories in 1971, he has worked on the millimeter waveguide system and recently on the fiber-optic transmission system. His main interest is in reliability theory, filter design, communication system simulation, microwave transient behavior measurement, and transmission system evaluation. Member, IEEE, American Physical Society, and Sigma Xi.

W. E. Cohen, B.M.E., 1961, College of the City of New York; Western Electric Co., 1968—. Prior to working on waveguide he was involved in designing numerical control machinery at Kearny. As a member of the waveguide manufacturing group at Forsgate, Mr. Cohen was responsible for the design and manufacture of helix waveguide. Presently he is a senior engineer at Kearny and is involved in the production of metal printed wiring boards. Member, ASME, Numerical Control Society.

W. P. Doran, B.S. in M.E., 1956, Newark College of Engineering; M.S. in I.E., 1964, Stevens Institute of Technology; Western Electric Co., 1956—. He has been engaged in manufacturing engineering for key equipment, power coils, miniature relays, and power equipment. While at Western Electric's Forsgate Laboratory he was responsible for tubing development, waveguide coupling and mechanical processing, mechanical measuring and electrical testing. He is currently responsible for product line planning for energy systems. Member, National Society of Professional Engineers.

Charles N. Dunn, B.S., 1958, M.S., 1960, Ph.D., 1964, University of Minnesota; Bell Laboratories, 1964—. Mr. Dunn was first involved in developmental studies on backward and tunnel diodes. Later he worked on microwave and millimeter wave diodes for solid-state oscillator sources. Now he is involved in the design and development of integrated circuits. Member, IEEE, American Physical Society, Sigma Xi, Eta Kappa Nu, Tau Beta Pi.

Michael P. Eleftherion, A.S., 1955, Wyomissing Polytechnic Institute; B.S.M.E., 1958, Pennsylvania State University; M.S.I.E., 1965, Lehigh University; Bell Laboratories 1958–1959; Western Electric 1959–. Mr. Eleftherion worked as a development and senior engineer on transistor and sealed contact facility and product engineering. From 1965 to 1968, he was the department chief responsible for new product manufacturing development at the Allentown Plant. Since 1968, Mr. Eleftherion has been assistant director, research and development at the Western Electric Engineering Research Center. A past resident head of the Forsgate Laboratory, his current responsibilities include thermal energy, integrated circuit, and PWB interconnection manufacturing research. Member, IEEE, Tau Beta Pi, and Pi Tau Sigma.

Paul E. Fox, B.S.E.E., 1963, Newark College of Engineering; Bell Laboratories 1957—. Since joining Bell Laboratories Mr. Fox has worked mostly in the design of control and measuring circuits. He is presently working on automatic remote test equipment for use in the single sideband radio project.

Milton A. Gerdine, B.S., 1961, M.S., 1962, Ph.D. (E.E.), 1965, University of Colorado, Bell Laboratories, 1965—. Mr. Gerdine has worked on microwave radio and millimeter waveguide transmission systems.

He now heads the Measuring Systems Design Department. Member, Eta Kappa Nu, Tau Beta Pi, and Sigma Tau.

R. W. Gretter, S.B. in M.E., 1950, S.M. in M.E., 1951, Mech. E., 1953, and Sc.D. in M.E., 1956, Massachusetts Institute of Technology; Bell Telephone Laboratories 1955—. Initially Mr. Gretter did analytical work in cable mechanics. This was followed by participation in the development of cable machinery for C.S. Long lines. From 1964 to 1971 he led a group responsible for physical design of digital transmission equipment including the D2 channel bank, the M12 multiplex, and the voiceband interface frame for No. 4 ESS. He then joined the WT4 project and supervised the design of the coupling and the support and protection system for the sheathed-waveguide medium. His group also developed techniques and machinery for waveguide installation by the insertion method as well as methods of designing sheath profiles for economical, low-curvature installation. Since May 1977 he has supervised a group responsible for physical design of VF facility terminals. He is a licensed professional engineer and a member of Pi Tau Sigma, Tau Beta Pi, and Sigma Xi.

R. P. Guenther, B.S.M.E., 1960, State University of Iowa; M.M.E., 1962 New York University; U. S. Army 1962–1964; Bell Laboratories 1960–62, 1964–70, 1973—. At Bell Labs, Mr. Guenther worked on paired cable development, outside plant maintenance and cable upkeep survey, and the WT4 feasibility study. In 1970 he was appointed AT&T assistant engineering manager, outside plant upkeep. Since 1973, he has been supervisor of a group developing the maintenance systems and special hardware for the WT4 medium. This group is developing radio transmission surveillance systems.

E. T. Harkless, B.S.E.E., 1947, M.S. (physics), 1949, Case Institute of Technology; Bell Laboratories, 1949—. He has designed filters for use in various microwave radio relay systems and equalizers for the L3 coaxial cable system. Mr. Harkless developed the array of systems combining networks used to feed the microwave radio systems through the horn reflector antenna. He designed the Telstar satellite communication antennas and has most recently been supervising a group developing millimeter wave circuits for the WT4 repeater.

Smith Harris, B.A., 1938, Emory University; Bell Laboratories, 1952—. Mr. Harris has worked on various loop and transmission projects,

including test sets, armored and armorless submarine cable, and millimeter waveguide. He was a member of the development team for the MAC-4 microprocessor. He is currently a member of the Transmission Surveillance Group.

William M. Hauser, B.S.M.E., 1967, Swarthmore College; M.S. and Ph.D., 1968 and 1973, respectively, Massachusetts Institute of Technology. Western Electric Company 1968–1970; Bell Laboratories 1972—. Mr. Hauser has worked on installation mechanics and maintenance systems for millimeter waveguide. He is currently engaged in engineering for digital systems outside plant. Member, Phi Beta Kappa, Tau Beta Pi, ASME.

Larry W. Hinderks, B.S. (physics), 1966, University of Kansas; Ph.D. (physics), 1970, University of Kansas. Bell Laboratories, 1970–1977. Mr. Hinderks was involved in test set design and fabrication for millimeter wave measurements using minicomputers. This work included hardware design and software data manipulation algorithms. He also worked on microprocessor controlled test sets for the evaluation of the surface properties of copper at millimeter wave frequencies.

P. T. Hutchison, B.S. (E.E.), 1944, Mississippi State College; M.S. (E.E.), 1947, California Institute of Technology; Ph.D. (E.E.), 1960, Georgia Institute of Technology. Mr. Hutchison taught at Mississippi State and Georgia Tech and worked for Raytheon Mfg. Co. before coming to Bell Laboratories in 1960. His experience at Bell Labs includes work on satellite communications, terrestrial microwave repeaters, and the WT4 millimeter-waveguide system. He is now head of the TASI-C and Undersea Network Department, working on TASI-C development and studying suitability of lightwave systems for undersea cables.

William J. Liss, Jr., B.S.M.E., 1969, Lehigh University; M.S.M.E., 1971, Rutgers University; Bell Laboratories 1969—. In addition to work on WT4 waveguide, Mr. Liss has recently been involved in developing fire and smoke control methods for central offices and the economic evaluation of engineering projects. He is currently working in the area of energy conservation and solar energy utilization in telephone buildings. Member Tau Beta Pi, Pi Tau Sigma.

Milton Lutchansky, B.S., 1960, Michigan State University; M.S., 1962, and Ph.D, 1973, New York University; Bell Laboratories, 1960—. Mr. Lutchansky participated in design studies for radar antenna structures and was involved in analyses of the effects of nuclear weapons on communications facilities. On the WT4 project, he was concerned with characterization of the waveguide installation environment and design of the mechanical filtering. Member Tau Beta Pi, Pi Tau Sigma, Phi Kappa Phi, and ASME.

Donald R. Marcotte, A.A.S. (industrial electronics), 1969, New Hampshire Technical College; A.A.S. (electronics eingineering) 1974, Lowell Technological Institute; B.S. (electronics engineering) 1977, University of Lowell; Bell Laboratories, 1969—. Mr. Marcotte has worked on the design of high-frequency analog circuits and has done systems engineering on protection switching for digital communications systems. More recently he has worked on the design of solid state switches and amplifiers for single sideband radio applications.

S. C. Moorthy, B.S., 1961, Kerala university, India; M.S., 1963, and Ph.D., 1966, University of Pennsylvania; Bell Laboratories 1967—. He has worked on phased-array antennas, electromagnetic pulse effects and the millimeter waveguide transmission (WT4) system. His work on the WT4 system included design of special components, development of automated test sets, and analysis of multimode waveguide propagation. He is currently working on problems concerning the Iranian domestic satellite system. Member, IEEE, American Physical Society, Sigma Xi.

Richard W. Muise, B.S.(E.E.), 1966, Northeastern University; M.S.(E.E), 1968, Ph.D.(E.E.), 1972, Polytechnic Institute of Brooklyn; MITRE Corporation 1962–1966; Bell Laboratories 1966—. Mr. Muise has been involved in WT4 waveguide system performance studies and in the development of high-speed decision and timing recovery circuits. Currently, he is supervisor of a group developing a Time Assignment Speech Interpolation (TASI) system for international applications. He is a member of Eta Kappa Nu, Tau Beta Pi, Phi Kappa Phi, and Sigma Xi.

Armand J. Nardi, B.S.M.E., 1959, Polytechnic Institute of Brooklyn; M.M.E. 1961, New York University; Bell Laboratories 1959—. Mr. Nardi

engaged initially in physical design work associated with missile guidance systems and the *TELSTAR*™ telemetry antenna. He later supervised the physical design of the WT4 system. He is currently supervisor of the Coaxial System Physical Design Group responsible for the design of long-haul carrier systems.

Daniel Olasin, B.S.M.E., Newark College of Engineering; Bell Laboratories, 1957—. In addition to work on the WT4 waveguide, Mr. Olasin's previous experience includes antenna design for the military and mechanisms design for the ocean cable plow. He is presently working on international satellite earth station engineering.

J. W. Osmun, B.S.E.E., 1953, University of Nevada; Bell Laboratories, 1953—. Mr. Osmun is a power systems engineer in the Energy Systems Engineering Department at the Whippany, New Jersey location of Bell Laboratories. He is presently responsible for systems engineering of small dc-dc converters for communications equipment. His early work was in ringing, tone and cadence systems and transistorized dc-dc power converter design. Member, of Phi Kappa Phi, Sigma Tau, and IEEE.

Owe G. Petersen, B.S.E.E., 1963, University of Wisconsin; M.S.E.E., 1965, Ph.D., 1971, University of Pennsylvania; Bell Laboratories, 1963—. Mr. Petersen was engaged in high-frequency semiconductor device development, including PIN, varactor, step-recovery, and Schottky diodes. Since 1976 he has been involved in integrated circuit process and circuit development. Member, Tau Beta Pi, Eta Kappa Nu.

Duane C. Redline, A.S. Assoc., 1954, Milwaukee School of Engineering; Bell Laboratories, 1954—. Mr, Redline has worked on the development and design of germanium, silicon, and gallium arsenide microwave semiconductor diodes used in Bell System radio systems.

Donald R. Rutledge, P.E.; B.S.C.E., 1966, Texas Technological College; M.S.C.E., 1968, Lehigh University; Bell Laboratories, 1968—. In 1966 he worked for Pan American Research Center investigating pipeline laying techniques in deep water and drill stem failures in deep wells. At Lehigh University, Mr. Rutledge was a research associate in the Fritz Engineering Laboratory specializing in failure mechanisms of built-up plate structures. He joined Bell Laboratories as a member of

the Outside Plant Installation Department, where he was concerned with the design of a standard series of prefabricated reinforced concrete manholes. Currently, he is a member of the Facility Terminal Systems Engineering Department.

John J. Schottle, B.S.E.E., 1962, Illinois Institute of Technology; M.S.E.E., 1964, New York University; Bell Laboratories, 1962—. Mr. Schottle has worked on the design of mode couplers for the *TELSTAR*™ project, on networks for use in a digital radio system, and, on equalization of the WT4 system. He is presently engaged in the development of a TASI system for use on the overseas cable network. Member, Eta Kappa Nu, Tau Beta Pi.

S. Shapiro, B.M.E., 1969, City College of New York; M.S.(M.E.), 1971, Columbia University; Bell Laboratories, 1969—. Mr. Shapiro's initial work was conducting studies on heat transfer and hardening aspects of underground repeater buildings for the WT4 system. Subsequent work on WT4 included the design of band diplexer assemblies, repeater frames and waveguide pressure windows. In 1975, he was involved with designing waterproof repeater and apparatus housings for use with filled cable on T-carrier systems. His current work, began in 1976, is the physical design of multiplex equipment for the new L5E cable system.

William E. Studdiford, Bell Laboratories, 1956—. Mr. Studdiford has worked on the development of TH radio, TH radio protection switching, Telstar ground station and cryogenic apparatus, TM klystron replacement, and the WT4 regenerator and timing recovery loop. He is currently working on L5 coaxial line equipment.

David J. Thomson, B.S., 1965, Acadia University; MS, 1967, Ph.D., 1971, Polytechnic Institute of Brooklyn; Bell Laboratories, 1965—. In the past Mr. Thomson has been involved in multipair and coaxial cable. He also worked on WT4 in measurement, analysis, and specification of geometric imperfections in addition to time series analysis and spectrum estimation techniques. Currently Mr. Thomson is working on the high-capacity mobile telephone system. Member, IEEE, IMS, SIAM.

Peter J. Tu, B.S.E.E., 1960, National Taiwan University; M.S.E.E., 1963, Ph.D., 1966, University of Denver; Bell Laboratories 1966—. Mr.

Tu has worked on the FM feedback transmitter, the development of millimeter waveguide system, and the systems aspects of domestic satellite system. Currently, he is responsible for the multiplexer of the L5E coaxial cable system. Member, Eta Kappa Nu.

R. D. Tuminaro, B.S., 1957, M.F., 1959, New York University; Bell Laboratories, 1966—. Mr. Tuminaro's first assignment involved studying the coupling of nuclear-generated electromagnetic pulses into telephone networks. Later he joined the Millimeter Wave Medium Department working on the design of millimeter waveguides. More recently he has been working on long-haul coaxial cable telecommunications systems. Member of Tau Beta Pi, Eta Kappa Nu, IEEE.

H. C. Wang, B.S.E.E., 1955, Cheng-Kung University, Taiwan, China; M.S.E.E. 1960, University of Notre Dame; Ph.D. 1965, Polytechnic Institute of Brooklyn; Bell Laboratories, 1965—. mr. Wang has worked on microwave and millimeter wave networks for various systems. Since 1969, he has supervised a microwave network group responsible for the development of many passive and active components for radio systems.

William D. Warters, A.B., 1949, Harvard University; M.S., 1950, Ph.D., 1953, California Institute of Technology; Bell Laboratories, 1953—. Did research in multimode waveguide transmission and millimeter-wave repeaters; later was director of a laboratory responsible for transmission performance standards and objectives. In 1969–70, responsible for technical staff employment, education, and salary administration. In 1970 became director of laboratory responsible for development of the WT4 waveguide system. Presently director of Toll Transmission Laboratory with responsibility for development of coaxial cable and satellite transmission systems. Member, American Physical Society, Phi Beta Kappa, Sigma Xi. Fellow, IEEE.

Albert B. Watrous, B.M.E., 1943, The Cooper Union; Bell Laboratories, 1936—. Mr. Watrous was concerned with the design and development of gear trains and servomechanisms on several military projects between 1943 and 1961. He also had design responsibility for plotting boards, safety and arming mechanisms, and a boresight motion picture camera. Since 1961 he has worked on Bell System projects including Telstar, TD2/TH radio and the WT4 millimeter waveguide system. Mr. Watrous was concerned with the WT4 waveguide installation, coupling

design and the application of the electron-beam welding process for attaching flanges to waveguide tubing. Since late 1975 his assignment has been with the Loop Plant Laboratory.

Thomas J. West, B.E.E., 1954, Clarkson College of Technology; M.S.E.E., 1957, Michigan State University; W. L. Maxson Corporation, 1954–1956; Bell Laboratories, 1957—. Mr. West participated in the development of a number of transmission media, including paired cable, armorless ocean cable, and millimeter waveguide. He has also worked on the development of apparatus and test sets for the maintenance of paired cable. Member, IEEE, Eta Kappa Nu.

Stuart D. Williams, B.S.E.E., 1957, University of Virginia; M.S.E.E., 1959, New York University; Bell Laboratories 1957—. Mr. Williams since 1969 has worked on automated measurements for millimeter waveguide and single sideband radio transmission systems. Earlier Bell Laboratories experience included work in the fields of inertial stabilization and control of magnetic tape transports.

D. T. Young, B.S., 1956, M.E.E. 1960, Ph.D. 1966, University of Oklahoma. Mr. Young joined the Guided-Wave Research Department of Bell Laboratories in 1960. He initially worked on millimeter solid-state devices. Later he was involved in optical-fiber transmission research. He is presently working in the toll transmission laboratory on satellite transmission systems. Member IEEE, Sigma Xi, Tau Beta Pi, and Eta Kappa Nu.

Douglas N. Zuckerman, B.S. (E.E.), 1969, M.S. (E.E.), 1971, Eng. Sc.D. (E.E.), 1976, Columbia University; Bell Laboratories, 1969—. Mr. Zuckerman has been involved in WT4 waveguide system performance studies and the development of frequency multiplexing networks. He has participated in exploratory satellite antenna work and is presently engaged in the design of specialized antennas for satellite communications. Member, IEEE, Eta Kappa Nu, Tau Beta Pi, Sigma Xi.

Papers by Bell Laboratories Authors

CHEMISTRY

Molecular Dissociation by Electron Impact: Optical Emission from Fragments of Methane, Ethylene and Methanol. D. E. Donohue, J. A. Schiavone, and R. S. Freund, J. Chem. Phys., *67* (July 1977), pp. 769–780.

The Molecular Dynamics of Polysulfones in Solution as Observed by ^{13}C NMR Relaxation Measurements. R. E. Cais and F. A. Bovey, Macromolecules, *10*, No. 4 (July–August 1977), pp. 757–762.

ELECTRICAL AND ELECTRONIC ENGINEERING

Forward Scattering Due to Rain at 11 GHz. T. Li, W. C. Jakes, Jr., and J. A. Morrison, IEEE Trans. Ant. Propag., *AP-25* (September 1977), pp. 646–649.

Vibration-Induced Modulation of Fiberguide Transmission. D. F. Nelson, D. A. Kleinman, K. W. Wecht, Opt. Fiber. Trans. II (February 1977), pp. TuE7-1–TuE7-3.

MATERIALS SCIENCE

Etching Technique for Delineating Hard Gold Electroplate from Soft Gold Electroplate. T. M. Paskowski, Metallography, *10*, No. 3 (July 1977), pp. 355.

Transmission Electron Microscopy at Interfaces in III-V Compound Semiconductors. P. M. Petroff, J. Vacuum Sci. Technol., *14* (July/August 1977), pp. 973–978.

Beryllium Doping and Diffusion in Molecular Beam Epitaxy of GaAs and $Al_xGa_{1-x}As$. M. Ilegems, J. Appl. Phys., *48* (March 1977), pp. 1278–1287.

Electronic Structure of Tetragonal Tungsten Bronzes and Electrochromic Oxides. G. K. Wertheim, M. Campagna, J. N. Chazalviel, D. N. E. Buchanan, and H. R. Shanks, Appl. Phys., *13* (1977), pp. 225–230.

Carbon-13 NMR Observations of the Microstructure and Molecular Dynamics of Poly(Phenyl Thiirane). R. E. Cais and F. A. Bovey, Macromolecules, *10*, No. 4 (July–August 1977), pp. 752–757.

Impurity Effects in the Nucleation of Alpha (bcc)-Tantalum or Beta-Tantalum Films. N. Schwartz and E. D. Feit, J. Electrochem. Soc., *124* (January 1977) pp. 123–131.

PHYSICS

Many-Body Effects in X-ray Photoemission from the Nolte Metals. Y. Yafet and G. K. Wertheim, J. Phys. F: Metal. Phys. *7*, No. 2 (1977), pp. 357–366.

Spin Polarization of Field-Emitted Electrons and Magnetism at the (100) Surface of Ni. M. Landolt and M. Campagna, Phys. Rev. Lett., *38* (March 1977), pp. 663–666.

Lateral Current Confinement by Reverse Biased Junctions in GaAs-$Al_xGa_{1-x}As$ DH Lasers. W. T. Tsang and R. A. Logan, Appl. Phys. Lett., *30* (May 1977), pp. 538–540.

PSYCHOLOGY

On Stress and Linguistic Rhythm. M. Y. Liberman and A. Prince, Linguist. Inq., *8*, No. 2 (Spring 1977), pp. 249–336.